Inhibition of Monocarboxylate Transporter 1 by AZD3965 as a therapeutic approach in oncology

Richard A Noble

Thesis submitted in partial fulfilment of the requirements of the regulation for Doctor of Philosophy

Newcastle University

Faculty of Medical Science Graduate School

Northern Institute for Cancer Research

September 2016

Abstract

Many tumours display a metabolic phenotype distinct from non-malignant cells, with an increased reliance on glycolysis. This results in a greater production of lactate even under aerobic conditions. Lactate efflux is facilitated by monocarboxylate transporters 1-4 (MCT1-4) and is essential to maintain energy homeostasis. A sub-group of cancers express only MCT1 and are therefore exclusively reliant on this transporter to export lactate.

Inhibition of MCT1 has been proposed as a therapeutic approach to prevent lactate export in tumour cells with low MCT4. In this thesis, inhibition of monocarboxylate transporter 1 (MCT1) was investigated using the oral MCT1 inhibitor AZD3965 which is currently undergoing phase I clinical development.

Low MCT4 expression was found to be a common characteristic of Burkitt lymphoma (BL) and Diffuse Large B-cell Lymphoma (DLBCL) in immortalised cell lines and patient samples. In cell line models AZD3956 treatment caused a rapid accumulation of intracellular lactate and altered cellular metabolite profiles consistent with feedback inhibition of glycolysis including an increase in TCA cycle intermediates.

A substantial growth inhibitory response was observed *in vitro* in BL and DLBCL cell lines and also in an *in vivo* model of BL following daily oral AZD3965 treatment. The combination with a mitochondrial Complex I inhibitor, BAY 87-2243, triggered significant lymphoma cell death *in vitro* and also reduced disease burden *in vivo*.

This work supports the use of AZD3965 in the treatment of lymphoma patients who have become refractory to standard therapy but also highlights the potential need for combination strategies to optimally target the altered tumour metabolic phenotype.

Acknowledgements

Firstly, I would like to express my sincere gratitude to my supervisor Steve Wedge for his continuous support of my research, for his patience allowing me to pursue my own ideas, his motivation and insight. Also, my industrial supervisor Susan Critchlow (AstraZeneca) for supporting my placement at Alderley Park which was a great experience and has contributed substantially to this work, and my progress review panel Chris Bacon and Ross Maxwell for their invaluable feedback throughout.

I would like to acknowledge all the collaborators who have contributed to the project especially Natalie Bell who was key to generating *in vivo* data. I'd also like to thank Noel Edwards who introduced me to the lab and trained me in a number of techniques used in this thesis.

I'm very grateful to the other members of the lab and the Drug Discovery team who have provided technical advice, camaraderie, a stimulating and fun environment to work in, and cake.

A special mention to my friends and family outside the lab especially to my parents who have always given me their fullest support.

Finally, I would like to thank the Biotechnology and Biological Sciences Research Council (BBSRC) and AstraZeneca for funding this CASE studentship and to the British Association for Cancer Research (BACR) for funding a travel grant to present some of this work.

Contents

List of Figures and Tables

List of Abbreviations

2-PG: 2-phosphoglycerate, 2
3-PG: 3-phosphoglycerate, 1
Adenosine triphosphate, 1
ADP: Adenosine diphosphate, 1
Aldo: Aldolase, 1
B-ALL: B-cell acute lymphocytic leukaemia, 70
BCA: Bicinchoninic acid, 45
BL: Burkitt lymphoma, 62
BSA: Bovine serum albumin, 46
BTK: Bruton's tyrosine kinase, 129
CCRC: Clear cell renal carcinoma, 20
CHC: 2-Cyano-3-(4-hydroxyphenyl)-2-propenoic acid, 21
dH_2O: deionised H_2O, 49
DHAP: Dihydroxyacetone phosphate, 1
DIDS: 4,4'-Diisothiocyano-2,2'-stilbenedisulfonic acid, 21
DLBCL: Diffuse large B-cell lymphoma, 61
DMSO: dimethyl sulfoxide, 43
EBV: Epstein-Barr virus, 72
ECAR: Extracellular acidification rate, 59
ENO1: Enolase, 2
F1,6 BP: Fructose 1,6 bisphosphate, 1
F2,6 BP: Fructose 2,6 bisphosphate, 1
F6P: Fructose-6-phosphate, 1
FBS: Foetal bovine serum, 43
FDG-PET: [^{18}F] Fluorodeoxyglucose positron emission tomography, 6
G6P: Glucose-6-phosphate, 1
GAP: Glyceraldehyde-3-phosphate, 1
GAPDH: Glyceraldehyde-phosphate-dehydrogenase, 1
GBP: 1,3-Bisphosphoglyceric acid, 1
GLS: Glutaminase, 13
GLUT1: Glucose transporter 1, 1
GPI: Glucose phosphate isomerase, 1
HIF-1α: Hypoxia inducible factor-1α, 9
HnRNP: Heterogenous nuclear ribonucleoprotein, 8
LDH: Lactate dehydrogenase, 2
MRM: multiple reaction monitoring, 53
mTOR: Mammalian target of rapamycin, 128
NAC: N-acetyl-ι-cysteine, 58
NAD: Nicotinamide adenine dinucleotide, 1
NFAT: Nuclear factor of activated T-cells, 19
NF-kB: Nuclear factor kappa-light-chain enhancer of activated B-cells, 9
NHL: non-Hodgkin lymphoma, 72
NMR: Nuclear magnetic resonance, 57
NSCLC: Non-small-cell lung carcinoma, 18
NSG: NOD/LtSz-scid IL-2Rγ-/-, 49

OCR: Oxygen consumption rate, 59
OXPHOS: Oxidative phosphorylation, 3
PBS: Phosphate-buffered saline, 45
PDH: Pyruvate dehydrogenase, 2
PEP: Phosphophenolpyruvate, 2
PFK: Phosphofructokinase, 1
PGK: Phosphoglycerate kinase, 1
PI3K: Phosphoinositide 3-kinase, 8
PKM: Pyruvate kinase, 2
PTEN: Phosphatase and tensin homolog, 128
RIPA: Radio Immunoprecipitation Assay, 45
RMA: Robust multi-array averaging, 67
ROS: Reaxtive oxygen species, 3
RPMI: Roswell Park Memorial Institute, 43
SDS: Sodium dodecyl sulfate, 47
TCA cycle: Tricarboxylic acid cycle, 3
TIGAR: TP53-Induced Glycolysis and Apoptosis Regulator, 9
TPI: Triosephosphate isomerase, 1
VHL: Von Hippel–Lindau, 9

Chapter 1. Introduction

1.1. Cellular metabolism

Otto Warburg first reported in 1924 that cancer cells generate increased amounts of lactate from the fermentation of glucose even under aerobic conditions (1). This shift away from oxidative phosphorylation (OXPHOS) towards a more glycolytic phenotype is now widely referred to as the 'Warburg effect' (Figure 1-1) (1-3). The high glycolytic rate of tumours has also been recognised as an emerging 'Hallmark of Cancer' and approaches to target this for therapeutic benefit are being sought (4).

1.1.1. Glycolysis

Glycolysis is a multi-step reaction, which ultimately uses glucose to produce two molecules of pyruvate, a process which also generates a net gain of 2 molecules of ATP (adenosine triphosphate) (5). The process is often broken into "preparatory" and "pay-off" phases (6). During the preparatory phase of glycolysis, glucose is initially taken up into the cell by the transmembrane glucose transporter 1 (GLUT1) and then phosphorylated by hexokinase II (HKII) to form glucose-6-phosphate (G6P). This requires a molecule of ATP and prevents passive diffusion of glucose out of the cell. G6P is then converted to fructose-6-phosphate (F6P) by glucose phosphate isomerase (GPI). The subsequent conversion of F6P to fructose 1,6 bisphosphate (F1,6 BP) by phosphofructokinase (PFK) is one of the key regulatory steps in the pathway and requires the investment of another molecule of ATP (7). Increased formation of fructose 2,6 bisphosphate (F2,6BP) by the isoenzyme PFK2 acts as an allosteric regulator, increasing the enzymatic activity of PFK1. F1,6BP is then converted to two 3 carbon molecules, glyceraldehyde-3-phosphate (GAP) and dihydroxyacetone phosphate (DHAP) by aldolase (Aldo). Triosephosphate isomerase (TPI) can then catalyse the conversion of DHAP to GAP. The formation of GAP signals the start of the pay-off phase where net gains in ATP are made. The next step is an oxidation reaction coupled to the reduction of Nicotinamide adenine dinucleotide $(NAD)^+$ catalysed by glyceraldehyde-phosphate-dehydrogenase (GAPDH) to produce 1,3-Bisphosphoglyceric acid (GBP). As a result, phosphoglycerate kinase (PGK) catalyses the transfer of a phosphate group from GBP to ADP forming 3-phosphoglycerate (3-PG). This is the first ATP generating step of glycolysis. Phosphoglycerate

mutase (PGM) then converts 3-PG to 2-phosphoglycerate (2-PG), allowing 2-PG to subsequently be converted to phosphophenolpyruvate (PEP) by enolase (ENO1). Finally, PEP is converted to pyruvate by pyruvate kinase (PKM), yielding further ATP. Pyruvate may then undergo two fates, either being converted to Acetyl-CoA by Pyruvate dehydrogenase (PDH) to fuel the TCA cycle, or be reduced by lactate dehydrogenase (LDH) to form lactate. Preference for this latter pathway, even under aerobic conditions, is characteristic of the Warburg effect.

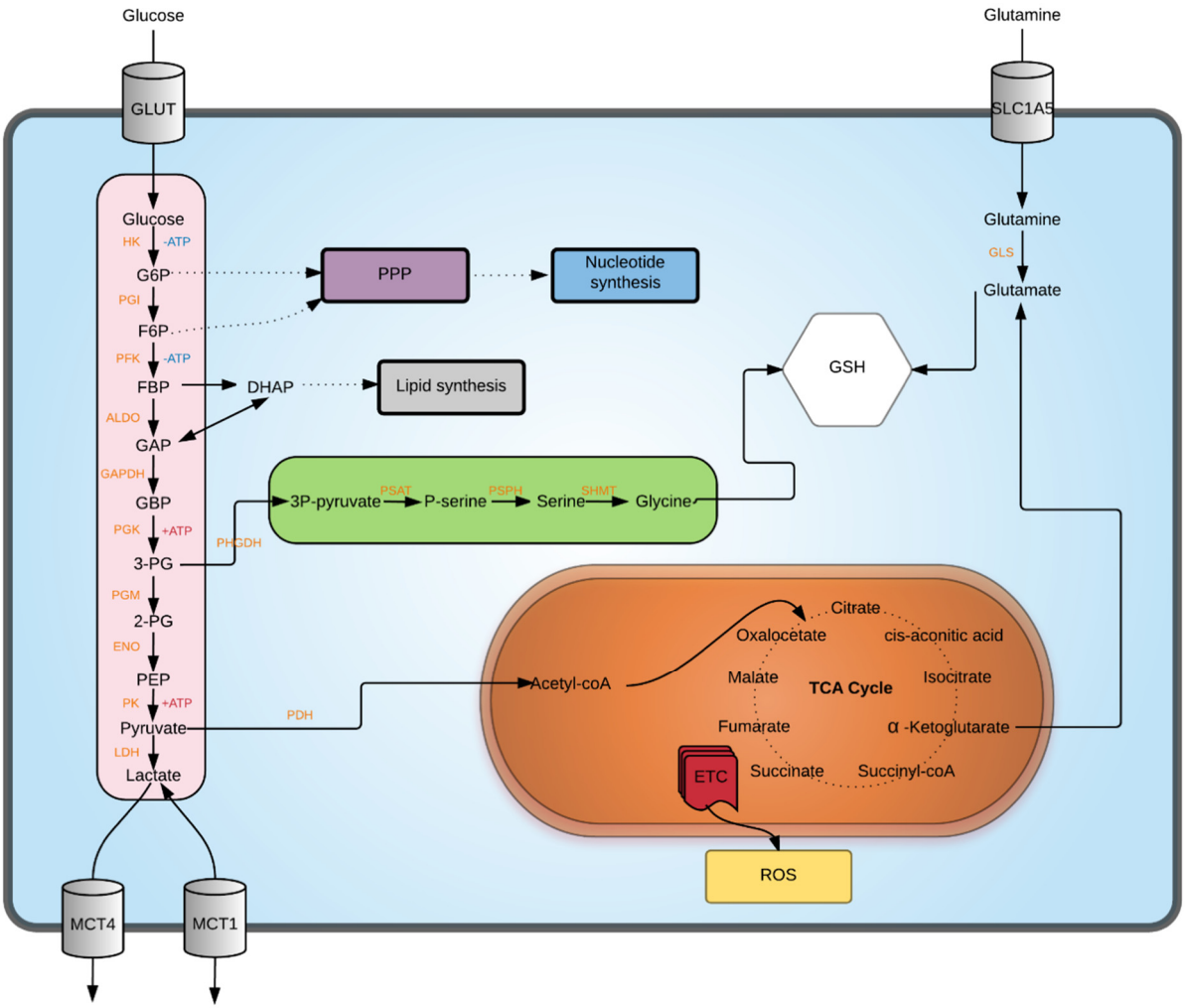

Figure 1-1: Cellular metabolism
Glycolysis generates a net gain of 2 ATP molecules per molecule of glucose, with complete oxidation of the pyruvate generated potentially yielding a further 36 molecules of ATP via OXPHOS. However, proliferating cells must also satisfy their need for biosynthetic intermediates by diverting intermediates away from ATP production. Abbreviations used: aldolase (ALDO), 1,3-Bisphosphoglyceric acid (GBP), dihydroxyacetone phosphate (DHAP), electron transport chain (ETC), enolase (ENO1), fructose 1,6 bisphosphate (FBP), fructose-6-phosphate (F6P), glyceraldehyde-3-phosphate (GAP), glyceraldehyde-phosphate-dehydrogenase (GAPDH), glutathione synthesis (GSH), glucose transporter 1 (GLUT1), glucose-6-phosphate (G6P), glucose phosphate isomerase (GPI), hexokinase (HK), lactate dehydrogenase (LDH), pyruvate dehydrogenase (PDH), phosphophenolpyruvate (PEP). phosphofructokinase (PFK), 2-phosphoglycerate (2-PG), 3-phosphoglyceric acid (3-PG), phosphoglycerate kinase (PGK), phosphoglycerate mutase (PGM), pyruvate kinase (PKM), reactive oxygen species (ROS), triosephosphate isomerase (TPI).

1.1.2. Oxidative phosphorylation

Mitochondria play a dual role in cellular metabolism with the tricarboxylic acid (TCA) cycle generating intermediates for anabolic pathways as well as the more recognised role in ATP generation.

Warburg's original hypothesis to explain his observation of aerobic glycolysis in cancer cells was that cancer cells had dysfunctional mitochondria and were therefore unable to produce ATP through oxidative phosphorylation (OXPHOS). This has now largely been disproved, as several studies have shown no evidence of mitochondrial dysfunction in the majority of tumour cell lines and oxidative phosphorylation still plays a key role in energy generation in cancer cells. Indeed mitochondrial metabolism is now recognised as being crucial to most cancer cells as a source of ATP, generating precursor molecules and providing reactive oxygen species (ROS) which help to promote genome instability and tumorigenesis (8). Mutations in mitochondrial enzymes such as fumarate hydratase as well as succinate and isocitrate dehydrogenases (IDH) are exceptions to this where dysfunctional mitochondria drive tumorigenesis. These mutations are rare in the wider context of all cancers but are found at higher frequencies in certain cancer subtypes. For example mutations in IDH occur in 12% of glioblastoma cases (9).

The tricarboxylic acid cycle

The TCA cycle begins with acetyl-coA which can be generated from pyruvate via PDH or through a variety of other pathways such as fatty acid oxidation. The TCA cycle utilises a number of carbon sources, including pyruvate to produce reducing equivalents, NADH and $FADH_2$. Three molecules of NADH and one molecule $FADH_2$ are generated per cycle. These reducing equivalents donate electrons which are required by the electron transport chain to ultimately generate ATP.

The TCA cycle is not a purely catabolic pathway and several TCA cycle intermediates also support anabolic pathways including amino acid synthesis (alpha-ketoglutarate and aspartate) and nucleotide synthesis (aspartate). Specifically, alpha-ketoglutarate can form glutamine, proline and arginine (5). Aspartate also contributes to pyrimidine synthesis. Since carbon in the form of CO_2 is lost as waste during the cycle, there is a requirement for the replenishment of substrates such as acetyl-coA in order for the cycle to continue.

The electron transport chain (ETC)

The indirect transfer of electrons from these reducing equivalents to O_2 occurs through a number of multi-protein complexes (I-IV) as part of the electron transport chain (ETC) (Figure 1-2). The transfer of electrons along the electron transfer chain is coupled to the maintenance of a proton gradient across the intermembrane space.

Complexes I, III and IV contribute to this by removing protons from the mitochondrial matrix and transferring them to the intermembrane space. Electrons are transferred from NADH, via Complex I through a multi-step reaction forming reduced ubiquinone to supply complexes III and IV. Complex II also converts ubiquinone to its reduced form but this is instead coupled to the formation of fumarate from succinate as part of the TCA cycle. Electrons are then transferred from ubiquinone to cytochrome C by Complex III. Reduced cytochrome C is then used as a substrate to reduce O_2 to form water. This proton gradient generated is then used to drive the generation of ATP from ADP by ATP synthase through the movement of protons back into the mitochondrial matrix through the proton channel (Complex V).

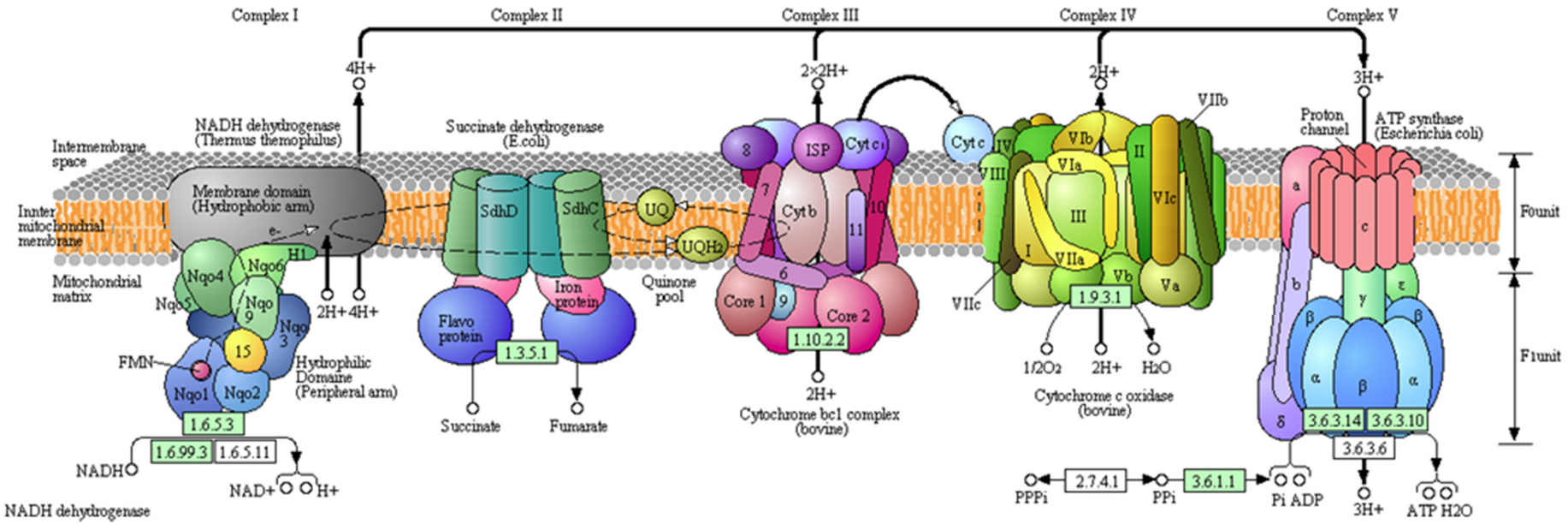

Figure 1-2: The electron transport chain (ETC)
Figure from the Kyoto Encyclopaedia of Genes and Genomes (KEGG) pathway database (10)

1.2. Reprogramming energy metabolism - An emerging hallmark of cancer

There are several characteristics which differentiate both tumour cells and the tumour microenvironment from normal tissue. Abnormal features of tumour cells include unbridled proliferation and alterations in cellular metabolism with which to support this. Within the tumour microenvironment there are changes in blood flow, vascular structure, oxygenation, nutrient availability and pH. Exploiting these differences through the use of selective targeted agents, rather than targeting proliferation *per se* with existing treatments, should provide an improved therapeutic window, resulting in fewer side effects than existing treatments. One such approach involves targeting the altered metabolic profile of tumour cells typified by the "Warburg effect".

1.2.1. The Warburg effect

Cancer cells exhibit an altered metabolic phenotype which supports their rapid and uncontrolled proliferation. An increased demand for glucose is exploited diagnostically through Fludeoxyglucose-Positron emission tomography (FDG-PET) scanning of solid tumours (Figure 1-3). Here an analogue of 2-deoxyglucose (2-DG) is labelled with radioactive fluorine isotope [^{18}F]. Positrons emitted from [^{18}F] trigger the emission of γ-rays from electrons which can be detected by the PET scanner. FDG enters cells via glucose transporters, once within the cell, FDG is phosphorylated by hexokinase but cannot proceed any further through the glycolytic pathway and so becomes trapped within the cell.

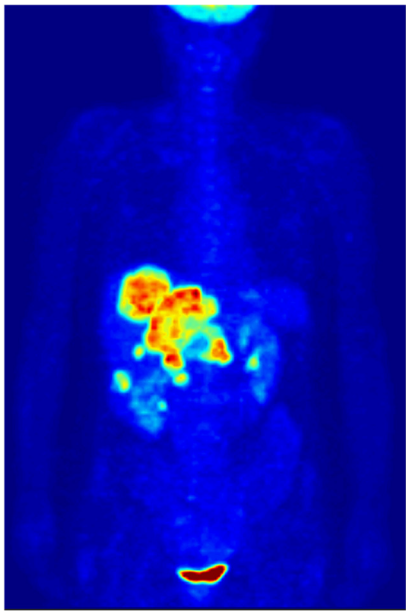

Figure 1-3: FDG-PET scanning
18F-FDG scan showing high accumulation of the radiolabelled glucose-analogue in a colorectal tumour with liver metastases. Normal high accumulation in the bladder is also evident. Image from Jens Langer (11). It is important to stress that although tumourigenic cells undergo a relative shift towards glycolysis, in comparison to normal comparable cell types, the balance between OXPHOS and glycolysis used to generate ATP is cell type and context dependent and varies widely.

If glucose metabolism is purely viewed as a means to generate ATP, then it seems counter-intuitive that during highly proliferative states cells would opt for a less efficient means of ATP generation. It is now known that this preference for glycolysis is not only shown by most cancer cells but is also shared by 'normal' cells when undergoing rapid proliferation, including lymphocytes. Although in terms of ATP generating efficiency, glycolysis is inferior to oxidative phosphorylation, glycolysis is able to generate ATP at a faster rate and so, under conditions where glucose availability is a non-limiting factor, may be a more productive means of ATP synthesis (12).

Perhaps the most attractive hypothesis to explain the selective advantage of utilising glycolysis is that a high level of glycolytic flux supports various biosynthetic pathways through the generation of glycolytic intermediates which help to provide much of the carbon backbone required for macromolecular biosynthesis and reducing equivalents needed for proliferation. For example:

- G6P can enter the pentose phosphate pathway which supports nucleotide synthesis through the generation of ribose-5-phosphate.

- DHAP is a precursor to Glycerol-3-phophate, which is required for phospholipid synthesis needed to produce cellular membranes.
- The glycolytic intermediate, 3-PG, supports the serine/glycine synthetic pathway. This pathway in particular appears to be particularly important to cancer cell proliferation.

In support of this hypothesis a number of key enzymes that regulate these branch points away from the canonical glycolytic pathway are upregulated in cancer as discussed in the following section.

1.2.2. Regulation of cellular metabolism in cancer

A relative shift in the metabolic profile of tumours is regulated by multiple signalling pathways linked to oncogenes (e.g. *c-MYC, KRAS* and *PI3K)* and tumour suppressor genes, (e.g. *TP53)* as well as the tumour microenvironment itself (Figure 1-4).

c-MYC

The prevalence of c-MYC deregulation in cancer through translocations, amplifications of the *c-MYC* gene, or through aberrant activation of signal transduction pathways are testament to its importance in cell growth and survival. c-MYC promotes a glycolytic phenotype through the upregulation of the glucose transporter GLUT1, and glycolytic enzymes such as HKII, PFKM, ENO1 and LDHA (13-16). In addition, c-MYC also increases glutamine uptake and glutaminase expression favouring glutaminolysis as another important energy source particularly under low glucose or oxygen conditions (17, 18). Similarly c-MYC influences the expression of genes involved in the serine-glycine pathway (19).

c-MYC also alters cellular metabolism indirectly through alterations in micro RNA (miRNA) and heterogeneous nuclear ribonucleoprotein (HnRNP) expression (20, 21). For example deregulated c-MYC indirectly increases the formation of PKM2 through altered splicing of the *PKM* gene (21). Pyruvate kinase (PK) catalyses the final ATP-generating step of glycolysis where pyruvate is formed from PEP. Uniquely amongst PK isoforms, PKM2, can exist as a dimer with intermediate activity or the usual tetrameric complex with high activity. This allows for graded regulation of PK activity depending on nutrient availability. PKM2 is also subject to a number of post-translational modifications which reduce its activity by preventing tetramer formation. A number of cancer types preferentially express PKM2 to promote the Warburg effect. Specific deletion of PKM2 has recently revealed that non-proliferating cancer cells may express the high activity PKM2 isoform where efficient

generation of ATP is more advantageous as the need for biosynthetic intermediates decreases (22).

HIF1α

Hypoxia inducible factor-1α (HIF-1α) is induced under hypoxic conditions and increases the transcription of a number of glycolytic genes in concert to sustain ATP production under anaerobic conditions. Target genes include monocarboxylate transporter 4 (*MCT4*) to deal with an increased production of lactate, resulting from the decreased utilization of pyruvate in the TCA cycle under hypoxic conditions.

Aside from the synonymous upregulation under hypoxia, HIF-1α is also responsive to other stimuli. Increased levels of succinate and fumarate have been shown to alter HIF stability *in vitro* via inhibition of HIF-prolyl 4-hydroxylases therefore increasing HIF activity (23). HIF-1α synthesis is also increased via the PI3K/Akt/mTOR pathway and its stability is increased following p53 loss of function (24, 25). HIF-1α also plays a major role in a sub-set of renal cell carcinomas, where the tumour suppressor function of Von Hippel–Lindau (VHL) has been lost thereby preventing effective ubiquitination of HIF-1α (26).

p53

Conversely p53 and its transcriptional targets, TP53-inducible glycolysis and apoptosis regulator (*TIGAR*) and Cytochrome C oxidase (*SCO2*) work to suppress glycolysis and favour oxidative phosphorylation. Loss of p53 function, which is commonly observed in a wide range of cancers, therefore, favours a more glycolytic phenotype. p53 inhibits the expression of glucose transporters directly. And also, through the inhibition of NF-κB , p53 also inhibits PGM (27). Originally TIGAR was postulated to be a fructose-2,6 bisphosphatase, thus limiting the availability of F2,6BP, reducing the activity PFK1 and inhibiting glycolysis (28). Whilst there is evidence to support this view, Gerin *et al*. have recently contested this theory by demonstrating that TIGAR is a comparatively poor fructose-2,6-bisphosphatase and that it is several orders of magnitude more active towards other substrates such as 2-3-bisphosphoglycerate and glycolytic intermediates such as 2-PG and PEP (29). This calls into question the exact role of TIGAR in metabolic regulation. Also, the negative regulator of p53, MDM2, has been suggested to influence cellular metabolism, in particular serine/glycine metabolism and ROS homeostasis, through its chromatin binding independent of p53 function (30).

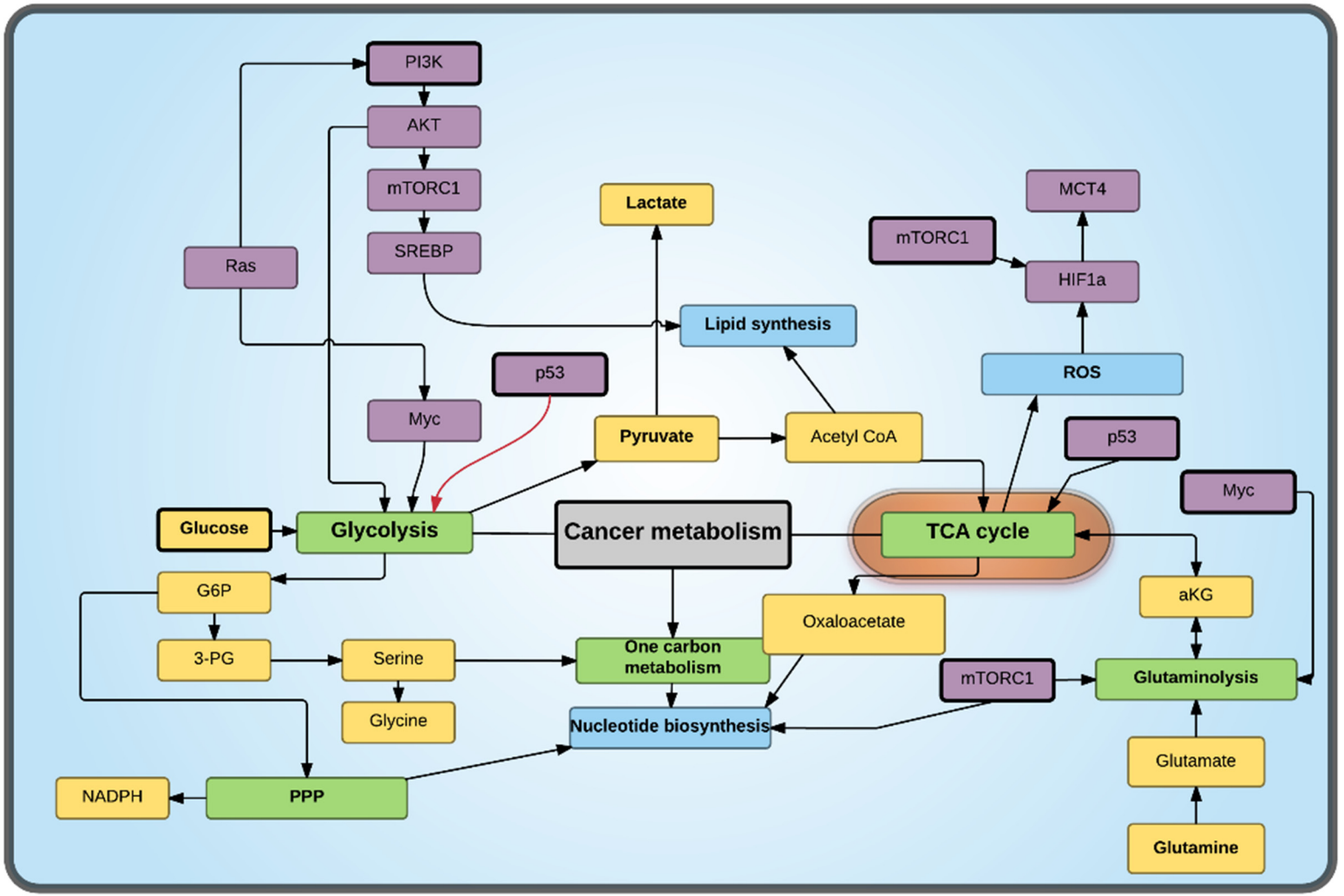

(Figure legend on next page)

Figure 1-4: Signaling pathways and cancer metabolism.
Figure adapted from Fundamental of Cancer Metabolism (31). A number of signal transduction pathways ■ converge on major metabolic pathways ■. In cancer dysregulation of these pathways shift the balance of energy generation pathways from OXPHOS towards glycolysis. Increased glycolytic flux generates increased levels of metabolites ■ which can fuel anabolic pathways. Directional arrows indicate where a metabolite is a substrate or intermediate/product of a given pathway. Abbreviations used; αKG (alpha-ketoglutarate); G6P (glucose-6-phosphate); 3-PG (3-phosphoglycerate); OAA (oxaloacetate). Therapeutic targeting of tumour metabolism

1.3. Therapeutic targeting of tumour metabolism

Recently there has been much interest in targeting metabolism in cancer through a number of diverse approaches from direct targeting of metabolic pathways to targeting signal transduction pathways (Figure 1-5) (32). The majority of these approaches aim to exploit a specific metabolic pathway that tumour cells are especially reliant upon. However, a potential concern in targeting tumour metabolism is the inherent plasticity between metabolic pathways as well as metabolic heterogeneity within tumours.

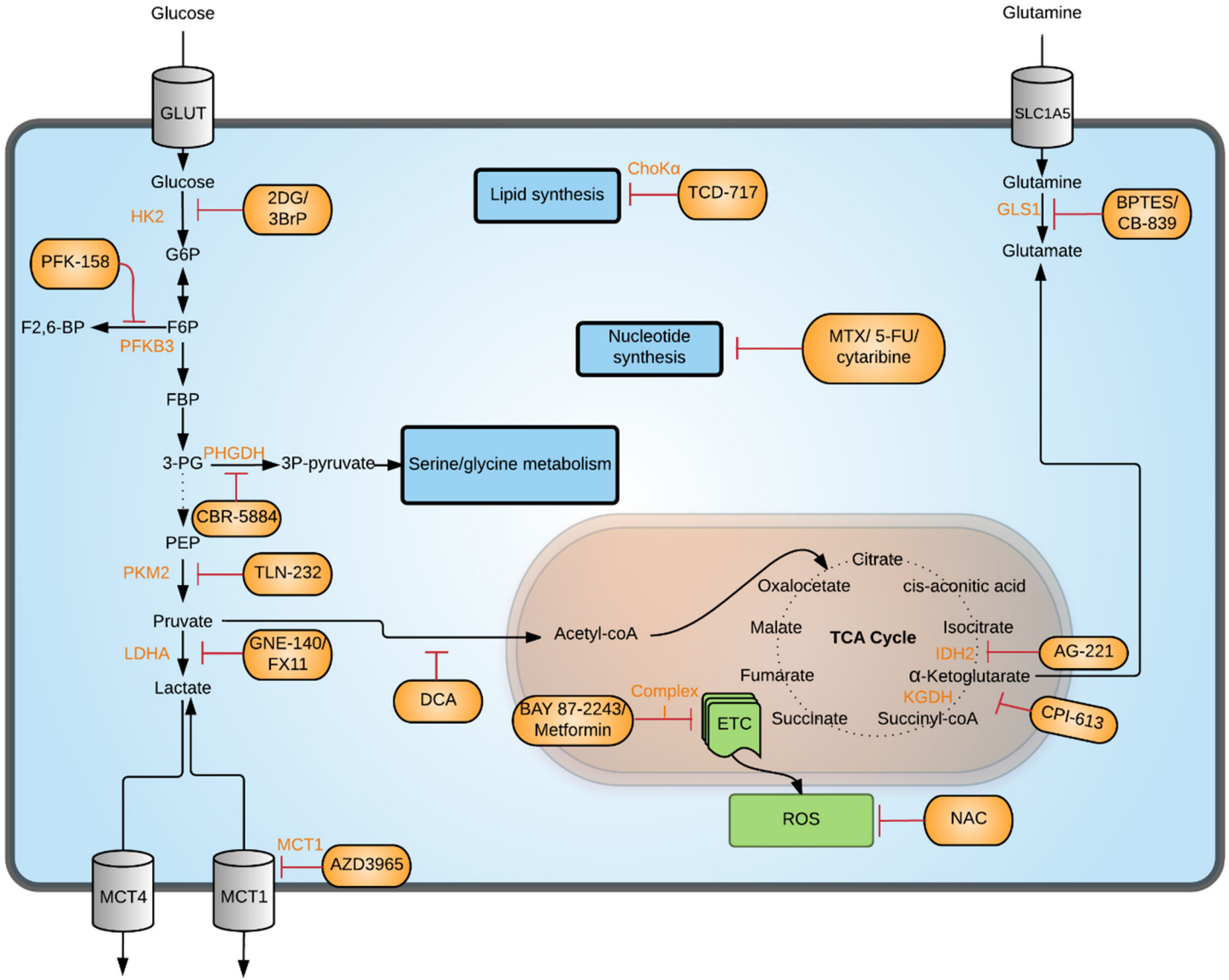

(Figure legend on next page)

Figure 1-5: Therapeutic approaches targeting the altered metabolic phenotype in cancer
A multitude of different approaches have been investigated as a means of targeting the altered metabolic phenotype in cancer cells. Molecular targets of the named compounds are indicated in orange. Adapted from (32).

1.3.1. Nucleotide biosynthesis

A number of cytotoxic chemotherapeutics used clinically target different stages of nucleotide synthesis. For example, one of the first classes of chemotherapies, the anti-folates, target rapidly proliferating cells and their increased requirement for nucleotides through inhibiting the formation of thymidylate. In the case of methotrexate, inhibition of dihydrofolate reductase, which catalyses the formation of tetrahydrofolate, reduces the availability of a key co-factor for nucleotide synthesis. Although the molecular mechanisms behind agents like methotrexate and 5-fluorouracil were retrospectively deduced they represent examples of targeted agents that have clinical utility to this day, commonly being used in a range of cancers (33).

1.3.2. Amino acid metabolism

As well as their increased uptake of glucose many cancers also demonstrate high levels of glutamine consumption. High levels of glutamine uptake are particularly associated with c-MYC activated tumour types (17). Once glutamine has been transported into the cell, glutaminase (GLS) catalyses the conversion of glutamine to glutamate. Glutamate acts as a precursor to glutathione production and a can feed into the TCA cycle via conversion to alpha-ketoglutarate supporting ATP synthesis which has been shown to be a particularly important under glucose-deprived conditions (18). Owing to the importance of glutamine/glutamate, small molecule inhibitors of GLS, with distinct mechanisms of action, have been developed showing efficacy both *in vitro* and *in vivo* (34-36).

The most advanced GLS inhibitor, CB-839 demonstrates preclinical efficacy in triple negative breast cancer and this is associated with mechanistically relevant changes in intracellular metabolites consistent with reduced activity of GLS, in particular reductions in aspartate and glutamate (37). CB-839 is under phase I/II clinical investigation in several trials for utility in both solid and haematological malignancies. Aside from glutamine, preclinical studies have also demonstrated an importance of serine/glycine metabolism and aspartate synthesis (38-40). Subsequently, attempts have been made to design inhibitors to target these pathways.

Recently, for example, a selective inhibitor of phosphoglycerate dehydrogenase (PHGDH) CBR-5884, has been described (40).

1.3.3. Oxidative phosphorylation

Interest in the biguanides, phenformin and metformin, were sparked by epidemiological evidence suggesting that patients who had been prescribed metformin for the treatment of type II diabetes exhibited a lower incidence of cancer formation (41). Subsequent mechanistic studies have shown metformin to be efficacious in various *in vitro* and *in vivo* preclinical models (42-45). Although the exact mechanism of action of metformin is still under debate, its efficacy is at least in part due to inhibition Complex I of the electron transport chain (46, 47).

Recently more potent inhibitors of the electron transport chain have been designed such as BAY 87-2243 and ME-433. BAY 87-2243 inhibits Complex I with nanomolar potency and has been shown to have growth inhibitory activity in a number of *in vitro* an *in vivo* preclinical models (48, 49). ME-344, a partial inhibitor of Complex I and III, is currently under investigation with results from a phase I clinical trial showing it to be well-tolerated (50). However, ME-344 also binds tubulin at lower concentrations than those required to observe reductions in oxygen consumption rate (51, 52). A further electron transport chain inhibitor, VLX600, has also been described which partially inhibits complexes I, II and IV (53).

1.3.4. Glycolysis

Previously, as discussed, many cancer types maintain high levels of lactate secretion allowing cells to maintain a high glycolytic flux in addition to regenerating NAD^+. A potential therapeutic approach is to target the more glycolytic phenotype in cancer cells through the interference of lactate transport governed by the monocarboxylate transporter family 1-4. A number of other approaches have also been explored both pre-clinically and in clinical trials, in order to target this increased reliance on glycolysis in cancer cells (Figure 1.5).

Hexokinase

Inhibition of the phosphorylation of glucose by hexokinase is inhibited by both of the glucose analogues, 2-deoxyglucose (2-DG) and 3-bromopyruvate. Despite preclinical efficacy in a wide range of models these agents have failed to demonstrate significant efficacy clinically and have been found to cause substantial toxicity in clinical trials (54). The discrepancy

between preclinical and early clinical investigations are likely to stem from a lack of target specificity in the case of 3-bromopyruvate and lack of tumour selectivity in the case of 2-DG. For example 2-DG is heavily incorporated into all glycolytic tissues not just cancer cells which can be visualised with FDG-PET scanning.

Pyruvate kinase M2

PKM2 is a crucial regulatory point in the glycolytic pathway expressed in foetal tissues, proliferative adult cells and commonly in cancer cells. PKM2 unlike other isoforms can exist as low-activity dimers and high activity tetrameric forms which allows fine-tuning of the rate of glycolytic flux, allowing flexibility to shift between the supply of anabolic intermediates and energy production. Consequently interfering with PKM2 has been investigated as a therapeutic strategy (55). An activator of PKM2, SGI-9380, has been shown to reduce cell proliferation *in vitro* under serine starved conditions indicating that serine biosynthesis is compromised by high PKM2 activity (56). Conversely, an inhibitor of PKM2 inhibition, TLN-232, (TT-232, CAP-232), has reduced tumour growth in a number of xenograft models (57, 58).

Fructose-2,6-biphosphatase 3

Another isoenzyme preferentially expressed in cancer cells is the PFKFB isoform, PFKFB3. PFKFB catalyses the reversible phosphorylation of F6P to form a potent allosteric activator of PFK, F2,6 BP. PFKFB3 promotes a higher rate of glycolytic flux through increased kinase activity relative to other isoforms (59). A novel inhibitor of PFKFB3, PFK-158, has recently been described with efficacy in a number of *in vitro* and *in vivo* preclinical models through the selective inhibition of PFKFB3 activity which reduces glycolytic activity and cell proliferation (60). PFK-158 is currently under phase I clinical investigation (NCT02044861).

Lactate dehydrogenase A

As mentioned, LDH catalyses the reversible conversion of pyruvate to lactate. Increased LDH-A expression, as observed in multiple cancers, favours the formation of LDH isoform (LDH5) which preferentially converts pyruvate to lactate (61). FX11 has been shown to reduce the growth of patient derived tumour xenografts decreasing the lactate:pyruvate ratio, consistent with decreased production of lactate (62). Similarly, an LDHA inhibitor with nanomolar potency, GNE-140, strongly reduces intracellular lactate *in vitro* having anti-proliferative effects in pancreatic cell lines demonstrating a glycolytic phenotype (63).

1.4. Monocarboxylate transporter 1

1.4.1. Structure

Based on hydrophobicity analysis, the predicted topology of MCT1 involves 12 α-helical transmembrane domains with intracellular C and N-termini and a large intracellular loop between domains 6-7 where the sequence homology between the isoforms is lowest and is important for substrate specificities (64). Conversely, sequence homology between the MCT isoforms is greatest within the transmembrane domains (65). The X-ray crystal structure of MCT1 has yet to be defined. However, a homology model based upon the known crystal structure for the *Escherichia coli* glycerol-3-phosphate transporter, GlpT, exists, which supports the predicted model (Figure 1-6) (66, 67).

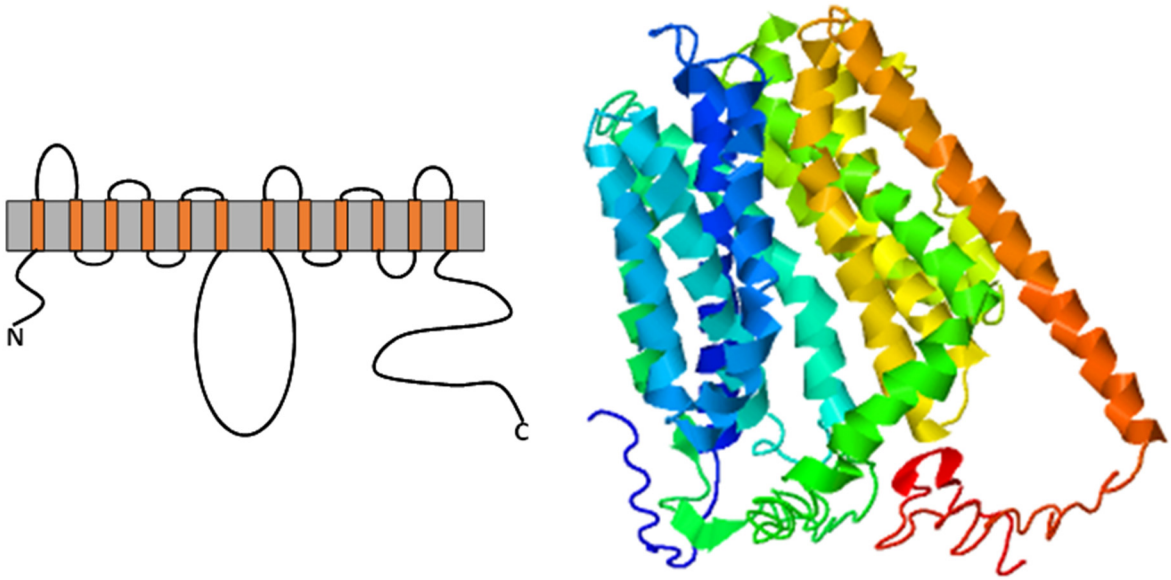

Figure 1-6: Structure of MCT1
Predicted topology of MCT1. Homology model of MCT1 based upon the Glycerol-3-Phosphate Transporter from *Escherichia coli* (1pw4A) as previously described (67). The model was generated using the FASTA amino acid sequence of hsMCT1 in I-TASSER (68-71)

1.4.2. Function of monocarboxylate transporters 1-4

MCT1 belongs to a larger transporter family of which only monocarboxylate transporters 1-4 (MCT1-4) have been experimentally demonstrated to be *bona fide* plasma membrane transporters of monocarboxylates, with MCT1 and 4 being the best studied. Transport of monocarboxylates is coupled to proton uniport allowing for bidirectional transport of substrates in to and out of cells dependent upon the concentration gradients.

Monocarboxylate transporters 1,2 and 4 differ in their relative affinities for their substrates. MCT2 displays the highest affinity for both lactate and pyruvate followed by MCT1 then MCT4. MCT4 displays an especially poor affinity for pyruvate compared to lactate.

	MCT1 (SLC16A1)	MCT2 (SLC16A7)	MCT3 (SLC16A8)	MCT4 (SLC16A3)
L-Lactate	3.5	0.74	6	28
D-Lactate	>60	-	-	519
Pyruvate	1	0.08	-	153
α-Ketobutyrate	0.2	-	-	57

Table 1: Substrate affinities of MCTs
K_m values (mM) for selected substrates of MCTs from studies expressing MCT1, 2 and 4 in *Xenopus* oocytes or in yeast (MCT3). Gene names are displayed in brackets as per HUGO nomenclature (72, 73).

MCT1 is ubiquitously expressed at low levels throughout the body with the exception of pancreatic β-cells and is the predominant isoform in most tissues (74). Consequently, MCT1 can be co-expressed with other MCT members. The substrate affinities of MCT1 allow it to facilitate the exit or entry of lactate to and from cells dependent on the substrate gradients present in their environment. As the ubiquitous isoform, in most cells it is MCT1 which exports lactate/H^+ out of the cell under anaerobic conditions of low O_2 concentrations. MCT1 also facilitates this role in some normal cell types such as red blood cells and in T-lymphocytes where MCT1 upregulation facilitates a highly proliferative activated state, demonstrating a glycolytic phenotype regardless of oxygenation status (75, 76). As discussed earlier, this is similar to cancer cells which exhibit a highly glycolytic phenotype generating high levels of lactate even under aerobic conditions which can be exported by MCT1.

The expression of the lower affinity MCT4 is more selective and limited to highly glycolytic cells including astrocytes, white blood cells and white skeletal muscle (77, 78). MCT4 has distinct substrate affinities from MCT1 reflecting its tissue specific distribution. MCT4 has a reduced affinity for lactate but a higher maximal rate for lactate transport (V_{max}). This allows MCT4 to remove lactate from the cell during anaerobic respiration to allow glycolysis to continue. In addition, MCT4 has also has a 150-fold greater K_m for pyruvate which prevents the efflux of pyruvate from the cell under anaerobic conditions where intracellular pyruvate can accumulate. If under such conditions, pyruvate was transported out of the cell without

its conversion to lactate, the NAD+/NADH ratio in the cell would fall, undermining glycolytic flux, by inhibiting the generation of GBP from GAP (79).

MCT2 and 3 are more specialised in their expression profiles. MCT2 is largely co-expressed with MCT1 in cells which demonstrate significant uptake of lactate but not efflux, either using it as a respiratory fuel as is the case in cardiac myocytes or neurons or alternatively to facilitate gluconeogenesis in liver parenchymal cells (80, 81). MCT3 is found limited to the basolateral membrane of the choroid plexus and retinal pigment epithelium however detailed knowledge on substrate affinities are to-date poorly defined (73, 82).

1.4.3. Mechanism of lactate transport

The translocation cycle of MCT1 has been best studied. The proposed model of transport suggests proton binding occurs prior to binding of a lactate anion and that these are released in the opposite order (66, 83). Initial proton binding requires the transporter to be in an open conformation allowing access to a lysine residue (K38) within the transport channel, which is crucial for subsequent transporter activity; site-directed mutagenesis of this lysine being shown to result in a complete loss of transporter activity. The negatively charged lactate anion is then able to access K38 forming an ion pair. Binding of both substrates triggers a conformational change in MCT1 which switches the open face of the transporter to the opposite side of the plasma membrane. This allows movement of the proton to an aspartic acid residue (D302) deeper within the channel allowing lactate to also move to a site deep in the channel as the aspartic acid side chain becomes neutralised. This allows lactate/H^+ to diffuse from the transporter if a sufficient concentration gradient exists.

1.4.4. Regulation

Transcriptional regulation

Recently *MCT1* has been shown to be a direct transcriptional target for MYC, adding to the list of MYC target genes linked to a glycolytic phenotype (84, 85). *MYC* expression therefore is found to correlate strongly with *MCT1* expression in a number of cancer types including Burkitt lymphoma, breast adenocarcinoma and squamous cell non-small-cell lung cancer (84). Aside from direct transcriptional activation by MYC, MYC also indirectly influences MCT1 expression through repression of a micro RNA, miRNA29, which leads to elevated *MCT1* levels (85). miR29a,c is highly expressed in pancreatic β-cells and is involved in the

strict regulation of *MCT1* expression in these cells, as failure to suppress *MCT1* results in hyperinsulinemic hypoglycaemia (85).

5' AMP activated protein kinase (AMPK) activation is also postulated to play a role in the upregulation *MCT1* following exercise but the exact mechanisms behind this remain to be elucidated (86). The *MCT1* promoter also contains numerous nuclear factor of activated T-cells (NFAT) consensus sequences, which may have importance in the upregulation of *MCT1* during T-cell activation (74).

Conversely, the tumour suppressor, p53 attenuates the transcription of *MCT1* through a direct interaction with the *MCT1* promoter region (87). In support of this *TP53* mutant breast cancer patients show higher levels of MCT1 which is consistent with p53 having a negative effect on MCT1 expression (87). In the same study the authors show NFκB to have a positive effect on *MCT1* transcript levels

MCT4 but not *MCT1* transcription can be induced under hypoxic conditions mediated by the transcription factor HIF-1α (88). The promoter region of *SLC16A3* (MCT4) contains two hypoxia response elements (HREs) which are absent from both *SLC16A1* (MCT1) and *SLC16A7* (MCT2). This supports the physiological role of MCT4, for example the increased anaerobic capacity of white skeletal muscle following training is supported through a greater capacity for lactate export via this transporter (89).

Post-translational regulation

The membrane trafficking and functional activity of the MCTs is facilitated by chaperone proteins. A crucial factor for functional expression of MCT1 and MCT4 is the co-expression of the single-pass, membrane bound, glycoprotein, CD147. In respect to both MCT1 and 4, CD147 (basigin) is the preferred partner. In contrast, GP70 (embigin) is the preferred chaperone for MCT2 (90). Consequently CD147 and MCT1 can be seen to co-immunopreciptate and co-localize at the plasma membrane. In addition, co-transfection with CD147 was found to be necessary in order to observe plasma membrane expression of MCT1 in HeLa cells. The crucial role for CD147 can be demonstrated by interfering with the chaperone CD147 through siRNA approaches which inhibit lactate transport and reduce the expression of MCT1 and 4 (91, 92).

There is also evidence that MCT1 transporter activity is enhanced by the presence of carbonic anhydrases. Carbonic anhydrase II can physically associate with the C-terminal tail

of MCT1 and alter its transporter activity (93). In this model carbonic anhydrase II can transfer protons to and from available sites on CA to associated MCTs, effectively altering the local availability of the MCT co-substrate (93-95).

MCT1 expression has also been shown to be influenced by glutamine availability, being enhanced under glutamine deprivation, through an increase in transporter half-life (96). The exact mechanisms behind this phenomena and its physiological relevance have not been defined but Cardaci *et al*. suggest glutamine may enhance the ubiquitination of MCT1 (96).

1.5. MCT1 as a therapeutic target in cancer

1.5.1. Differential expression of MCTs in cancer

MCT1

Although MCT1 is widely expressed in normal tissues, MCT1 expression is increased in a number of human tumours which may reflect a greater dependency on MCT1 function. Several studies have highlighted associations between *MCT1* gene expression and outcome. For example, high *MCT1* expression correlated with worse overall survival in breast cancer patients with *TP53* mutations, and has also been reported to associate with hypoxic tumours as indicated by *CAIX* expression (87). A number of studies also show increased protein expression of MCT1 to have prognostic relevance. Increased levels of MCT1 have been identified in malignant breast and lung tissue with high expression correlating with high grade and poor prognosis (97, 98). Similarly, high MCT1 expression also correlates with worse prognosis in small cell lung cancer (SCLC) and clear cell renal carcinoma (CCRC) (99, 100). In CCRC high levels of MCT1 were shown to have a negative impact on progression-free survival which was significant independent of stage (100). Increased MCT1 and CD147 chaperone expression is also associated with decreased overall survival in urothelial carcinoma as is the co-expression of MCT1 and CD147 in gastrointestinal stromal tumours (101-103).

MCT4

MCT4 but not MCT1 is a target gene of HIF-1α consistent with its physiological role as a lactate export mechanism (88). Therefore, in areas of low pO_2 where glycolysis becomes the obligate source of ATP, MCT4 becomes upregulated to support increased glycolytic flux and lactate production. Consequently, MCT4 is found to be overexpressed in a number of cancers

and has been found to have prognostic significance. Whilst pancreatic ductal adenocarcinoma's (PDAC) generally have a dismal prognosis, high MCT4 expression has been associated with even worse overall survival particularly when expressed in both tumour and the associated stroma (104). MCT4 expression has also been shown to be elevated in CCRC where, elevated expression is a poor prognostic factor associated with increased metastasis and worse relapse-free survival (105). In this same study the authors also show CCRC cell lines to exhibit high *MCT4* gene expression and sensitivity to MCT4 knockdown. Immunohistochemical staining of head and neck cancer samples revealed the presence of epithelial regions of high MCT4 are associated with greatly reduced disease free-survival with such patients approximately 6 times as likely to relapse (106). In prostate cancer expression of MCT4 and CD147 has also been associated with cases which displayed biochemical recurrence (107). A number of these studies also show a correlation between MCT4 expression and a glycolytic phenotype (104, 106).

Owing to the increasing amounts of clinical and preclinical data that suggest MCT4 plays an important role in certain cancer types, specific inhibitors are reported to be under development (AstraZeneca) but no MCT4-specific compounds are currently available (32).

1.5.2. Lactate shuttle hypothesis

Tumours are metabolically heterogeneous and do not exist in isolation but interact with the surrounding stroma. A model has been proposed whereby hypoxic tumour cells generate lactate through anaerobic glycolysis which is transported out of the cell via MCT4. This 'waste-product' is then utilised as a metabolic substrate under more oxygenated conditions, imported through MCT1 or 2 into other tumour cells or the surrounding stroma (108). In this way, cells with greater access to oxygen within the tumour microenvironment spare glucose and instead oxidise lactate, benefitting hypoxic cells which must rely on non-oxidative metabolism. Similarly a model has been proposed that cancer cells can trigger metabolic changes in cancer associated fibroblasts causing them to release lactate and pyruvate into the tumour microenvironment (109). This relationship somewhat mirrors the situation that occurs between astrocytes and neurons (80).

1.5.3. MCT1 inhibition in *in vitro* and *in vivo* cancer models

2-Cyano-3-(4-hydroxyphenyl)-2-propenoic acid (CHC) and 4,4'-Diisothiocyano-2,2'-stilbenedisulfonic acid (DIDS) exhibit inhibitory activity towards monocarboxylate

transporters and have been utilised in earlier transporter studies to define substrate affinities and kinetics as well as more recently in *in vitro* and *in vivo* cancer studies (Table 2) (Figure 1-7) (108, 110, 111). In addition, a number of other compounds have been described as having MCT1 inhibitory activity including quercetin and 3-bromopyruvate. A caveat of these studies is the lack of specificity of these inhibitors to MCT1. CHC and DIDS have greater affinities towards mitochondrial pyruvate transporter and a chloride/bicarbonate transporter, respectively (112). Lonidamine, seldom used as an MCT1 inhibitor, has inhibitory activity against a number of targets and is also a more potent inhibitor of the mitochondrial pyruvate transporter than MCT1 (113). Quercetin has been used as an MCT inhibitor but inhibits a broad spectrum of kinases with similar potency (114). 3-bromopyruvate is now appreciated to act as a competitive substrate of MCT1 but also inhibits hexokinase (115). The lack of specificity of these compounds makes their use in experiments aimed at studying the effects of pharmacological MCT1 inhibition difficult to interpret.

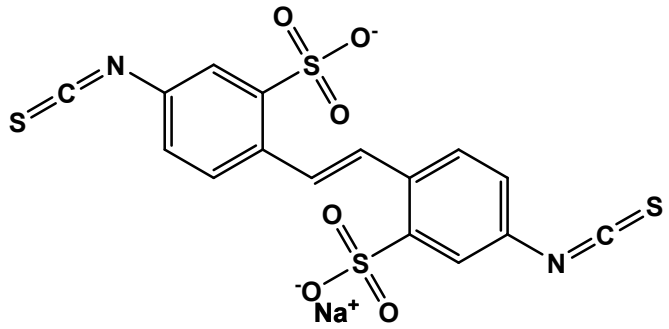

Disodium 4,4'-diisothiocyanatostilbene-2,2'-disulfonate (DIDS)

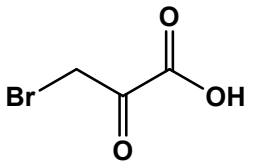

3-Bromopyruvate

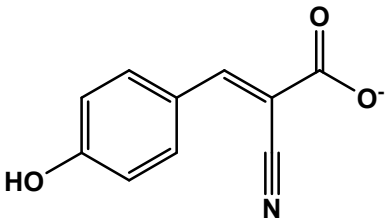

a-cyano-4-hydroxycinnamate (CHC)

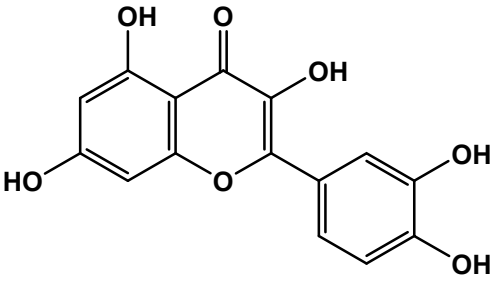

Quercetin

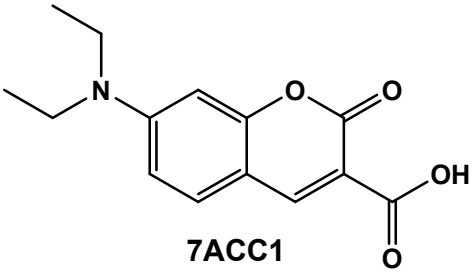

7ACC1

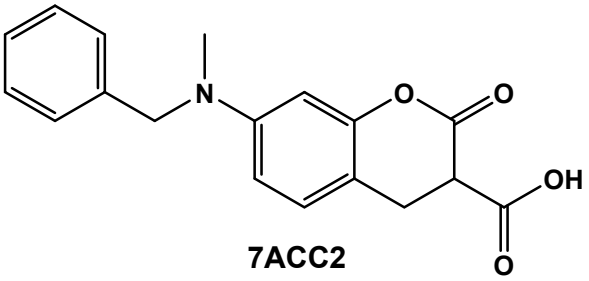

7ACC2

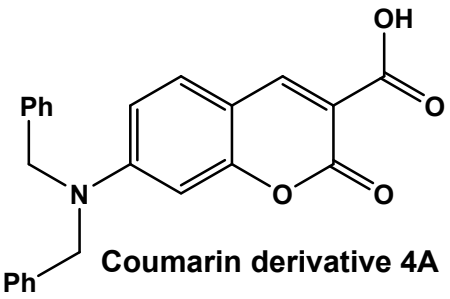

Coumarin derivative 4A

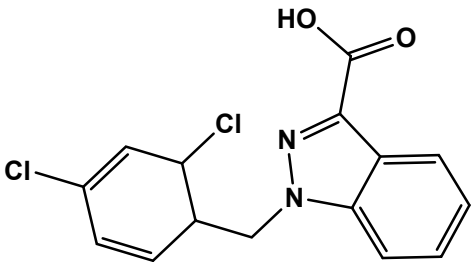

Lonidamine

Figure 1-7: Chemical structures of non-selective MCT1 inhibitors
Chemical structures recreated from Chemspider or using the following references; 7ACC (116), Coumarin derivate 4A (117)

More recently, preliminary work with MCT1 specific compounds such as AZD3965 and AR-C155858 have shown that they cause a rapid and sustained accumulation of lactate in cell lines that express MCT1 but not MCT4 (118, 119). Lactate accumulation appears to have no impact upon MCT1/4 protein expression. This accumulation of lactate coincides with significant anti-proliferative effects in some, but not all, tumour cell lines expressing only

MCT1. Favourable MCT1:MCT4 expression is therefore required but not sufficient for AZD3965 to have effects on cellular growth. Cell lines expressing both MCT1 and MCT4 possess intrinsic resistance to AZD3965 and related compounds due to the specificity of the compound to MCT1. This leaves MCT4 to provide a route for lactate efflux (92, 99). However, even where MCT1 inhibition causes an increase in intracellular lactate, the largely undetermined downstream events following this appear to be context dependent in terms of their effect on cellular proliferation (119). A working hypothesis to explain how lactate accumulation, following MCT1 inhibition, is antiproliferative has recently been proposed by Doherty *et al*. (84) The authors propose that lactate accumulation ultimately causes a feedback inhibition of glycolysis, impairing ATP generation. Inhibition of glycolysis has also been shown to be a downstream effect of MCT1 inhibition in other studies (92). Quantification of various glycolytic intermediates following MCT1 inhibition showed an increase in G6P and FBP and a decrease in 2 and 3-PG as well as pyruvate. They therefore postulate that accumulation of lactate inhibits the conversion of pyruvate to lactate via LDH, which in turn, decreases levels of available NAD^+, a cofactor required for GAPDH mediated generation of GBP. This idea of a "bottleneck" within the glycolytic pathway explains the accumulation of earlier stage intermediates but a lack of intermediates from the pay-off phase of glycolysis. Alternative MCT1 inhibitors such as 7ACC1 have been developed which also demonstrate improved selectivity. However, this family of compounds are distinct from AZD3965 in that they specifically inhibit MCT1 mediated lactate influx but not efflux (116).

Method of inhibition	Model MCT1/MCT4 expression (+/-)	Lactate	Cell growth and viability	*In vivo*	Other comments	Reference
3-BrPA (MCT substrate)	• Neuroblastoma: Kelly, SKN-BE-2C, • Breast adenocarcinoma: MDA-MB-231.	• Extracellular lactate reduced by 40-50% in high *MYCN/C-MYC* cells (Kelly, BE-2C) (6h 50 µM).	• Growth inhibition (40-60%) in high *MYC* expressing cells. (MTT assay 72h 50 µM.)	• Daily 2.5 $mg.kg^{-1}$ I.P (14-days treatment) • Reduced tumour weight in Kelly xenografts (50%) • Reduced tumour size in BL (*Eμ-Myc;Arf− / −)* allografts	• Substantiates MCT4 as a resistance factor • Kaplan-Meier analysis of neuroblastoma patient data reveals high MCT1 is associated with worse survival. • Combination with L-γ-glutamyl-p-nitroanilide (ASCT2 inhibitor) induced cell death	*Gan 2016* (85)

Method of inhibition	Model MCT1/MCT4 expression (+/-)	Lactate	Cell growth and viability	*In vivo*	Other comments	Reference
7ACC1/2	• Cervical squamous cell carcinoma: SiHa (+/+) • Colorectal cancer: HCT-116 (+/+) • Acute myeloid leukaemia: HL60 (+/-) • Breast adenocarcinoma MCF-7 (+/-,) MDA-MB231 (-/+) • Bladder cancer: UM-UC-3 (-/-)	• Lactate uptake reduced ~50% (SiHa) • No effect on lactate release • 24h ≤1 µM.	• 80% growth inhibition SiHa. • No effect in (+/-) or (-/-) cells. • MTT/Presto blue assay or cell counts 72h 10 µM	• Daily 3 $mg.kg^{-1}$ I.P (12-days treatment) • Range of growth inhibitory activity (30-75%) (MCF-7)> (SiHa)> (HCT-116) • No effects observed in UM-UC-3 (No MCT1 or 4)	• 7ACC1/2 specifically target lactate influx. • ACC1/2 potentiates the effect of cisplatin and 3-BrPA *in vivo*	*Draoui 2014* (116)
CHC	• Cervical squamous cell carcinoma: SiHa (+/?) • Head and neck squamous cell carcinoma $FaDu_{dd}$ (+/?)	Bioluminescent detection of lactate showed no change *in vivo* after a single dose (1.5, 4h 1 mM/kg) or daily treatment across 4-days	*In vivo* only study	No increase in necrosis.		*Busk 2011* (120)

Method of inhibition	Model MCT1/MCT4 expression (+/-)	Lactate	Cell growth and viability	*In vivo*	Other comments	Reference
CHC	Colorectal cancer: HCT-15 (+/+), RKO (+/+),	Extracellular lactate decreased by 50% (24h IC_{50} dose for 10h) HCT-15 only	• Cell number decreased - 70% (24h IC_{50} dose SRB assay). • Decreased cell viability - 25% (24h IC_{50} dose Annexin V/PI).	N/A	• Effects much weaker with siRNA possibly reflecting off-target effects of CHC. • Mildly potentiated response in combination with 5-FU (CI value 0.4)	*Amorim 2015* (121)
CHC	Breast cancer: MDA-MB-468 (+/+) MDAMB-231 (-/+) Hs578T (+/+) BT-20 (+/-) MCF-7/AZ (+/-) and SkBr3 (+/+)	50% inhibition lactate production (24h IC_{50}) most strongly	Proliferation (BrdU) decreased MDA-MB-488 (60%), MCF-7/AZ (55%), SkBr3 (50%), Hs578T (50%) (24h 1/2-IC_{50})	N/A	• CHC- Growth inhibition observed in absence of altered glucose uptake/lactate production. • MCT1 inhibition via CHC also reduced migration	*Morais-Santos* 2014 (122)
CHC	• Cervical squamous cell carcinoma: SiHa (+/-) • Colon adenocarcinoma: WiDr • Lewis lung carcinoma (LLc)	• Vehicle treated cells decrease extracellular lactate in culture. • Extracellular lactate is unaltered by $MCT1_i$ over 6 days (5 mM).	Cell death observed under glucose deprivation (siRNA)	• Growth delay (LLc mouse carcinoma, WiDr cells). Daily 25 µM I.P (Until endpoint).		*Sonveaux 2008* (108)

Method of inhibition	Model MCT1/MCT4 expression (+/-)	Lactate	Cell growth and viability	*In vivo*	Other comments	Reference
CHC	Osteosarcoma: U2OS (+/?), MG63, SAOS2 and MNNG/HOS (+/?)	• N/A	• ~50% inhibition of cell proliferation (5-day MTT assay)	• ~50% reduction in tumour volume in two SC xenografts (Daily 25 µM I.P until endpoint) • Potentiates efficacy of doxorubicin *in vivo*	• shMCT1/CHC inhibits migration and invasion *in vitro* • *In vitro* and *in vivo* effects potentiated by doxorubicin • Overall patient survival significantly associated with MCT1 protein expression (MCT1-/+ = 46/64 months)	*Zhao 2014* (123)
CHC	Glioblastoma: U251 (+/+), SW1088 (+/-) and others	• ~25% decrease in lactate production (10 mM ≤24h U251 cells)	Proliferation (BrdU) decreased by 80% (≤24h 10 mM U251 cells)	• Reduced U251 tumour size (31%) and vascularisation (22%) in a chicken Chorioallantoic Membrane assay (72h 5mM).	MCT1 inhibition via CHC also reduced migration	*Miranda-Gonzalez* (124)

Method of inhibition	Model MCT1/MCT4 expression (+/-)	Lactate	Cell growth and viability	*In vivo*	Other comments	Reference
CHC (ACCA)	Glioblastoma cells; U87-MG, U251-MG	*In vivo* – intracellular lactate mildly reduced (22%) (40 mM)	*In vivo* only study	Increased survival 48% (20 mM), 224% (40 mM). (14-day 40 mM delivery through osmotic pump)	• Orthotopic glioblastoma model. Dosing administered by convection enhanced delivery to tumour bed. • Metabolite concentrations taken from non-tumour bearing mice sections	*Colen 2011* (110)
CHC	Multiple myeloma cell lines (+/+)	Reduced extracellular lactate 50-95% (3h ≥10 mM)	50-100% growth inhibition (24h WST-assay ≥10 mM)	N/A	Also shows reduced intracellular pH with AR-C155858	*Hanson 2015 (125)*
DIDS/ Quercetin	Lung adenocarcinoma: A110L (+/+)	N/A	• DIDS GI_{50} > 50µM • Quercetin GI_{50} = 50µM • (72h WST assay)	N/A		*Izumi 2011* (126)
Lonidamine	Neuroblastoma: IMR-32; B, Sk-N-SH; C, NGP.	N/A	25% (IMR-32) 75% (NGP) (160 µM 48h MTS assay)	N/A		*Fang 2006 (127)*

Method of inhibition	Model MCT1/MCT4 expression (+/-)	Lactate	Cell growth and viability	*In vivo*	Other comments	Reference
shRNA	• Cervical squamous cell carcinoma: SiHa • Colon adenocarcinoma: WiDr • Cervical carcinoma: HeLa • Head and neck squamous cell carcinoma: FaDu	• Oxidative cells (SiHa, FaDu and HeLa) increase HIF-1α levels under lactate rich normoxic conditions which can be inhibited by MCT1 shRNA.	N/A	$MCT1_i$ completely inhibits lactate-fuelled tumour growth (SiHa matrigel plugs 30 mM lactate).	• No effect on tumour growth without the addition of exogenous lactate. • Suggests influx of lactate via MCT1 is an important fuel for oxidative tumours.	*De Saedeleer 2012* (128)
shRNA	• Colorectal adenocarcinoma; WiDr (+/+) • Breast adenocarcinoma; MDA-MB231 (+/+)	MCT1 shRNA had no effect on extracellular lactate (WiDr)	MCT1 shRNA had no effect on cell growth (WiDr)	MCT4 shRNA lowers tumour volume compared to MCT1 shRNA matrigel plugs *in vivo* (WiDr and MDA-MB231)	• This +/+ model is sensitive to MCT4 knockdown but not MCT1 knockdown. • Suggests WiDr cells are dependent on MCT4 for lactate efflux.	*Vegran 2011* (129)

Method of inhibition	Model MCT1/MCT4 expression (+/-)	Lactate	Cell growth and viability	*In vivo*	Other comments	Reference
siRNA	Lung adenocarcinoma: A110L (+/+)	• Basal extracellular lactate did not correlate with MCT1 expression • Knock down did not alter extracellular or intracellular lactate	50% growth inhibition siMCT1 (72h WST assay)	N/A	• 90% decrease in invasion. • siRNAs with similar knockdown have differing effects on cell proliferation and invasion indicating potential off target effects.	*Izumi 2011* (126)

Table 2: Preclinical studies on the effects of non-specific or genetic MCT1 inhibition in cancer
Abbreviations used: CHC (α-Cyano-4-hydroxycinnamic acid), 3BrPa (3-Bromopyruvic acid), 7ACC (7-aminocarboxycoumarin and derivatives) Where available the protein expression of MCT1 and 4 are indicated (+/-). Concentrations of intracellular and extracellular lactate were determined by biochemical assay unless otherwise stated.

Method of inhibition	Model MCT1/MCT4 expression (+/-)	Lactate	Cell growth and viability	*In vivo*	Other comments	Reference
AR-C122982 **AR-C155858**	• Burkitt lymphoma: Raji (+/-) • Breast adenocarcinoma: MCF7 (+/-)	• Raji: Rapid (T_{max} 4h) increase (~6-fold) in intracellular lactate • Raji: ~3-fold in intracellular lactate (MS). • MCF7: 90% inhibition of lactate transport (^{14}C lactate) • 100 nM $MCT1_i$	• Complete growth inhibition (cell counts 100 nM) • Raji GI_{50} AR-C155858 (28 nM), AR-C122982 (5 nM) (72h, MTT assay). • Viability: 72h-100%, 120h-50% (Trypan blue, 5 nM)	• 30% increase in median survival (IV Raji) • Reduced growth in tumour volume (SC T47D) • Daily 30 $mg.kg^{-1}$ I.P	• Demonstrates MCT1 to be transcriptional target for c-MYC • *In vivo* effects potentiated by metformin oral dosing (5 $mg.ml^{-1}$)	*Doherty 2014* (85)
AR-C155858	Pancreatic adenocarcinoma: PL45 (+/+) MIA PaCa-2 (+/+) Capan-2 (+/+)	N/A	• Cell number decreased 40-50% in comparison to MCT4 knock down alone (72h ATP 100 nM)	N/A	• Substantiates MCT4 as a resistance factor. $MCT1_i$ was not effective in MCT4 expressing cells.	*Baek 2014* (104)
AR-C155858	Breast cancer; MDA-MB-231, MCF7	N/A	Upto 50% reduction in mamosphere formation (120h ≤2 μM)	N/A		*Lamb 2016* (130)

Method of inhibition	Model MCT1/MCT4 expression (+/-)	Lactate	Cell growth and viability	*In vivo*	Other comments	Reference
AR-C155858	Rat erythrocytes and *Xenopus* oocytes	• ^{14}C lactate maximal inhibition observed after 45min (100 nM)	N/A	N/A	• MCT1/MCT4 co-expression abrogates effects of MCT1i • AR-C155858 inhibits lactate transport (14C) via MCT1 MCT2 but not MCT4.	*Ovens* (131)
AR-C155858 (*in vitro*) AZD3965 (*in vivo*)	Colon adenocarcinoma: LS174T (+/+) derived cell lines. CD147 or MCT4 knock-outs (Zinc-finger Nuclease)	• 4-fold increase in intracellular lactate (AR-C155858 + MCT4 k.o) (300 nM ≤6h)	• 66% inhibition of growth in (AR-C155858 + MCT4 k.o). (120h, cell counts, 300 nM) • Combination with phenformin induced cell death	Reduction in tumour volume v.s. control. AZD3965 (BID 100 $mg.kg^{-1}$ oral) +/- phenformin. • WT: 50% / 25% • MCT4 k.o: 75% / 84%	• MCT4 knock out required for sensitivity to MCT1i • *In vitro* effects were enhanced under hypoxic conditions	*Marchiq 2014* (132)
AZD3965	Small cell lung cancer: DMS114 and H526.	• Intracellular lactate increased in 2/3 cell lines ~3-5-fold (100 nM). • Reduced 50% uptake of ^{14}C lactate (24h 100nM) • Tumour lactate increased by 2-fold *in vivo*	N/A	• Increased time to reach endpoint (tumour size) by 50% (BID 100 $mg.kg^{-1}$ oral) • Increased MCT4 staining in xenografts (IHC)	Potentiated response to radiation *in vivo*	*Bola 2014* (133)

Method of inhibition	Model MCT1/MCT4 expression (+/-)	Lactate	Cell growth and viability	*In vivo*	Other comments	Reference
AZD3965	Small cell lung cancer: (normoxic conditions); COR-L103 (+/-), DMS114 (+/-), DMS79 (-/+), NCI-H1048 (+/-).	• Intracellular lactate increased by 2-fold *in vitro* (72h 8 nM) • Intracellular lactate increased *in vivo* ~50%+ (daily 100 $mg.kg^{-1}$ oral)	Normoxia/hypoxia COR-L103: 40/90% NCI-H1048: 40/40% DMS114: 0/20% DMS79: 0/0% (72h SRB/resazurin assay ≤10 µM)	~30% reduction in tumour volume after 21 days (COR-L103). (BID 100 $mg.kg^{-1}$ oral)	• MCT4 siRNA increases sensitivity to AZD3965 in DMS114 and DMS79 (resistant lines). • High (>median) MCT1 expression score was associated with worse survival in patient (IHC TMA)	*Polanski 2014* (134)
AZD3965	• Prostate cancer: DU145 (+/+) • Breast cancer: HCC1806 (+/+) • Burkitt Lymphoma: Raji (+/-)	• DU145/Raji 50%/90% reduction in lactate uptake (^{14}C) was observed (1h 100 µM)	MCT1 shRNA has no effect on cell confluency (72h IncuCyte)	N/A		*Gray 2016* (135)

Method of inhibition	Model MCT1/MCT4 expression (+/-)	Lactate	Cell growth and viability	*In vivo*	Other comments	Reference
AZD3965	Breast cancer; HS578T, SUM149PT, SUM159PT	No consistent effect on lactate export or influx (^{13}C-lactate) (4-24h 250 µM)	• 40-50% reduction in proliferation (250 nM, 120h cell count) • Additive effects in combination with biguanides	• Reduced tumour growth • AZD3965 (BID 100 mg.kg^{-1} oral) treated xenografts at day 0 and 7 were comparable in size	• Only report of *in vivo* efficacy in MCT4+ model. • In this setting, MCT4+ breast cancer, MCT1i prevents pyruvate export, having growth inhibitory activity.	*Hong 2016* (98)

Table 3: Preclinical studies AZD3965 and structurally related MCT1 specific inhibitors
Where available the protein expression of MCT1 and 4 are indicated (+/-). Concentrations of intracellular and extracellular lactate were determined by biochemical assay unless otherwise stated.

1.6. AZD3965: A potent, selective orally-bioavailable MCT1 inhibitor

1.6.1. Development

AZD3965 has been developed by AstraZeneca as an orally bioavailable MCT1 specific inhibitor. The compound was initially identified in a high throughput screen which identified structurally related compounds to have immunosuppressive activity through the inhibition of lactate efflux in activated T-cells (75). T-cells reprogram their metabolic profile on recognition of a foreign antigen switching from OXPHOS and fatty acid oxidation to a highly glycolytic profile to support rapid proliferation (76, 136). Subsequently these compounds were identified to target MCT1 and possess anti-neoplastic properties in a range of tumour types (118). Further development led to the production of lead compound, AZD3965 (137).

AZD3965 is currently undergoing phase I clinical evaluation in Newcastle and London (NCT01791595) for a range of advanced solid tumours and lymphoma. Currently within the dose escalation phase, the aim is to establish a maximum tolerated dose in a wider cohort of patients before expansion into a patient population predicted to be sensitive to MCT1 inhibition.

1.6.2. Selectivity

AZD3965 has been previously shown to be selective towards MCT1 with a binding affinity of 1.5 nM equating to a 6-fold greater affinity relative to the most closely related MCT family member, MCT2. AZD3965 has no inhibitory activity towards MCT4 or MCT3 at 10 µM (133, 138). Recent studies using site directed mutagenesis and modelling approaches have proposed a number of residues responsible for the selectivity of AR-C155858 towards MCT1 over MCT4, which appear to indicate a two-stage binding model (83). However, this cannot be confirmed due to the lack of X-ray crystal structures for MCT1 or MCT4.

Selectivity of AZD3965 comes not only from the relative potency of the compound towards MCT1 but also the increased reliance of cancer cells on glycolysis and therefore lactate transport. Whilst certain non-malignant cells also display a glycolytic phenotype, as discussed earlier, the majority of these co-express alternative MCT isoforms, particularly MCT4, and so have a compensatory mechanism for lactate transport. Therefore, AZD3965 affords the

opportunity to specifically target cancer cell metabolism in cells reliant on MCT1 for lactate transport.

1.6.3. Structure

The structure of AZD3965, (S)-5-(4-hydroxy-4-methylisoxazolidine-2-carbonyl)-1-isopropyl-3-methyl-6-((3-methyl-5-(trifluoromethyl)-1H-pyrazol-4-yl)methyl)thieno[2,3-d]pyrimidine-2,4(1H,3H)-dione , has been previously published (99). It is structurally related to earlier MCT1 inhibitors such as AR-C155858 sharing a thiopurine core (Figure 1-8).

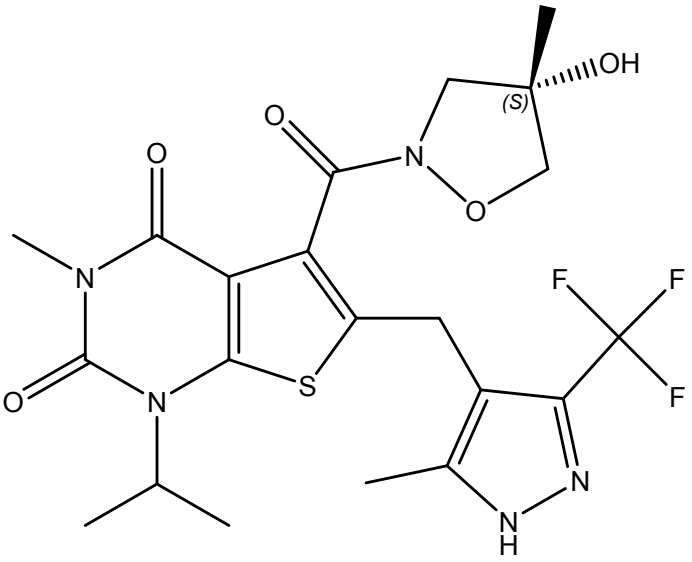

AZD3965

(*S*)-5-(4-hydroxy-4-methylisoxazolidine-2-carbonyl)-1-isopropyl-3-methyl-6-((5-methyl-3-(trifluoromethyl)-1*H*-pyrazol-4-yl)methyl)thieno[2,3-*d*]pyrimidine-2,4(1*H*,3*H*)-dione

Molecular Weight: 515.51

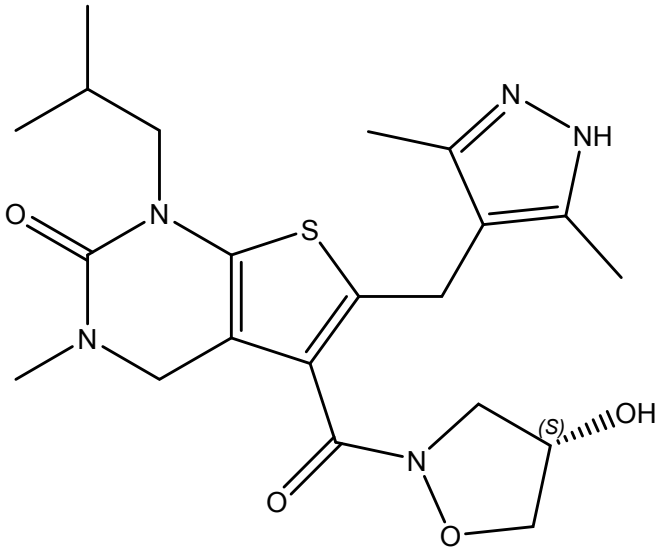

AR-C155858

(*S*)-6-((3,5-dimethyl-1*H*-pyrazol-4-yl)methyl)-5-(4-hydroxyisoxazolidine-2-carbonyl)-1-isobutyl-3-methyl-3,4-dihydrothieno[2,3-*d*]pyrimidin-2(1*H*)-one

Molecular Weight: 447.55

Figure 1-8: Chemical structure of selective MCT1 inhibitors AZD3965 and AR-C155858

1.6.4. Mode of binding

Whilst the mode of binding for AZD3965 has not specifically been determined, studies using the structurally related compound, AR-C155858 reveal that it binds on the intracellular face of the transporter when in an inward-open conformation between transmembrane helices 7-10 (83, 131). This initial binding induces a conformational change allowing access to a binding site further into the binding pocket. AR-C155858 also binds to a number of key residues implicated in the proposed translocation cycle of MCT1, namely K38, R306 and D302 (66, 83). Furthermore, Nancolas *et al.*, have reported on the key residues which are crucial to the binding of AR-C155858 and its selectivity to MCT1 over MCT4 identifying N147, R306 and S364 as the key residues dictating selectivity. This information could potentially aid in the development of MCT4 specific inhibitors (83).

1.6.5. Safety

The safety of AZD3965 is currently under investigation in humans however it has been shown to be well-tolerated in mouse models (99, 133). Twice-daily oral dosing of 100 $mg.kg^{-1}$ AZD3965 has been shown to be well-tolerated in mice for 21 days, and is associated with increased tumour lactate confirming it as a pharmacologically active dose (99).

Despite being comparatively well tolerated, based on the physiological role of MCT1 a number of on-target toxicities could be anticipated. Genetic mutations in the *MCT1* gene, associated with systemically reduced MCT1 function, are linked to severe exercise induced muscle pain, reduced red blood cell lactate transport and of greater concern, greater risk to ketoacidosis (Online Mendelian inheritance in man OMIM; 245340, 616095) (139, 140). Furthermore, since MCT1 inhibition has been shown to reduce T-cell activation AZD3965 may also have immunosuppressive activity. MCT1 inhibition may also be predicted to affect male fertility as MCT1 plays an important role in spermatogenesis where sertoili cells supply lactate to germ cells as an energy substrate. In addition, the establishment of a therapeutic window allowing sufficient MCT1 inhibition whilst limiting inhibition of MCT3 will be necessary to avoid ocular toxicities due to inhibition of MCT3 in the retinal pigment epithelium.

1.7. Project objectives

Inhibitors of MCT1 exemplify an important new class of cancer therapeutics that are designed to exploit defects in tumour cell metabolism. Such inhibitors are proposed to have selectivity for tumours that have a specific dependency on MCT1 alone for lactate efflux *versus* normal tissues that have a broader MCT isoform expression or are more metabolically oxidative. As with all targeted agents, the optimal development of MCT1 inhibitors will require the co-development of predictive pharmacodynamic biomarkers, and appropriate patient selection. The aim of the project will be to inform patient selection as to where an MCT1 inhibitor may be most efficacious using both *in vitro* and *in vivo* methods.

Specifically this thesis will aim to;

- Use both gene and protein expression data to identify disease areas of potential interest based on a low MCT4 phenotype.
- Define the anti-tumour activity of AZD3965 in cell line models *in vitro*.
- Describe the metabolic consequences of MCT1 inhibition downstream of lactate accumulation.
- Investigate acquired resistance to AZD3965
- Investigate the efficacy and metabolic consequences of MCT1 inhibition *in vivo.*
- Identify combination approaches to enhance the efficacy of AZD3965 and also explore these *in vivo*.

Chapter 2. Materials and methods

2.1. Preparation of AZD3965 and BAY 87-2243

The MCT1 inhibitor, AZD3965, was supplied by AstraZeneca. AZD3965 was dissolved in dimethyl sulfoxide (DMSO) to give a stock solution of 10 mM and stored at –20°C for *in vitro* studies. For *in vivo* administration of AZD3965 an oral formulation (10 $mg.ml^{-1}$) was prepared as an aqueous solution of 0.5% hydroxypropylmethylcellulose (HPMC), 0.1% Tween 80 (Sigma, St Louis, USA) (99). BAY 87-2243 (Selleckchem) was prepared in ethanol to give stock solutions of 1 mM for *in vitro* use. BAY 87-2243 (0.9 $mg.ml^{-1}$) was prepared as a formulation of ethanol, solutol (Kolliphor® HS 15) and water (10:40:50) for oral *in vivo* administration. The sources of all other reagents and materials are detailed within the relevant experimental methods.

2.2. Cell culture

Cells were maintained at 37°C, 5% CO_2 and 100% humidity in a SANYO CO_2 incubator (Panasonic, NV, Netherlands). Cells were handled under sterile conditions using a class II BioMat2 laminar flow hood (Biomat2, MedAir® Inc. Boston, USA). Unless expressly stated all cell lines were cultured in Roswell Park Memorial Institute (RPMI) 1640 (Sigma) supplemented with 10% v/v foetal bovine serum (FBS) (Gibco, Paisley, UK) in the absence of antibiotics. Sterile cell culture plastic wear was supplied by Corning (NY, USA). The absence of mycoplasma contamination was confirmed approximately every 8 weeks (Lonza, Basel, Switzerland). Cell lines were authenticated at the end of the study by short tandem repeat DNA analysis (NewGene, Newcastle, UK). A cell line identity threshold was set at 85% allelic match between the reference and tested samples.

Name	Source	Cell origin	Patient details	Subclassification	c-MYC translocation	Reference
BL41	DSMZ	Tumour material	Primary diagnosis - M (8)	N/A	t(8;14)	(141)
Daudi	DSMZ	Tumour material	Primary diagnosis - M (16)	Endemic BL	t(8;14)	(141)
CA46	DSMZ	Ascites fluid	M	Sporadic BL	t(8;14)	(141)
Raji	DSMZ	Tumour material	M (11)	Endemic BL	t(8;14)	(141)
Ramos	DSMZ	Tumour material	M (3)	Sporadic BL	t(8;14)	(141)
BJAB	DSMZ	Tumour material	F (5)	GCB/?	t(2;8)	(142)
Farage	ATCC	Lymph node biopsy	Primary diagnosis - F (70)	GCB/BCR	None reported	(143, 144)
OCILY18	DSMZ	Pleural fluid	Relapse - M (56)	GCB/BCR	t(8;14;18)	(145)
Pfeiffer	ATCC	-	M (adult)	GCB/OXPHOS	t(8;14)	(146)
Toledo	ATCC	Peripheral blood leukocytes	Relapse - F (adult)	GCB/OXPHOS	?	(146)
RIVA	Prof. Alison Banham	Peripheral blood leukocytes	Relapse - F (57)	ABC/?	t(4;8)	(147)

Table 4: Cell panel details
Source of cell lines used in our study along information regarding their origin including patient sex, age and disease state (diagnosis or relapse) are indicated. Disease subtypes for Burkitt lymphoma (Sporadic/endemic) and Diffuse large B-cell lymphoma cell lines (COO: GCB/ABC, CCC: BCR/OXPHOS) and presence of MYC translocations are also listed where available.

2.2.1. Subculturing cells

Cells were passaged every 2-3 days or when at 80% confluency under sterile conditions within a laminar flow hood. All cell lines used were grown in suspension culture and therefore, did not require detachment for passaging. Cell counts were performed using a haemocytometer and viability assessed by trypan blue exclusion (0.4% w/v, Sigma) and seeded into new flasks at a density of approximately 2-3 x 10^5 cells ml^{-1}.

2.2.2. Cryopreservation

To generate cell stocks sub-confluent cells were centrifuged at 500 x g and resuspended in cryopreservant containing 80% complete growth media, 10% DMSO (v/v) and 10% FBS (v/v) to a density of 5 x 10^6 cells $ml^{-1.}$ Cell stocks were stored as 1 ml aliquots in cryogenic vials (NUNC™, New York, USA) and stored at -80°C for a day before transferring to liquid nitrogen.

2.3. Protein extraction and quantitation

2.3.1. Protein extraction

Cell pellets were collected and washed in phosphate-buffered saline (PBS) before lysing in Radio Immunoprecipitation Assay (RIPA) buffer (Sigma) including Halt Protease Inhibitor Cocktail (Sigma). Lysed samples at were centrifuged 14,000 x g for 10 minutes at 4°C to remove cellular debris. Supernatants were collected and stored at -80°C ready for downstream applications.

2.3.2. Protein quantitation – BCA protein assay

Background principles

Protein quantification for various downstream applications was performed using the bicinchoninic acid (BCA) assay (Thermo Scientific, Northumberland, UK). This reaction takes place in two steps; the biuret reaction where cupric ions (Cu^{2+}) (Reagent B) chelate with peptides longer than two amino acids under alkaline conditions to produce cuprous ions (Cu^{1+}), followed by the chelation of the cuprous ions with BCA (Reagent A) to produce a purple coloured complex. The absorbance of this complex at 562 nm is proportional to the protein concentration of the sample.

Assay

Bovine serum albumin (BSA) standards were prepared (0, 0.125, 0.25, 0.5, 1 and 2 mg ml^{-1}) PBS and an aliquot (20 µl) of each standard or unknown sample were plated in duplicate in 96-well plates before the addition of 200 µl working reagent per well. Where protein concentrations were above the linear range of the assay i.e.> 2 $mg.ml^{-1}$, samples were diluted in PBS. Working reagent was prepared by adding combining reagent A and reagent B in a 50:1 ratio. Samples were then incubated at 37°C for 25 minutes before measuring absorbance values at 570 nm using FLUOstar Omega (BMG Labtech) plate reader.

Data analysis

Mean absorbance values attributed to standard samples with known protein concentrations were used to construct a standard curve, from which to calculate protein concentration of unknown samples through linear regression analysis. R^2 values were typically ≥ 0.99. These were then corrected for initial dilutions made to samples in order to give the final protein concentration expressed as $mg.ml^{-1}$.

2.4. SDS-Page and Western Blot

2.4.1. Sodium dodecyl sulfate polyacrylamide gel electrophoresis (SDS-PAGE)

Samples were prepared in 4x XT sample buffer (Bio-Rad, Hercules, USA) and dH_2O to produce a 2.5 $µg.µl^{-1}$ protein solution. Samples were denatured through incubation at 98°C for 2 minutes.

2.4.2. Western Blot and ECL detection

Protein samples (50 µg) were loaded into wells of a 4-20% Criterion™ TGX™ (Tris-Glcyine eXtended) pre-cast gel (Bio-Rad) and separated at 100V in 1x running buffer. PrecisionPlus™ pre-stained protein standards (Bio-Rad) were used in order to estimate the molecular weight of the protein of interest following detection. Proteins separated by size were then transferred to a Hybond-C nitrocellulose membrane (GE Healthcare, Buckinghamshire, UK) using 1x Novex® Tris-Glycine Transfer Buffer (Thermo Scientific) solution with 4% (v/v) methanol at 100V for 1 hour. The transfer assembly was arranged as shown in Figure 2-1,

with the gel sandwiched between supports and filter papers with the nitrocellulose membrane laying on top of the gel closest to the cathode.

After protein transfer, the membrane was blocked in 5% (w/v) skimmed milk powder in TBS-T for 1 hour at room temperature. Following this the membrane was incubated overnight at 4°C with the appropriate primary antibody diluted in 5% (w/v) milk in TBS-T, working concentrations of which are indicated in Table 5.

Protein	Dilution	Raised in	Manufacture	Product
MCT1	1:200	Goat	Santa Cruz	sc-14916
MCT4	1:1000	Rabbit	Santa Cruz	sc-50329
CD147	1:200	Mouse	Ancell	376-820
c-MYC	1:1000	Rabbit	Abcam	ab32072
PARP	1:1000	Rabbit	Santa Cruz	sc-7150
β-actin	1:5000	Mouse	Abcam	ab-8227

Table 5: Primary antibodies used for western blotting
All primary antibodies were prepared in 5% milk TBS-T and incubations were performed overnight at 4°C.

The membrane was then thoroughly washed in TBS-T to remove unbound primary antibody and less stringent non-specific binding to proteins other than the target protein of interest. Horseradish peroxidase conjugated secondary antibodies were incubated for 1 hour at room temperature before thorough washing in TBS-T. Protein expression was then estimated using chemiluminescence substrate and exposure to X-ray film (Kodak).

Where necessary the membrane was stripped and reprobed using mild stripping buffer (1.5% glycine (w/v), 0.1% SDS (w/v), 1% Tween20 (v/v) pH 2.2). Here membranes were incubated in stripping buffer 10 minutes before repeating this step in fresh buffer. Duplicate 10 minute wash steps in PBS followed by 5 minute washes in TBS were then performed to ready the membrane for the blocking stage.

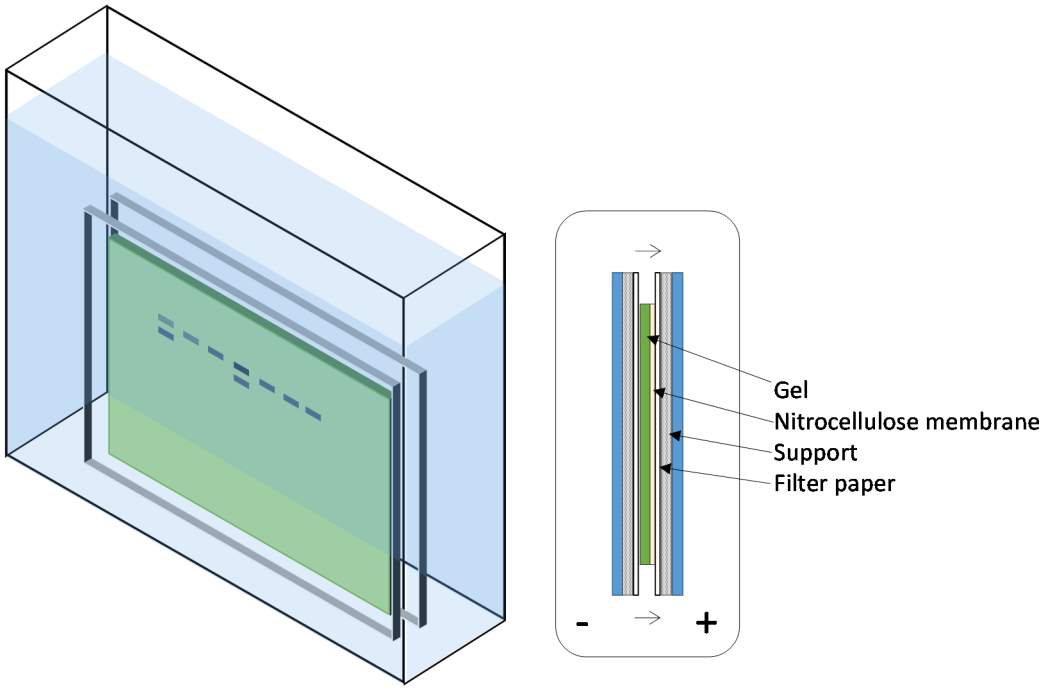

Figure 2-1: Western blotting procedure
Proteins carry a net negative charge and so transfer towards the positively charged anode.

2.5. *In vitro* and *ex vivo* lactate quantification

2.5.1. Background principles

The intracellular concentration of L-Lactate was measured using a commercially available biochemical assay (Trinity Biotech, Co Wicklow, Ireland). The principle of the assay is summarised in Figure 2-2. Lactate oxidase converts L-lactate present in the sample is to H_2O_2 and pyruvate. H_2O_2 generated then catalyses the conversion of a chromogen dye precursor by horseradish peroxidase yielding a colour change with maximal absorbance at 540 nm.

2.5.2. *In vitro* sample preparation

Cells were seeded at a density of $5x10^4$ ml^{-1} in 6-well plates (Corning) and incubated for 24 hours. Cells were then dosed with AZD3965 (10-1000 nM) or a DMSO (0.01%) control solution and re-incubated for a further 0.5-72 hours. Suspension cells were centrifuged at 500 x g for 5 minutes, the supernatant aspirated and pellets washed in 5 ml of 4°C PBS, followed by re-centrifugation and aspiration, a procedure which was repeated a total of 3 times. Cell pellets were then lysed in 100 µl of RIPA buffer (Thermo Scientific). Preparation was similar for adherent cell types however, washing steps were performed with cells adhered to the well surface before lysing in 120 µl of RIPA buffer. Cellular lysates were then

centrifuged at 10,000 x g for 30 minutes at 4°C, and supernatant collected and either stored at -20°C or assayed immediately.

2.5.3. *Ex vivo* sample preparation

A suspension of approximately 10^7 CA46 or Raji cells were implanted subcutaneously in NSG mice on the right flank and allowed to reach an appropriate size (2-4 weeks). Mice were given a single dose of AZD3965 (100 $mg.kg^{-1}$) or a 0.5% control solution by oral gavage before being humanely killed. Tumours were excised and snap-frozen in liquid nitrogen immediately following cervical dislocation. Tumour samples were then stored at -80°C until homogenisation. Samples were weighed and then homogenised in RIPA buffer (1000 µl/100 mg) using a handheld tissue homogeniser. Samples were briefly centrifuged at 500 x g for 1 minute to remove frothing. Samples were then rested on ice for 30 minutes to allow for complete cell lysis to take place before centrifugation at 12,000 x g for 10 minutes at 4°C. Supernatants were collected and assayed immediately or stored at -20°C.

2.5.4. Assay

L-lactate standards of different concentrations (0.0025, 0.0125, 0.025, 0.05, 0.1, 0.2 and 0.4 $\mu g.\mu l^{-1}$) were prepared periodically in PBS and stored at -20°C. 20 µl of standard solution or unknown sample were plated in duplicate in 96-well plates before the addition of 200 µl working reagent per well. Working reagent was prepared by adding 10 ml deionised H_2O (dH_2O) per bottle of lactate reagent. Samples were then incubated at room temperature for 15 minutes with protection from ambient light before measuring absorbance values at 540 nm using a FLUOstar Omega (BMG Labtech, Germany) plate reader installed with the Omega data analysis software.

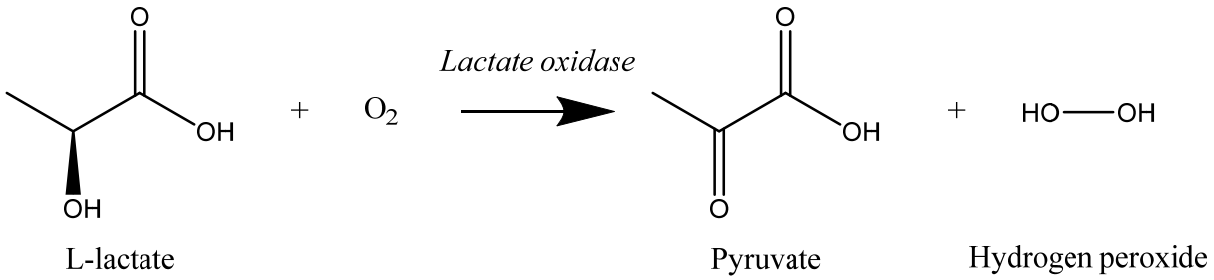

Figure 2-2: Principle of biochemical assay used to quantitate intracellular lactate

2.5.5. Data analysis

Lactate concentrations of unknown samples were derived through linear regression using a set of lactate standards with defined lactate concentrations (0.0025-0.4 µg.µl^{-1}) and making adjustments for any initial samples dilutions. R^2 values were typically ≥0.99. Lactate concentrations were normalised to the protein content of each sample as determined by BCA assay.

$$\frac{\text{Lactate (µg.µl}^{-1})}{\text{Protein (µg.µl}^{-1})} \times 1000 = \text{Lactate [µg.(mg protein)}^{-1}]$$

2.6. Cell viability assays

2.6.1. XTT assay

Background principles

Cell metabolic activity was assessed using the reduction of the tetrazolium dye, XTT (sodium 3'-[1-(phenylaminocarbonyl)-3,4-tetrazolium]-bis (4-methoxy-6-nitro) benzene sulfonic acid hydrate), to its orange formazan derivative (Figure 2-3). This occurs due to the activity of mitochondrial dehydrogenase enzymes present within viable cells. Whilst XTT reduction is routinely interpreted as a measure of cell viability or cell number, it is more accurate to interpret it as a direct measure of cellular metabolism (148).

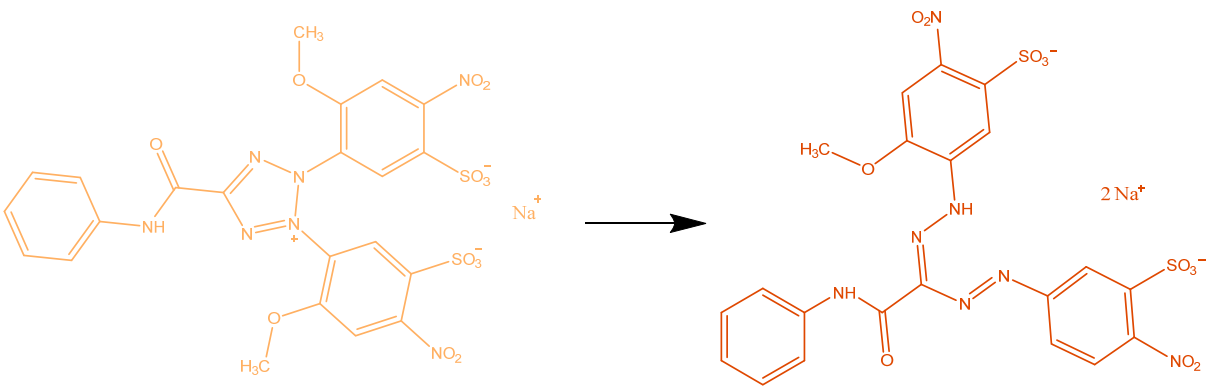

Figure 2-3: Principle of XTT assay
The production of the formazan derivative, which has maximal absorbance at 450 nm, is catalyzed by mitochondrial reduction of XTT therefore; absorbance is proportional to the metabolic activity of a given population of cells.

Assay

Cells were seeded in quadruplicate at a final density of $1.25x10^4$-$1x10^5$ cell.ml^{-1} in 96-well plates (Corning). Cells were incubated for 24 hours before dosing. Following 72 hours of drug exposure, metabolic activity was assessed using the XTT-based colourimetric assay as per the manufacturer's instructions (Cell Proliferation Kit II, Roche, West Sussex, UK). The XTT working reagent consists of a 50:1 mixture of XTT and an electron-coupling agent, PMS (N-methyl dibenzopyrazine methyl sulphate). For the assay, XTT working reagent (50 µl) was added to each well and incubated at 37°C in a 5% CO_2 atmosphere for 4-6 hours before measuring absorbance at 450 nm and 655 nm using a FLUOstar Omega microplate reader (BMG Labtech, Germany). T_0 absorbance values were also collected 24 hours after seeding to account for any proliferation during the pre-treatment phase, as the lymphoma cell lines have a comparatively rapid proliferation rate, thus enabling a more accurate determination of growth inhibition over the period of drug incubation.

Data analysis

Absorbance at 450 nm was corrected for non-specific absorbance using the reference wavelength, 655 nm. No-cell absorbance was also subtracted from all wells; this value was obtained from an average of quadruplicate wells containing media and compound vehicle but without cells. Absorbance at 450-655 nm was then expressed as a percentage of control values. Pre-dose measurements were made, establishing a baseline measurement of metabolic activity, (T_0). The drug concentration required to cause 50% growth inhibition, GI_{50} values, were calculated. Data were analysed using Microsoft Excel and Graph Pad Prism 6.

2.6.2. Cell counts

Background principles

A haemocytomer has predefined etched grids of known sizes and depths thus allowing for accurate measurement of total cell number within a sample. Coupled with counting total cell number, a trypan blue exclusion assay can be used to assess the viability of a given cell population. The intact, selectively permeable plasma membrane of a viable cell prevents trypan blue from entering the cell, whereas the dye is able to penetrate dead or dying cells and stain them blue.

Assay

For suspension cells, a homogenous suspension was achieved by repeated pipetting. Cell number and viability was then assessed using a Neubauer haemocytometer (Hawksley, Sussex, UK) after diluting 10 µl of cell suspension 1:1 with 0.4% trypan blue solution (Sigma). 10 µl of the stained cell suspension was then used to fill the haemocytomer chamber which has a volume of 10^{-4} ml. Cell counts were made in three 1x1 mm squares by recording the number of live, trypan blue excluding cells and dead stained cells.

Data analysis

The average number of live and dead cells were calculated for each sample before multiplying by $2x10^4$ in order to give cell number (ml^{-1}) and account of dilution with trypan blue.

2.7. Metabolomics

2.7.1. LC-MS

Sample preparation

Extraction solvents were prepared using LC-MS grade acetonitrile (ACN), methanol (CH_3OH) and UltraPure water (FischerScientific, USA). All eppendorfs were pre-labelled and kept at -20°C along with extraction solvents in preparation for metabolite extraction. For all metabolomics experiments cells were cultured in RPMI 1640 supplemented with dialysed foetal calf serum (Gibco) to minimise the presence of nutrients in the serum.

Suspension cells

Following the desired incubation period a single cell suspension was collected and centrifuged (13,000 rpm x 2 min; 4°C). A sample of media (100 µl) was added to media extraction buffer (ACN 50%, CH_3OH 50%; 400 µl) and incubated at -20°C for 10 minutes. During this incubation step crude cellular extracts were prepared by removing media from the cell pellet and rapidly quenching cell metabolism by applying 400 µl cell extraction buffer (ACN 40%, CH_3OH 40%, H_2O 20%) and incubating for 10 minutes on dry-ice. Any debris present in the crude cellular extracts was then removed by centrifugation (13,000 rpm x 2 min; 4°C). Then supernatants were collected and transferred to fresh pre-chilled Eppendorfs for storage at -80°C before analysis.

Adherent cell lines

Following the desired incubation period 100 µl media was collected and added to 400 µl media extraction buffer (ACN 50%, CH_3OH 50% v/v) and incubated on dry ice for 10 minutes. During this incubation step crude cellular extracts were prepared by removing media from each well and rapidly quenching cell metabolism by applying 400 µl cell extraction buffer (ACN 40%, CH_3OH 40%, H_2O 20% v/v) and scraping the well surface on dry-ice. The collected crude extract was then incubated for 10 minutes on dry-ice. Any debris present in the crude cellular of media extracts was then removed by centrifugation (13,000 rpm x 2 min; 4°C), supernatants were collected and transferred to fresh pre-chilled eppendorfs for storage at -80°C before analysis.

Sample loading

On the day of the analysis a 50 µl aliquot of each sample was transferred to individual 0.3 ml microvials and dried in a vacuum centrifuge without heating to a volume of approximately 5 µl. Dried metabolic extracts were then resuspended in 150 µl of UltraPure water. Various quality control samples were also prepared, termed 'total QC' and 'spike QC'. Total QC represents a pooled sample of each sample to be analysed. This was prepared by collating 15 µl of each sample into a single 1.5 ml Eppendorf and transferring to 300 µl of the pool to microvials in duplicate. The contents were then dried using a vacuum centrifuge without heat and resuspended in 150 µl of UltraPure water. A collection of metabolite standards were used to prepare 'test mix' by adding 5 µl from six separate metabolite mixes to 70 µl UltraPure water. This therefore contains all detectable metabolites with the scheduled multiple reaction monitoring (MRM) transitions.

LC-MS analysis

LC-MS operation was performed by Dr. Lai-Rowcroft (AstraZeneca). Chromatographic separation was achieved using a reverse-phase C18 100 x 2.1 mm, 1.8 µm particle size, Acquity HSS T3 column (Waters, Hertfordshire, UK). The analytical column was maintained at a constant temperature of 60 °C in an oven housing. Solvent flow was delivered by a Dionex Ultimate 3000 system equipped with a Rapid Separation pump operated at a consistent rate of 400 µl per minute. Buffer A was composed of tributlamine (TBA) (10 mM) and acetic acid (15 mM) in HPLC-MS grade UltraPure water. Buffer B was composed of methanol (80% v/v) and isopropanol (20% v/v). The time-table used for the gradient elution is shown in Table 6.

Time post injection (min)	% Buffer A	% Buffer B
0	100	0
0.5	100	0
4	95	5
6	95	5
6.5	80	20
8.5	80	20
14	45	55
15	0	100
17	0	100
17.1	100	0
20	100	0

Table 6: Chromatographic gradient composition

Parameter	
Curtain gas	10
Ionspray voltage	3500 V
Source temperature	550°C
Gas 1	60
Gas 2	50
Interface heater	On
CAD gas	5
Exit potential	-10

Table 7: Mass spectrometry settings

An ABI Sciex 4000 QTRAP mass spectrometer was operated in negative polarity schedules multiple reaction monitoring mode under conditions listed in Table 7

Data analysis

Peak integration was performed using MultiQuant software version 2.0.45 (AB Sciex, Framingham, USA) the chromatographic peak for each metabolite was visually compared to the corresponding peak in test mix and spiked QC injections in order to select the appropriate peak for integration. Integrated peak areas were then exported to MS Excel for further processing.

Metabolites, which were present in less than two replicate samples, were not included in the analysis. Metabolites not present in at least 60% of total QC injections were also excluded from the analysis as the detection of these metabolites had altered during the run and therefore may not be reliable.

Integrated peak areas were Log_2 transformed. Log_2 transformed data was then normalised to the median fold change since this is recognised as a relatively robust method with regard to dilution effects (149). Log_2 peak areas for all identified metabolites in a given sample were normalised by median fold change of log_2 peak areas for each individual analyte across all injections. Coefficient of variance (CV) values were calculated for each metabolite in the QC samples. Metabolites with a CV value >30% were excluded from further analysis. Log_2FC values were calculated in order to determine the effects of treatment with AZD3965 for each sample relative to a time-matched control. The statistical significance of any observed changes were assessed using a Student's *t*-test. Significantly altered metabolites ($P \leq 0.05$) with log_2FC changes ± 0.5 were considered altered by AZD3965 treatment.

Log_2FC and P-values were exported to Spotfire (Tibco Software, Boston, USA) or Tableau (Tableau Software, Seattle, USA) for visualisation. Using the R-package "Pathview" log_2FC and P-values were also used to map metabolic changes onto defined metabolic pathways listed on the KEGG database. The R-script used is provided in Appendix A.

2.7.2. GC-MS

Ex vivo sample preparation

A suspension of approximately 10^7 CA46 cells were implanted subcutaneously in NSG mice on the right flank and allowed to reach an appropriate size (2-4 weeks). Mice were given a single dose of AZD3965 (100 $mg.kg^{-1}$) or a 0.5% control solution by oral gavage before being humanely killed. CA46 tumour were excised as previously described in section 2.5.3 then stored at -80°C before sending for metabolomic analysis.

Metabolite extraction and GC-MS analysis was performed at Imperial College London by Arti Sikka using the following protocol and keeping the samples on dry ice throughout. Tumour samples were weighed and added to screw-cap tubes containing 0.1 mm glass beads. 800 µl of pre-chilled 80% methanol was added and samples were homogenised using a Precellys 24 bead beater (Bertin Technologies, Montigny-Le-Bretonneux, France) set to 6500 rpm x 20

seconds x 2 cycles. Supernatants were collected after centrifugation (12,000 x g, 5 min, at 4°C). The extraction was repeated and the fractions for each sample were pooled. Supernatants were then dried in a vacuum concentrator and subjected to dual-phase extraction. Chloroform/methanol of (2:1; 300 µl) was added to each sample followed by vortexing. Water (300 µl) of was then added to each sample followed by vortexing and centrifugation (14,000 rpm, 10 min; 4°C). The aqueous (upper) layer from each sample was transferred to silanized GC-MS vials. The dual-phase extraction was repeated and fractions were pooled for each sample. A 20 mg sample of each tumour extract was dried in a vacuum concentrator and analysed by GC-MS.

GC-MS analysis

The analytical protocols used were adapted from a previously reported method (150). Myristic acid-d27 (10 µl of 1.5 mg.ml^{-1} solution), was added to each dried extract as an internal standard. Metabolite extracts were derivatised using the two-step method of derivatisation: methoxymation and silylation (151). When required, samples were diluted with anhydrous pyridine. Samples were analysed in a splitless mode on an Agilent 7890 GC with a 30m DB-5MS capillary column and a 10m Duraguard column. This GC was coupled to an Agilent 5975 MSD. GC-MS data was deconvoluted and metabolites were assigned using FiehnLib assisted processing in 'Automated Mass spectral Deconvolution & Identification System' (AMDIS) and manually assessed using the GC–MS Assignment Validator and Integrator (GAVIN) package (150-152).

2.7.3. NMR

Sample preparation

For metabolite analysis of media samples all cells were seeded and compounds prepared, in freshly prepared aliquots of RPMI media supplemented with 10% dialysed FBS. CA46 or CA46-R cells were incubated for 24 hours (37°C, 5% CO_2) in the presence of AZD3965 (100 nM) or DMSO (0.01%). Occasionally DMSO related metabolic effects can be observed, and in order to evaluate this, samples not including the compound vehicle were also included. Matched culture media controls were also prepared, where media with or without DMSO vehicle or AZD3965 (100 nM) were cultured alongside cell containing samples. Conditions were performed in quadruplicate within 6-well plates (4 ml/well) at a cell density of 2x10^5 cells.ml^{-1}.

To prepare media samples for metabolite analysis, cell suspensions were prepared by thoroughly resuspending the contents of each well to ensure a homogenous cell distribution. An aliquot of cell suspension (100 µl) was removed in order to determine cell number and viability by counting, as described previously, for normalisation. The remaining cell suspension was centrifuged 500 x g, 5 minutes at room temperature before collecting the media fraction into sterile and labelled Eppendorf tubes. Samples were collected on a plate by plate basis to minimise the time spent outside incubator conditions (37°C, 5% CO_2). Samples were then frozen on dry ice and stored at -80 °C.

NMR analysis

Nuclear magnetic resonance (NMR) analysis of cell culture supernatants were performed at Imperial College London by Ms. Arti Sikka using the below method.

An internal standard of 4,4-dimethyl-4-silapentane-1-sulfonic acid (DSS) was prepared in deuterated oxide (D_2O). A 550 µl aliquot of each cell culture medium sample was mixed with 50 µl of sodium phosphate (0.5 M) buffer containing DSS (12 mM, pH 7) and transferred to 5 mm glass NMR tubes. High Resolution One dimensional (1D) ^{1}H NMR spectra were acquired using a Bruker AVANCE spectrometer (Bruker Bio Spin, Rheinstetten, Germany) at 298K, 14.1 T and 400 MHz ^{1}H frequency. All spectra were acquired using a ZGPR pulse sequence, 32 free induction decays (FIDs), a spectral width of 6402.049 Hz and 0.3 Hz line broadening.

^{1}H NMR spectra were imported into MATLAB (MathWorks, Natick, Boston, USA) using an in-house script written by Dr. T. M. D Ebbels, Dr. Hector C. Keun, Dr. J.T.M. Pearce, Dr. O. Cloarec and Dr. R. Cavill at Imperial College London. Spectra were automatically phased, baseline corrected and referenced to the DSS resonance at δ 0. Manual assessment ensured that the automatic processing and water suppression were appropriate. Peaks were integrated and the resonances were assigned to metabolites using spectral comparison with the Human Metabolome Database (HMDB).

Jain *et al.,* (2012) previously described metabolite CORE profiling as the difference between the concentration of a given metabolite ‘X’ in spent and fresh media, normalised to the area under the growth curve. CORE profiling was normalisation to cell number (153).

2.8. Assessment of intracellular reactive oxygen species with CellROX® via Fluorescence-activated cell sorting (FACS) analysis

2.8.1. Background principles

The levels of intracellular reactive oxygen species (ROS) were measured in live cells using a proprietary cell-permeable fluorogenic probe CellROX® green (Life Technologies). The fluorescence of CellROX® green is substantially increased upon its oxidation relative to in its reduced state. A number of tool compounds were utilised to alter cellular ROS. Firstly menadione was used to increase cellular ROS. Cellular metabolism of menadione creates ROS by futile redox cycling , where its one-electron reduction generates a reactive semiquinone radical. In the presence of O_2 the semiquinone can be oxidized back to the parent species generating further ROS (154). Conversely, N-acetyl-ι-cysteine (NAC) reduces ROS by increasing levels of cellular glutathione and cysteine, and in addition, the thiol groups of NAC provide alternative sites of action for ROS oxidation thereby decreasing the likelihood of ROS causing cellular damage.

2.8.2. Sample preparation

CA46 cells were seeded at $2x10^5$ ml^{-1} in standard media, with or without, anti-oxidant NAC (5 mM) for 1 hour prior to dosing with AZD3965, BAY 87-2243 or both compounds. All groups received equal vehicle concentrations, of DMSO and ethanol respectively. Cells were cultured for 48 hour before staining and FACS analysis.

On the day of analysis, a number of control treatments were also included to validate that the observed shifts in FL-1 fluorescence coincided with alterations in cellular ROS. A positive control cell population was created by treating cells for 1 hour with menadione (50 μM). A negative control cell population was created as above, but with pre-treatment with NAC for 1 hour.

2.8.3. FACS Analysis

Samples were analysed using a FACS Calibur (BD Biosciences) equipped with a 488 nm laser and a 530/30 nm filter. Using forward and side scatter profiles, live cells were selected for, and dead cells and cell debris were eliminated from the analysis. The FL-1 signal was

adjusted to enable the minimum (negative control) and maximum (positive control) cell populations to be viewed.

2.9. Measuring extracellular acidification (ECAR) and oxygen consumption rate (OCR) using the SeaHorse Bioanalyser XF24

2.9.1. Background principles

The SeaHorse Bioanalyser allows for real-time measurement of two parameters through the creating of a series of transient microchambers; extracellular acidification rate (ECAR) and oxygen consumption rate (OCR) (Figure 2-4). A large contributor to extracellular acidification is the efflux of lactate produced through the glycolytic pathway. Conversely, OCR, reflects the oxygen consumption rate of the cell which largely reflects mitochondrial oxidative phosphorylation. By measuring these two parameters simultaneously in response to a number of tool compounds the relative contributions of these two major energy producing pathways can be assessed in real-time in live cells.

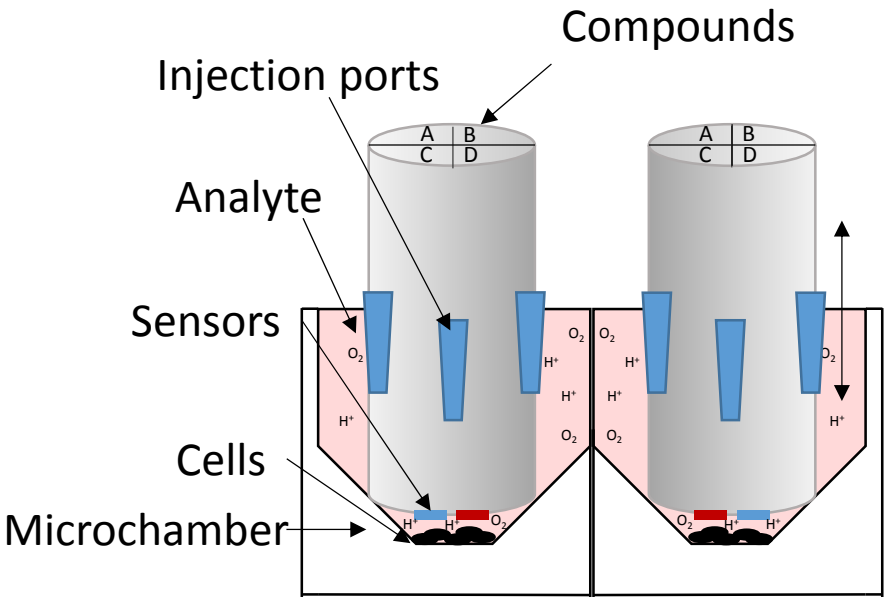

Figure 2-4: Seahorse bioanalyser technology
To measure oxygen consumption and proton extrusion a transient microchamber is formed by the sensor moving towards the bottom of the well. Four injection ports are preloaded with compounds of interest which can be added between measurements. Adapted from (155).

FCCP (Carbonyl cyanide 4-(trifluoromethoxy)phenylhydrazone)

The protonophore, FCCP, essentially uncouples ATP generation from oxygen consumption triggering a maximal rate of oxygen consumption. Protons continue to be pumped across the inner mitochondrial membrane requiring the reduction of molecular oxidation. However FCCP, allows protons to freely pass back across membrane therefore there is no electron gradient to drive ATP generation by ATP synthase.

Oligomycin

Oligomycin binds to the F_o subunit of ATP synthase and in doing so blocks the passage of protons from the intermembrane space to the mitochondrial matrix which drives the addition of P_i to ADP to form ATP. Therefore, the effects of oligomycin on OCR are representative of the OCR associated with mitochondrial ATP production.

Antimycin

Antimycin is an inhibitor of Complex III of the ETC. It inhibits the oxidation of ubiquinol by cytochrome c reductase (Complex III) disrupting the proton gradient. This completely inhibits mitochondrial oxygen consumption.

2.9.2. Experimental methods

Preparation of suspension cells for SeaHorse Bioanalyser experiments

SeaHorse Bionalyser requires that cells are immobile for analysis as we are using suspension cells they must be adhered to the well surface. CellTak® (Corning) cell and tissue adhesive is a formulation of polyphenolic proteins isolated from *Mytilus edulis* which allow the marine mussel to fix to solid surfaces. XF microplates were coated with 50 µl CellTak (22.4 $\mu g.ml^{-1}$) solution in sterile $NaHCO_3$ (0.1 M). This was prepared from a stock solution (2.03 $mg.ml^{-1}$ in 5% acetic acid). In order to neutralise the pH of the solution NaOH (1 M) equal to half the volume of CellTak stock solution used was immediately added to trigger adsorption of CellTak to the well surface at room temperature over a 20 minute incubation. CellTak solution was subsequently removed and remaining bicarbonate solution was removed by washing with sterile dH_2O. Coated XF cell culture plates were either used immediately or stored at 4°C for up to 1 week before cell attachment.

On the day of the experiment, CA46 lymphoma cells (200,000 cells/well) were adhered to CellTak® (Corning) coated 24-well proprietary XF24 cell culture plates excluding background

control wells. A cell suspension was prepared at an appropriate density in XF assay media without FBS, as the presence of FBS was found to be detrimental to attachment (data not shown). Cells were attached evenly to the bottom of the plate by centrifuging immediately at 200 x g for 1 minute with no braking. The attached cells were incubated at (37^{o}C, 0% CO_2) for 30 minutes for ensure cell attachment before beginning SeaHorse analysis. An additional 400 µl of assay media containing FBS (3% final concentration) were added to each well.

Assay media

Fresh XF assay media was prepared on the day of the experiment from XF base media supplemented with glucose (5 mM), L-Glutamate (2 mM) and pyruvate (1 mM). XF Base media does not contain bicarbonate or other buffering compounds as these would interfere with the measurement of extracellular acidification as such fresh batches of media were adjusted to pH 7.4. FBS was added following cellular attachment to a final concentration of 3%.

Cartridge loading

Before compound loading the cartridge required hydration in calibrant solution overnight. Compounds to be injected during the assay were freshly prepared in XF assay media at 10x final assay concentration and loaded into the cartridge. The SeaHorse sensor cartridge contains 4 injection ports and a central sensor channel for each well of the 24-well plate.

Running the assay

FCCP (0.3 µg.ml^{-1}), oligomycin (1 µg.ml^{-1}) and antimycin A (2.5 µM) were injected sequentially through ports in the Seahorse Flux Pak cartridge.

2.9.3. Data analysis

Oxygen consumption rate and extracellular acidification rate data were normalised to the protein content of each well (determined by BCA assay) to account for any inter-well variability in cell number.

2.10.Immunohistochemical staining of MCT1 and MCT4

Immunohistochemical method development, data acquisition and scoring was performed by the MRC/EPSRC Newcastle Molecular Pathology Node, Newcastle upon Tyne. Formalin-fixed paraffin-embedded pre-treatment diagnostic diffuse large B-cell lymphoma (DLBCL) and

Burkitt lymphoma (BL) tissue samples were obtained from the Newcastle Haematology Biobank (National Research Ethics Service Committee Reference 07/H0906/109+5) and the Children's Cancer and Leukaemia Tissue Bank (National Research Ethics Service Committee Reference (08/H0405/22+5) respectively. Most DLBCLs were combined into 3 tissue microarrays containing duplicate 1 mm cores; other samples were assessed as individual sections. Immunohistochemistry for MCT1 and MCT4 was performed on the Ventana Benchmark automated immunostaining platform using Optiview detection, following optimisation using kidney, lymphoid and solid tumour control tissues and cell lines of known MCT1/MCT4 expression status. Semi-quantitative measurement of MCT1/4 in tumour cells was performed by assessing staining extent (%) and intensity (absent = 0, weak = 1+, moderate = 2+, strong = 3+) to produce a summary H-score from 0-300 calculated (H = (1 x % 1+) + (2 x % 2+) + (3 x % 3+)) (156). This was performed by two haematopathologists (Dr. Chris M Bacon and Dr. Despina Televantou, Cellular Pathology, Newcastle upon Tyne Hospitals NHS Foundation Trust). In selected cases, double 11 immunohistochemical staining for PAX5 (SP34 rabbit monoclonal antibody, Ventana) and MCT4 was used to distinguish MCT4 expression on non-tumour versus tumour cells. DLBCL cell-of-origin classification was determined by immunostaining as described in Culpin *et al.* using the Hans algorithm (157, 158).

2.11.*In vivo* experiments

The efficacy of AZD3965 was assessed *in vivo* using an intravenous CA46 cells transfected with the pSLIEW vector engineered to express luciferase (pSLIEW) which allows monitoring of their engraftment via bioluminescent imaging on the IVIS Spectrum® (Figure 2-5). Imaging and histological studies have previously shown that cells engraft in the bone marrow, spleen and kidneys reflective of the clinical manifestation of the disease (159). *In vivo* engraftment of transfected CA46 cells, IVIS® imaging and preparation of post-mortem tissues were performed by Dr. Natalie Bell and Dr. Helen Blair.

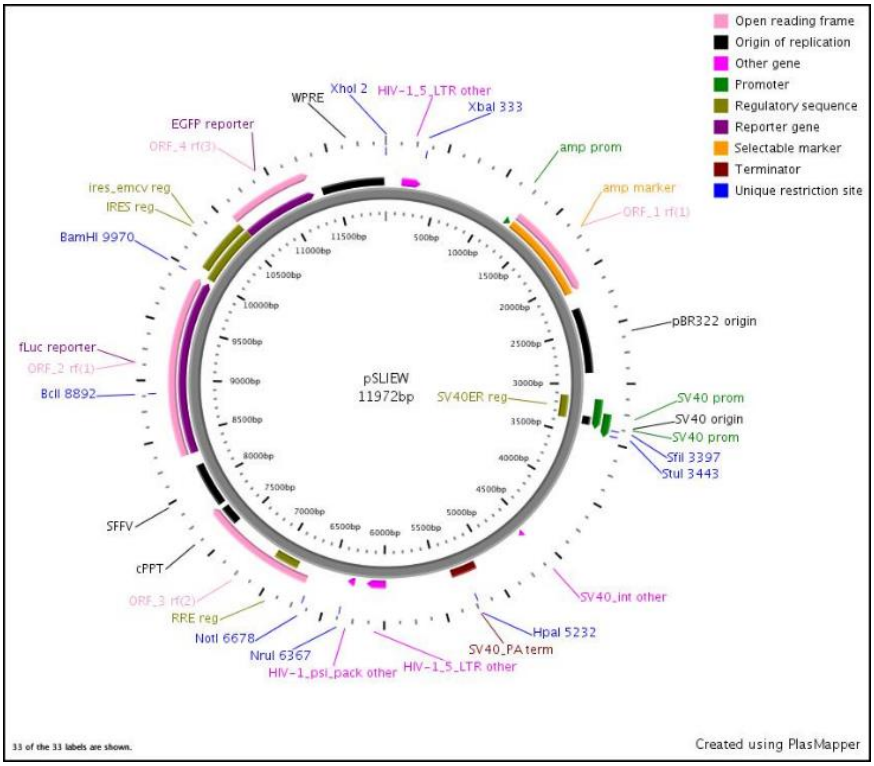

Figure 2-5: Plasmid map of pSLIEW
pSLIEW vector containing, enhanced green-fluorescent protein (EGFP), and firefly luciferase (fLuc) genes. Transduced GFP expression was used to sort transduced CA46 cells via FACS. Luciferase expression was used to track CA46 cell engraftment *in vivo*. Diagram from (159).

For efficacy experiments 10^4 CA46 pSLIEW cells in 100µl of RPMI1640 medium were delivered intravenously via the tail vein to NOD/LtSz-scid IL-2Rγ-/- (NSG) mice. Tumour cell engraftment was assessed at the described intervals via IVIS® Spectrum imaging. Here, D-luciferin (150 $mg.kg^{-1}$) was administered intraperitoneally before anaesthetising mice with isoflurane 5 minutes after injection. Initially a kinetic curve will be constructed to determine the time to peak flux detection after luciferin injection.

Bone marrow, spleen and kidneys were harvested and fixed in formalin, paraffin embedded and sectioned at 4 µm to allow immunohistochemical staining of human CD20. IHC was performed in the Department of Pathology, Royal Victoria Infirmary, Newcastle using either a Ventana Benchmark XT or Benchmark Ultra and Ventana Ultraview detection system.

Treatment schedules are described below.

2.11.1. Monotherapy study

An initial IVIS® scan was performed 6 days following implantation to confirm engraftment and assigned to mice to treatment groups. Mice received AZD3965 (100 $mg.kg^{-1}$) or vehicle

by oral gavage twice-daily (8 hour interval) Monday to Friday and once-daily at weekends for a period of 24 days. Scans were performed on the first day of treatment and then on day 3, 10, 17 and 24.

2.11.2. AZD3965 and BAY 87-2243 combination study

An initial IVIS® scan was performed 12 days following implantation to confirm lymphoma engraftment and assigned to mice to treatment groups. Mice were split into four treatment groups; vehicle, AZD3965, BAY 87-2443 or AZD3965 and BAY 87-2243. A post-treatment scan was conducted 72 hours after the last dose of AZD3965

AZD3965 or the corresponding vehicle was dosed twice-daily orally, BAY 87-2243 or the corresponding vehicle dosed orally roughly 2 hours after the AM dose of AZD3965 daily. Control mice received a combination of vehicles.

2.12.Statistical analysis

Unless otherwise stated statistical significance was assessed using a two-tailed Student's *t*-test. P-values below 0.05 were considered as significant.

Chapter 3. Diffuse large B-cell lymphoma and Burkitt Lymphoma are potential targets for AZD3965 treatment

3.1. Introduction

As summarised in Table 2 and Table 3 previous preclinical studies using AZD3965 demonstrate that MCT4 expression can preclude sensitivity to MCT1 inhibition (84, 118, 134). MCT4, which is overexpressed in a number of cancers, can compensate for the loss of MCT1 activity by exporting lactate allowing cellular metabolism and growth to continue unimpeded. Therefore, the identification of cancer types where MCT4 expression is particularly low will be key to ascertaining a disease area where MCT1 inhibition is most likely to be clinically efficacious.

3.2. Aims

Two potential areas of interest are diffuse large B-cell lymphoma (DLBCL) and Burkitt lymphoma (BL). The work in this chapter will describes the identification of DLBCL and BL, as cancer types consistently low in MCT4 (mRNA and protein) making them attractive areas in which to further characterise the *in vitro* effect of AZD3965.

The aims of this chapter are:

- To assess the gene expression of *MCT1* and *4* in cancer cell lines using publically available data to determine cancer type where low MCT4 expression is a common feature.
- To determine MCT 1 and 4 protein expression profile in a selected patient population via IHC.

3.3. Identifying candidate cell lines from SLC16A1 (*MCT1*) and SLC16A3 (*MCT4*) expression in human cancer cell lines

Cell lines with high expression of MCT4 have been shown to be refractory to MCT1 inhibitor treatment (118). We therefore sought to identify potential disease areas where low *MCT4* expression is most prevalent based on publically available mRNA expression data (Affymetrix u133p2) from the Cancer Cell Line Encyclopaedia (CCLE) in order to select disease area(s) for further *in vitro* investigation (160). To do this we first categorised cell lines by tumour type, using available primary site and histological subtype metadata. Tumour categories with ≥ 4 representative cell lines were pre-selected. We then compared the RMA (Robust multi-array

averaging)-normalised expression levels of SLC16A1 (*MCT1*) and SLC16A3 (*MCT4*) mRNA in 11 solid cancer types and 8 haematological cancer types representing 610 cell lines (Figure 3-1).

MCT1 mRNA expression was found to be largely consistent across disease sub-types possibly reflective of its physiologically less tissue-specific expression pattern. There was little difference in median expression across the categories (8.45-9.61) although particular cell lines within these categories could be considered as having high or low *MCT1* mRNA expression such as the neuroblastoma cell line, IMR-32 and NSCLC cell line, NCI-H1373, respectively.

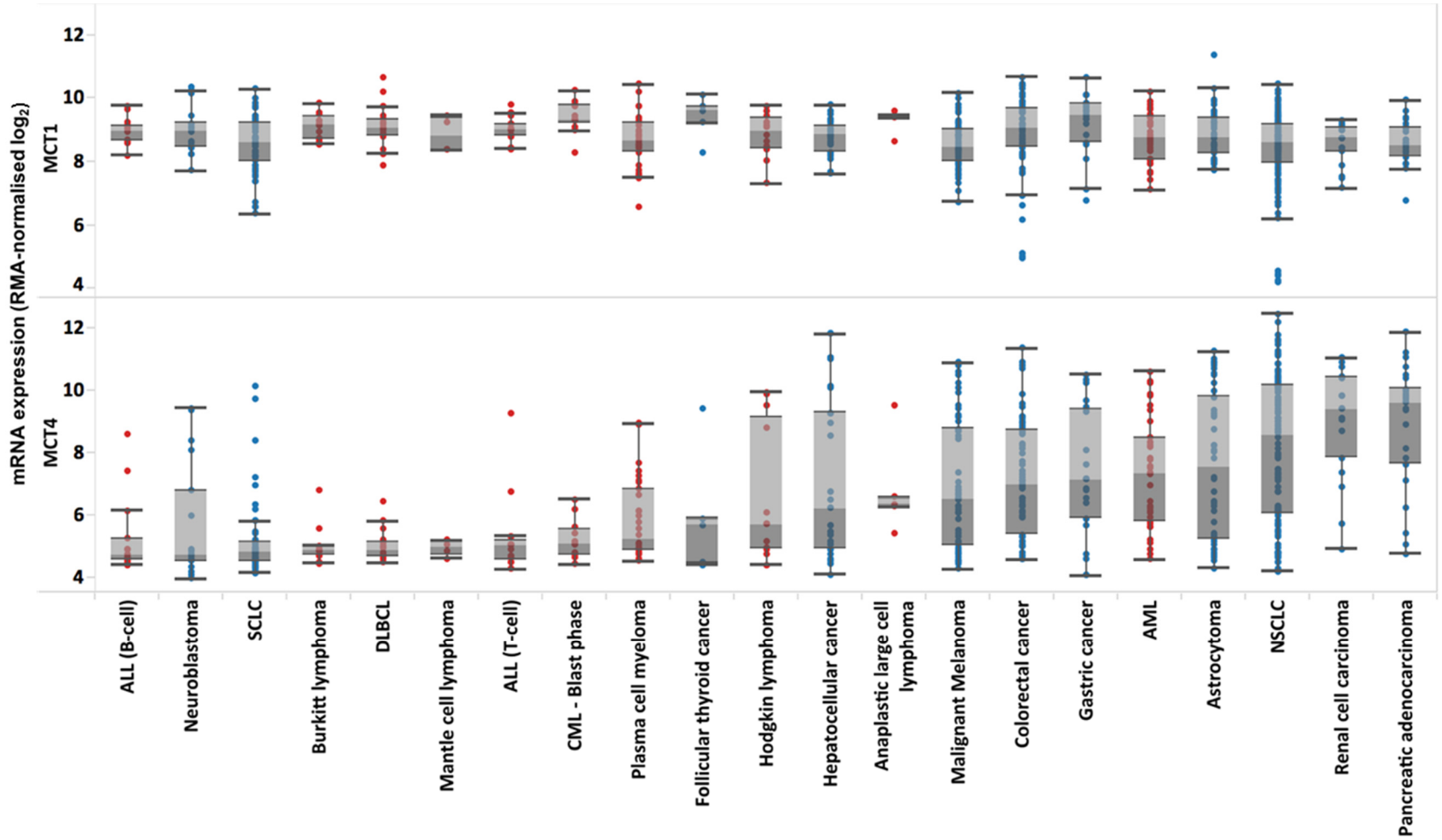

Figure 3-1: *MCT1* and *MCT4* mRNA expression across disease subtypes
A subset of 610 cell lines from CCLE (Affymetrix U133 +2) with gene expression data for *MCT1* and *MCT4* were categorized by disease type. Disease categories were sorted by the median of *MCT4* expression. Individual hematological and solid cancers cell lines are displayed as ■ and ■ respectively. Abbreviations used: acute lymphocytic leukaemia (B/T-ALL), small-cell lung cancer (SCLC), diffuse large B-cell lymphoma (DLBCL), chronic myeloid leukaemia (CML), acute myeloid leukaemia (AML), non-small-cell lung cancer (NSCLC).

In contrast, *MCT4* mRNA expression was highly variable between disease sub-types, median values ranging from 4.7-9.6. *MCT4* mRNA levels were particularly low in a number of haematological cancers, as evidenced in Figure 3-2.

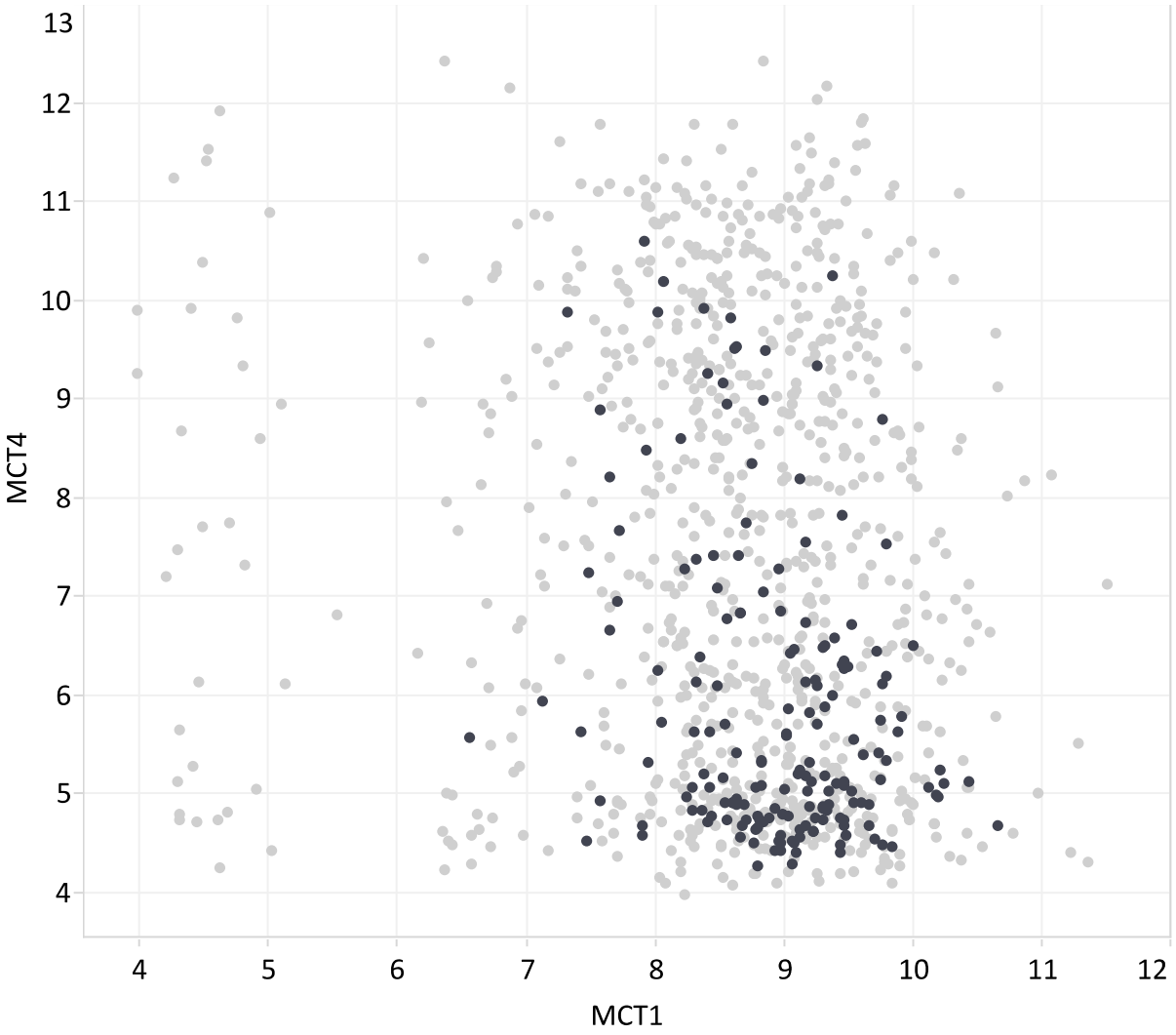

Figure 3-2: Summary of *MCT1* and *MCT4* mRNA expression in the Cancer Cell Line Encyclopedia
Scatterplot of normalized *MCT1* and *MCT4* expression in cancer cell lines from the Cancer Cell Line Encyclopedia. Hematological and solid cancers are indicated as ■ and ■ respectively.

Haematological malignancies with low *MCT4* included DLBCL, BL, B-cell acute lymphocytic leukaemia (B-ALL) and plasma cell myeloma. Conversely most solid tumour types had notably higher *MCT4* levels with pancreatic adenocarcinoma having the highest average expression. Neuroblastoma cell lines were a notable exception to this, in that they appear to have the desired MCT profile based on mRNA expression data. There was also great diversity in the expression of *MCT4,* within several solid-tumour cell line cohorts, such that there are examples of cell lines with very high and very low expression of *MCT4* in a given disease. A

good example of this is in SCLC where there are examples of high (SW-1271) and low (NCI-H1048) *MCT4* expressing cell lines.

3.3.1. Diffuse Large B-cell lymphoma

DLBCL is the most common form of non-Hodgkin lymphoma accounting for around 5,000 annual cases in the UK (161). The median age at diagnosis is approximately 60 years old. DLBCL is a genetically diverse disease and several classification systems have been described using gene expression profiling (162).

The Cell of Origin (COO) classification system describes distinct subgroups enriched with genes associated with different stages of B-cell development; Activated B-cell (ABC-DLBCL), Germinal centre B-cell (GCB-DLBCL), primary mediastinal B-cell lymphoma (PBML) (163). These subgroups are associated with expression of genes associated with a particular development phase of B-cells. Additionally, they are characterised by distinct drivers of tumourigenesis for example ABC-DLBCL is commonly driven by constitutively active NFκB signalling. Common features in GCB-DLBCL include *BCL2* translocations and *PTEN* deletions which are found in 34% and 15% of patient samples respectively. These different subgroups also have distinct prognostic profiles with GCB-DLBCL having better prognosis than the rarer ABC-DLBCL subtype (164). In addition, GCB and non-GCB tumour types can be identified using surrogate IHC markers (158). Despite the available information on the distinct drivers of these genetic subtypes and their prognostic relevance are yet to impact on the ways patients are treated (165).

An alternative molecular subgroup termed, Consensus cluster classification (CCC), is based on gene expression analysis in DLBCL patient samples where genes involved in oxidative phosphorylation (OXPHOS), B-cell receptor signalling (BCR) or the Host-Response are found to form three distinct clusters (166). The OXPHOS signature includes multiple subunits of the ETC complex and TCA cycle. Subsequently OXPHOS cell lines are found to exhibit increased expression of mitochondrial proteins, enhanced glucose oxidation, decreased lactate production and increased fatty acid oxidation (167). The BCR subset show enrichment of genes in the B-cell receptor signalling cascade such as Spleen tyrosine kinase (*SYK*) and cell cycle regulatory genes such as *CDK2* (166) The two classification systems are independent of each other such that a particular COO subtype is not associated with a certain CCC subtype in tumours (166).

The standard of care for DLBCL is currently a combination of cytotoxic drugs and antibody therapy and steroid, typically R-CHOP therapy; R-Rituximab, C-Cyclophosphamide, H-(Hydroxy)doxorubicin, V-Vincristine, P-Prednisolone. The incorporation of anti-CD20 antibody rituximab has been demonstrated to be superior to CHOP therapy in elderly and younger patients (168, 169). Although curative in around 50% of cases, 30-40% of patients become refractory with dismal outcome, accounting for the vast majority of mortality associated with DLBCL (170, 171). Additionally, a number of patients are not able to tolerate the aggressive chemotherapy schedule owing to toxic side effects therefore there is scope to improve patient survival in both such cases using more targeted agents.

3.3.2. Burkitt Lymphoma

BL is a much rarer but highly aggressive B-cell lymphoma characterised by *c-MYC* translocations most commonly with the *IgG* heavy chain locus. The pathogenesis of BL is therefore heavily driven by this aberrant activation of c-MYC, a potent oncogene. *c-MYC* translocations are found in approximately 90% of cases but *MYC* is also commonly mutated in BL (172, 173). In contrast to DLBCL cases of sporadic Burkitt lymphoma are more common in young adults and children, indeed, BL is the most common form of non-Hodgkin lymphoma (NHL) in children. There are three distinct types of Burkitt lymphoma; endemic, sporadic and immunodeficiency-associated Burkitt lymphoma. Endemic Burkitt lymphoma is most common in sub-Saharan Africa and is associated with infection with Epstein-Barr virus (EBV). Sporadic Burkitt is the most commonly observed form in the western world although it represents only 1-2% of all non-Hodgkin lymphoma diagnoses.

BL is currently treated with a variety of short-term high-dose combination chemotherapy regimens with high response rates such as R-CODOX-M (Rituximab, cyclophosphamide, vincristine, doxorubicin, methotrexate) / R-IVAC (Rituximab, ifosphamide, etoposide, cytarabine). Recently the inclusion of rituximab has been shown to improve event free survival in adult BL (174). However, as with DLBCL, when refractory cases occur the aggressive nature of the disease mean 5-year survival rates are very low, approximately 10% (175, 176).

3.4. Expression of MCT1 and MCT4 and CD147 in DLBCL and BL cell lines

Publically available mRNA expression data suggested DLBCL and BL cell lines possess the required MCT profile consistent with sensitivity to MCT1 inhibition. It is also important to note that mRNA expression does not necessarily translate to the level of protein or indeed to functional MCTs expressed at the plasma membrane. We therefore profiled the MCT1 and MCT4 protein expression in a range of DLBCL and BL cell lines by western blot analysis aiming to confirm the suggested MCT phenotype from mRNA data (Figure 3-3). MCT1 was detectable in all cell lines although the level of expression was variable across the cell panel. Raji showed the highest level of MCT1 expression and Farage showed the lowest level of expression. We observed that the vast majority of the cell lines analysed expressed undetectable levels of MCT4, with the exception of BJAB. The chaperone glycoprotein, CD147 was detectable across the cell panel, but with a variable molecular weight, which can be attributed to the various glycosylation states of CD147. Of the cell lines examined by western blot, BL-41, CA46, Daudi, Raji, Pfeiffer, RIVA and Toledo had publically available mRNA data. BL-41 were found to have the highest MCT1 expression by both mRNA and protein. All cell lines with low *MCT4* mRNA also had low or undetectable MCT4 protein. These data suggest that cell line gene expression appears to be a reasonably approximation to identify cell lines with the appropriate MCT phenotype.

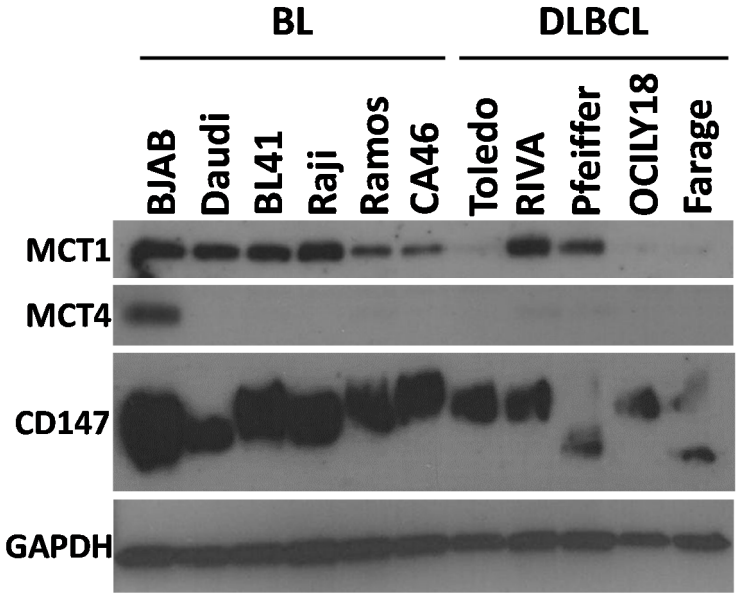

Figure 3-3: Characterization of MCT1 and MCT4 expression in BL and DLBCL cell lines
Western blot showing the expression of MCT1 (54 kDa), MCT4 (49 kDa) and CD147 (42 kDa) in the panel of DLBLC and BL cell lines representative of two blots. Samples are whole cell lysates from untreated cells.

We also confirmed plasma membrane expression of MCT1 and MCT4 in a sub-set of cell lines via immunohistochemistry. Here CA46, Raji, Ramos and BJAB all show high homogeneous staining for MCT1 but only BJAB shows MCT4 staining (Figure 3-4). The majority of staining for both transporters can be seen localized to the plasma membrane.

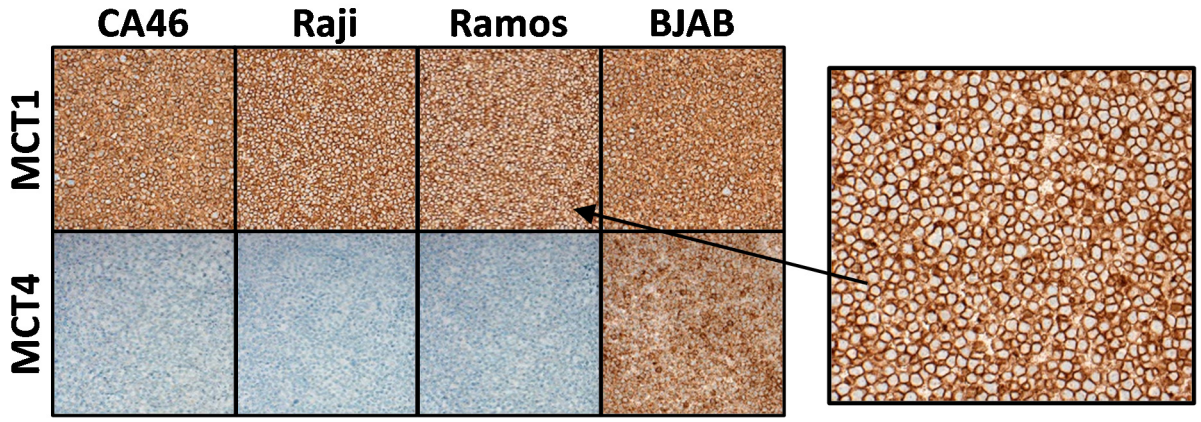

Figure 3-4: Immunohistochemical staining of MCT1 and MCT4 in B-NHL cell lines
Paraffin embedded cell pellets were prepared from B-NHL cells cultured under normal conditions.

3.5. Immunohistochemical characterisation of MCT1 and MCT4 in DLBCL and BL patient samples

We next examined a cohort of 120 DLBCL and 10 BL patient samples by immunohistochemistry for both MCT1 and MCT4 protein using antibodies developed by AstraZeneca. The staining procedure and antibody optimisation was developed in collaboration with Dr. Chris Bacon and Anna Long using cell line samples and a selection of both of normal and tumour control tissues. Staining of patient BL/DLBCL samples was performed by the MRC/EPSRC Newcastle Molecular Pathology Node. H-scores (Scored 0-300) were calculated based upon the coverage (% of cells) and intensity of staining (Section 2.10).

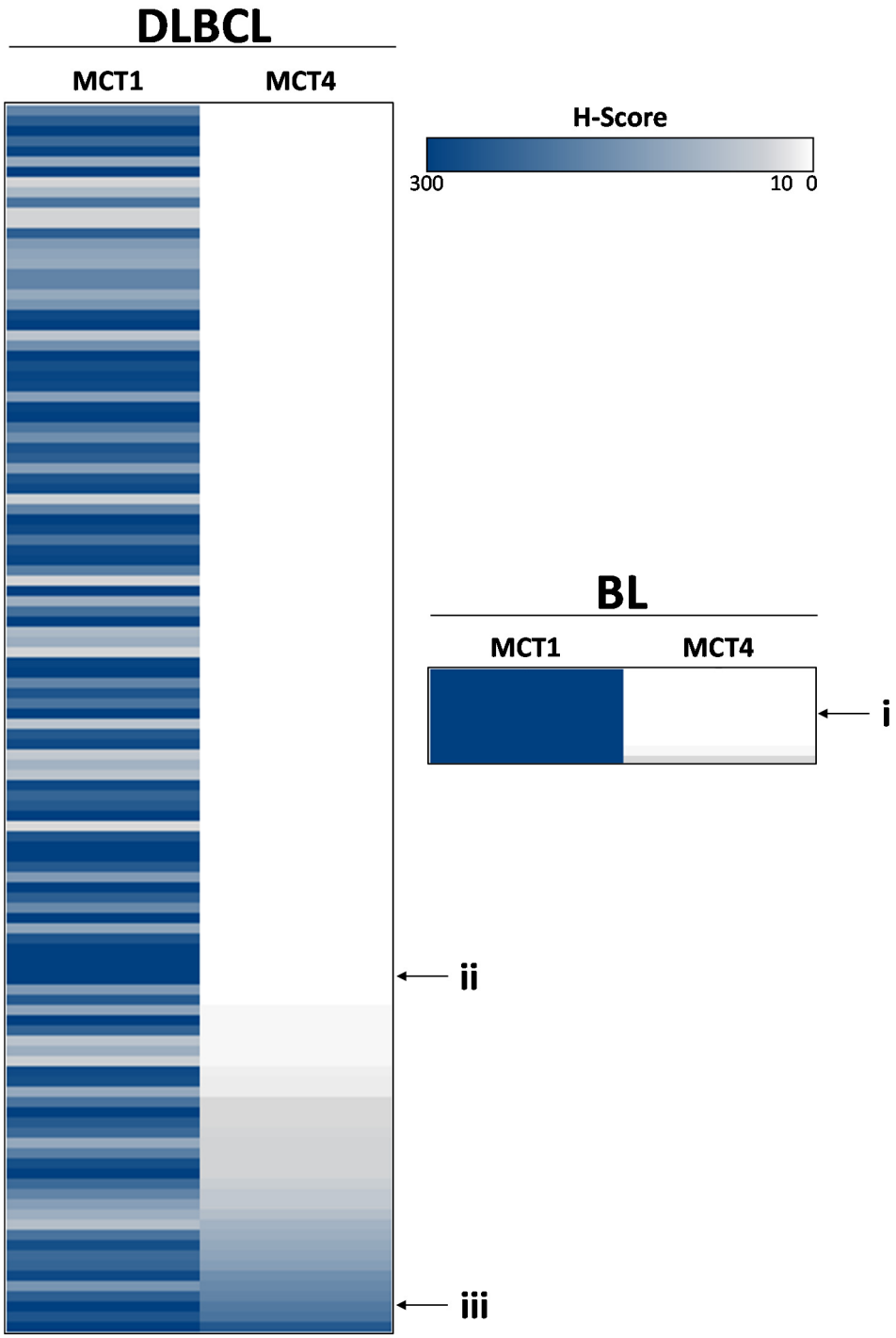

Figure 3-5: Heat map distribution of MCT1 and 4 scoring in BL and DLBCL patient cohorts.
BL and DLBCL patient samples were scored for intensity and extent of staining to produce a single expression score (H-score). Individual cases were sorted by MCT4 expression. Representative examples covering the range of MCT1/4 expression are marked (i-iii) with corresponding IHC images available in Figure 3-6. H-scores, Cell of Origin status and sample identifiers can be found in Appendix B.

All DLBCL samples were positive for MCT1 staining although there was a large range in the intensity of staining with H-scores of 20 to 300 (Figure 3-5). The median H-score for MCT1 was 230/300 in the DLBLC samples indicating that the majority of samples had medium to high expression of MCT1. In contrast, only 26% of the specimens were positive for MCT4, of these 10% of the full cohort were only very weakly positive (H-score ≤ 10). Tumour cell staining of MCT1 and 4, where present, was localised to the cell membrane (Figure 3-6). There was however varying amounts of MCT4 expression in stromal cells as distinguished by morphology and staining for the B-cell marker Pax5 (*data not shown*). Figure 3-6i and ii show representative staining for high MCT1 and low MCT4 H-score in BL and DLBLC respectively Figure 3-6iii is an example of DLBCL specimen with high MCT1 and 4 H-score.

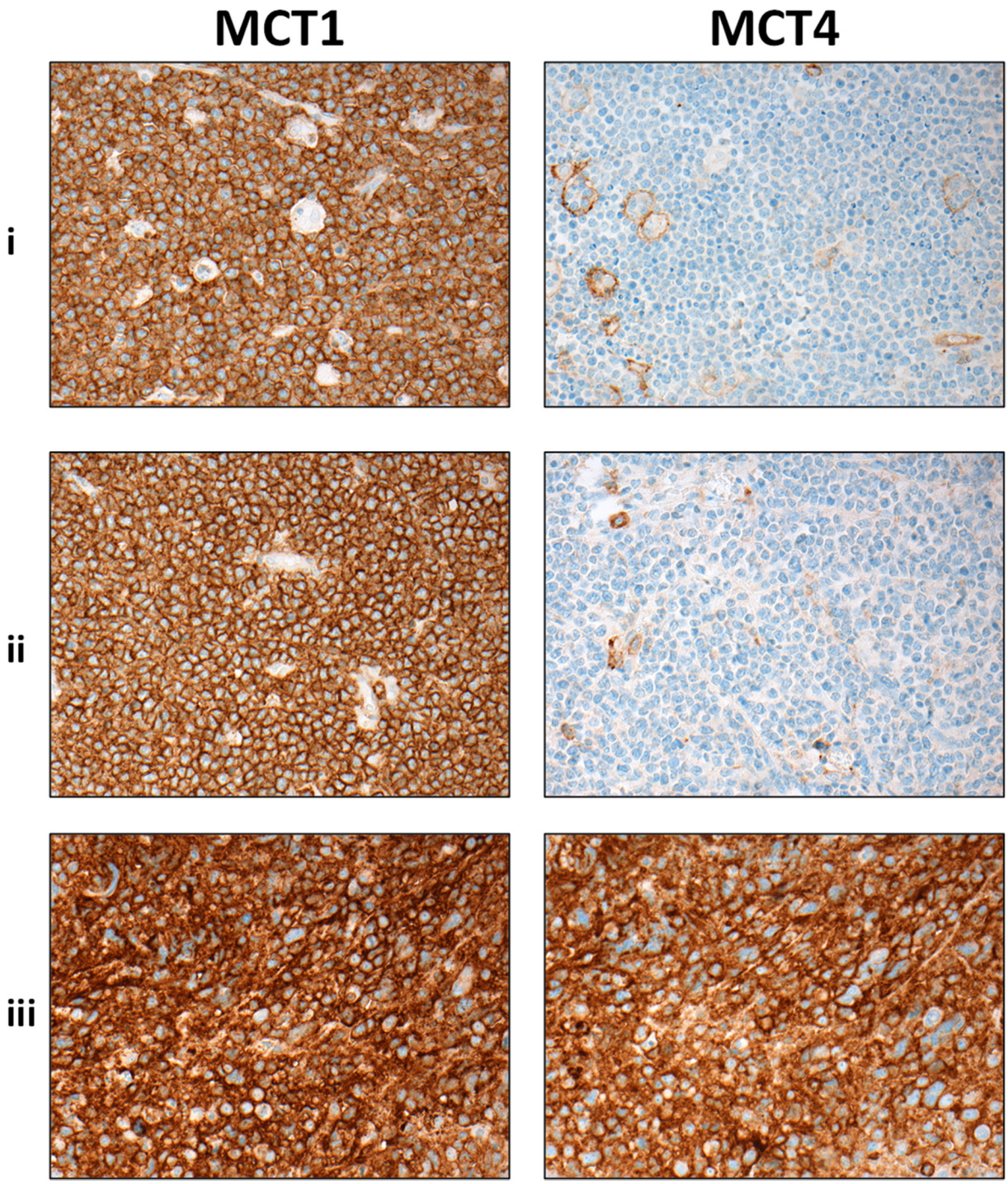

Figure 3-6: Representative MCT1 and 4 staining in BL and DLBCL patient cohorts. Representative images corresponding to the indicated H-scores (i-iii) in Figure 3-5.

The cohort of DLBCL samples contained 39 ABC and 81 GCB samples (32 and 67% respectively) (Figure 3-7). The proportion of MCT4 negative samples (H-score = 0) between Cell of Origin subtypes was identified as 72% and 74% of ABC and GCB respectively and was very comparable (P = 0.83 Fisher's exact test) (Figure 3-8).

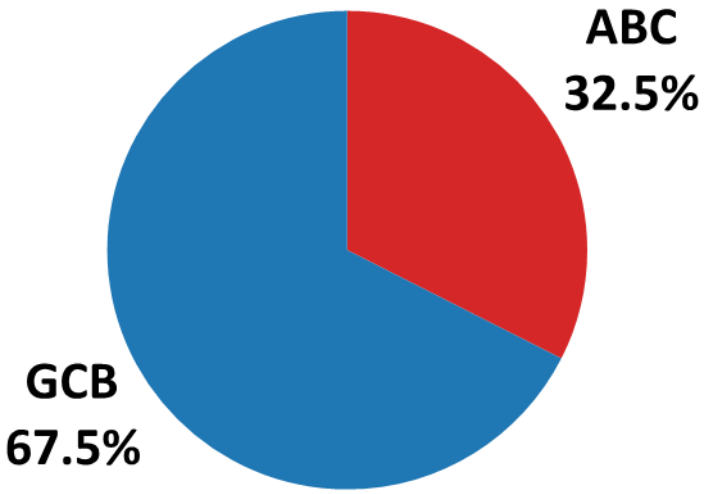

Figure 3-7: Distribution of COO subtypes in DLBCL cohort
Cell of origin subtype classification as assessed by IHC.

The DLBCL cohort also contained a number of samples with *MYC* rearrangement as previously detected by fluorescence in situ hybridisation (FISH) (Unpublished data: Dr. Chris Bacon–Newcastle University). Of the samples which were successfully analysed 14 of 84 showed evidence of *MYC* rearrangement two of which were double-hit lymphomas with *MYC* and BCL2 translocations. *MYC* rearrangement in these samples was not associated with altered MCT1 expression (P = 0.32). Median MCT1 H-scores were 265 (*MYC* rearranged) and 220 (Not rearranged).

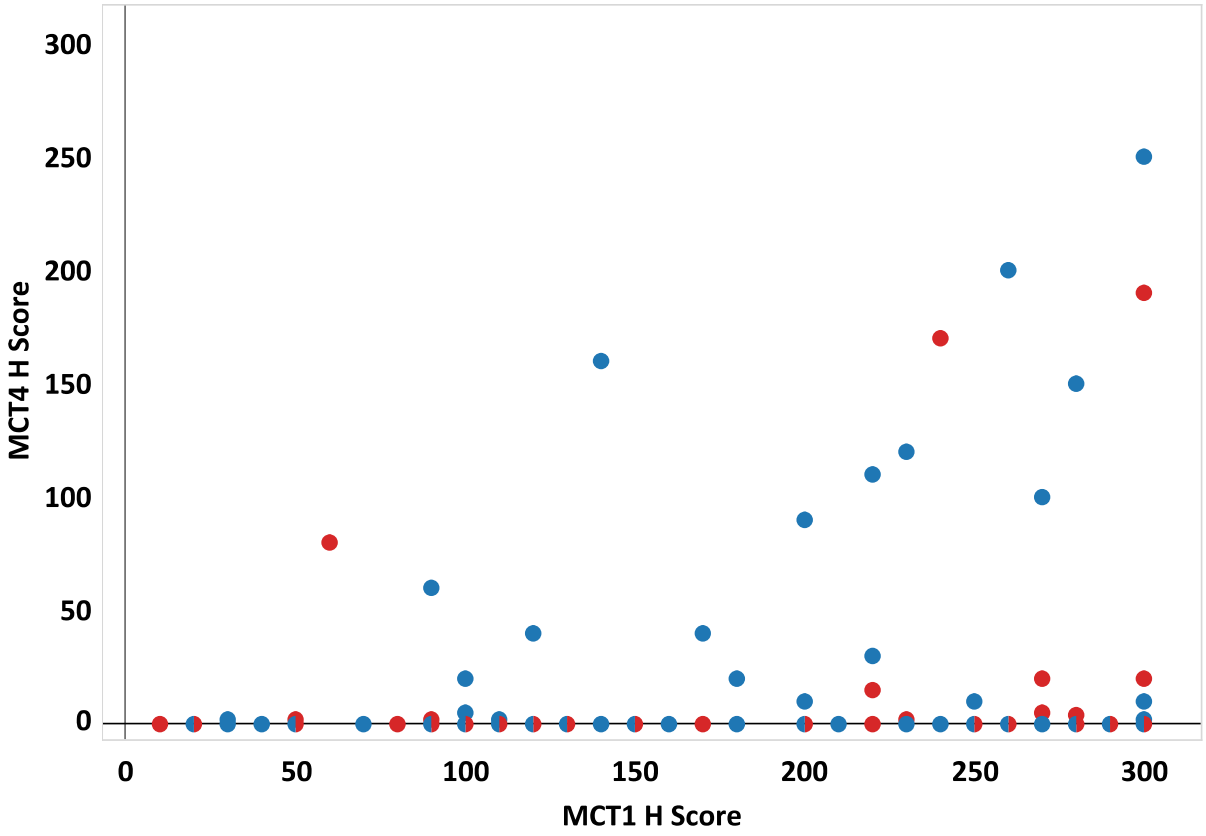

Figure 3-8: COO sub-types do not exhibit specific expression profiles of MCT1/4
Summary of immunohistochemical staining using H-scores for MCT1 and MCT4 in 120 DLBLC samples. Cell of origin classification are shown as ■(ABC), ■(GCB).

BL tumour specimens were less variable with a uniform high MCT1 with maximal H-scores for MCT1 in all samples and an absence of MCT4 protein in most cases although two samples from ulcerated intestinal BL tumours showed weak MCT4 staining concentrated to a small percentage of cells (H-score ≤10).

3.6. Discussion

Analysis of gene expression data (CCLE) showed the majority of DLBCL and BL cell lines to have comparatively low *MCT4* mRNA expression, which would be predicted to render them susceptible to MCT1 inhibition. This is in contrast to a number of solid tumour types which also express appreciable levels of *MCT4* mRNA. Indeed, MCT1 and 4 co-expression has been reported in a wide number of solid tumours, for example, in pancreatic adenocarcinoma (104)

Our analysis of BL indicates high levels of MCT1 protein expression largely in the absence of MCT4. MCT4 expression in BL where observed was extremely minor and associated with

ulcerated samples with high levels of inflammation which is potentially more consistent with MCT4 expression in macrophages as part of an inflammatory response (177).

Doherty *et al.* previously reported high levels of *MCT1* expression in BL correlating with high *MYC* expressing tumours, as well as *MYCN,* in *MYCN* amplified neuroblastoma (84). In such tumours, concurrently low *MCT4* expression was also a common feature. However, the same study also included analysis of 129 DLBCL patient samples and showed DLBCL to have comparatively low *MCT1* expression as well as increased expression of *MCT4* (GSE4475). This is in contrast to our IHC data where MCT4 expression was undetectable in the majority of DLBCL patient specimens. We also found no association between *MYC* rearrangement and MCT1 expression which may have been expected based on the role of MYC in the transcriptional regulation of *MCT1*.

Aside from post-transcriptional regulation of mRNA, which can of course influence protein translation and expression, the discrepancy between our data and that previously published may stem from methodological differences between IHC and gene expression analysis. IHC allows for information to be garnered about the location of a given protein within a cell but also which cells in a mixed population express that protein. Gene expression data will reflect a mixed cell population and not exclusively tumour cells; for example, in our IHC samples we observed MCT4 positive immune infiltrate, which could not be distinguished by gene expression analysis.

Previously, a subset of SCLC patient samples was identified as exhibiting high MCT1 and low MCT4 expression and (99). There was however a wide range of expression in both MCT1 and 4 across the patient cohort as a whole and this preferred phenotype represented the minority of patients where high MCT1 expression was found to be a poor prognostic factor. Therefore, identifying that low MCT4 expression is a common feature in DLBCL, in not only immortalised cell lines but also, more importantly, in patient samples regardless of COO classification, makes DLBCL an attractive patient population to target with MCT1 inhibition where patients have become refractory to current treatment options. Our analysis of MCT1 and 4 expression in cancer cell lines also highlights the potential for investigation into other disease types particularly in haematological malignancies such as B- and T-cell acute lymphoblastic leukaemia, chronic lymphocytic leukaemia, blast phase chronic myeloid leukaemia and mantle cell lymphoma.

Chapter 4. Anti-tumour activity of AZD3965 in BL and DLBCL models

4.1. Introduction

As previously discussed, the majority of pre-clinical data suggest that MCT4 expression is associated with resistance to MCT1 inhibition, offering a compensatory mechanism for lactate efflux (118). Consistent with this, knockdown of MCT4 sensitises cells to MCT1 inhibitors whereas over-expression of MCT4 or upregulation by HIF-1α activation increases resistance to MCT1 inhibition (99). Therefore our findings that, low MCT4 protein expression is found in the majority of DLBCL and almost all BL tumours suggest that MCT1 inhibition warrants further investigation in these diseases (Chapter 3). DLBCL and BL are both highly aggressive, highly proliferative malignancies (172). As such they demonstrate a particularly glycolytic phenotype thought to be due to an increased need for biosynthetic intermediates (178). Despite this, to date no studies have been reported on use of an MCT1 inhibitor in DLBCL. Together this provides a strong rationale for exploring the efficacy of AZD3965 in this setting.

The efficacy of AZD3965 and structurally related inhibitors has been investigated in a number of tumour models (Table 2). These and alternate approaches to MCT1 inhibition using less specific inhibitors or genetic approaches are discussed in Section 1.5. Previous literature data on MCT1 inhibition suggests a mixture of anti-proliferative and cell death effects in tumour cell lines with negligible expression of MCT4. In these settings MCT1 inhibition prevents lactate efflux attenuating cellular proliferation.

In vitro efficacy of AZD3965 has been examined in a number solid tumour models including small cell lung cancer, glioblastoma, colon adenocarcinoma and breast adenocarcinoma (Section 1.5.2.) (84, 98, 99, 132). In these solid tumour models growth inhibitory responses are partial. For example in SCLC, under normoxic conditions AZD3965 had maximal growth inhibitory responses of approximately 40% in cell models which lacked MCT4 expression, (99). *In vivo* MCT1 inhibition has been demonstrated to increase median survival by 30% in an intravenous Burkitt lymphoma model and also attenuates tumour growth in SCLC and breast adenocarcinoma xenograft models (84, 99). The *in vivo* efficacy of MCT1 inhibition *in vivo* has also been shown to be potentiated by radiotherapy or metformin treatment (133).

4.2. Aims

Having identified a number of BL and DLBCL cell lines without MCT4 by analysis of available gene expression data, western blotting and immunohistochemistry (Section 3.4); we aimed to use these models to examine the activity of AZD3965 *in vitro* and *in vivo*.

In each cell line *in vitro* we aimed to determine:

- The extent of lactate accumulation
- The effect this had on tumour cell growth
- The effect on tumour cell viability

In addition, we also aimed to examine the *in vivo* efficacy of AZD3965 treatment in a BL model.

4.3. MCT1 inhibition causes lactate accumulation in BL and DLBCL cell lines which express MCT1 but lack MCT4

As a key transporter of lactate, one of the primary pharmacodynamic endpoints predicted following inhibition of MCT1 is an increase in intracellular lactate. We analysed the intracellular lactate concentrations in our cell panel using a biochemical assay (Figure 4-1).

The basal level of intracellular lactate varied across the cell panel potentially reflecting differences in glycolytic flux, ranging from undetectable levels to 7 $\mu g.mg^{-1}$ protein. Vehicle treatment had no effect on this intracellular lactate (<10 $\mu g.mg^{-1}$). A number of published studies have measured lactate ≤24 hours (133). We therefore measured intracellular lactate following 24 hour treatment with AZD3965 (1 µM). All MCT4 negative cell lines showed a significant increase in the level of intracellular lactate relative to vehicle control ($P \leq 0.05$). This dose was chosen as previous studies indicated it was a dose associated with a maximal growth inhibitory response but was unable to inhibit MCT4 activity (119, 138). In these cell lines the mean lactate concentration was 49 $\mu g.mg^{-1}$, with fold increases ranging from 4.6 to 33.3 fold of control. There was, however, great variability, both in terms of the absolute levels of lactate achieved and the fold-increase over vehicle treated cells. The highest intracellular lactate concentrations achieved following AZD3965 treatment were measured in Farage cells (>100 $\mu g.mg^{-1}$), which were observed to be particularly proficient at acidifying media, as indicated by the change in phenol red indicator colour in the media (red to yellow)

evident during cell culture under basal conditions. This is in line with a high rate of lactate/H^+ efflux and may indicate an especially glycolytic phenotype. BL cell lines, Raji and Ramos displayed the greatest fold-increase over vehicle treated cells because of their particularly low basal intracellular lactate concentrations. Basal levels of intracellular lactate were undetectable in Raji and AZD3965 induced a 33-fold increase in basal lactate concentrations in Ramos.

In contrast, the MCT4 expressing cell line, BJAB, did not demonstrate significantly elevated intracellular lactate following AZD3965 treatment (P = 0.16). This supports the compensatory role of MCT4 as an alternative lactate transporter following MCT1 inhibition in these cells.

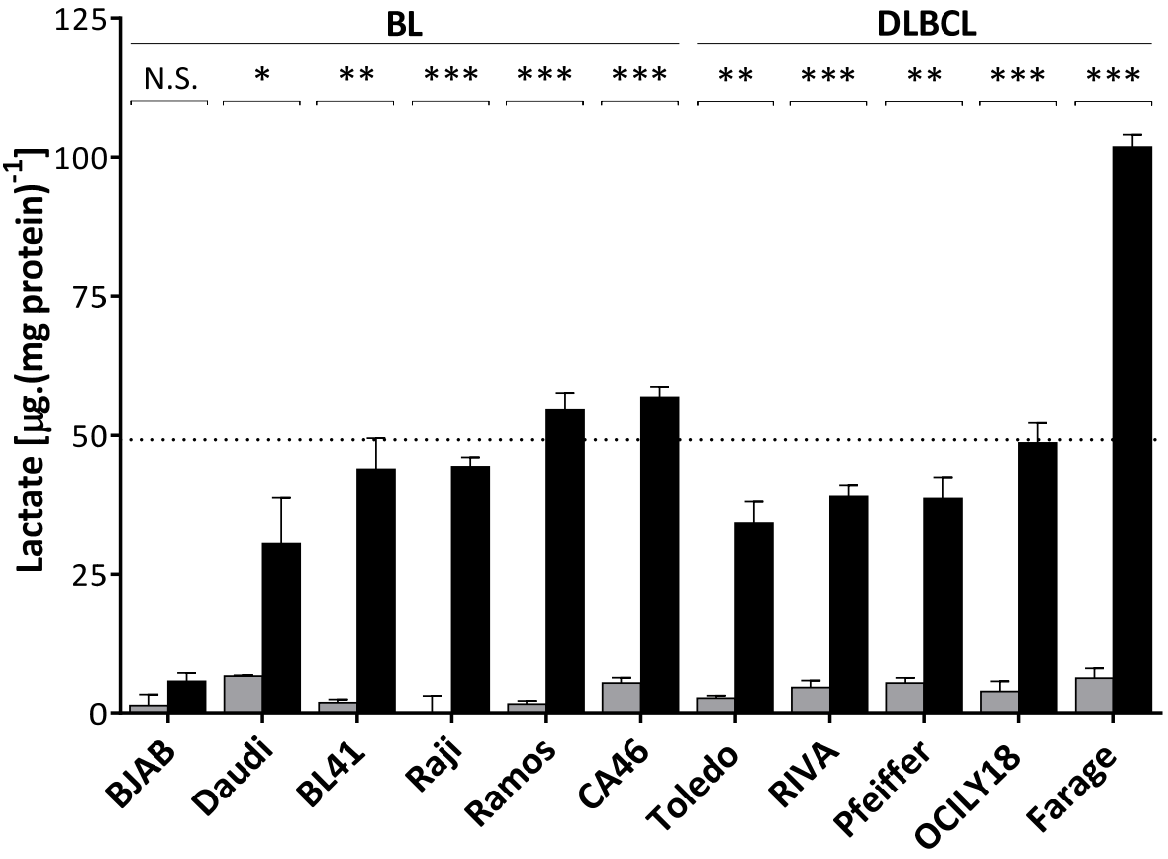

Figure 4-1: AZD3965 increases intracellular lactate in human lymphoma cell lines
Intracellular lactate was measured in cells following exposure to AZD3965 (1 µM) (■) or DMSO (■) vehicle for 24 hours as described in Section 2.5. Values shown have been normalised to protein content via BCA assay. The mean concentration of intracellular lactate following treatment with AZD3965 in MCT4 negative cell lines is indicated (┅). Data shown are the mean + SEM of at least three independent experiments. P-values were calculated using an unpaired Student's *t*-test (*P ≤ 0.05, **P ≤ 0.01 ***P ≤ 0.001).

4.4. Time and dose-dependency of lactate accumulation in CA46 cells

After demonstrating that 24-hour exposure to AZD3965 was sufficient to observe significant increases in intracellular lactate we sought to determine how rapidly lactate accumulation could be detected and whether it was maintained over a period that would be consistent with any potential growth mediated effects of the compound. In CA46 cells AZD3965 induced a rapid accumulation of intracellular lactate which was detectable after 30 minutes exposure at a dose of 100 nM or greater (Figure 4-2). At lower doses, (10 nM) lactate accumulation occurred at a slower rate. Despite this, the time to reach maximal concentration of lactate, $T_{max,}$ was observed at 6 hours across all tested doses of AZD3965. Conversely, the maximal concentration achieved, C_{max}, showed some dose dependency after 6 hours (82-105 µg.mg^{-1} protein) but increases from 10-1000 nM were not dose proportional and levels were equivalent after 24 and 72 hours. Also, whilst the intracellular lactate remained significantly elevated relative to control, after 72 hours, lactate was not maintained at peak levels with a notable reduction from 6 to 24 hours. Levels between 24 and 72 hours were largely similar.

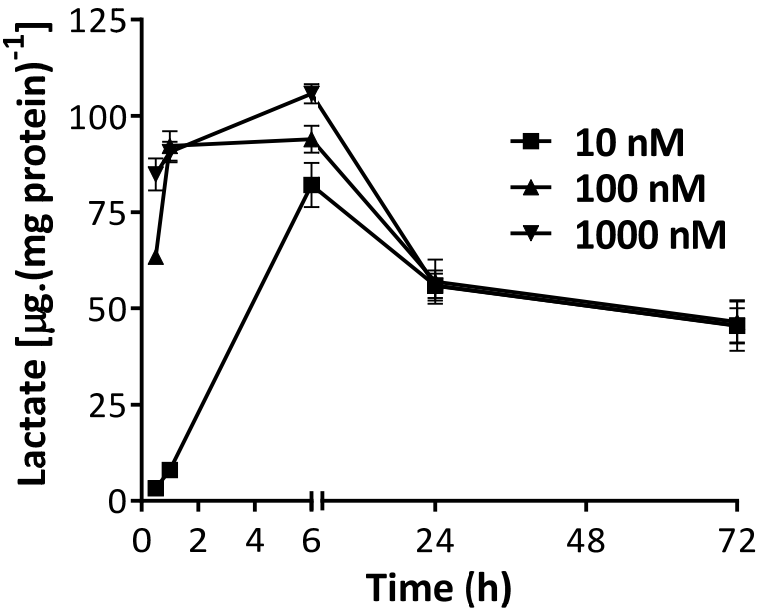

Figure 4-2: AZD3965 triggers a rapid and sustained accumulation of lactate in CA46 cells
Intracellular lactate was measured in CA46 cells following exposure to AZD3965 (10-1000 nM) or DMSO vehicle at the indicated time-points (0.5-72 hours) as described in Section 2.5. Values shown have been normalised to protein content via BCA assay. Data shown are the mean + SEM of three independent experiments.

4.5. Growth inhibitory effects of AZD3965 in Burkitt and DLBCL cell line models

The effect of AZD3965 treatment on lymphoma cell proliferation was investigated in cell lines over 72 hours using an XTT assay. Data were normalised to DMSO vehicle treated cells and expressed as percentages of control. Any cell growth between cell seeding and dosing was also accounted for. AZD3965 potently inhibited the growth of both BL and DLBCL in cell lines where significant lactate accumulation was observed. The half-maximal growth inhibitory concentration or the concentration associated with 50% growth inhibition (GI_{50}) values ranged from 3-40 nM (Figure 4-5). In contrast, AZD3965 did not affect the proliferation of BJAB cells (GI_{50} > 10 µM) which express MCT4 and consequently do not exhibit lactate accumulation following AZD3965 treatment. The maximal level of growth inhibition observed in AZD3965 sensitive cell lines ranged from 64-99% (Figure 4-3, Figure 4-4). BL41 and RIVA were marginally less sensitive than the other MCT4 negative cell lines which all shared GI_{50} values below 10 nM and ≥ 90% growth inhibition. The remaining cell lines exhibited comparable levels of sensitivity.

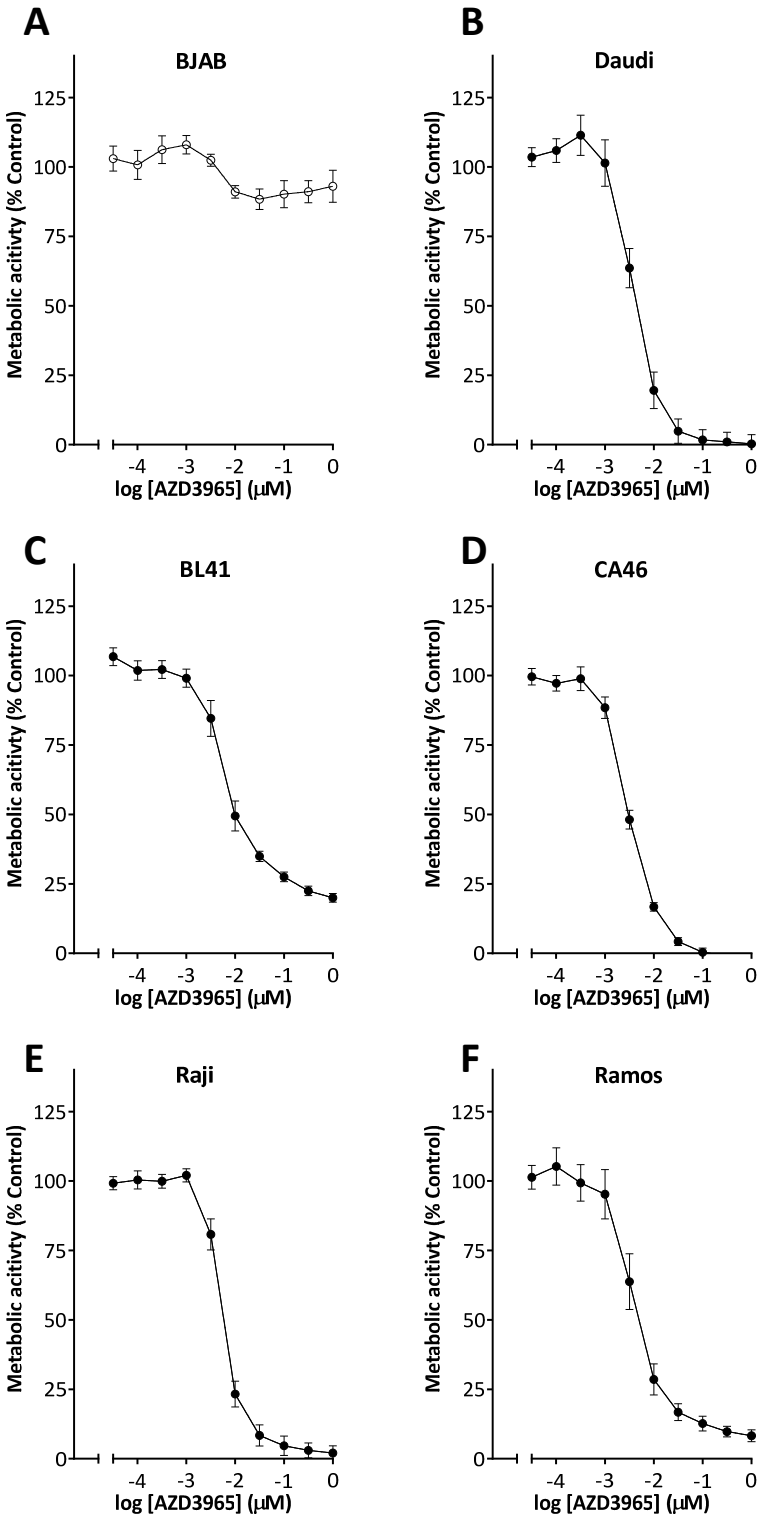

Figure 4-3: AZD3965 has growth inhibitory activity in BL cell lines
Exponentially growing Burkitt lymphoma cells were treated with increasing concentrations of AZD3965 for 72 hours before assessing metabolic activity in the cell population as a surrogate for cell number using an XTT assay, as described in Section 2.6. Individual dose-response curves are shown for BJAB (A), Daudi (B), BL41 (C), CA46 (D), Raji (E) and Ramos (F). Metabolic activity as a percentage of control was calculated relative to DMSO (0.01%) treated control cells after correcting for proliferation between seeding and dosing T_0. Data shown are the mean ± SEM of between three and nine independent experiments.

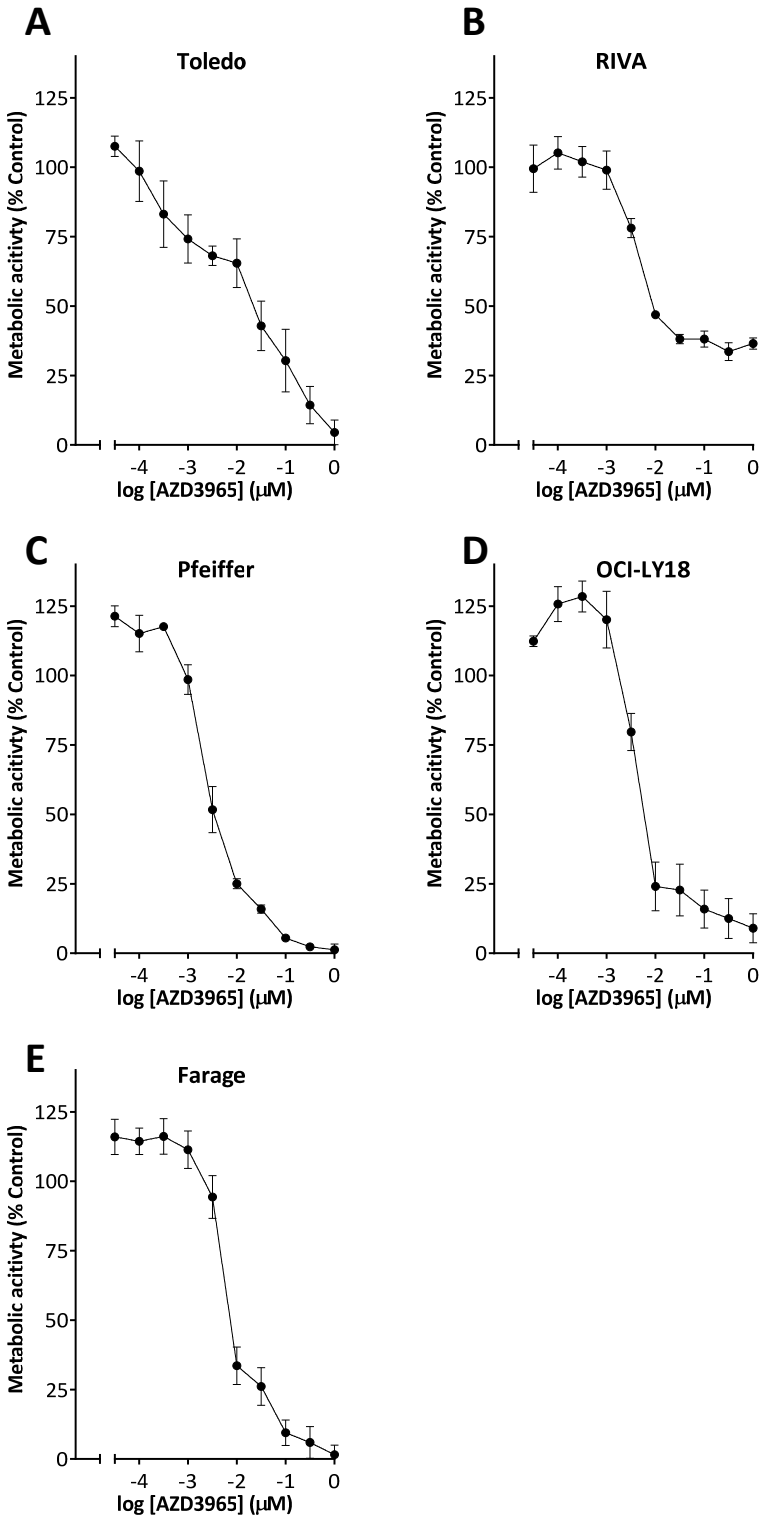

Figure 4-4: AZD3965 has growth inhibitory activity in DLBCL
Exponentially growing Diffuse Large B-cell lymphoma cells were treated with increasing concentrations of AZD3965 for 72 hours before assessing metabolic activity in the cell population as a surrogate for cell number using an XTT assay, as described in Section 2.6. Individual dose-response curves are shown for Toledo (A), RIVA (B), Pfeiffer (C), OCILY18 (D) and Farage (E). Metabolic activity as a percentage of control was calculated relative to DMSO (0.01%) treated control cells after correcting for proliferation between seeding and dosing T_0. Data shown are the mean ± SEM of between three and nine independent experiments.

Although lactate accumulation appears a prerequisite for sensitivity to AZD3965 neither GI_{50} values nor the maximal growth inhibition observed were found to correlate with the level of lactate accumulation observed. For example, Farage were subject to the highest concentrations of intracellular lactate by around two-fold but shared a similar GI_{50} with a number of other cell lines including OCILY18, Raji and Ramos.

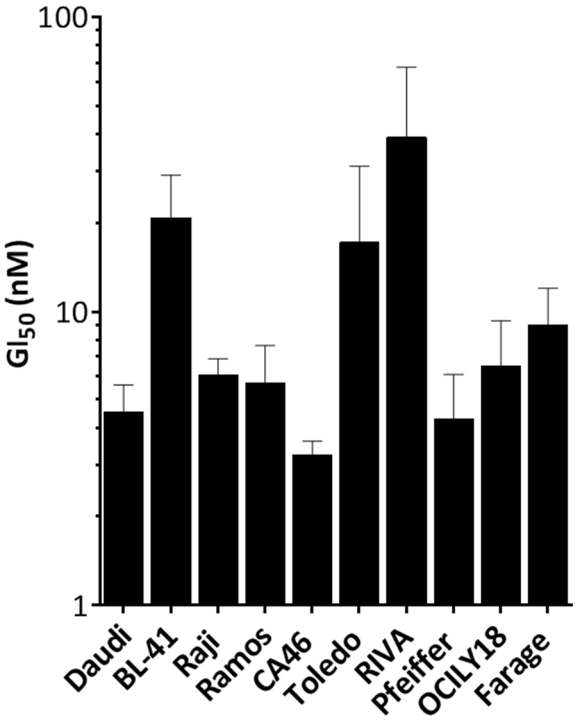

Figure 4-5: Sensitivity of B-NHL cell lines to AZD3965
GI_{50} values as determined by XTT assay after 72 hour treatment with AZD3965. GI_{50} was defined as the dose required to inhibit the metabolic reduction of XTT by 50%. Data shown are the mean + 95% CI of between three and nine independent experiments.

4.6. AZD3965 is predominantly cytostatic as a monotherapy

As the XTT assay is a measure of metabolic activity within a cell population it does not definitively indicate an alteration in cell number or inform the mechanism behind any such changes (Section 2.6.1.). We therefore performed cell counts across the cell panel following 72 hours exposure to AZD3965 or a known cytotoxic agent, doxorubicin. Doxorubicin is utilised as part of combination chemotherapy regimen, R-CHOP, for the treatment of both BL and DLBLC. A dose of doxorubicin (1 μM) was chosen based on previous dose-response data using daunorubicin in Raji where this dose was associated with ~95% growth inhibition by XTT assay following 72 hour exposure (119).

Cell viability was assessed using trypan blue. Viable cells with intact plasma membranes are non-permeant to trypan blue whilst those who have lost membrane integrity through late-apoptosis or necrosis stain blue. We found that despite profound reductions in cell number relative to vehicle treated control there was little evidence of reduced cellular viability suggesting an anti-proliferative cytostatic rather than a cytotoxic effect (Figure 4-6). Following 72 hour exposure to AZD3965, a significant decrease in cell viability relative to vehicle treated control was detected in one cell line only. A decline of approximately 15% in cell viability was detected in Farage cells however the observed reduction would be insufficient to account for such a marked reduction in cell number ($P = 0.005$). In contrast to the response to AZD3965, all cell lines exhibited significantly reduced cell viability > 50% following exposure to the topoisomerase II poison, doxorubicin (1 µM) ($P < 0.001$).

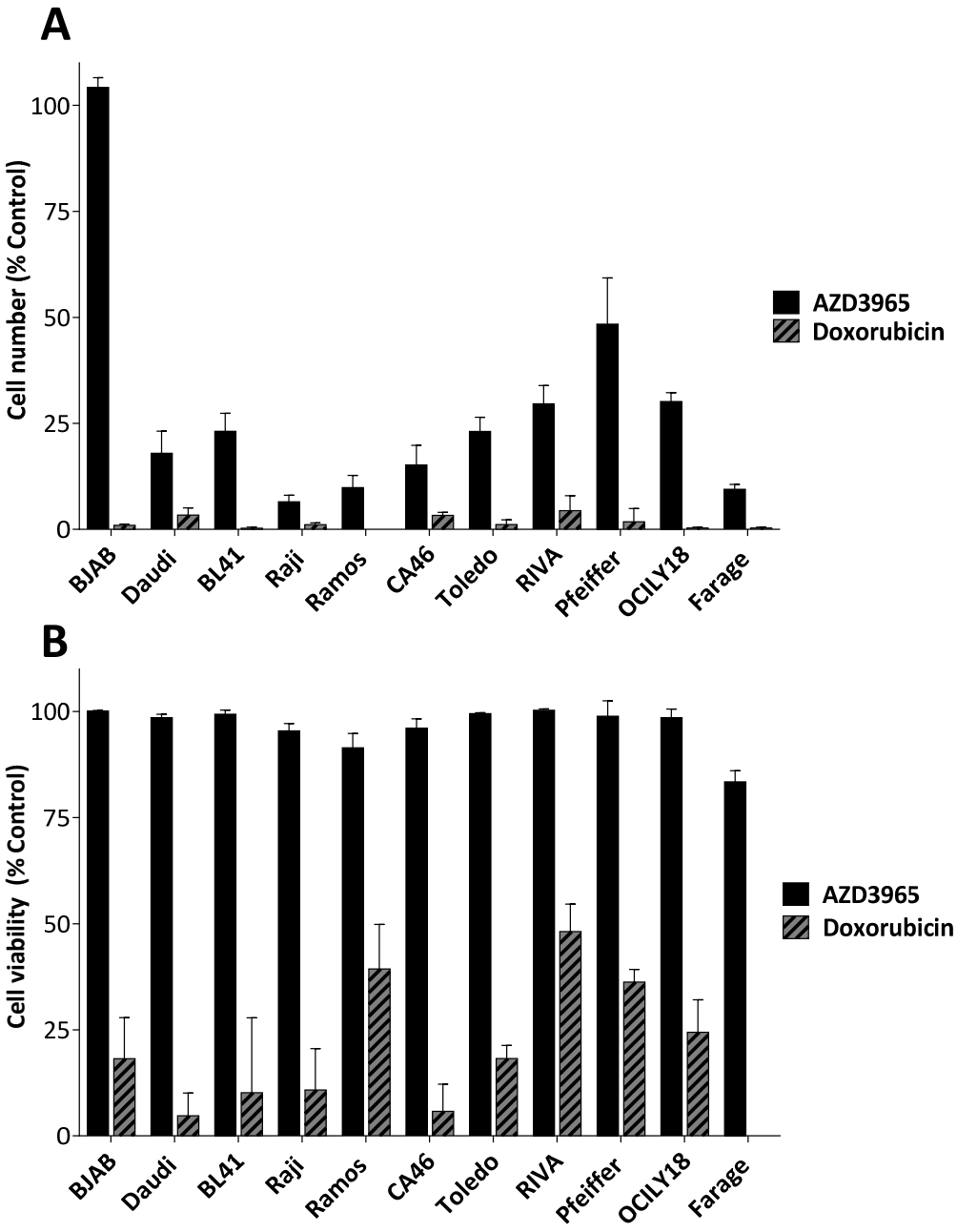

Figure 4-6: AZD3965 is cytostatic in DLBCL and BL which lack MCT4
Exponentially growing BL or DLBCL cells were treated with AZD3965 (100 nM) or doxorubicin (1 μM) for 72 hours before performing cell counts using a hemocytometer. Cell number (A) data are shown as a percentage of each corresponding cell line matched DMSO (0.01%) treated control population. Cell viability (B) as assessed by trypan blue exclusion are shown as percentage of trypan blue excluding cells. Data shown are the mean ± SEM of three independent experiments.

A previous report has shown treatment with 100 nM of two other selective MCT1 inhibitors (AR-C122982 and AR-C155858) to be initially growth inhibitory but induce a protracted cell death following extended incubations of 72 – 120 hours in Raji cells (84). We took 100 nM, equivalent to a GI_{95} dose determined over a 72 hour incubation, and looked for evidence of

cell death after a 120 hour drug incubation. We observed a maximum of 24% reduction in cell viability after 120 hours in Raji (P = 0.023), substantially less than the reported 50% reduction reported by Doherty *et al.* under comparable conditions with AR-C155858 (84). In contrast, CA46 cells did not show any appreciable change in cell viability (>95% of vehicle control) after a 120 hour drug incubation (Figure 4-7).

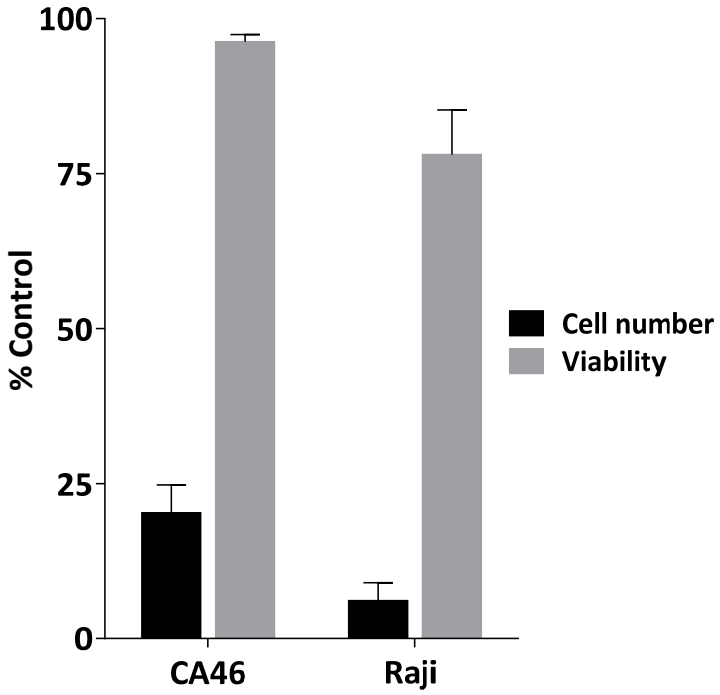

Figure 4-7: Extended incubation with AZD3965 does not induce substantial cell death
CA46 or Raji cells were treated with AZD3965 (100 nM) for 120 hours before performing cell counts using a heamocytometer. Cell number (■) and cell viability (■) data are shown as a percentage of the respective cell line matched, DMSO (0.01%) treated control population. Cell viability was assessed by trypan blue exclusion. Data shown are the mean ± SEM of three (CA46) or four (Raji) independent experiments.

4.7. AZD3965 causes lactate accumulation *ex vivo*

Before testing the efficacy of AZD3965 *in vivo* we wanted to confirm that acute oral treatment with AZD3965 (2 hours) was sufficient to induce significant lactate accumulation in comparison to tumours from vehicle treated mice (Figure 4-8). The chosen oral dose of AZD3965 (100 $mg.kg^{-1}$) is sufficient to yield non-protein bound plasma concentrations of AZD3965 consistent with MCT1 inhibition (99). Subcutaneous Raji or CA46 tumours were allowed to establish in NSG mice to an approximate volume of 500 mm^3 and then dosed with a single oral dose of AZD3965 (Section 2.5.3.). Basal levels of lactate were higher *in vivo* versus *in vitro.* Although statistically significant (P < 0.05), the degree of lactate accumulation

relative to control tumours was less pronounced than observed in this cell line *in vitro*. The protein-normalised lactate concentrations were also lower *in vivo* in both CA46 and Raji, relative to the cell-line matched *in vitro* measurements.

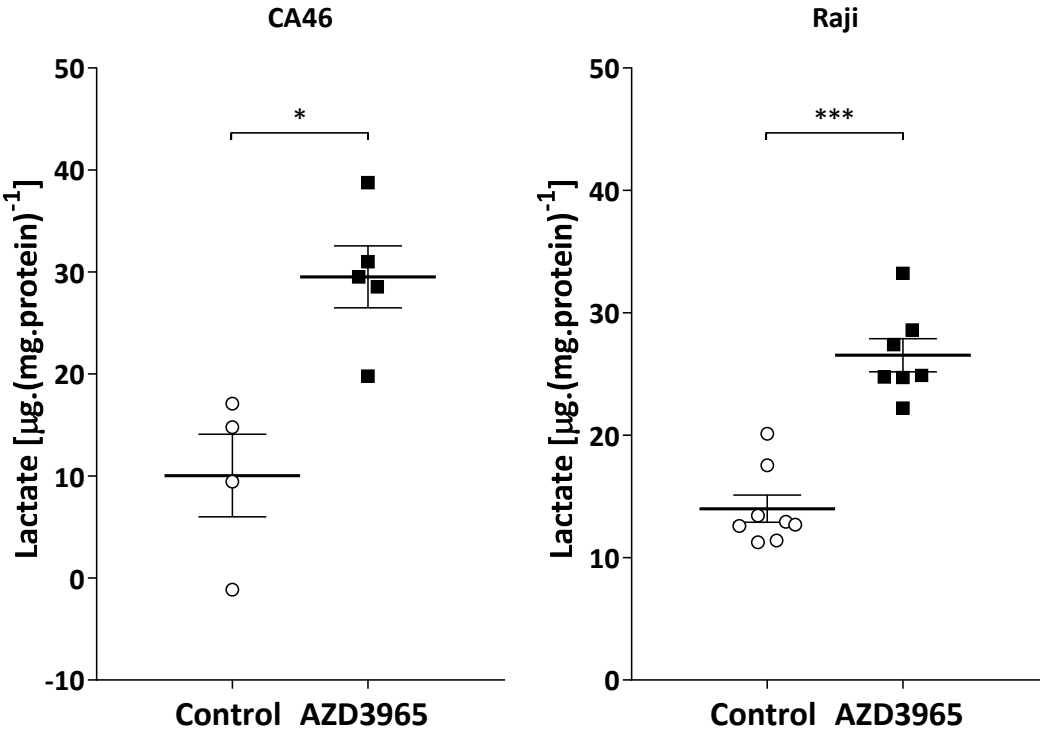

Figure 4-8: Acute oral treatment with AZD3965 induced lactate accumulation in BL tumour xenografts
Concentrations of tumour lactate were measured in subcutaneous BL xenografts taken 2 hours following oral administration with AZD3965 (100 mg.kg^{-1}) or vehicle as indicated. Intracellular lactate concentrations were determined *ex vivo* by biochemical assay and normalised to protein as described in Section 2.5. P-values were calculated using an unpaired Student's *t*-test (*P ≤ 0.05, **P ≤ 0.01 ***P ≤ 0.001).

4.8. AZD3965 monotherapy substantially reduces CA46 cell proliferation *in vivo*

Having shown that the necessary elevation in intracellular lactate could be detected *ex vivo* following AZD3965 treatment we next sought to assess the efficacy of AZD3965 *in vivo*. CA46 cells were chosen to investigate the *in vivo* efficacy of AZD3965 as they were representative of a highly sensitive but predominantly cytostatic phenotype and we were interested to define what level of *in vivo* efficacy this may achieve.

Drs. Natalie Bell and Simon Bomken (NICR), engineered CA46 tumour cells to ectopically express firefly luciferase allowing their growth to be determined by bioluminescent *in vivo* imaging following intravenous inoculation as described in Section 2.11. Briefly, the tumour cells were engineered to express the luciferase gene so upon intraperitoneal injection of luciferin a luminescent signal can be detected which is proportional to the number of CA46 cells present in the mouse. This allows disease progression burden and localisation to be tracked non-invasively in an intravenous model. The intravenous model more accurately recapitulates human BL versus subcutaneous models of lymphoma, in that tumour engraftment is evident in the spleen, bone marrow of and the kidneys of mice.

Initial tumour engraftment was confirmed 6 days after the inoculation of CA46 cells as described in Section 2.11. On commencement of dosing, treatment groups had comparable levels of engraftment ($P > 0.05$ unpaired *t*-test). Mice were treated orally with either AZD3965 (100 $mg.kg^{-1}$) or vehicle (both administered twice-daily Monday to Friday and once-daily at weekends) for a period of 24 days. This dosing schedule was similar to that used previously and was found to be well tolerated with no significant changes in body weight observed (*data not shown*) (99, 133).

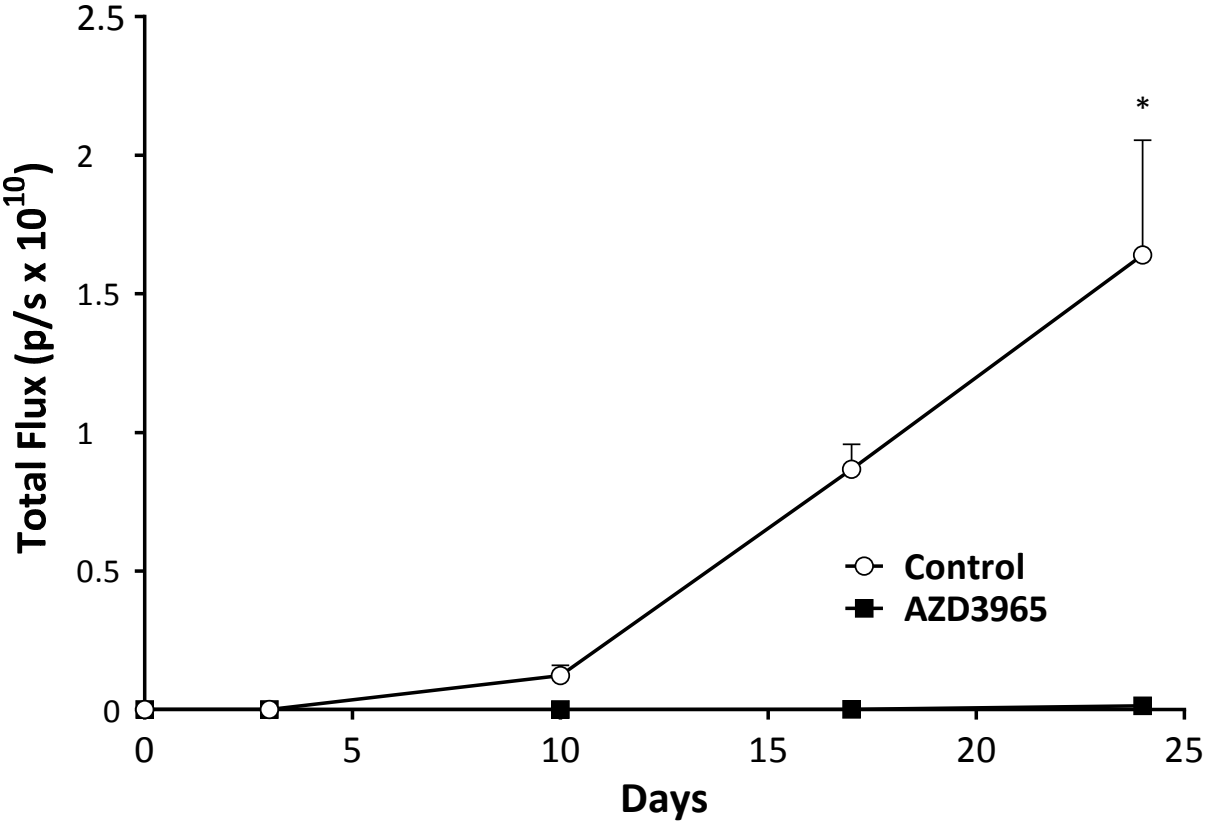

Figure 4-9: Efficacy of AZD3965 in an intravenous *in vivo* model of Burkitt lymphoma
NSG mice were transplanted with luciferase-expressing CA46 cells and treated with AZD3965 (100 mg.kg^{-1}, BID) or vehicle control for 24 days, following successful engraftment (6 days). Scans were performed at 3,10,17 and 24 days of treatment as described in Section 2.11. Data points show the mean + SEM of n=8 vehicle treated n=7 AZD3965 treated animals on a linear scale.

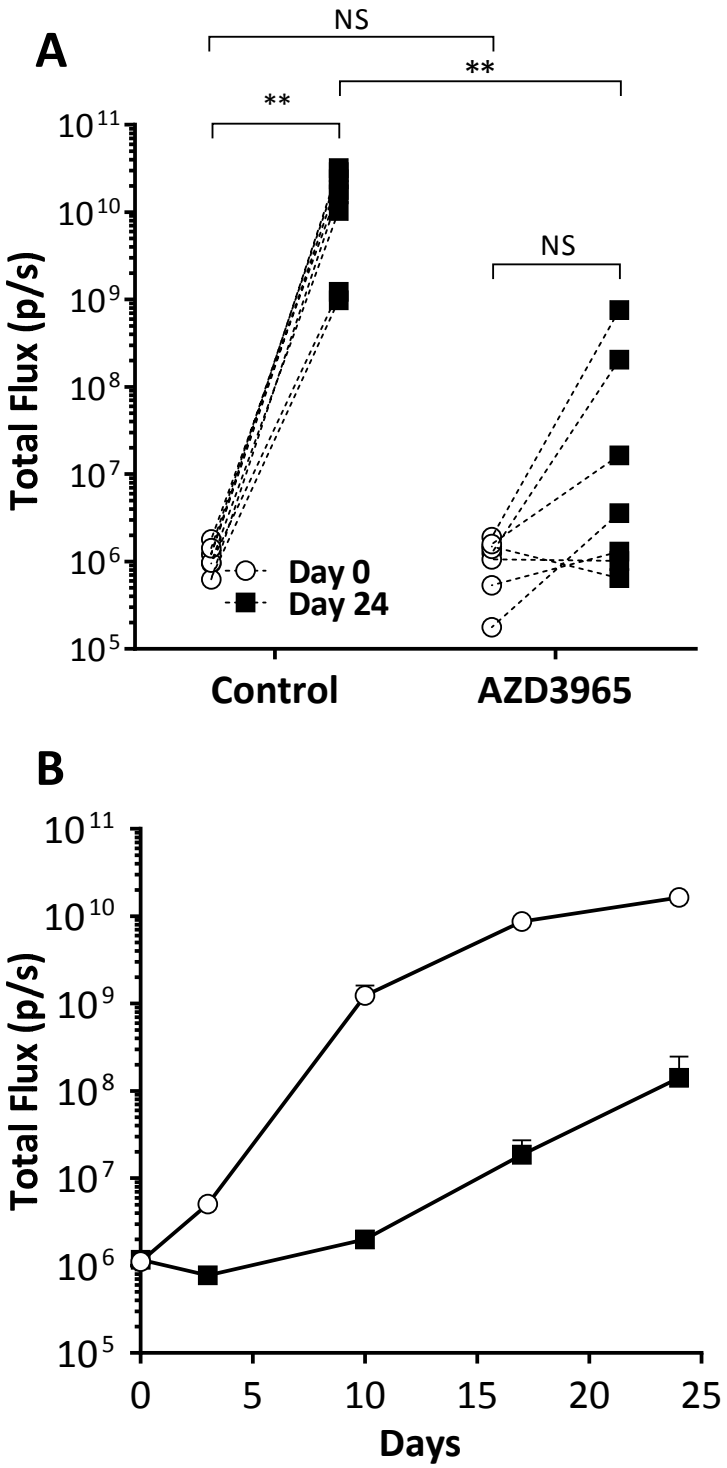

Figure 4-10: AZD3965 attenuates CA46 xenografts growth
NSG mice were transplanted with luciferase-expressing CA46 cells and treated with AZD3965 (100 mg.kg^{-1}, BID) or vehicle control for 24 days, following successful engraftment (6 days). A, the individual responses of mice treated with vehicle or AZD3965 pre-treatment (day 0) and post-treatment (day 24). Comparisons of paired samples pre-treatment and post-treatment. Significance was assessed by paired two-tailed *t*-test. Comparison between treatment groups before and after treatment. Significance was assessed by unpaired two-tailed *t*-test (*P ≤ 0.05, **P ≤ 0.01 ***P ≤ 0.001). B, Scans were performed at 3,10,17 and 24 days of treatment as described in Section 2.11. Data points show the mean + SEM of n=8 vehicle treated n=7 AZD3965 treated animals.

Bioluminescence was measured using the IVIS Spectrum® 3 days after the start of treatment and at weekly intervals to determine total tumour burden. AZD3965 treatment for 24 days was associated with a profound and statistically significant cytostatic response, inhibiting tumour burden relative to vehicle treated animals by 99%, as ascertained by bioluminescence imaging (P = 0.0029 unpaired two-tailed *t*-test) (Figure 4-9).

Luminescence signal was significantly higher in vehicle treated mice post treatment (day 24) in comparison to pre-treatment levels consistent with increased engraftment (P = 0.0055 paired *t*-test) (Figure 4-10, Figure 4-11). The post-treatment signal was not significantly elevated in the AZD3965 treated group (P > 0.05 paired two-tailed *t*-test) (Figure 4-10, Figure 4-12). Although not statistically significant, a small but consistent increase in flux values across the timecourse was observed in the AZD3965 treated group indicating some tumour progression still occurred under treatment as indicated by increasing flux values (Figure 4-9, Figure 4-11)

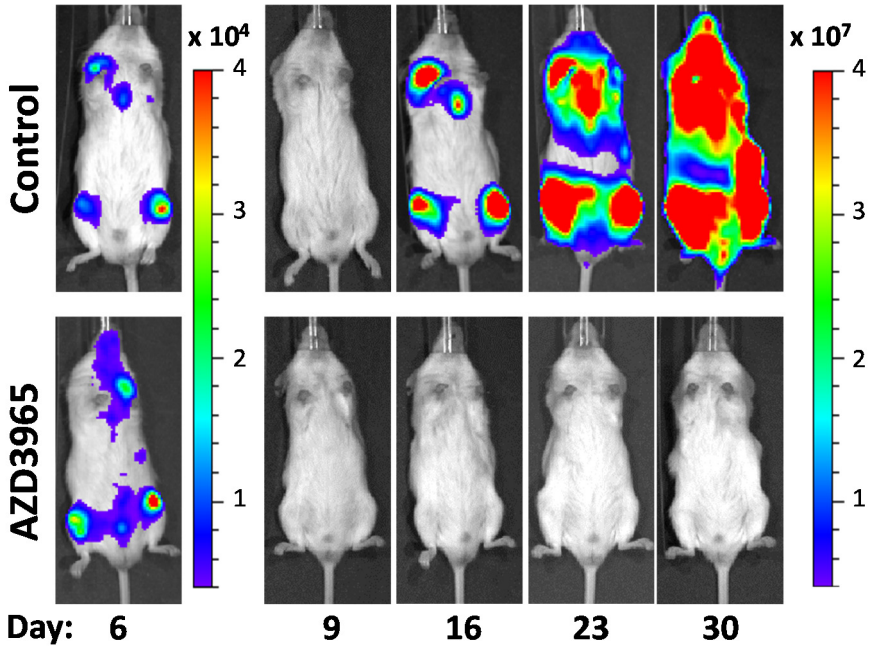

Figure 4-11: Bioluminescence of CA46 xenografts following treatment with AZD3965
Representative images of an individual mouse from AZD3965 and vehicle treated groups showing the expansion of luciferase-expressing transduced CA46 cells over time. Mice prior to treatment period (day 6) and during treatment are shown on different radiance scales (p/sec/cm^2/sr) to avoid excessive image saturation.

The bioluminescent signal was localised to the femurs, spleen and head of mice. Tissues taken at necropsy confirmed substantially reduced signs of engraftment in AZD3965 treated animals evidenced by the complete lack of human CD20 staining in spleen and bone marrow

sections and normal spleen weight in contrast to vehicle treated mice which showed enlarged spleens positive for human CD20 (Figure 4-13). Only 8% (1/13) of recovered femurs from AZD3965 treated mice showed engraftment in contrast to 86% (12/14) of vehicle treated mice.

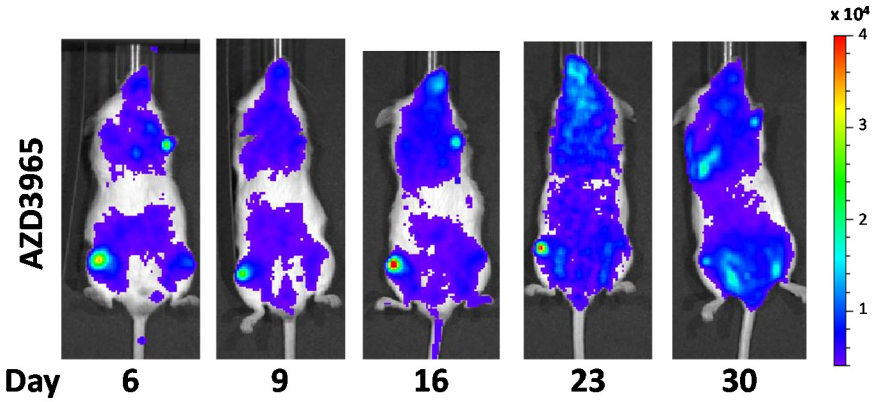

Figure 4-12: Time course of CA46 engraftment in mice receiving AZD3965
Representative images of an individual AZD3965-treated mouse showing the expansion of luciferase-expressing transduced CA46 cells over time on a consistent radiance scale (p/sec/cm^2/sr).

.

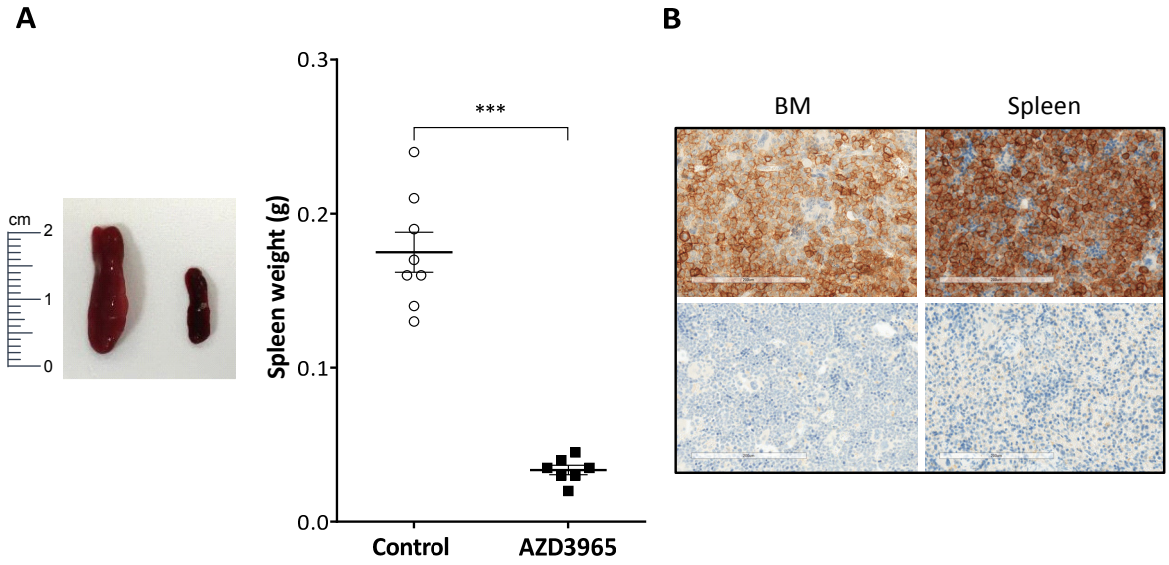

Figure 4-13: AZD3965 reduces spleen and bone marrow engraftment of BL
Spleen weights were recorded post treatment, a representative image of an enlarged vehicle treated spleen is shown alongside a spleen taken from an AZD3965 treated mouse. Also shown are the individual spleen weights for each mouse (A). Reference non-engrafted spleen weights of NSG mice are typically 0.025-0.03 g (*data not shown*) (159). Representative immunohistochemical analysis of human CD20 in spleen sections and bone marrow sections from mice treated with AZD3965 or vehicle control. Scale bar = 200 μM (B)

4.9. Discussion

AZD3965 had a highly potent and significant growth inhibitory effect, inducing lactate accumulation across a panel of BL and DLBCL cell lines. The accumulation of intracellular lactate following MCT1 inhibition in cell lines lacking MCT4 is consistent with a blockade of lactate efflux. In contrast, the MCT4 expressing cell line, BJAB, did not accumulate lactate nor were they subject to growth inhibitory effects of AZD3965. In MCT4 negative cells intracellular lactate was comparable between 24 and 72 hour measurements which may indicate either an equilibrium between lactate generation and utilisation or that lactate generation via glycolysis ceases and only the remaining lactate is trapped within the cell. AZD3965 caused a rapid accumulation of lactate in CA46 (< 30 min) and to better define T_{max}, associated with tested doses of AZD3965 an increased number of timepoints giving a higher resolution timecourse may be necessary.

AZD3965 appears to induce a predominantly growth inhibitory effect rather than a cytotoxic response even under prolonged exposures. This is in line with published data using knock-down approaches and low-specificity MCT1 inhibitors where MCT1 inhibition did not induce cell death under standard growth conditions (108). A statistically significant 24% drop in cell viability was observed in Raji following 120 hour exposure but to a lesser extent than previously suggested using the similarly potent and selective compound AR-C155858 (84). This suggests some cell death may occur, but conversely the very limited cell death in CA46 cells, suggests that a purely cytostatic response may be evident in responsive tumours.

Interestingly, the degree of lactate accumulation did not correlate with levels of MCT1 expression or magnitude of antiproliferative effect as indicated by GI_{50} value. This suggests MCT1 expression alone may be a poor predictor of cell line sensitivity to AZD3965 treatment. It remains unclear whether there is a threshold concentration of intracellular lactate beyond which cells cannot continue to proliferate or whether the basal phenotype of the cell influences this threshold such that certain cells can tolerate a higher concentration of lactate than others can. It is notable, considering the vast plasticity between metabolic pathways, that targeting a single transporter, MCT1, has such profound effects on cell proliferation.

In respect to lactate accumulation, AZD3965 caused a greater fold-accumulation in CA46 and Raji cells *in vitro* (> 10-fold), than when grown as subcutaneous xenografts *in vivo* (2-3 fold). In addition to differences between the *in vitro* and *in vivo* environments, *in vitro* lactate

measurements were made following longer exposure to AZD3965 which may partly explain the higher lactate concentrations observed.

Despite the profound growth inhibition observed *in vivo*, we also detected increasing tumour burden across the treatment period. We hypothesise that AZD3965 does not induce CA46 cell death *in vivo* in line with our *in vitro* observations. The pharmacokinetics of AZD3965 necessitate twice-daily dosing in order to maintain plasma drug levels consistent with MCT1 inhibition (138). Similarly, twice-daily dosing of the compound is also under investigation in first-in-man studies. In doing so, the dose-limiting toxicities associated with higher doses that are necessary to maintain active concentrations throughout for 24 hours will hopefully be avoided (179). Therefore, our once-daily dosing over weekends may have potentially allowed for some level of increased proliferation as MCT1 inhibition is not maintained throughout the entire treatment period and so this may have led us to underestimate the efficacy of AZD3965. Alternatively, a minor clone within the tumour cell population may have developed adaptive resistance to AZD3965 which may account for the increase in tumour burden.

A sub-set of DLBCL lines have been classified by Consensus cluster classification (CCC) using gene expression profiles enriched in oxidative phosphorylation (OXPHOS) genes or B-cell receptor signalling (BCR) (Section 3.3.1.) (167, 180). Perhaps surprisingly, we identified no discernible difference between, Farage and OCILY18 (BCR) and Pfeiffer and Toledo (OXPHOS) in their sensitivity to AZD3965. (167), (181). Although we did not assess the relative contributions of oxidative phosphorylation and glycolysis in these lines, previous reports by Caro *et al.* show that the functional differences (OXPHOS vs. BCR) in OCR contribution are greatest in terms of mitochondrial fatty acid oxidation of palmitate, but that OCR was not different between OXPHOS and BCR subtypes being fuelled by glucose (167). This suggests that Pfeiffer and Toledo may not exhibit increased OXPHOS in standard RPMI media conditions with high glucose (11 mM) and no palmitate or other fatty acids, which might explain why the comparable responses to MCT1 inhibition between OCR and BCR subtypes were observed in this study. An alternative classification system, Cell of origin (COO), splits DLBCL into cells derived from germinal centre B-cells (GCB) or activated B-cells (ABC). Both GCB and ABC-DLBCL are represented although RIVA, represent the only activated B-cell (ABC-DLBCL) line studied (182, 183). Since RIVA are not as sensitive as the other MCT4 negative cell lines tested in terms of maximal growth inhibition without other examples of ABC-

DLBCL, we cannot definitely conclude whether this is a property linked to Cell of Origin status.

Although in the context of the BL and DLBCL lines studied here, lactate accumulation in the absence of MCT4 appears necessary for the growth inhibitory effects of the compound, lactate accumulation *per se* is not sufficient to denote sensitivity to AZD3965. Previous work in the neuroblastoma cell line, SH-SY5Y, show that despite the desired MCT profile and lactate accumulation, growth inhibition was not observed (119). Similarly the SCLC cell line, COR-L103 were as resistant to AZD3965 under normoxic conditions but became more sensitive under hypoxic conditions (99). AZD3965 also significantly inhibited growth of COR-L103 xenografts but did not cause tumour regression. This is consistent with AZD3965 having growth inhibitory rather than cytotoxic effects.

Here we show AZD3965 has a profound cytostatic effect in BL and DLBCL, including in an *in vivo* model of BL. These effects are associated with increased intracellular lactate in cells lacking MCT4. This corroborates previous work, with other MCT1 inhibitors in Raji cells but now confirms the efficacy of the clinical candidate, AZD3965 in a wider cohort of BL cell lines, and demonstrates efficacy in a novel disease area, DLBCL. However, the lack of cell death *in vitro* or inability to induce tumour regression *in vivo,* indicates a need to identify effective combination strategies in order to reduce tumour burden.

Chapter 5. Metabolic consequences of MCT1 inhibition

5.1. Introduction

The increased generation of lactate as an end-product of glycolysis even under aerobic conditions is believed to support the increased anabolic demands cancer cells have for ATP and biosynthetic intermediates (184). We have demonstrated in Chapter 4 that interfering with the removal of this lactate from cells by inhibiting MCT1 causes a rapid and sustained accumulation of lactate which is detrimental to cell proliferation. However, how lactate accumulation interferes with cellular metabolism to limit proliferation is less clear.

A number of studies have reported downstream metabolic changes following MCT1 inhibition but these show varying effects depending upon the cell model being studied. In glycolytic *MYC* amplified cells lacking MCT4, Doherty *et al.* reported that treatment with an MCT1 inhibitor AR-C122982 increased levels of early glycolytic intermediates, G6P and F6P, and decreased levels of pyruvate and other downstream metabolites (84). They proposed lactate accumulation to reduce the availability of NAD^+ in the cell, which undermines glycolytic flux that requires NAD^+ for the conversion of GAP to GBP. This favours the formation of DHAP over GAP. Consequently this reduces flux through the ATP-generating phase of glycolysis, reducing levels of 3-PG and pyruvate, thereby leading to decreased cellular concentrations of ATP and undermining proliferation (84).

Similar changes in G6P, F6P and pyruvate were observed by Bola *et al.* (133). However, different conclusions were made in their small cell lung and gastric cancer models. They conclude the metabolic response to MCT1 inhibition is increased glycolytic flux as cells can no longer import lactate for oxidation, somewhat mimicking the response to hypoxia (133). This corroborates earlier studies showing under certain circumstances lactate is also utilised as oxidative fuel. Consequently, MCT1 inhibition may target the hypoxic portion of solid tumours, forcing normoxic cells to switch from lactate oxidation to glucose utilisation, and thereby starving obligatory glycolytic hypoxic cells (108).

Recent reports suggest there are conditions where MCT1 inhibition can also have detrimental effects on the growth of MCT4 expressing cells by inhibiting pyruvate export and increasing oxidative metabolism in breast cancer (98). Here MCT4 is unable to compensate for the loss of pyruvate transport as a result of MCT1 inhibition, due to the 150-fold lower affinity of MCT4 for pyruvate. In this context MCT1 inhibition causes cells to undergo transcriptional changes to adopt increased oxidative metabolism through upregulation of

components of the electron transport chain, such as NDUFB3, and enzymes involved in the TCA cycle, such as succinate dehydrogenase. In such cells pyruvate levels increase under MCT1 inhibition without any impact on glycolytic flux contrary to earlier examples. Collectively these studies indicate inhibition of MCT1 can be detrimental to cell proliferation by interfering with cellular metabolism.

5.2. Aims

This chapter will discuss the *in vitro* metabolic changes that occur as a consequence AZD3965 treatment in DLBCL and BL cell lines, and the *ex vivo* effect of treatment in BL tumour xenografts. In addition, the creation and metabolic characterisation of a resistant cell type based on the BL cell line CA46 with a partial acquired resistance to AZD3965 treatment will be described.

5.3. MCT1 inhibition triggers an increase in TCA cycle intermediates *in vitro*

To determine the effects of inhibiting lactate transport on other metabolic pathways, 130 intracellular metabolites (Appendix D) were analysed by LC-MS with assistance from L. Rowcroft (AstraZeneca). Three BL lines (CA46, Daudi and Raji), two DLBLCs (Farage and OCILY18) and two neuroblastoma (IMR-32 and SH-SY5Y) cell lines were prepared *in vitro* for analysis following 2 hour inhibition with AZD3965 (100 nM) or DMSO control (Figure 5-1, Appendix E). Samples were prepared and analysed as previously described (133). Neuroblastoma cell lines, IMR-32 and SH-SY5Y had previously been shown by us to be relatively insensitive to the growth mediated effects of the compound despite significant lactate accumulation and undetectable levels of MCT4 protein and were included with an aim to determine a potential resistance mechanism (119).

Lactate accumulation in AZD3965 treated cells was observed by the LC-MS method in the majority of cell lines, in line with biochemical measurements of intracellular lactate, with the exception of Farage. Fold increases in intracellular lactate were lower than values from the biochemical assay but similar to *ex vivo* measurements in CA46 and Raji xenografts following 2 hour exposure to AZD3965 (~ 2-fold). Small increases were also detected in Farage but these did not reach statistical significance (P = 0.35 unpaired Student's *t*-test). Since, lactate

is produced as an end-product of glycolysis, we also looked for changes in other glycolytic intermediates. MCT1 inhibition increased the levels of the early glycolytic intermediates G6P and F6P, and GAP. Strong reductions in FBP (Log_2 FC > -3, P ≤ 0.037) were detected in CA46 and Daudi cells but these metabolites remained unchanged in the other cell lines examined. FBP is an important positive allosteric regulator of pyruvate kinase and therefore reduced levels of FBP may trigger a reduction in glycolytic flux by reducing the production of pyruvate (185).

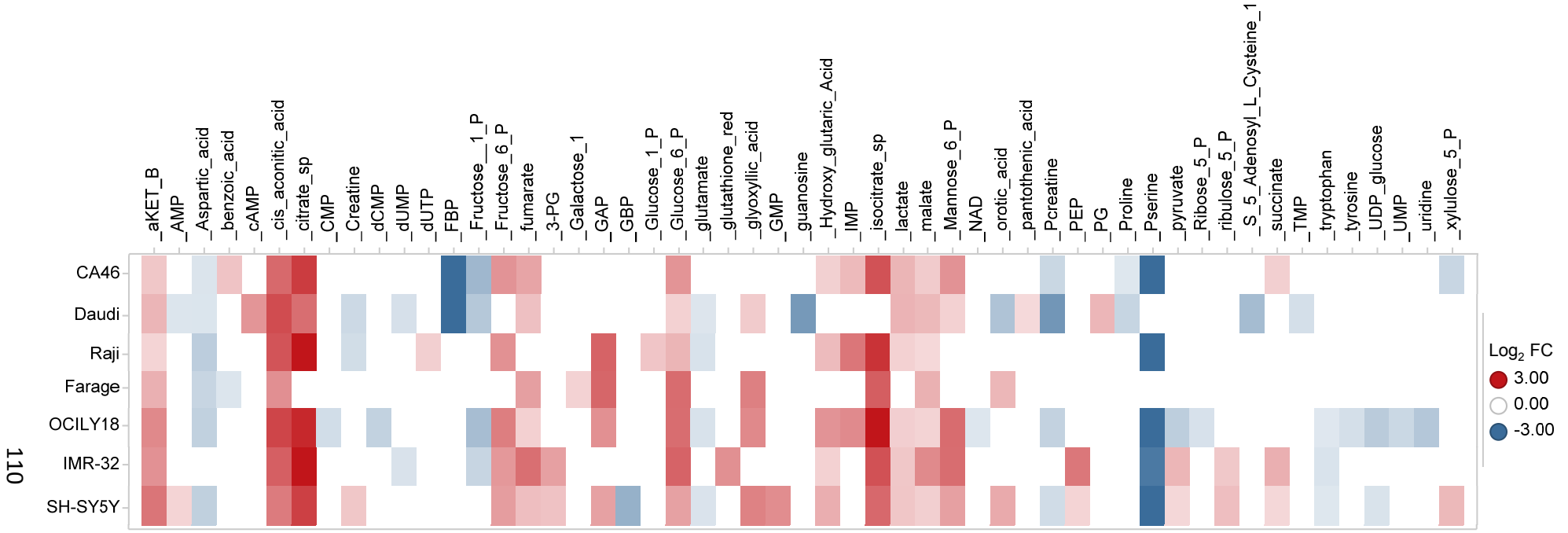

Figure 5-1: *In vitro* metabolic changes following acute treatment with AZD3965

Metabolic changes following 2 hour treatment with AZD3965 in BL (CA46, Daudi, Raji), DLBCL (Farage and OCILY18) and neuroblastoma (IMR-32, SH-SY5Y) cells. Significant (P-value ≤ 0.05) and substantial (+/- 0.5 Log_2 fold change) alterations in intracellular metabolite concentrations relative to time-matched DMSO controls, are labelled by metabolite name. Abbreviations used: aKET B (α-ketoglutarate or oxoglutarate), AMP (Adenosine monophosphate), CMP (Cytidine monophosphate), dCMP (2'Deoxycytidine monophosphate), dUMP (2'-Deoxyuridine 5'- triphosphate), dUTP (2'-Deoxyuridine 5'- triphosphate), Fructose-1-P (Fructose-1-phosphate), Fructose-6-P (Fructose-6-phosphate), FBP (Fructose bisphosphate), Glucose-1-P (Glucose-1-phosphate), Glucose-6-P (Glucose-6-phosphate), glutathione red (Reduced glutathione),GAP (Glyceraldehyde-3-phosphate), GBP (Glycerate bisphosphate), IMP (Inositol monophosphate), Mannose-6-P (Mannose-6-phosphate), NAD (Nicotinamide adenine dinucleotide) PG (Phosphogluconate), Pserine (Phosphoserine), Ribose-5-P (Ribose-5-phosphate), Ribulose-5-P (Ribulose-5-phosphate), TMP (Thymidine monophosphate), UDP-glucose (Uridine diphosphate glucose), UMP (Uridine monophosphate), Xyulose-5-P (Xyulose-5-phosphate).

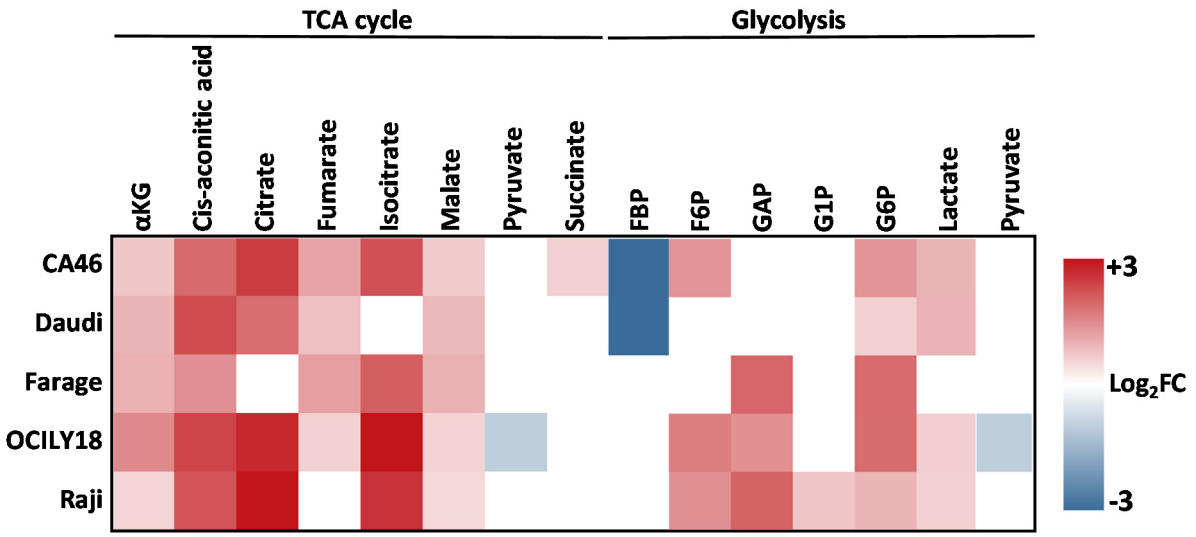

Figure 5-2: Summary of the AZD3965-induced changes in glycolytic and TCA cycle intermediates in B-NHL
Concentrations of intracellular metabolites significantly altered (P-value ≤ 0.05) relative to time-matched DMSO control, which are substantially altered (+/- 0.5 Log_2 fold change) are labelled by metabolite name. A number of metabolites were not detectable in both vehicle-treated and AZD3965-treated samples consequently log_2 FC values could not be derived. Metabolites exclusively detected in AZD3965 treated cells were isocitrate (Daudi) and GBP (Farage). Abbreviations used: αKG (α-ketoglutarate or oxoglutarate), F6P (Fructose-6-phosphate), FBP (Fructose bisphosphate), G1P (Glucose-1-phosphate), G6P (Glucose-6-phosphate), GAP (Glyceraldehyde-3-phosphate), GBP (1,3-Bisphosphoglyceric acid).

Across all cell lines we observed increased levels of various TCA cycle intermediates as shown in Figure 5-2. The distribution of changes is also shown for CA46 in detail (Figure 5-3) and highlights alterations in metabolites throughout the cycle. Elevated levels of citrate can inhibit PFK1 however since we also observed accumulation of GAP, which comes downstream of this enzyme in the glycolytic pathway this suggests this did not occur to a great extent (186). Unfortunately, alterations in two important regulators of TCA cycle activity, succinyl-coA and oxaloacetate could not be determined as these metabolites could not be detected within the QC sample from which integrals are matched.

One of the most consistent and marked changes observed were decreases in serine and phosphoserine. Although potentially interesting due to the magnitude of effect, decreases in serine and phosphoserine were also observed in resistant SH-SY5Y cells so the importance of this observation is unclear. We also observed decreased levels of aspartate in all cell lines with the exception of IMR-32. Aspartate has been shown to play an important role in nucleotide and protein synthesis (39, 187).

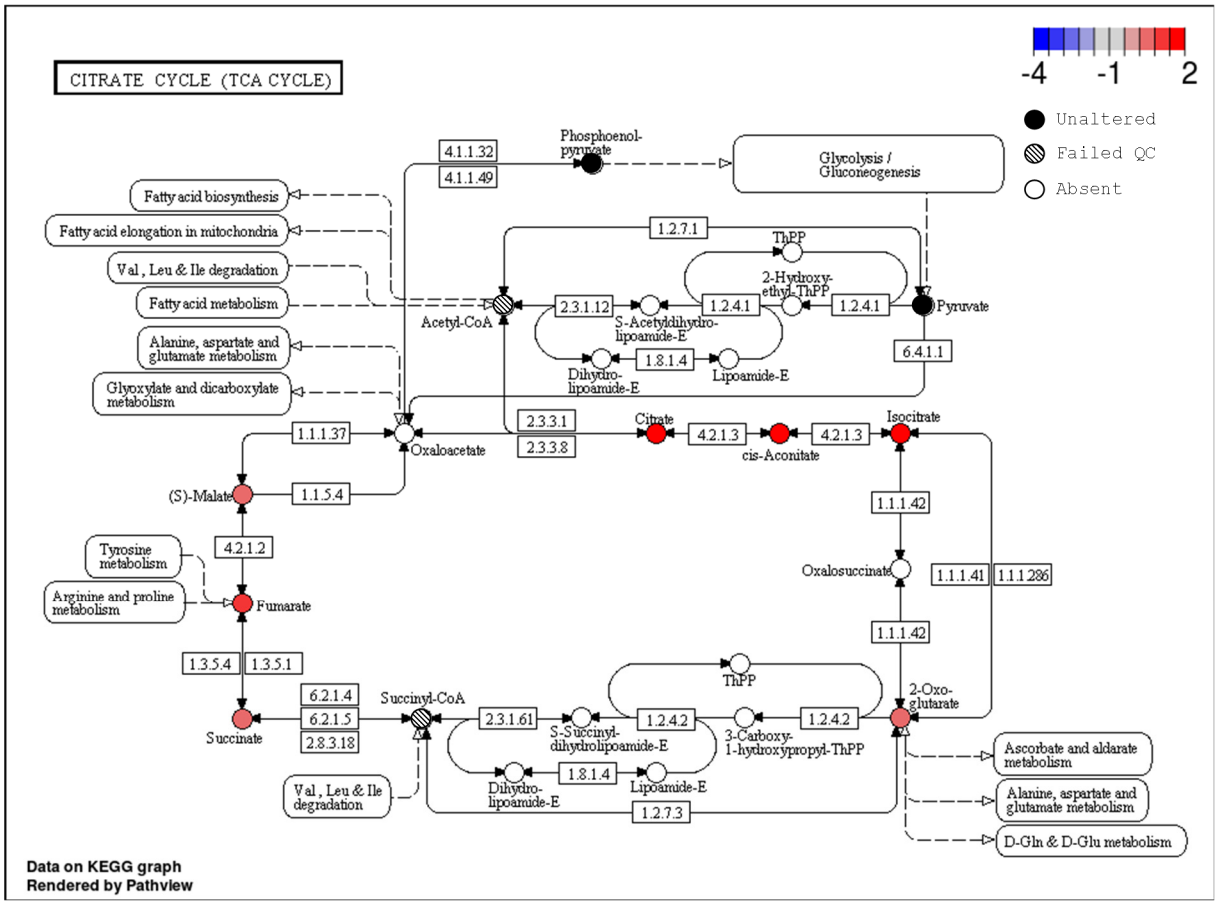

Figure 5-3: TCA cycle pathway analysis in CA46 cells
Log_2 fold changes in metabolites are plotted onto the KEGG pathway database (Hsa00020) using the R/Bioconductor package Pathview (188). Significantly ($P < 0.05$) altered metabolites are colour coded by log_2 fold change. In this example, data are taken from CA46 cells after 2 hour treatment with AZD3965 (100 nM). Metabolites not significantly altered by drug treatment (black nodes), those which failed LC-MS quality control (patterned nodes) or metabolites which were not part of the profile of quantifiable metabolites (non-shaded nodes) are also shown.

There are a number of similarities between AZD3965-resistant neuroblastoma and sensitive B-NHL cell lines in terms of the acute metabolic changes that occur following MCT1 inhibition. We observed increased levels of TCA cycle intermediates including; citrate, α-KG and fumarate in both groups. However, a number of glycolytic intermediates from the energy generating steps of glycolysis were specifically increased in IMR-32 and SHSY5Y which showed increased concentrations of 3-PG, PEP and pyruvate. This is in direct contrast to the reduced levels of these late-glycolytic intermediates observed in cells sensitive to MCT1 inhibition by Doherty *et al.*, and could that glycolytic flux is not impeded in these cells.

5.4. Acute treatment with AZD3965 alters metabolite profiles *ex vivo*

Following confirmation of lactate accumulation after 2 hour exposure to AZD3965 relative to a vehicle control, *ex vivo* in Raji and CA46, tumour material was sent for metabolomic analysis GC-MS (S. Solanki - Imperial College London). Raji and CA46 xenografts will be discussed separately.

Raji xenograft analysis revealed 36 significantly altered metabolites across a profile of 130 metabolites. *Ex vivo* we observed increased concentrations of intracellular glucose and glutamine. Increases in the TCA cycle intermediates, fumarate and malate, and increased levels of several amino acids (alanine, glutamine, aspartic acid, threonine and tryptophan) were also observed. Metabolites within the glycolytic pathway were also augmented by MCT1 inhibition. Increased concentrations of PEP were the highest both in terms of magnitude and significance, and the glycolytic intermediate, glyceraldeyde-3-phosphate (GAP) was also increased. The concentration of a smaller number of metabolites were decreased by AZD3965 treatment including a number of saturated (palmitic and stearic acid) and non-saturated (linoleic acid) fatty acids (Figure 5-4).

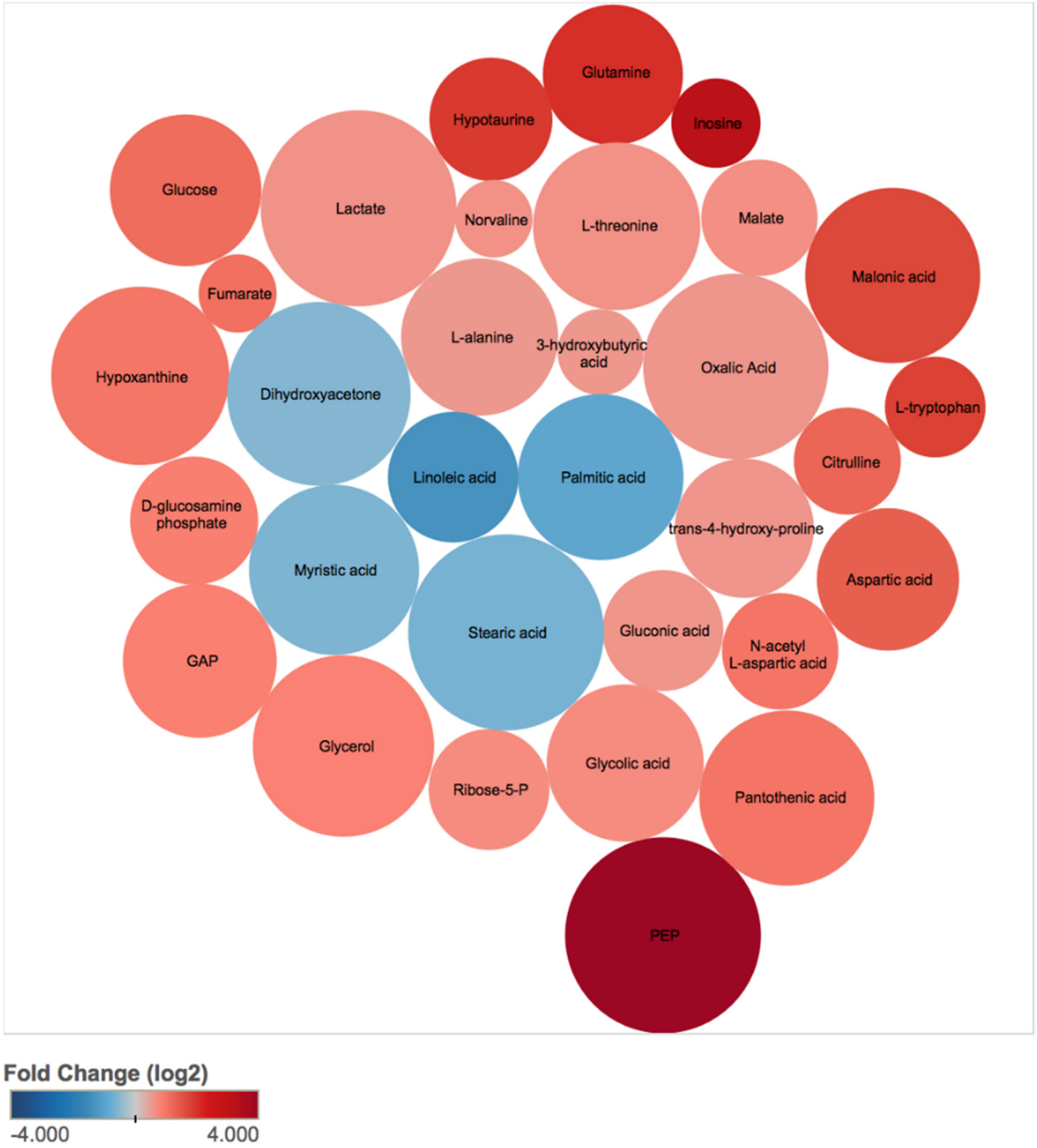

Figure 5-4: Metabolic alterations in Raji xenografts triggered by acute treatment of AZD3965
Changes in intracellular metabolites 2 hours after treatment with AZD3965 (100mg.kg^{-1}) in Raji xenografts. 130 metabolites were analysed using GC-MS by S. Solanki (Imperial College London). Concentrations of metabolites that were significantly altered (P value ≤ 0.05) relative to time-matched vehicle control, which are substantially altered (+/- 0.5 Log_2 fold change) are shown. Shapes are coloured according to log_2 fold change and sized by P-value where larger shapes equate to a lower P-value value.

In contrast, metabolite analysis (GC-MS) in CA46 xenografts revealed a limited number of alterations in comparison to Raji tumours and did not replicate any of the alterations identified in Raji with the exception of a significant elevation in lactate, albeit a more subtle change in CA46 tumours (Log_2FC; CA46= 0.34, Raji= 0.62) (Figure 5-5).

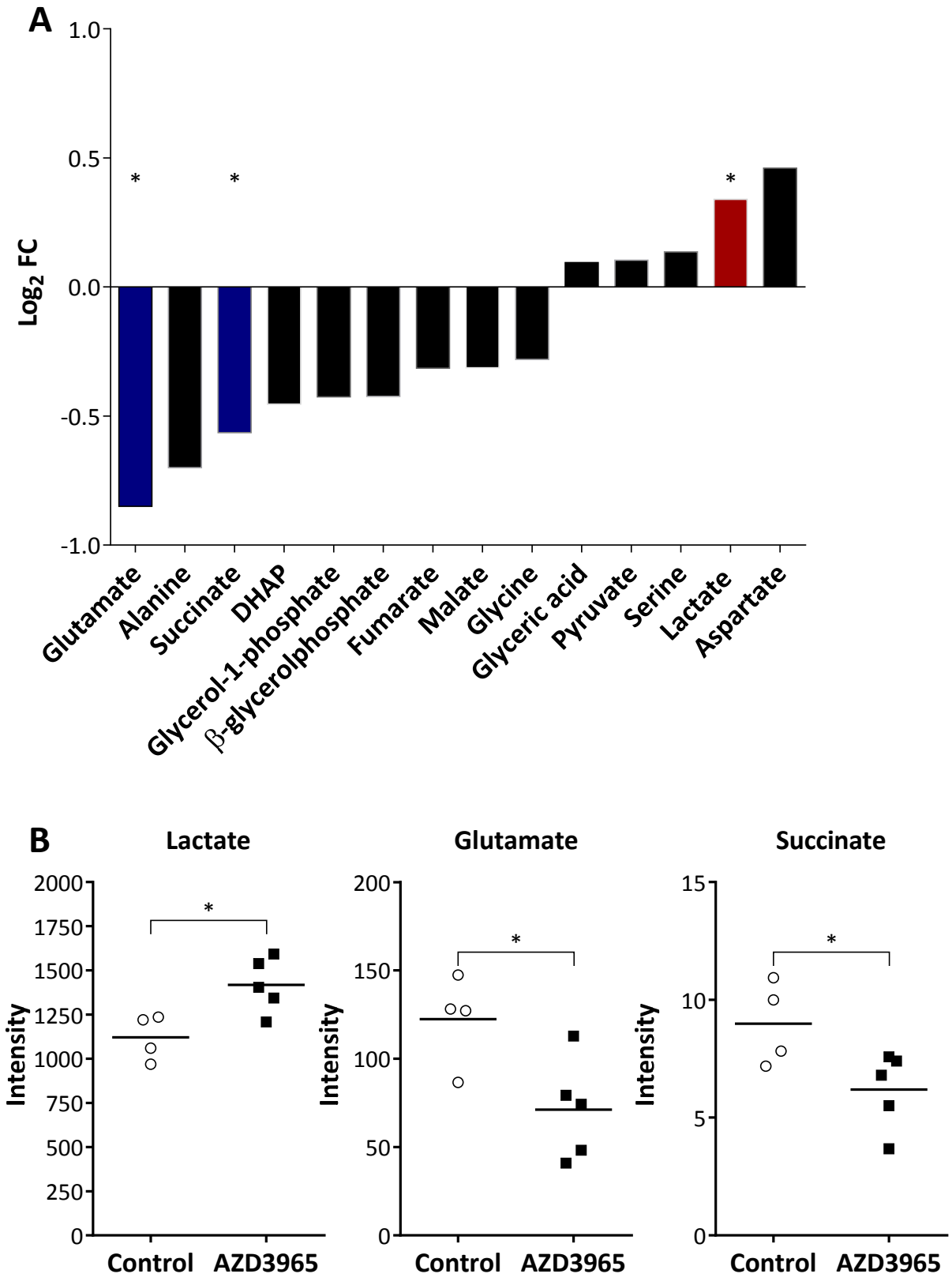

Figure 5-5: Metabolic alterations in CA46 xenografts triggered by acute treatment of AZD3965

A, Log_2FC changes following 2 hour treatment with AZD3965 (100mg.kg^{-1}) in CA46 xenografts relative to time-matched vehicle controls. Changes in intracellular metabolites. Samples were analysed using GC-MS by A. Sikka (Imperial College London). B, shows the individual metabolite intensity values (relative concentration) that were significantly altered (P value ≤ 0.05) between AZD3965 and time-matched vehicle controls.

5.5. A model of acquired resistance to AZD3965 displays an altered metabolic phenotype

We have shown AZD3965 induces a very significant cytostatic effect in CA46 cells. CA46 cells were chosen as a model where AZD3965 was cytostatic both *in vitro* and *in vivo*. To determine whether we could induce an acquired resistance to AZD3965 treatment we created an AZD3965-resistant cell line model (CA46-R). CA46 were initially cultured in continuous exposure to AZD3965 (10 nM) over a period of 5 weeks after which, reduced sensitivity to AZD3965 through a 72 hour XTT assay was apparent (*data not shown*). We then increased the concentration of AZD3965 (100 nM) for 3 weeks. We then characterised the phenotype of these cells in contrast to parental CA46 cells. Once established we found that these cells maintained their resistant phenotype following removal of AZD3965 for 2 weeks (*data not shown*).

5.5.1. Sensitivity

In CA46-R cells the sensitivity to the growth inhibitory effects of AZD3965 were reduced relative to CA46. The GI_{50} value was increased to 30 nM from 3 nM in parental CA46 cells (Figure 5-6). In addition, the maximal level of inhibition observed at 10 µM was decreased by 30% in CA46-R. Similarly, CA46-R were able to continue to proliferate, albeit at a reduced rate, in the presence of AZD3965 as indicated by greater number of cells being present after 72 hour exposure to the compound (Figure 5-7). Under these conditions, as with CA46, AZD3965 did not induce cell death in CA46-R (Figure 5-8). The resistance mechanism appeared to be specific to AZD3965 and the targeting of MCT1 as the level of cytotoxicity associated with doxorubicin treatment was comparable between CA46 and CA46-R cells.

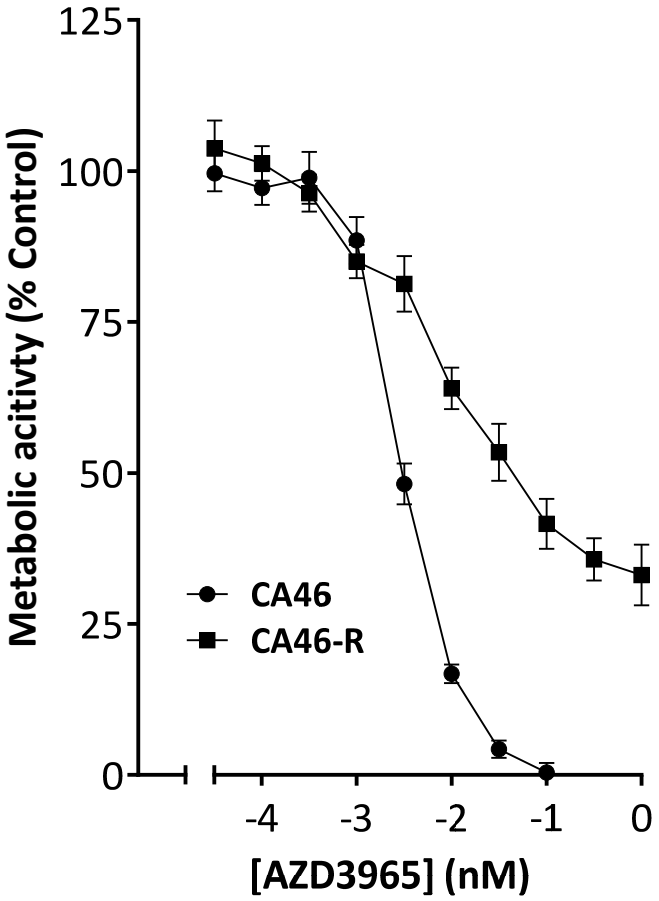

Figure 5-6: XTT assay of CA46 and CA46-R cells in response to AZD3965
Exponentially growing CA46 or CA46-R cells were treated with increasing concentrations of AZD3965 for 72 hours before assessing metabolic activity in the cell population as a surrogate for cell number using an XTT assay, as described in Section 2.6. Metabolic activity as a percentage of control was calculated relative to DMSO (0.01%) treated control cells after correcting for proliferation between seeding and dosing T_0. Data shown are the mean ± SEM of nine (CA46) and six (CA46-R) independent experiments.

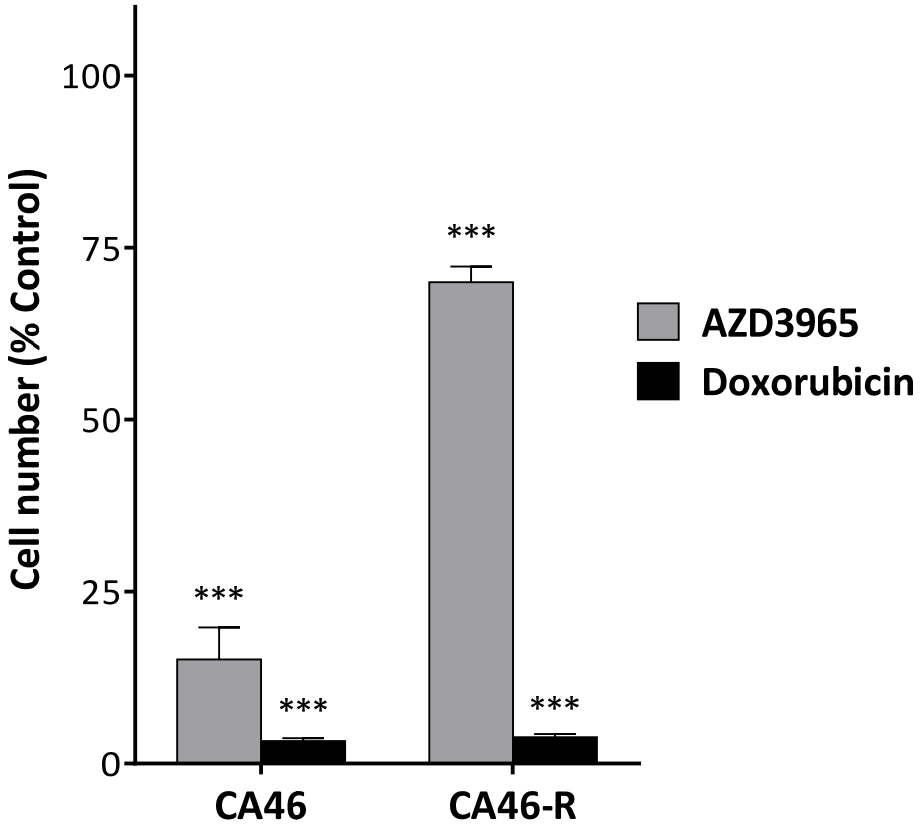

Figure 5-7: Sensitivity to AZD3965 and CA46 and CA46-R cells
Exponentially growing CA46 or CA46-R cells were treated with AZD3965 (100 nM) or doxorubicin (1 μM) for 72 hours before performing cell counts using a hemocytometer. Cell number data are shown as a percentage of a, cell line matched, DMSO (0.01%) treated control population. The significance of any changes relative to DMSO control was assessed using unpaired Student's *t*-tests (*P ≤ 0.05, **P ≤ 0.01 ***P ≤ 0.001). Data shown are the mean ± SEM of three independent experiments.

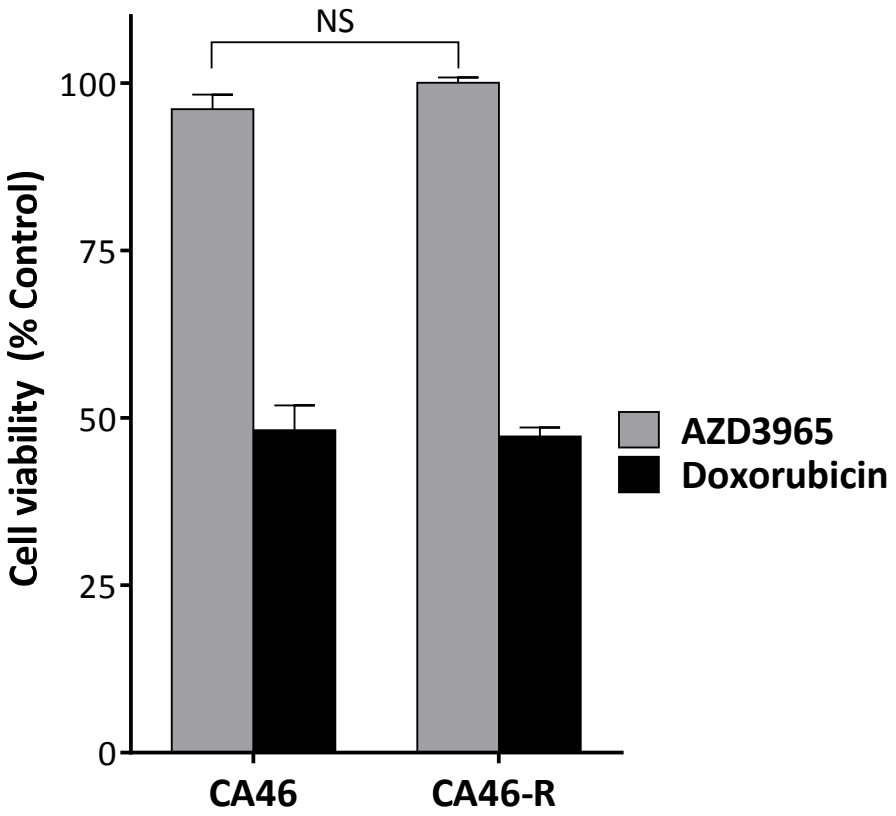

Figure 5-8: Cell viability in CA46 and CA46-R cells following AZD3965 or doxorubicin treatment
Exponentially growing CA46 or CA46-R cells were treated with AZD3965 (100 nM) or doxorubicin (1 μM) for 72 hours before assessing cell viability by trypan blue exclusion. Data are shown as a percentage of a cell line matched DMSO (0.01%) treated control population. Data shown are the mean ± SEM of three independent experiments

A reduction in cell doubling time in CA46-R cells could have conceivably led to an underestimate of the sensitivity to an anti-proliferative agent such as AZD9365. We therefore examined whether the reduction in AZD3965 sensitivity could be due to a differential proliferative rate in CA46-R cells (Figure 5-9). However, these were comparable between the two cell lines. Doubling times in CA46 and CA46-R, derived from cell counts in standard media over a 96 hour period were 20.57 hours (95% CI: 19.19-22.16) and 19.84 hours (95% CI: 19.13-20.61) respectively.

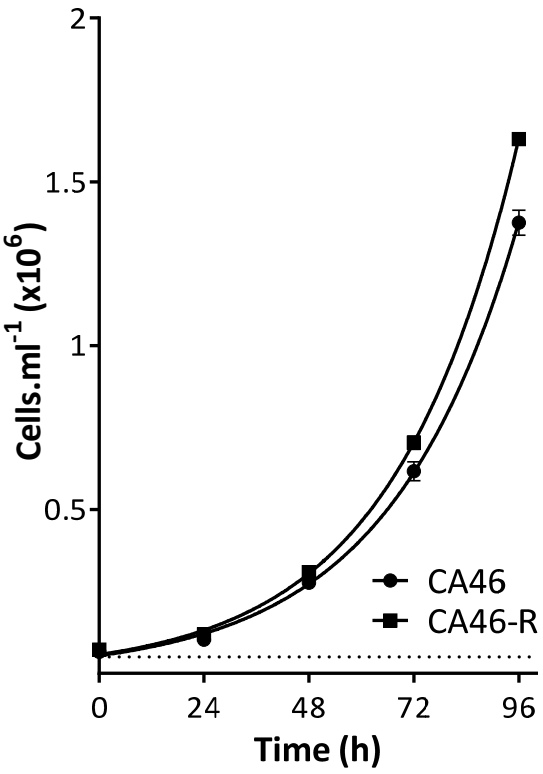

Figure 5-9: Doubling times of CA46 & CA46-R cells
Exponentially growing CA46 and CA46-R cells were seeded in their standard drug-free media and cell counts performed every 24 hours to determine proliferative rate. Doubling times were determined using an exponential growth equation in Graphpad. Data shown are the mean ± SEM of three independent experiments.

5.5.2. Lactate accumulation

Previously, increased MCT4 expression has been demonstrated to invoke resistance to AZD3965. We therefore sought to determine whether the reduced sensitivity to AZD3965 was a result of compensatory lactate transport through MCT4. Measurement of intracellular lactate following treatment with AZD3965 for 24 hours (1 µM) showed significantly elevated intracellular lactate in both CA46 and CA46-R cells (Figure 5-10), whilst intracellular lactate concentrations in CA46 and CA46-R cells were also similar across cell types following vehicle treatment ($P > 0.05$). The lactate accumulation following MCT1 inhibition was greater in CA46 cells than CA46-R cells ($P = 0.026$). However, CA46-R still displays a large increase in intracellular lactate following AZD3965 treatment, 72% of that displayed in parental CA46 cells, and greater than observed in multiple sensitive cell lines (Daudi, Pfeiffer, Toledo and RIVA) (Figure 4-1).

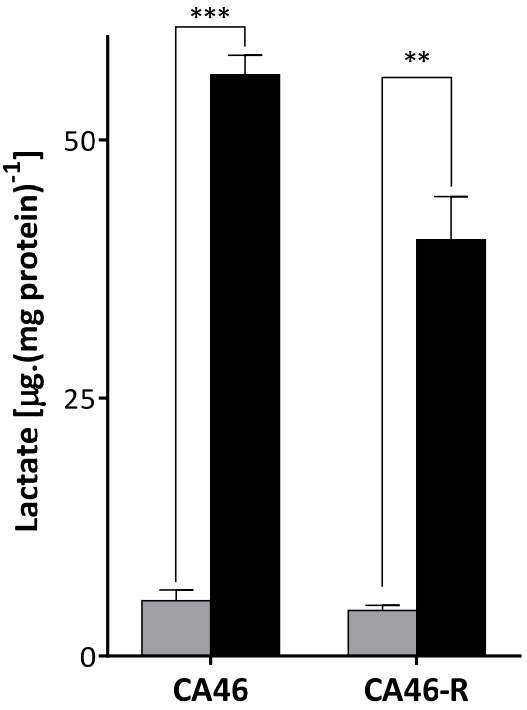

Figure 5-10: Intracellular lactate accumulation in CA46 & CA46-R following AZD3965 treatment
Intracellular lactate was measured in cells following exposure to (■) AZD3965 (1 µM) or (■) DMSO vehicle for 24 hours as described in Section 2.5. Values shown have been normalised to protein content via BCA assay. Data shown are the mean + SEM of at least 3 independent experiments. P-values were calculated using unpaired Student's *t*-tests. (*P ≤ 0.05, **P ≤ 0.01 ***P ≤ 0.001).

We sought to measure MCT4 protein expression by western blot. Consistent with the lactate accumulation data, MCT4 protein expression remained undetectable in CA46-R. A reduction in MCT1 expression and CD147 expression was observed in CA46-R cells (Figure 5-11).

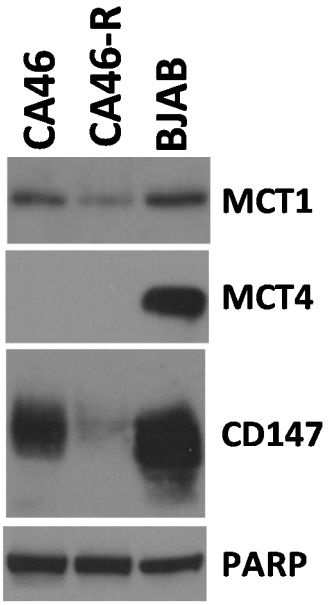

Figure 5-11: Expression of MCT1, MCT4 and CD147 in CA46 CA46-R cells
Protein expression of MCT1 (54 kDa) and MCT4 (49 kDa) and chaperone CD147 shown in comparison to parental CA46 cells. BJAB are included as an MCT4 expressing control. One representative blot of two separate lysate preparations is shown.

We reasoned that CA46-R might shift metabolic dependencies in order to circumvent the growth inhibitory effect of chronic lactate elevation. We therefore examined the relative consumption and release of metabolic substrates, comparing cell-naive culture medium and 'spent' media exposed to cells for 24 hours. This allows for changes in metabolite composition of the media to be measured following cell exposure which in turn informs the consumption and uptake of these components. CA46-R cells showed increased glutamine uptake, decreased lactate release and a minor increase in pyruvate export (Figure 5-12). This is consistent with a reduced production of lactate and increased oxidation of glucose and glutamate. This may suggest an increased entry of pyruvate and glutamate into the TCA cycle.

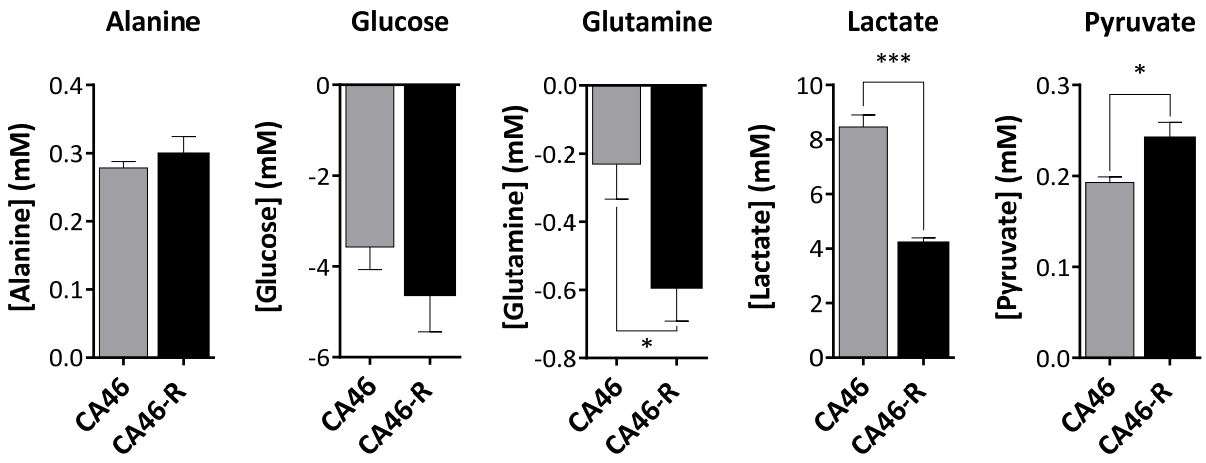

Figure 5-12: Extracellular metabolite analysis in CA46 and CA46-R cells
Extracellular metabolite concentrations were measured following exposure to AZD3965 (100 nM) or DMSO vehicle for 24 hours, as described in (Section 2.7.3.). Values shown have been normalised to cell number. Data shown are the mean + SEM of 4 technical replicates. P-values were calculated using an unpaired Student's *t*-test. (*P ≤ 0.05, **P ≤ 0.01 ***P ≤ 0.001).

5.5.3. Real-time measurement of OCR and ECAR in CA46 using the SeaHorse XF Bioanalyser

We reasoned that CA46-R may exhibit an altered metabolic phenotype with a lesser reliance on glycolysis and therefore performed analysis of the metabolic phenotype of these cells using the SeaHorse XF Bioanalyser. SeaHorse XF technology allows for real-time assessment of oxygen consumption rate and extracellular acidification rate, giving a phenotypic measure of oxidative phosphorylation and glycolysis respectively (Section 2.9)

The basal metabolic phenotype of CA46 and CA46-R cells differed greatly. Basal OCR was significantly higher in CA46-R cells (Figure 5-13). The raised OCR was shown to be associated with increased oxidative phosphorylation through acute treatment with the ATP synthase inhibitor, oligomycin, which highlights the proportion of OCR coupled to ATP generation. CA46-R also demonstrated a greatly increased reserve oxidative capacity following treatment with FCCP a protonophore, which dissipates the proton gradient maintained across the mitochondrial membrane. This altered response is indicative of a shift towards a more oxidative metabolic phenotype.

.

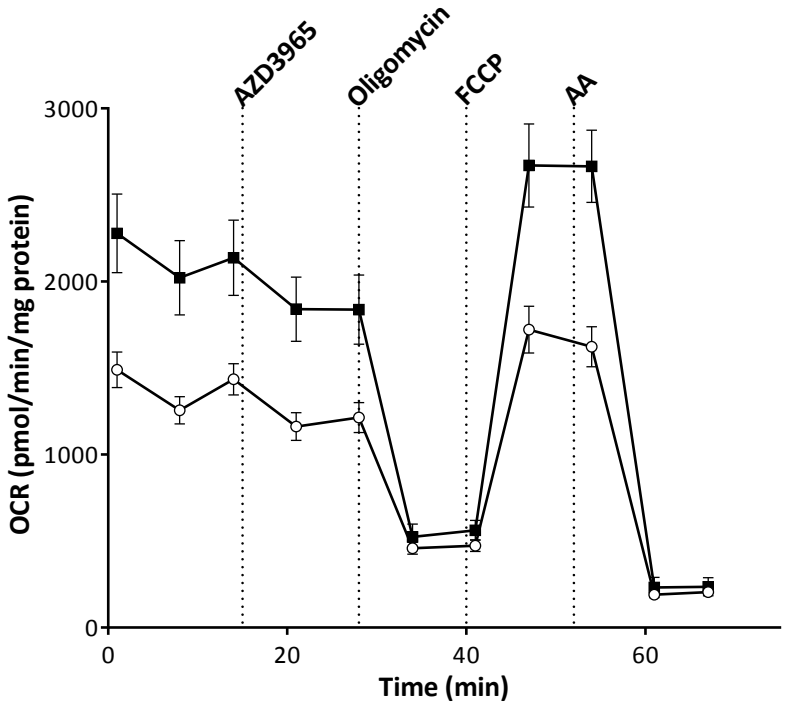

Figure 5-13: Oxygen consumption rate (OCR) in CA46 and CA46-R cells
Oxygen consumption rate in CA46 (□) and CA46-R (■) was normalised to protein concentration via BCA assay following phenotypic analysis using the SeaHorse XF24. Abbreviations used: FCCP (Carbonyl cyanide 4-(trifluoromethoxy)phenylhydrazone)); AA (antimycin A).

Acute treatment with AZD3965 resulted in a rapid decrease in ECAR in CA46 but not CA46-R cells (Figure 5-14). CA46-R also demonstrated a reduced basal ECAR which was below ECAR following AZD3965 in parental cells indicating a reduced production of lactic acid and decreased glycolytic activity (Figure 5-14). If glycolytic flux in these cells is low, then such an acute treatment is likely insufficient to detect further decreases in ECAR. The OCR augmenting compounds, oligomycin, FCCP, and antimycin, had little effect on ECAR in either CA46 or CA46-R cells.

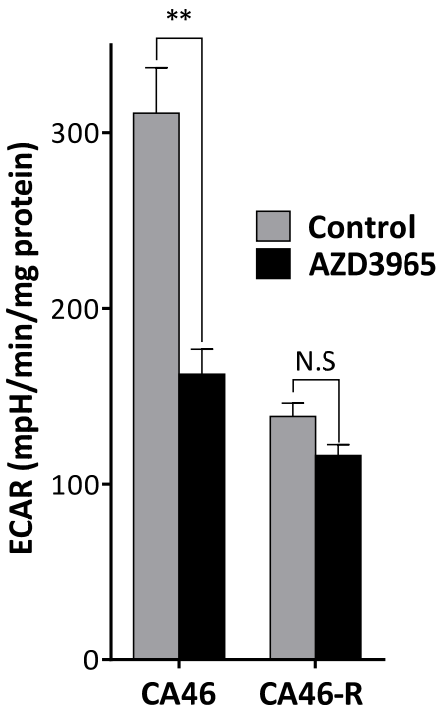

Figure 5-14: Extracellular acidification rate (ECAR) in CA46 and CA46-R cells
Extracellular acidification rate was normalised to protein concentration via BCA assay following phenotypic analysis.

5.6. Discussion

Lactate accumulation via MCT1 inhibition has a number of downstream effects on the concentration of various cellular metabolites, which impacts upon energy homeostasis inhibiting cell proliferation (Figure 5-15). Increased levels of early glycolytic intermediates measured across our DLBCL and BL cell panel are somewhat consistent with previous reports in solid and haematological cell line models. In the case of the model proposed by Doherty *et al.*, lactate accumulation as a result of MCT1 inhibition triggers an accumulation of early glycolytic intermediates including G6P and FBP, and decreased levels of those which make up the energy generating steps of glycolysis such as 3-PG and 2-PG.

From static measurements, such as those presented here, it is difficult to conclude whether increased concentrations of a particular metabolite are caused by increased flux through a given metabolic pathway, or an accumulation due to a bottleneck within that pathway. Also, not all metabolites passed QC, either because the metabolite could not be detected in the QC sample or because, the variability between QC samples was > 30%. This is important to consider when making conclusions about the absence of a metabolite, as it may not accurately inform as to whether its concentration has been altered by AZD3965 treatment.

Several commonalities exist between our *in vitro* and *ex vivo* data, in particular namely an increase in TCA cycle intermediates such as fumarate and malate. This, coupled with the accumulation of early glycolytic intermediates such as G6P and GAP supports a hypothesis that TCA cycle activity may be increased as a compensatory mechanism following inhibition of glycolysis. The increased levels of G6P reported here would also be predicted to inhibit hexokinase and reduce glycolytic flux. More directly lactate also favours the dissociation of PFK tetramers to less-active dimeric forms reducing glycolytic flux.

However, there were also instances where AZD3965 treatment *in vitro* had opposing effects *in vivo.* For instance, aspartate was reduced consistently *in vitro* but was elevated in Raji xenografts. Aspartate has been shown to play an important role in *de novo* purine synthesis but also can function as an electron acceptor which may have particular importance if NAD^+ pools are lowered by MCT1 inhibition as previously suggested by Doherty *et al.* where MCT1 inhibition prevents regeneration of NAD^+ by LDH (39, 84). The metabolic environment of cells *in vitro* differs greatly to that experienced *in vivo*. Cell culture conditions have been optimized to promote maximal proliferation in these cell lines so contain supra-physiological levels of several nutrients including glucose (11 mM) and glutamine (2 mM). Also, tumor cells interact with the surrounding stroma and can experience varied levels of oxygenation *in vivo* in contrast to the *in vitro* situation where a homogenous cell population are cultured under regulated conditions. A previous model has suggested a complex interplay between hypoxic and normoxic tumour cells where normoxic cells preferentially utilize lactate as an oxidative substrate sparing glucose for hypoxic cells which are obligatory glycolytic (109). Additionally the reverse Warburg hypothesis suggests additional changes *in vivo* may stem from stromal cells which export pyruvate and lactate via MCT1/4, providing energetic substrates to cancer cells (108).

The acute changes in metabolites observed which are suggestive of compensatory increase in TCA cycle activity, would also be consistent with a more oxidative phenotype. Chronic exposure to AZD3965 increased OCR and decreased lactate accumulation in CA46-R cells. CA46-R cells also showed changes in metabolite utilization suggestive of increased oxidation of glutamine (decreased extracellular glutamine). Glutamine anaplerosis can provide an alternative substrate for the TCA cycle through the conversion of glutamine to α-ketoglutarate which may become especially important if pyruvate generation becomes inhibited by lactate accumulation (189).

AZD3965 treatment also decreased cellular concentrations of phosphoserine in the majority of measured cell lines. Serine/glycine synthesis is integrally linked to glycolysis through 3-phosphoglycerate, which can be diverted to fuel the serine/glycine synthetic pathway. *De novo* serine synthesis has been found to occur *in vitro,* even in the presence of ample exogenous serine in culture media, indicating that this pathway serves other functions aside from serine synthesis. For example the conversion of phosphohydroxypyruvate to phosphoserine by PSAT1 is coupled to the generation of α-ketoglutarate from glutamate and so contributes towards TCA cycle intermediates (84, 190). Therefore the accumulation of α-ketoglutarate observed may reduce phosphoserine formation. Potentially, decreased levels of serine/phosphoserine could indicate a reduction in serine synthesis, which has been previously shown to decrease PKM2 activity and so favour a more oxidative mode of metabolism (191).

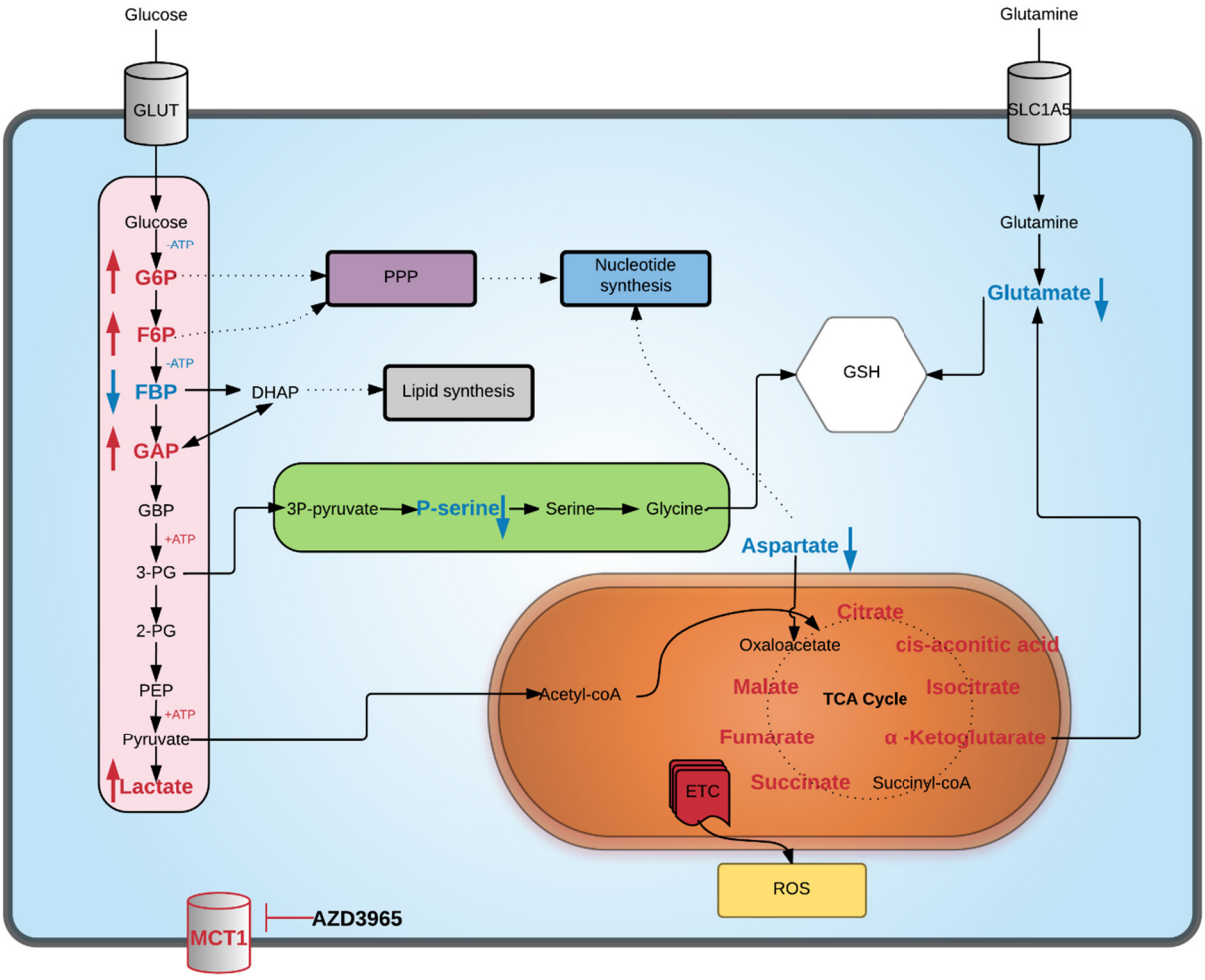

Figure 5-15: Summary of *in vitro* metabolic alterations following MCT1 inhibition with AZD3965.
Intracellular metabolites which were significantly by 2 hour exposure to AZD3965 (100 nM) altered in at least 3 of the 7 tested B-NHL cell lines are shown as (■) increased or (■) decreased.

We could not identify a distinct metabolic response associated with sensitivity to AZD3965 between our B-NHL cell lines and neuroblastoma cell lines. The *TP53* mutational status of all cell lines used in our study were publically available. Cell lines within our B-NHL cell panel are known to be *TP53* mutant whereas IMR-32 and SH-SY5Y are *TP53* wild-type (145, 192, 193). With the well-established role of p53 in metabolic regulation (Section 1.2.2.) differences in sensitivity to AZD3965 could stem from an altered basal metabolic phenotype or greater metabolic flexibility in cells with wild-type *TP53*. The potential influence of *TP53* status interest for future investigation and would require identification of *TP53* wild-type DLBCL or BL models with the desired MCT1/4 profile. Publically available gene expression data indicate that the majority of DLBLC and BL cell lines are *TP53* mutant, but there are wild-type cell lines including DOHH2, OCILY3 and OCILY10 available that have also have high *MCT1* and low *MCT4* mRNA expression which would be interesting to examine (160) (Appendix C).

Chapter 6. Identification of combination approaches to enhance the efficacy of AZD3965

6.1. Introduction

AZD3965 potently inhibits cell proliferation in DLBCL and BL models which commonly lack MCT4 expression. However, as the response is largely cytostatic *in vitro* and *in vivo* there is a clear need to identify effective combination strategies to induce cell death in cells which are sensitive to AZD3965, in order to achieve curative responses.

6.1.1. Novel targets for DLBCL

As the most common form of B-NHL, there is a lot of interest in developing new, more targeted therapies for use in DLBCL, which build upon the our understanding of the genetic basis of the disease (Table 8) (194). Although BL represents a much smaller patient population there is also interest in using molecular targeted therapies for patients who cannot tolerate current chemotherapy regimens or for those who have become refractory to treatment. Some potential targets for therapeutic intervention in DLBCL and BL are discussed below.

The PI3K (Phosphatidylinositol 3-kinase)/Akt/mTOR (mammalian target of rapamycin) pathway, transduce extracellular signals from receptor tyrosine kinases to control cell survival and proliferation. The family of catalytic PI3Ks (α,β,γ,δ) once activated, generate secondary messenger, PIP3, attracting Akt to the plasma membrane. Akt is a serine/threonine protein kinase that mediates various downstream effects including promoting cell proliferation and survival. mTOR (mTORC1) integrates a diverse range of signals, including PI3K/Akt signalling and regulates protein translation to control cell metabolism and cell proliferation. Of relevance to potential combination strategies with AZD3965, is the finding that aberrant activation of the PI3K/Akt/mTOR pathway results in distinct effects on cell metabolism and facilitating a more glycolytic phenotype.

Aberrant activation of the PI3K/Akt/mTOR pathway is a common feature of both BL and DLBCL as well as a number of solid tumours (195). Consequently, a number of agents have been designed to target the PI3K/Akt/mTOR pathway. One mechanism by which the PI3K pathway can become aberrantly activated in DLBCL is through the loss of negative regulator, PTEN (Phosphatase and tensin homolog). PTEN loss is a feature commonly found in GCB-DLBCL associated with sensitivity to PI3K (196). Akt inhibition has also been shown to have some efficacy in cell line models of GCB-DLBCL (197). The PI3K/Akt/mTOR pathway is also activated in BL, through tonic BCR signalling via SYK (198). Also in support of the role of the

PI3K pathway in BL pathogenesis, the transplantation of bone marrow from mice with combined constitutive c-MYC expression and PI3K activity triggers the formation of BL like tumours in recipient mice, but not in marrow from donor mice with only one pathway activated (199).

A key hallmark of cancer is the evasion of apoptosis which can occur through the overexpression of anti-apoptotic proteins such as BCL2 which inhibits pro-apoptotic proteins Bax and Bak to promote survival. BCL2 overexpression is a characteristic of GCB-DLBCL particularly through translocations (14;18) or mutations or (200, 201). BCL2 overexpression in ABC-DLBCL is more commonly associated with gene amplification or activation via aberrant NFκB signalling. Sensitivity to BCL2 specific inhibitor, ABT-199 correlates with the expression of BCL2 expression in DLBCL cell lines (202, 203).

The B-cell receptor signalling pathway is also activated in a number of B-cell malignancies including DLBCL and CLL. A key component of the BCR is Bruton's tyrosine kinase (BTK) BTK targeting inhibits downstream NFκB signalling which is a major driver of ABC-DLBCL (204). Ibrutinib, a potent irreversible inhibitor of BTK, is under clinical assessment as a potential treatment for DLBCL and has already been approved for the treatment of CLL (205, 206).

As mentioned previously, Burkitt lymphoma is characterised by *c-MYC* translocations but a number of other cancers are also driven by aberrant *c-MYC* activation, and various preclinical *in vitro* and *in vivo* models demonstrate the importance of MYC in tumourigenesis (207). MYC specific small molecule inhibitors have proved difficult to develop. However, the BET domain inhibitor JQ1 inhibits BRD4 which binds acetylated histones at gene enhancer sites reducing MYC target gene expression (208). JQ-1 has been demonstrated to be efficacious in BL and DLBCL (209, 210).

Novel agent (Target)	Combination	Phase	Population	NCT identifier
AT13387 (Hsp90)	None	2	Relapsed/refractory patients	NCT02572453
AZD2014 (mTOR)	+/- Rituximab	2	Relapsed/refractory patients	NCT02752204
Bortezomib (Proteosome inhibitor)	R-CHOP	2	Untreated patients	NCT02542111
Chidamide (HDAC)	VDDT	2	Relapsed/refractory patients	NCT02733380
CUDC-907 (HDAC)	+/- Rituximab	2	Relapsed/refractory patients	NCT02674750
Entospletinib (SYK)	None	2	Relapsed/refractory patients	NCT01799889
Ibrutinib (BTK)	R-GEMOX-Dexa	2	Relapsed/refractory patients	NCT02692248
Ibrutinib (BTK)	R-CHOP	2	Untreated EBV+ patients	NCT02670616
INCB18424 (JAK)	None	2	Relapsed/refractory patients	NCT01431209
Metformin (Complex I)	R-CHOP	2	Untreated patients	NCT02531308
Metformin (Complex I)	DA-EPOCH-R	2	Untreated patients	NCT02815397
Selinexor (CRM1)	None	2	Relapsed/refractory patients	NCT02227251
Sirolimus (mTOR)	Methotrexate	2	Relapsed/refractory patients	NCT01162551
Tazemetostat (EZH2)	Various	2	-	NCT02875548
TGR-1202 (PI3Kδ), Ibrutinib (BTK)	TGR-1202 + Ibrutinib	2	Relapsed/refractory patients	NCT02874404
Lenalidomide	+/- R-CHOP	3	Untreated patients	NCT02285062
Lenalidomide	+/- R-miniCHOP	3	Treated rituximab naïve patients	NCT02128061
TGR-1202 (PI3Kδ)	+/- Ublituximab	2|3	Relapsed/refractory patients	NCT02793583

Table 8: Ongoing Phase II and III trials with novel targeted compounds in BL and DLBCL
(Legend on next page)

The advanced search function of Clinicaltrials.gov was used to search for ongoing interventional phase 2 or 3 clinical trials for the treatment of 'Diffuse large B-cell lymphoma' or 'Burkitt lymphoma'. Trials investigating novel biologicals were not included. Where novel agents are being tested alongside existing or novel combination therapies this is stated. Combination acronyms; R-CHOP (Rituximab), R-GEMOX (Rituximab, gemcitabine, oxaliplatin, dexamethasone), DA-EPOCH-R (Dose-adjusted rituximab, etoposide, prednisone, vincristine, doxorubicin, cyclophosphamide.), VDDT (Vinorelbine, Liposomal doxorubicin or mitoxantrone , dexamethasone and thalidomide.

6.1.2. Targeting mitochondrial metabolism in cancer and the role of Complex I in the electron transport chain (ETC)

Far from being dysfunctional in cancer cells, as originally suggested by Warburg, mitochondria play an important role in tumorigenesis supplying biosynthetic intermediates via the TCA cycle but also helping to regulate redox homeostasis and epigenetics (211). Inhibition of Complex I prevents the oxidation of NADH and increases the generation of ROS which has been shown to reduce cell proliferation. A number of inhibitors of Complex I have been described.

Rotenone is a widely used pesticide and piscicide that acts as an inhibitor of Complex I resulting in an inhibition of the oxidation of NADH (212, 213). The compound is often utilised as a tool compound for investigating the effects of Complex I inhibition or as a mean to generate ROS.

Metformin is currently the most commonly prescribed medication for the treatment of type II diabetes. Recently there has also been interest in using metformin as an anti-cancer drug either as a chemopreventative agent or in combination with a range of other treatments. This interest was originally sparked by retrospective epidemiological studies suggesting a reduced incidence of cancer in patients receiving metformin (41). There have subsequently been a great number of preclinical studies using metformin in a range of *in vitro* and *in vivo* models as well as a number of ongoing clinical trials (214). Although still under discussion there is mounting evidence that metformin inhibits Complex I of the electron transport chain (46, 47). More recently, a compound developed by Bayer Pharmaceuticals, BAY 87-2243, has been demonstrated to inhibit Complex I (48).

6.1.3. *In vivo* combination approaches with MCT1 inhibitors

A number of attempts to combine MCT1 inhibition *in vivo* have already been investigated with a number of treatment modalities. One approach has been to investigate MCT1

inhibition in combination with components of current treatment regimens for particular diseases. For example, the combination of AZD3965 and ionising radiation had a beneficial effect, extending the time to reach a defined tumour volume (1,000 mm^3) in comparison to monotherapy or radiotherapy alone but without evidence of inducing any significant regression in SCLC xenografts (133). The MCT1 inhibitor, 7ACC1 when combined with cisplatin in cervical cancer xenografts also stabilised tumour volume during treatment and delayed tumour regrowth on cessation of treatment to a greater extent than either treatment alone (116).

We have shown that Complex I inhibition in combination with MCT1 inhibition triggers a rapid induction of cell death *in vitro*. The combination of parenteral MCT1 inhibitor, AR-C122982 and Complex I inhibitor, metformin, has previously been reported yielding increased survival in BL and breast cancer *in vivo* models (84). Similarly, AZD3965 has also been investigated in combination with phenformin, a more potent biguanide related to metformin (215). Here, Marchiq *et al*. reported a substantial 84% reduction in tumour growth relative to vehicle-treated mice at (132). These effects were specifically associated with tumour xenografts with an MCT4 negative phenotype. However, in both cases metformin and phenformin were dosed orally in drinking water making accurate assessments on dose received and their clinical relevance difficult. Also, a number of recent reviews have raised concerns about the physiological relevance of metformin doses used for many preclinical studies in cancer models (216-218)

6.2. Aims

This chapter will discuss attempts to identify synergistic combination strategies to partner with AZD3965 in BL and DLBCL in order to induce cell death and increase efficacy. Potential partners could be largely categorised into two groups; targets under preclinical or early clinical investigation in DLBCL or those interfering with cellular metabolism. In particular, it will focus on MCT1 inhibition and combinations which seek to target Complex I of the electron transport chain. As an extension of these studies the efficacy and tolerability of the novel combination of AZD3965 and BAY 87-2243 was also investigated in an intravenous model of BL.

6.3. Alternative combination approaches

We investigated the sensitivity of 2 BL and cell lines to range of small molecule inhibitors (Figure 6-1, Table 9). Neither cell line was sensitive to BTK (Ibrutinib), BCL2 (ABT-199) or PI3Kδ (CAL-101) inhibition (GI_{50} >1 μM). These three inhibitors have nanomolar potency towards their molecular targets and have been shown to reduce cell proliferation/viability by 50% at doses <1 μM in appropriate cell lines (202, 219, 220). CA46 have been previously reported to be resistant to the BCL2 inhibitor ABT-737 (198). Raji cells were particularly sensitive to GLS1 inhibition with BPTES and the more potent GLS1 inhibitor CB-839. Raji cells also showed greater sensitivity to JQ1 although this was less than had previously been reported in DLBCL cell lines (209). Both cell lines were sensitive to mTOR inhibitor, AZD8055 (GI_{50} < 100 nM), with CA46 cells being marginally more sensitive having lower GI_{50} and higher maximal inhibition being observed.

	AZD3965 (MCT1)	**Ibrutinib (BTK)**	**JQ1 (c-Myc)**	**AZD8055 (mTOR)**	**CAL-101 (PI3Kδ)**	**ABT-199 (BCL-2)**	**CB-839 (GLS1)**	**BPTES (GLS1)**
CA46	3 nM (n=5)	4.8 μM (n=3)	2.9 μM (n=2)	28 nM (n=3)	>10 μM (n=3)	8.8 μM (n=3)	6.66μM (n=2)	>10 μM (n=2)
Raji	6 nM (n=6)	>10 μM (n=3)	381 nM (n=1)	85 nM (n=3)	>10 μM (n=3)	>10 μM (n=3)	44 nM (n=1)	912 nM (n=1)

Table 9: GI_{50} values in CA46 and Raji
GI_{50} values calculated based on the mean metabolic activity measured by XTT assay across the indicated number of independent experiments.

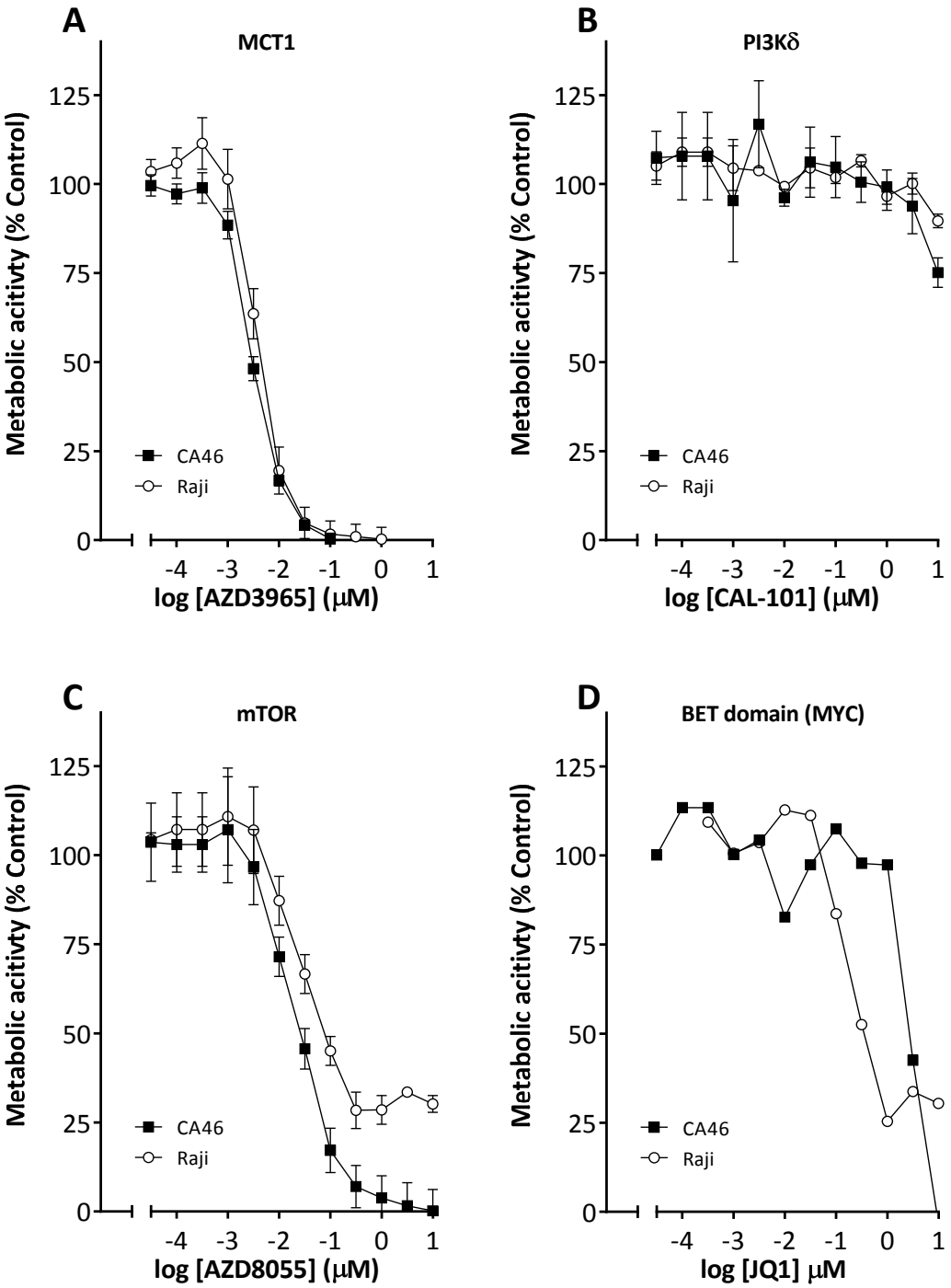
A
MCT1
Metabolic acitivty (% Control)
125
100
75
50
25
0
CA46
Raji
-4 -3 -2 -1 0 1
log [AZD3965] (μM)
B
PI3Kδ
Metabolic acitivty (% Control)
125
100
75
50
25
0
CA46
Raji
-4 -3 -2 -1 0 1
log [CAL-101] (μM)
C
mTOR
Metabolic acitivty (% Control)
125
100
75
50
25
0
CA46
Raji
-4 -3 -2 -1 0 1
log [AZD8055] (μM)
D
BET domain (MYC)
Metabolic acitivty (% Control)
125
100
75
50
25
0
CA46
Raji
-4 -3 -2 -1 0 1
log [JQ1] μM

.

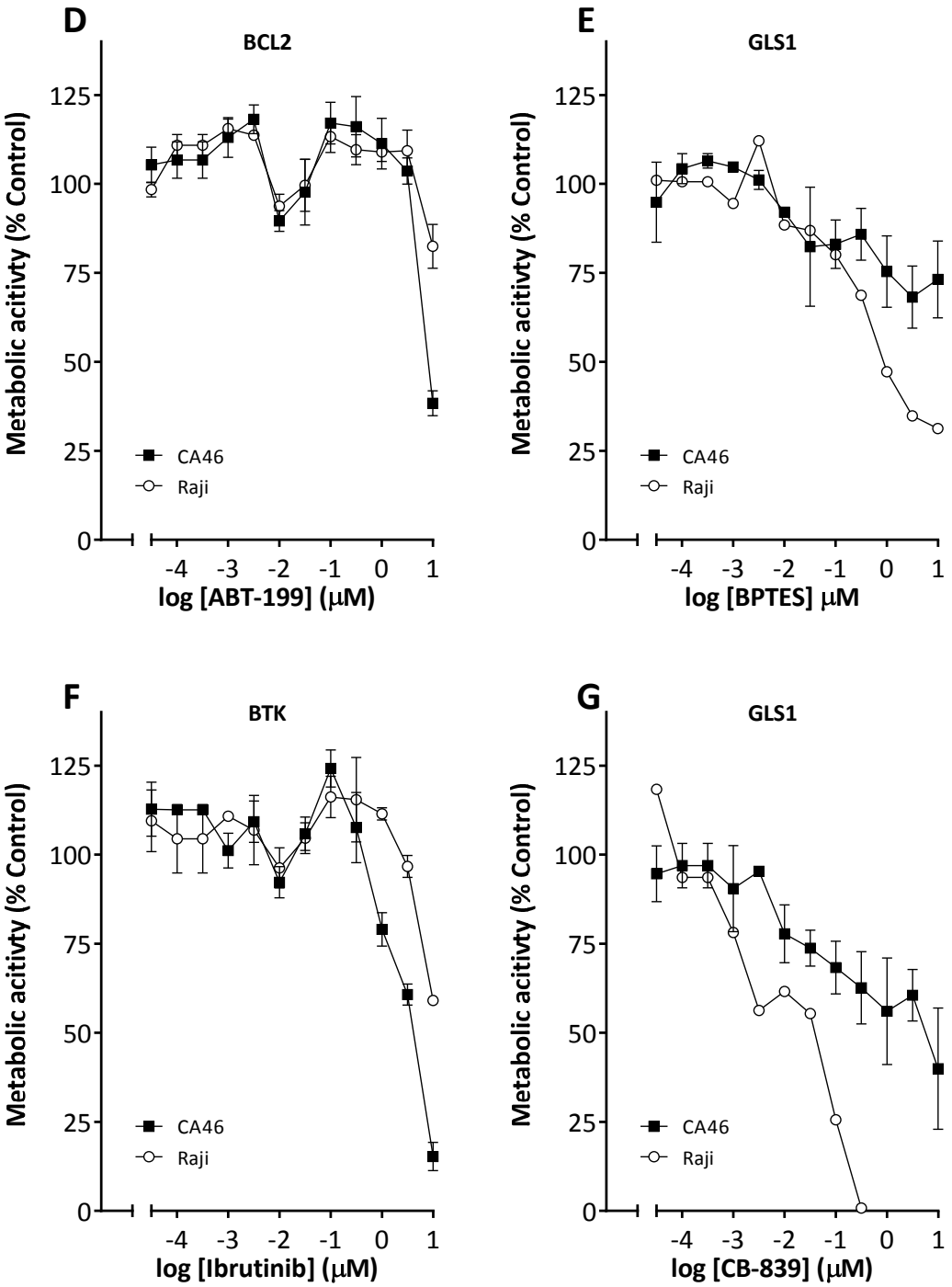

Figure 6-1: Inhibitor sensitivity in CA46 and Raji
Exponentially growing CA46 and Raji cells were treated with increasing concentrations of the indicated inhibitors for 72 hours. The molecular targets the named inhibitors are indicated in individual graph titles. Metabolic activity as a percentage of control was calculated relative to DMSO (0.01%) treated control cells after correcting for proliferation between seeding and dosing T_0. Data shown are the mean ± SEM of N experiments as indicated in Table 9, single experiments are shown as means without error bars.

We prioritized the investigation of mTOR inhibitor AZD8055 with AZD3965 as both cell lines examined, demonstrated sensitivity to both inhibitors alone. Combination index (CI) values were calculated using median effect analysis with Compusyn, using equipotent doses of

AZD3965 and AZD8055 alone and in combination across a range of multiples of GI_{50} allowing for computer aided calculation of CI values across the full range of effect levels in addition to those corresponding to experimental data points (221, 222). There are various alternative methods for determining synergy including the use of surface response methods which (223, 224)

$$CI = \frac{(D_{alone})_1}{(D_{combination})_1} + \frac{(D_{alone})_2}{(D_{combination})_2}$$

Combination index: Numerators are the dose associated with a given inhibitory effect for compound 1 and 2. Denominators are the dose of each compound necessary to illicit the same inhibitory response when used in combination. CI<1, C1=1, and CI>1 indicate synergism, additivity, and antagonism, respectively.

Treatment with equipotent doses of AZD3965 and AZD8055 in CA46 and Raji revealed a mild –moderate synergy at EC_{75} in CA46 and Raji cells (CI: 0.46, 0.52 respectively) (Figure 6-2). The levels of synergism or antagonism between two compounds can vary across different effect levels. Higher effect levels are more therapeutically relevant in relation to anti-cancer therapies therefore EC_{75} was chosen. This can be seen in Raji where the addition of AZD3965 only synergistic at higher effect levels.

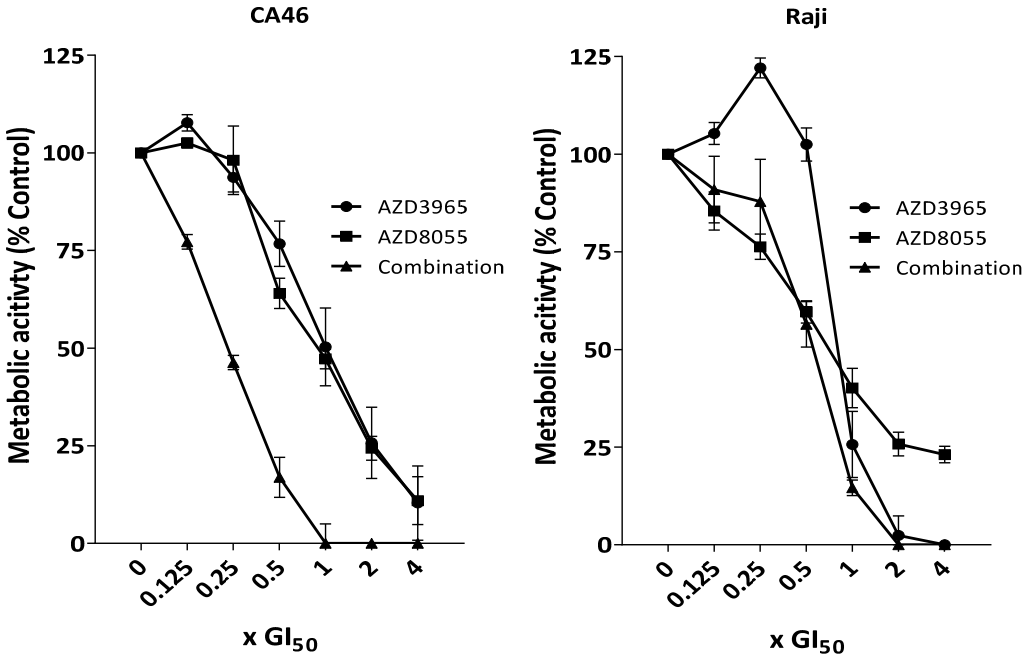

Figure 6-2: Combination of mTOR inhibitor AZD8055 and AZD3965 in CA46 and Raji cells
CA46 and Raji cells were treated with equipotent doses of AZD3965 and AZD8055 for 72 hours. Metabolic activity as a percentage of control was calculated relative to DMSO (0.01%) treated control cells after correcting for proliferation between seeding and dosing T_0. Data show the mean ± SEM of three experiments (CA46) or two experiments (Raji).

We also performed preliminary experiments in the DLBCL cell line OCILY18 with ABT-199. OCILY18 has a *BCL2* translocation resulting in the overexpression of this anti-apoptotic protein underlying the sensitivity of OCILY18 to ABT-199 (GI_{50} 5 nM) (203). We determined the GI_{50} of ABT-199 to be similar to that previously reported, 22 nM. Treatment with equipotent doses of ABT-199 and AZD3965 was mildly synergistic with CI at EC_{75} value of 0.47 (Figure 6-3).

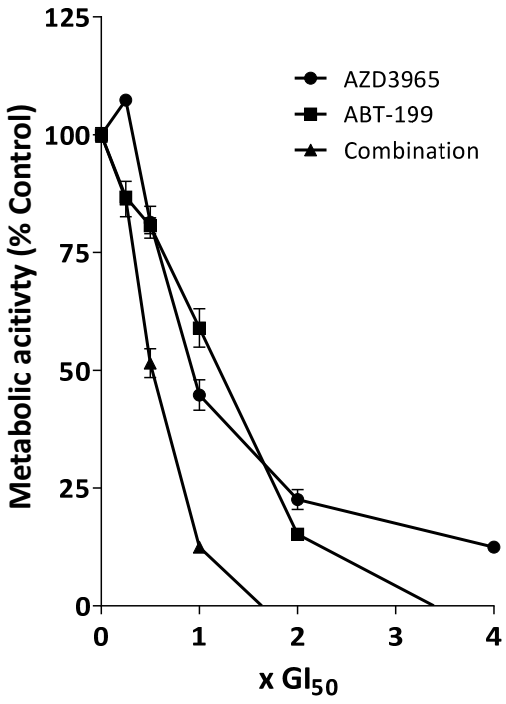

Figure 6-3: Combination with BCL2 inhibitor ABT-199 in OCILY18
OCILY18 cells were treated with equipotent doses of AZD3965 and ABT-199 for 72 hours. Metabolic activity as a percentage of control was calculated relative to DMSO (0.01%) treated control cells after correcting for proliferation between seeding and dosing T_0. Data show the mean ± SEM of quadruplicate wells in a single experiment.

6.4. Targeting oxidative phosphorylation in combination with MCT1 inhibition

We proposed that MCT1 inhibition in DLBCL or BL may result in an increased reliance on oxidative phosphorylation as glycolytic activity is inhibited by AZD3965. Concomitant targeting of MCT1 and OXPHOS may therefore trigger cell death. Initially we ran preliminary experiments using the potent Complex I inhibitor, rotenone, and metformin.

AZD3965, rotenone or metformin did not affect Raji cell viability when applied as monotherapy. However, AZD3965 in combination with either Complex I inhibitor caused a dramatic reduction in cell viability (Figure 6-4).

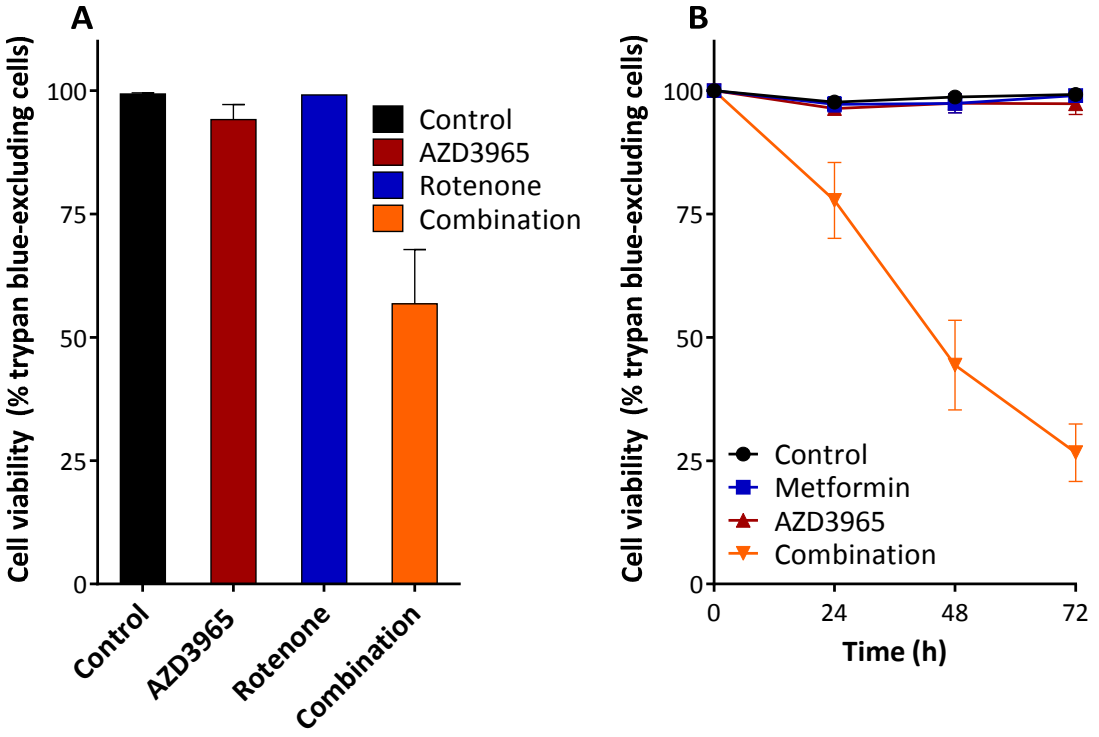

Figure 6-4: Combination of AZD3965 with a Complex I inhibitors reduces cell viability (A), exponentially growing Raji cells were treated with rotenone (5 nM), AZD3965 (100 nM), combination or a DMSO vehicle control for 72 hours before assessing cell viability by trypan blue exclusion. Data shown are the mean + SD of two independent experiments. (B) exponentially growing Raji cells were treated with metformin (1 mM), AZD3965 (100 nM), combination or a DMSO vehicle control for 72 hours before assessing cell viability every 24 hours across a 72 hour period by trypan blue exclusion. Data shown are the mean ± SEM of three independent experiments.

The *in vitro* concentrations of metformin necessary to induce cell death in combination with AZD3965 were substantially higher than levels achievable *in vivo*, a phenomenon which has been the topic of much comment when interpreting preclinical studies using metformin in

cancer (217, 218). We therefore sought to examine combinations with the potent Complex I inhibitor BAY 87-2243, which possesses suitable pharmacokinetic properties with which to enable serum drug concentrations to reach those active *in vitro* to permit inhibition of oxidative phosphorylation *in vivo* (34). We initially measured the response to combination with BAY 87-2243 in Raji cells as our previous data combining AZD3965 with Complex I inhibitors had been studied in this model (Figure 6-5). Combination treatment with AZD3965 and BAY 87-2243 induced profound cell death in contrast to either compound as monotherapy where cell viability remained above 90%.

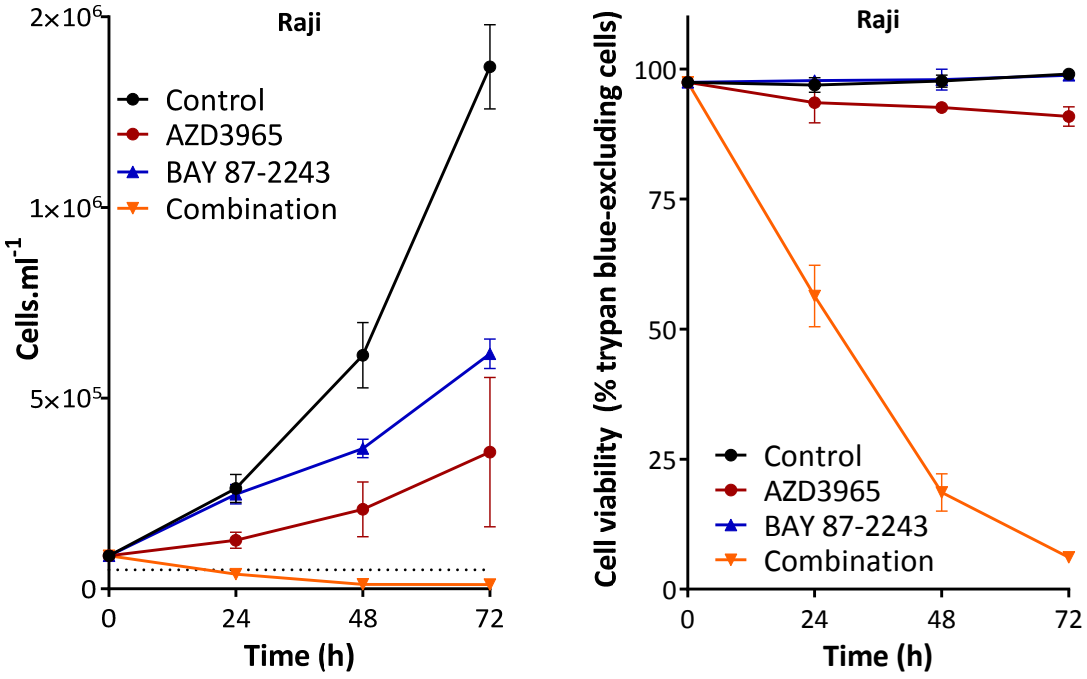

Figure 6-5: AZD3965 and BAY 87-2243 induces cell death in Raji
Exponentially growing Raji cells were treated after 24 hours with AZD3965 (5 nM) or BAY 87-2243 (100 nM) or both in combination a further 72 hours before performing cell counts using a hemocytometer. Cell number data are shown as a percentage of a cell line matched DMSO (0.01%) treated control population. Cell viability as assessed by trypan blue exclusion are shown as percentage of trypan blue excluding cells. Data shown are the mean ± SEM of three independent experiments.

We measured the effect of BAY 87-2243 (100 nM) on oxygen consumption rate in CA46 cells. Acute treatment with BAY 87-2243 decreased oxygen consumption rate and also abrogated spare respiratory capacity following treatment with FCCP (Figure 6-6). Previous reports demonstrate similar effects in melanoma cell models where BAY 87-2243 reduces OCR and spare respiratory capacity at higher doses than used here (49).

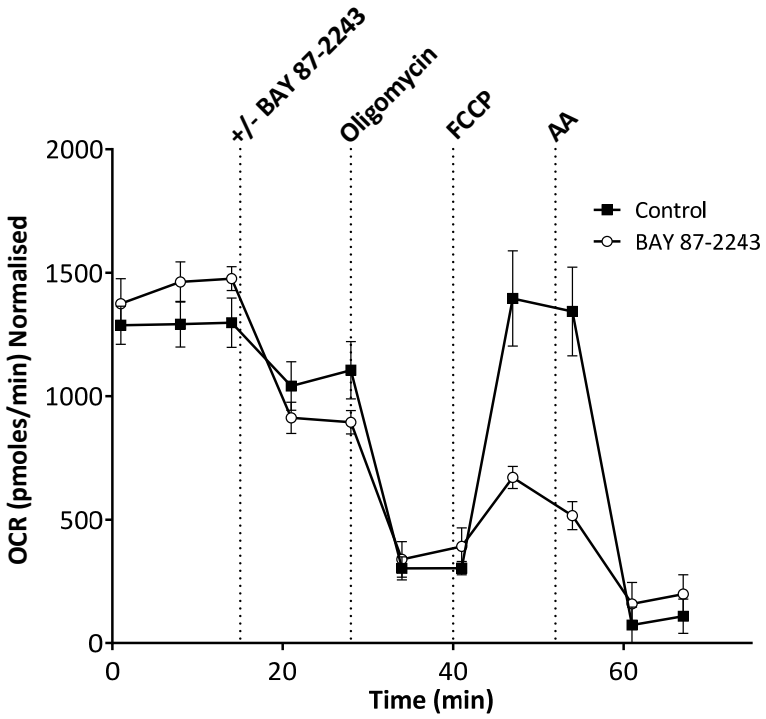

Figure 6-6: BAY 87-2243 reduces OCR and spare respiratory capacity
Oxygen consumption rate (OCR) was measured in CA46 cells. BAY 87-2243 (100 nM) or vehicle was added after establishment of a baseline measure of OCR. OCR was normalised to protein concentration via BCA assay following phenotypic analysis using the SeaHorse XF24. Abbreviations used: FCCP (Carbonyl cyanide 4-(trifluoromethoxy)phenylhydrazone)); AA (antimycin A).

As observed with Raji, CA46 were also insensitive to BAY 87-2243 monotherapy *in vitro* which likely reflects the metabolic profile of BL; a rapidly proliferating glycolytic tumour type (Figure 6-5, Figure 6-8). CA46-R cells were more sensitive to the growth inhibitory effect of BAY 87-2243 than parental CA46 cells consistent with a more oxidative metabolic phenotype exhibited by these cells (Figure 6-7).

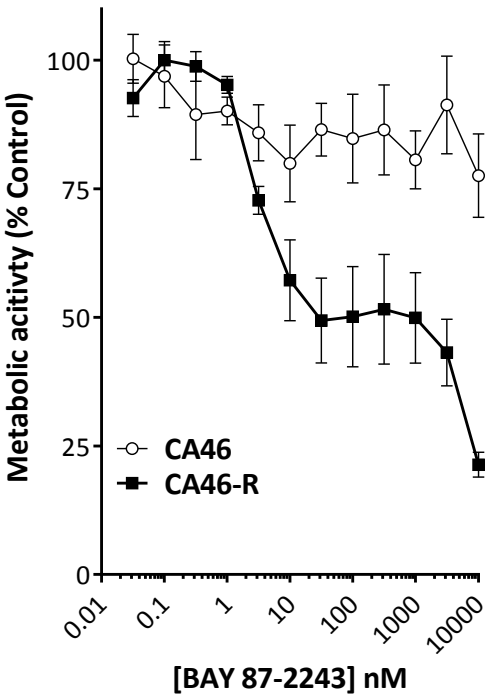

Figure 6-7: Increased sensitivity in CA46-R to BAY 87-2243
Exponentially growing CA46 or CA46-R cells were treated with increasing concentrations of BAY 87-2243 for 72 hours before assessing metabolic activity in the cell population as a surrogate for cell number using an XTT assay, as described in Section 2.6. Metabolic activity as a percentage of control was calculated relative to DMSO (0.01%) treated control cells after correcting for proliferation between seeding and dosing T_0. Data shown are the mean ± SEM of between three and nine independent experiments

In contrast to the disparate sensitivities to AZD3965 and BAY 87-2243 monotherapy, both CA46 and CA46-R were similarly sensitive to the combination (10 nM of each compound). After 72 hour exposure to combination treatment cell viability for CA46 and CA46-R were 37 and 34% respectively (Figure 6-8).

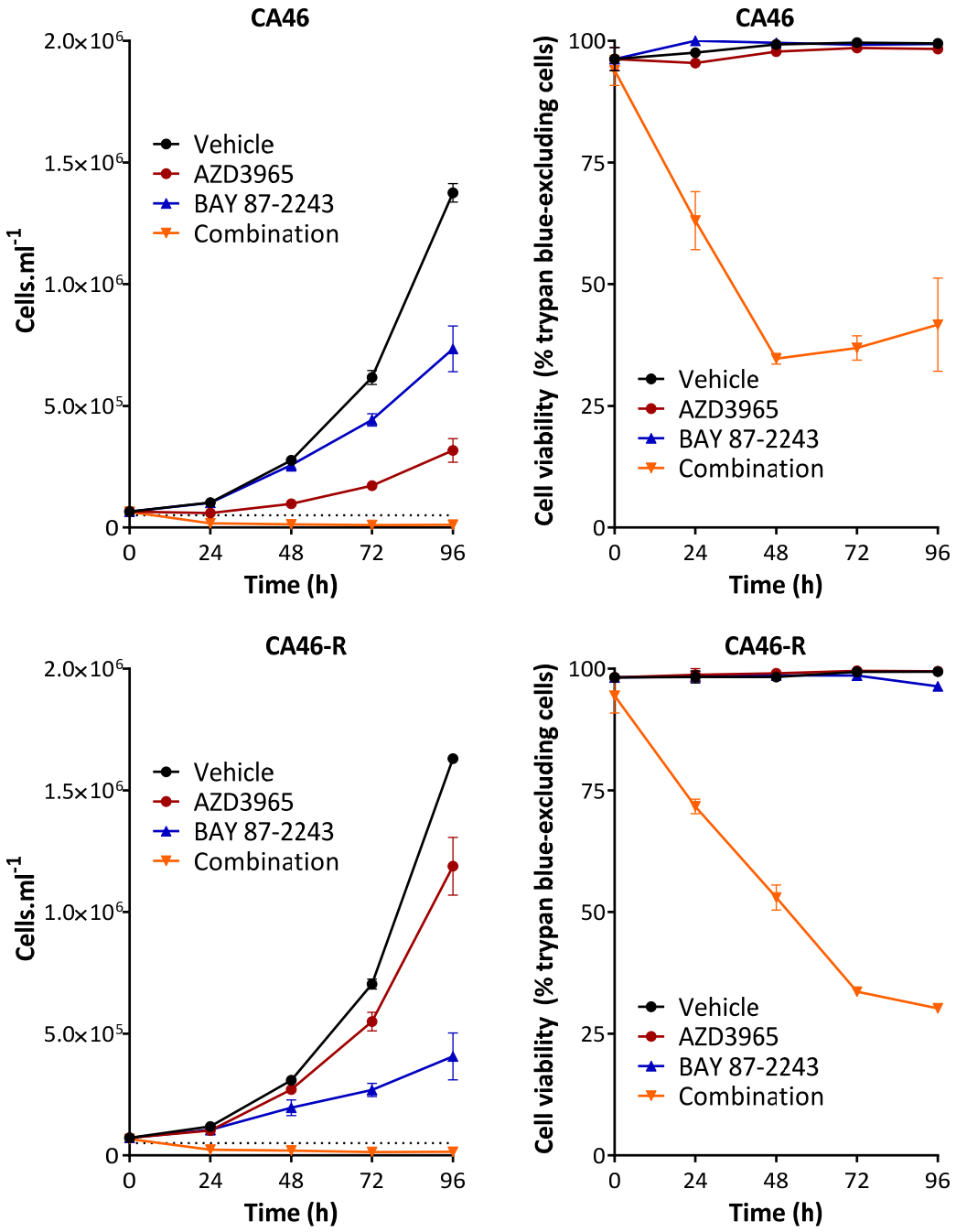

Figure 6-8: AZD3965 and BAY 87-2243 induces BL cell death
Exponentially growing CA46 or CA46-R cells were treated after 24h with AZD3965 (10 nM) or BAY 87-2243 (10 nM) or both in combination a further 72 hours before performing cell counts using a hemocytometer. Cell number data are shown as a percentage of a cell line matched DMSO (0.01%) treated control population. Cell viability as assessed by trypan blue exclusion are shown as percentage of trypan blue excluding cells. Data shown are the mean ± SEM of three independent experiments.

6.5. AZD3965 and BAY 87-2243 increase ROS

We investigated the levels of intracellular reactive oxygen species as a potential mechanism for the induction of cell death (Section 2.8). ROS plays a role in tumourigenesis increasing mutation rates through the induction of DNA damage, but high levels of ROS can also induce cell death (225). MCT1 inhibitors and BAY 87-2243 have previously been reported to increase intracellular ROS but have not been tested in combination (49, 84).

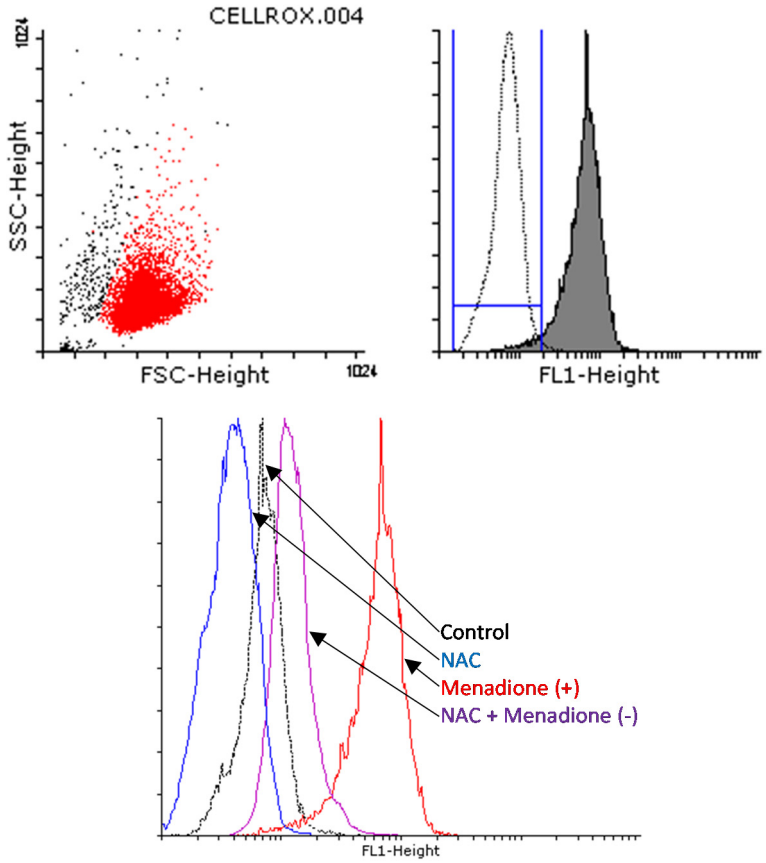

Figure 6-9: Positive and negative controls for Cell-ROX assays
Cellular debris was excluded using the FSC-SSC plot expressed in arbitrary units. Positive controls were prepared in CA46 cells using menadione (100 nM) for 1 hour prior to analysis. Negative controls were prepared using N-acetyl cysteine (NAC) pre-treatment for 1 hour before menadione or vehicle treatment. Intracellular ROS was measured flow cytometry for CellROX fluorescence (FL-1). Representative plots of 2 experiments.

We demonstrated the ability to detect changes in intracellular ROS using menadione and N-acetyl cysteine (NAC) to increase and decrease ROS respectively (Figure 6-9).The mechanisms by which these compounds modulate ROS are described in Section 2.8.1. N-acetyl cysteine was able to abrogate the increase in ROS generated as a result of menadione treatment. N-acetyl cysteine alone was also able to reduce intracellular ROS below that observed in vehicle treated cells.

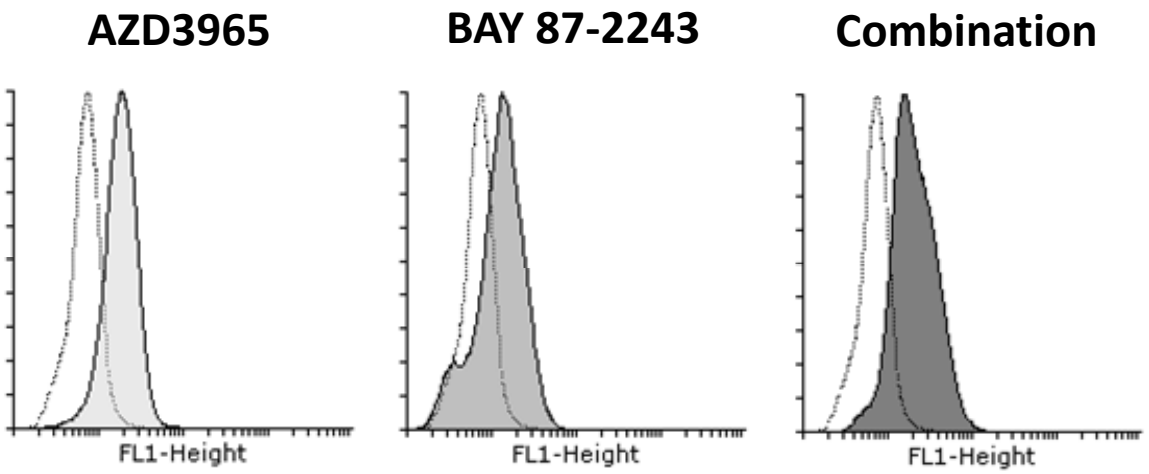

Figure 6-10: AZD3965 and BAY 87-2243 both increase intracellular ROS
CA46 cells were treated with vehicle, AZD3965 (100 nM), BAY 87-2243 (100 nM), or combination for 48 hours and analysed by flow cytometry for CellROX fluorescence (FL-1). Representative plots of 2 experiments.

Both AZD3965 and BAY 87-2244 increased fluorescence of Cell-ROX which is indicative of increased ROS. BAY 87-2243 and MCT1 inhibitor AR-C122982 has previously been shown to increase ROS. However, we did not observe a substantial increase in ROS on combination treatment therefore it seems unlikely that the significant shift in cytotoxicity observed with the combination is due to ROS (Figure 6-10).

6.6. *In vivo* efficacy of AZD3965 combined with BAY 87-2243

We decided to further investigate the combination approach *in vivo* using BAY 87-2243. BAY 87-2243 has been demonstrated to be well-tolerated and stabilise disease *in vivo* in melanoma, lung adenocarcinoma and prostate tumour models (48, 49, 226). However, it shows no efficacy in glycolytic models such as renal cell carcinoma in line with its mechanism of action, inhibiting oxidative phosphorylation (226).

Initially we established that dual oral administration of AZD3965 and BAY 87-2243 at doses individually shown to be safe *in vivo* could be tolerated in non-tumour bearing mice (49, 134). AZD3965 was administered twice-daily at 100 $mg.kg^{-1}$. BAY 87-2243 (1 - 9 $mg.kg^{-1}$) was administered once-daily. There was no major weight change observed in combination during the dose escalation, weight changes associated with the maximum tested BAY 87-2243 dose in combination with AZD3965 are shown in Figure 6-11.

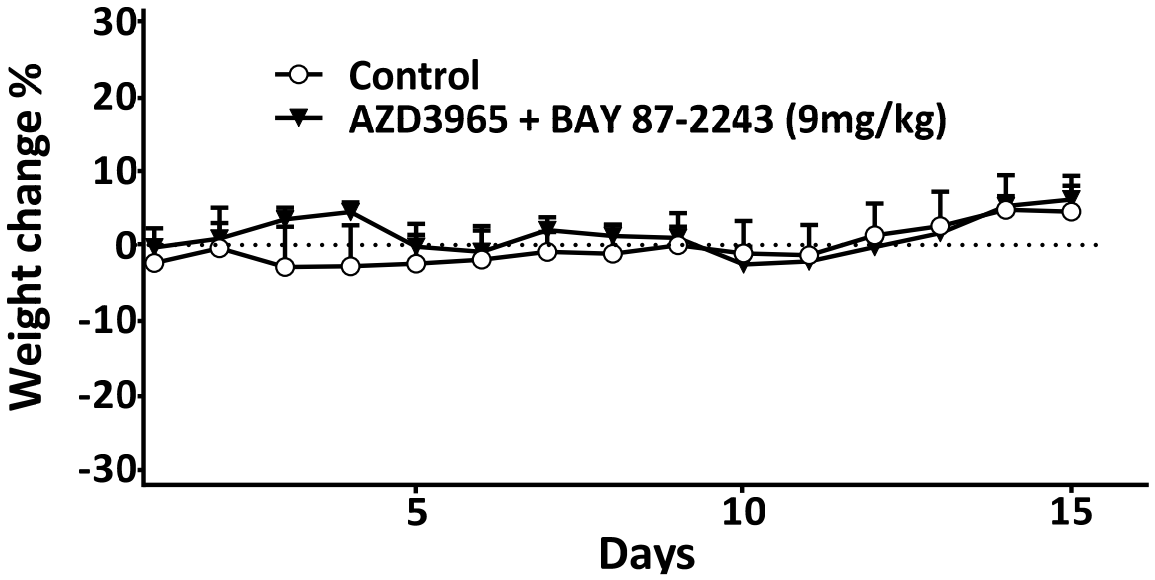

Figure 6-11: AZD3965 in combination with BAY 87-2243 in well tolerated in non-tumour bearing mice
Weights recorded at the indicated intervals were compared to individual mouse weights at the beginning of treatment to give a % change. Data points show the mean + SEM % change taken from 3 mice per treatment group.

To address whether MCT1 inhibition combined with Complex I inhibition can induce tumour regression *in vivo* we inoculated mice intravenously with luciferase expressing CA46 cells (Figure 6-12). We chose to extend the period of engraftment to 12 days before randomisation to ensure the radiance signal pre-treatment was well within the dynamic range of the IVIS® allowing us to be able to reliably detect tumour regression.

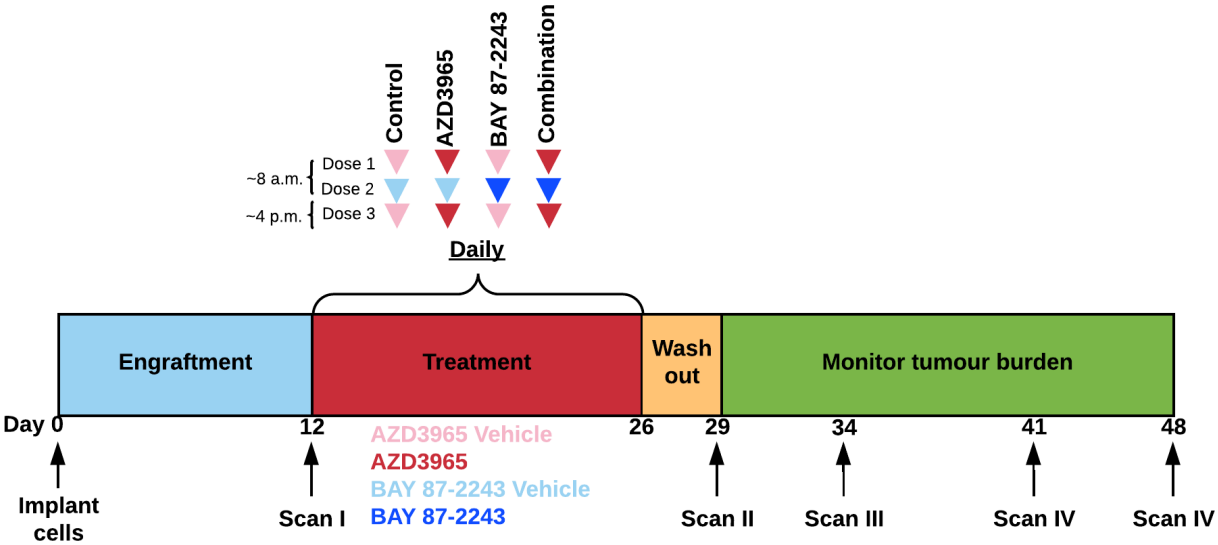

Figure 6-12: Study format for the assessment of AZD3965 and BAY 87-2243 *in vivo*
Twelve days post implantation mice were assigned to one of four treatment groups and treated as indicated. Following a drug-free wash-out period tumour burden was measured at the indicated intervals using bioluminescent imaging (Section 2.11.2.).

Tumour engraftment was not monitored during treatment since a lethal drug interaction had been observed in pilot studies where four animals receiving BAY-872243 alone or in combination died under anaesthesia. These animals displayed no histological evidence of any underlying major organ toxicity associated with combination drug treatment (*data not shown*). We therefore hypothesise the interaction to be between BAY 87-2243 and the isoflurane used to anaesthetise mice for bioluminescent imaging. We suggest this having shown AZD3965 does not interact under anaesthesia and that BAY 87-2243 in combination with AZD3965 is well-tolerated.

Animals were randomised to treatment groups receiving either AZD3965 (100 $mg.kg^{-1}$, BID), BAY 87-2243 (9 $mg.kg^{-1}$, OD), or the combination, for 14 days. Prior to commencement of the treatment regimen the mean level of engraftment between prospective treatment groups were comparable ($P > 0.05$ by two-way ANOVA).

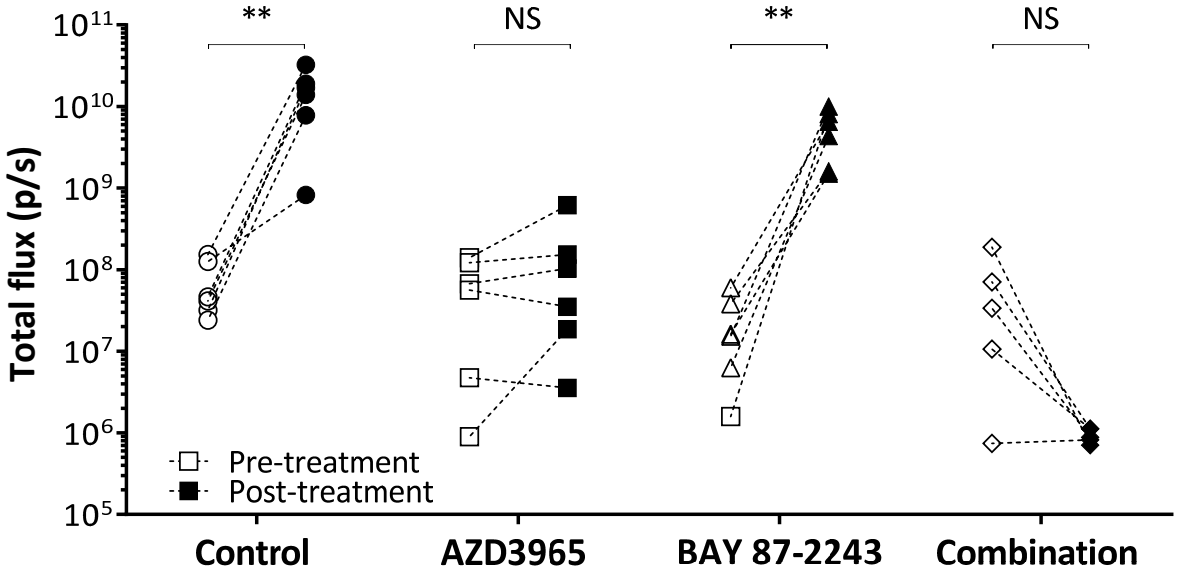

Figure 6-13: Efficacy of the combination of AZD3965 and BAY 87-2243 *in vivo*
NSG mice were intravenously inoculated with luciferase-expressing CA46 cells and allowed to engraft for 12 days prior to treatment with AZD3965 (100 $mg.kg^{-1}$, BID), BAY 87-2243 (9 $mg.kg^{-1}$, OD) or the combination of AZD3965 and BAY 87-2243, for 14-days. Control and monotherapy-treated mice received the relevant vehicle controls. Mice were re-imaged at intervals from 72 hours following treatment. A, bioluminescent signals for mice within each group. The individual responses of mice treated with vehicle or AZD3965 pre-treatment (day 12) and post-treatment (day 29). Comparisons of paired samples pre-treatment and post-treatment. Significance was assessed by two-tailed paired *t*-test (*$P \leq 0.05$, **$P \leq 0.01$ ***$P \leq 0.001$)

Post treatment, 72 hours after a final dose, engraftment was significantly increased in control and BAY 87-2243 treated mice ($P = 0.018$ and 0.013) respectively as assessed by a two-tailed

paired *t*-test. As observed in our previous *in vivo* experiment, AZD3965 monotherapy treatment caused a strong growth inhibitory effect, with pre and post treatment flux values being comparable (Figure 6-13). Emphasising this, the mean radiance signal in the AZD3965 treated group was just 1% of the control group at the end of the study. The combination of AZD3965 with BAY 87-2243 led to a reduction in mean tumour burden compared with the pre-treated value in 4 of 5 mice, with signal intensities being reduced by between 9.5 to 267 fold (P = 0.01 by Pearson χ2 test). This is consistent with the induction of lymphoma cell death *in vivo*.

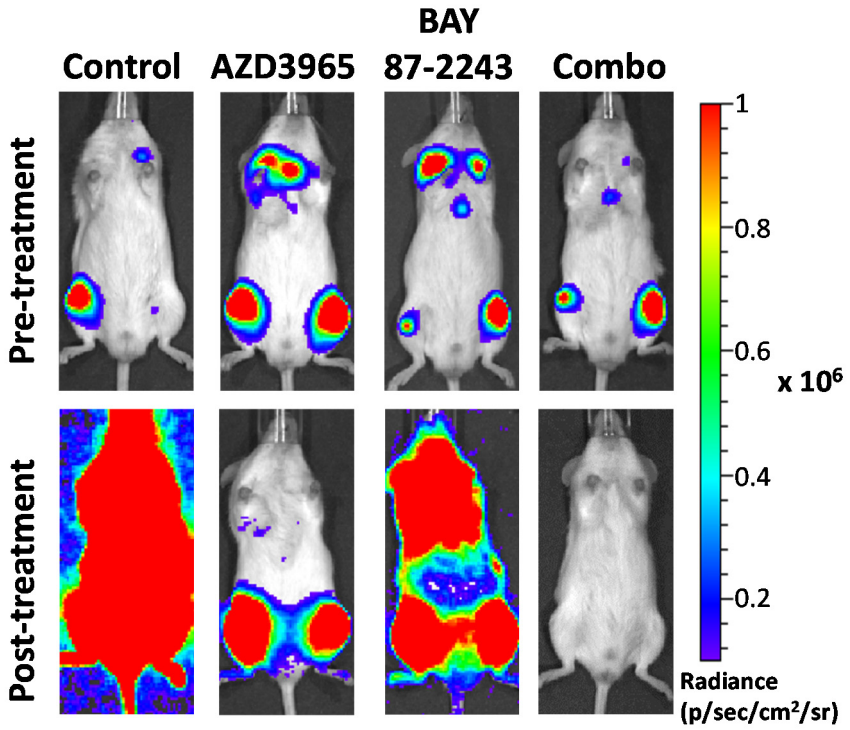

Figure 6-14: Visualisation of the efficacy of the combination of AZD3965 and BAY 87-2243 *in vivo*
NSG mice were intravenously inoculated with luciferase-expressing CA46 cells and allowed to engraft for 12 days prior to treatment with AZD3965 (100 $mg.kg^{-1}$, BID), BAY 87-2243 (9 $mg.kg^{-1}$, OD) or the combination of AZD3965 and BAY 87-2243, for 14-days. Representative images taken of a mouse from each treatment group are shown pre-treatment (day 12) and post-treatment (day 29). Images are displayed on a single radiance scale, due to the wide range in signal intensities pre and post treatment which necessitates post-treatment control images are overexposed in order to detect signal pre-treatment.

The change in burden post-treatment can be visualised in representative mice (Figure 6-14). The signal distributions show engraftment of both femurs pre-treatment. Post-treatment, mice which received vehicle or BAY 87-2243 treated images are over exposed and so prevent localisation of tumour burden. However, displaying the images at a higher scale reveals similar patterns of engraftment of femurs and the chest area (Figure 6-15).

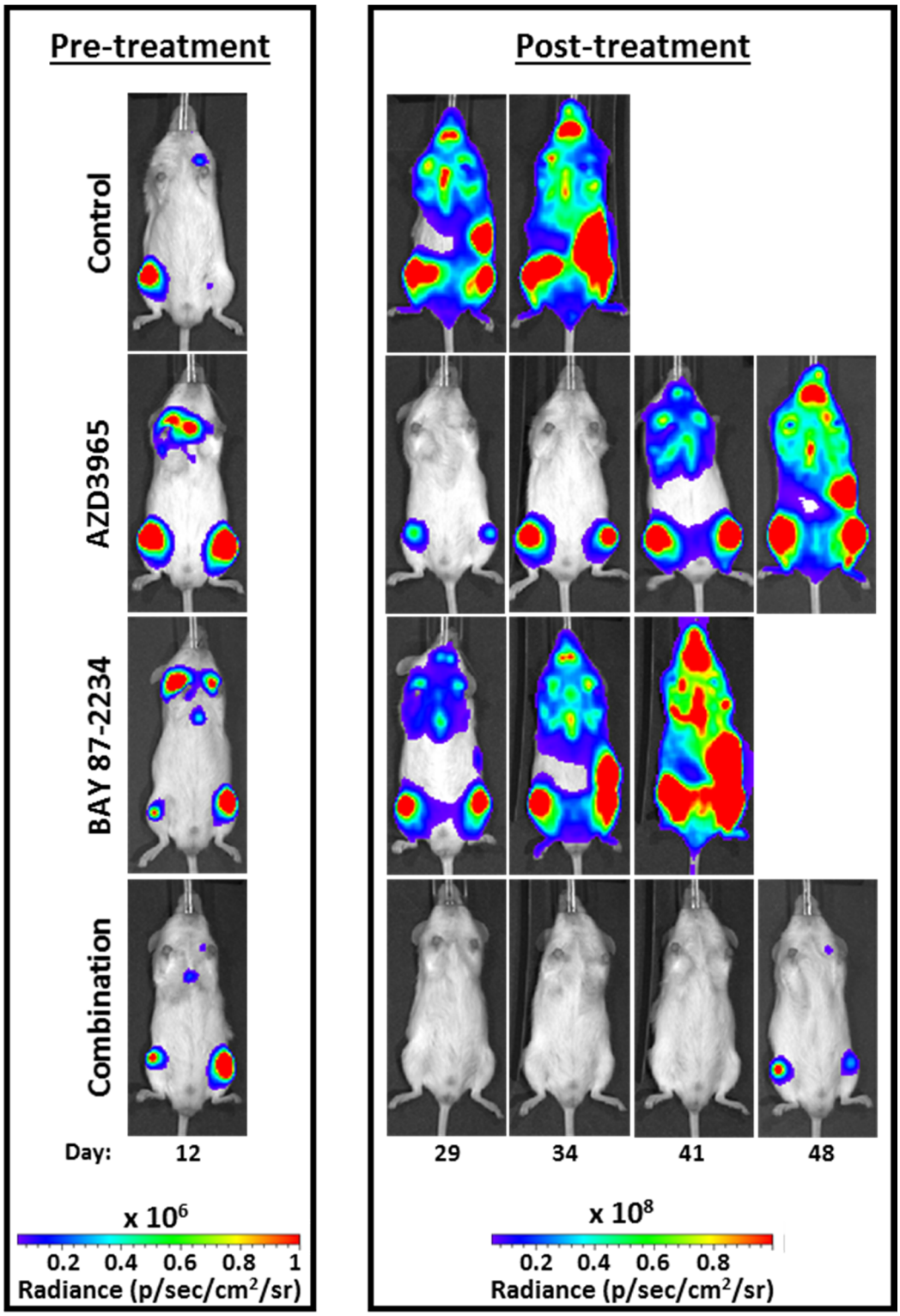

Figure 6-15: Visualisation of the progression of CA46 post-treatment *in vivo*.
NSG mice were intravenously inoculated with luciferase-expressing CA46 cells and allowed to engraft for 12 days prior to treatment with AZD3965 (100 $mg.kg^{-1}$, BID), BAY 87-2243 (9 $mg.kg^{-1}$, OD) or the combination of AZD3965 and BAY 87-2243, for 14-days. Representative images taken of a mouse from each treatment group are shown pre-treatment (day 12) and post-treatment (day 29, 34, 41, 48). Pre and post-treatment images are displayed on separate scales.

Post-treatment, mice previously receiving AZD3965 alone progressed at a rate comparable to control animals indicating continued dosing would be necessary and maybe sufficient for disease control (Figure 6-16). Similarly, despite the reduction in tumour burden following combination treatment, on cessation we observed regrowth such that at the end of the study (day 48) radiance values in the combination group were similar to those in control mice at day 29 (Figure 6-16).

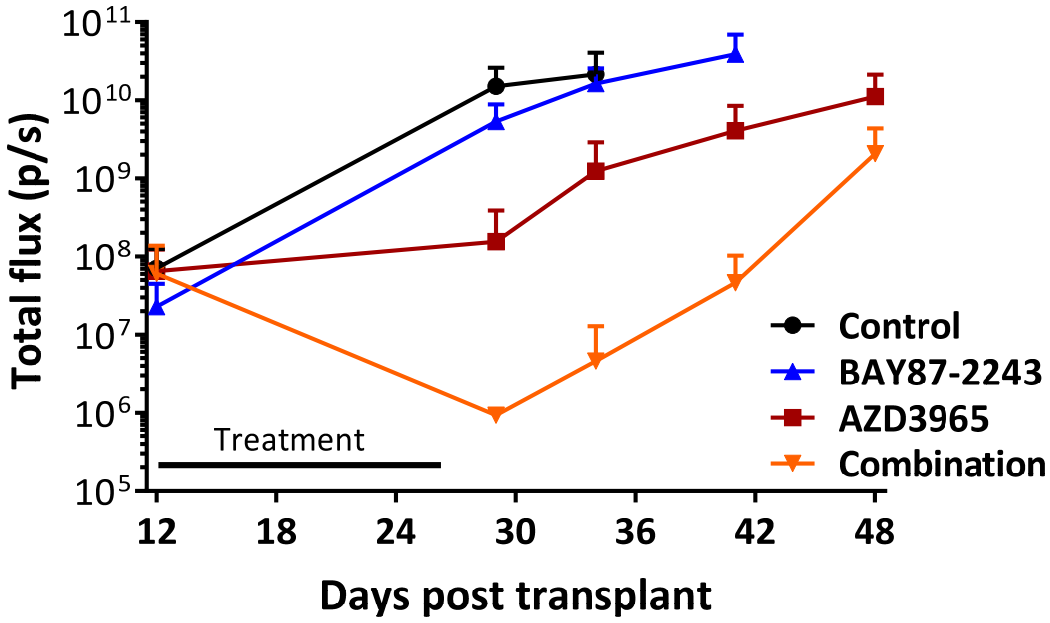

Figure 6-16: Progression of CA46 post-treatment *in vivo*.
NSG mice were intravenously inoculated with luciferase-expressing CA46 cells and allowed to engraft for 12 days prior to treatment with AZD3965 (100 mg.kg^{-1}, BID), BAY 87-2243 (9 mg.kg^{-1}, OD) or the combination of AZD3965 and BAY 87-2243, for 14-days. Control and monotherapy-treated mice received the relevant vehicle controls. Mice were re-imaged at intervals from 72 hours following treatment. Scans were performed at 12, 29, 34, 41 and 48 days of treatment as described in Section 2.11. Data points show the mean + SEM on a logarithmic scale.

The treatment regimen was well tolerated, with no significant decrease in body weight relative to control mice receiving vehicle gavages although some mild weight loss was observed most likely associated with the dosing regimen which involved 3 gavages per day (Figure 6-17).

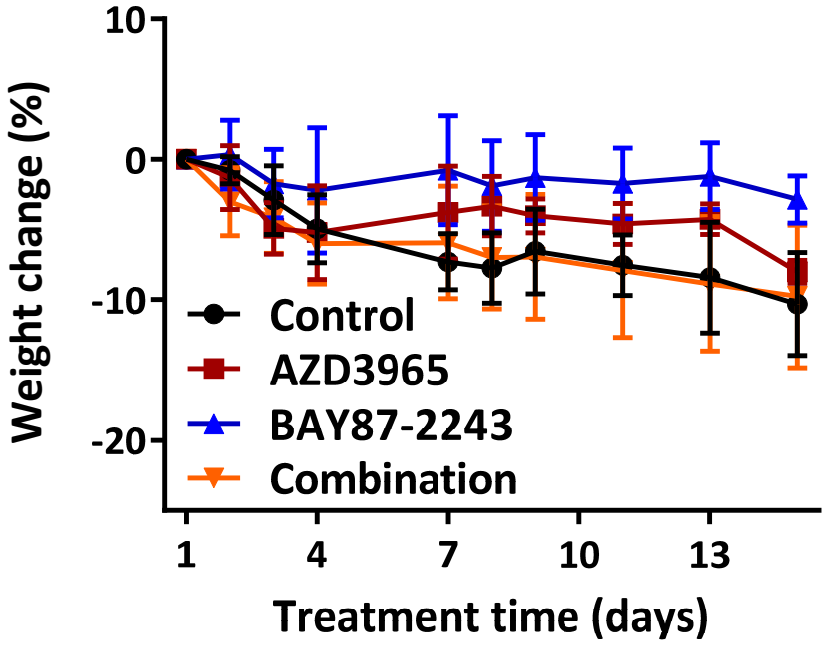

Figure 6-17: The oral dosing regimen of AZD3965 and BAY 87-2243 is well tolerated
Weights recorded at the indicated intervals were compared to individual mouse weights at the beginning of treatment to give a percentage change value. Data points show the mean + SEM % change.

6.7. Discussion

AZD3965 monotherapy produces a potent growth inhibitory effect in BL and DLBCL, however additional strategies are required to augment this activity, the most promising of which would be to identify combinations that could selectively trigger tumour cell death. We examined BL cell lines CA46 and Raji as these had the greatest amount of pre-existing data relating to the effects of AZD3965 monotherapy. These cell lines lacked sensitivity to the majority of the tested inhibitors. Previous studies have shown BL model, Eμ-Myc to be sensitive to a dual mTOR/PI3K inhibitior (227). However, here we also identified BL cell lines to be sensitive to the selective mTOR inhibitor AZD8055 monotherapy, and when we tested AZD8055 in combination with AZD3965 we observed mild to moderate synergy. Additional preliminary studies in DLBCL also suggest AZD3965 sensitizes cells to BCL2 inhibition in cells harbouring *BCL2* translocations.

We identified that Complex I inhibition using metformin in combination with AZD3965 was highly cytotoxic to CA46 and Raji cells and considered this a better strategy to pursue. However, metformin was only efficacious at millimolar doses *in vitro* which are not achievable *in vivo*. Human steady state plasma concentrations following a typical anti-

diabetic dose (2 g.day^{-1}) result in plasma metformin levels of 0.86 mg.L^{-1} (5.2 μM) (228). In mice, similar plasma concentrations to those achieved clinically in man (i.e. 5 μM), are only evident following administration of a very large 250 mg.kg^{-1} oral dose of metformin (229). Therefore even at high oral doses, plasma concentrations fall well short of *in vitro* concentrations required to see the dramatic combination effects. Importantly, metformin does not readily diffuse across cellular membranes and is reliant upon active transport mechanism such as organic cation transporters and therefore tumour transporter expression can also influence the intratumour drug concentrations attained. The relevance of *in vitro* metformin concentrations to mouse models and ultimately to potential human utility have been discussed (216, 217).

Despite this, due to its preclinical efficacy in cancer models and the widespread safe clinical use of metformin there is great interest in investigating the potential efficacy of metformin in cancer. Currently there are over 100 open clinical trial investigating the efficacy of metformin for treatment and prophylaxis of various cancer types. However, the first randomised controlled trial to report results, which studied metformin in combination with gemcitabine and erlotinib in PDAC, failed to show any additional survival benefit (230).

We selected a more potent Complex I inhibitor, BAY 87-2243, with favourable pharmacokinetics, to further investigate the combining Complex I inhibition with AZD3965. Our results investigating the combination of AZD3965 and BAY 87-2243 *in vivo* compare positively with recent reports combining MCT1 inhibition with Complex I inhibition using biguanides, metformin and phenformin *in vivo*. Our data also uniquely show a reduction in tumour burden *in vivo* as a result of combination treatment using an MCT1 inhibitor. However, as reported by Marchiq *et al.* tumour growth was observed on cessation of treatment (132). This may indicate the need for a longer treatment period to eliminate residual disease. Unfortunately, we were unable to monitor disease progression by bioluminescent imaging throughout the dosing period due to a severe adverse reaction to anaesthesia in mice receiving BAY 87-2243. Therefore, it is more difficult to draw conclusions about the effect of the combination on tumour growth. For example, if we had been able to observe a consistent trend towards decreasing tumour burden throughout the treatment period then it may have been reasonable to assume that a longer treatment period may have eradicated the tumour. Despite the relatively low metformin concentrations achievable i*n vivo,* the combination of metformin supplied in drinking water with an MCT1 inhibitor has

been shown to be efficacious, and led to some animals surviving beyond 80 days following cessation of combination treatment (84).

The combination with an oral small molecule inhibitor of Complex I clearly enhances the effects of AZD3965 *in vivo.* However, the development of BAY 87-2243 was stopped after its withdrawal from phase I clinical trials due to safety concerns as a result of severe adverse events which were not predicted by preclinical pharmacology (severe vomiting). This was despite efforts to reduce the dose and alter the formulation (231). Aside from metformin and phenformin there is a sparsity of other inhibitors which target Complex I, with potential utility. In addition to clinical examination of metformin, phenformin was also used clinically but withdrawn due to the risk of lactic acidosis estimated to be 40-64 cases for every 100,000 patient years (232). Whilst not acceptable for the management of diabetes this may present an acceptable risk profile for patients with refractory B-NHL. Speculative approaches with which to disrupt OXPHOS alongside MCT1 inhibition include targeting the mitochondrial HSP90 (TRAP-1) using the preclinical candidate Gamitrinib (233, 234). Gamitrinib has been shown to specifically target TRAP-1 clients including, succinate dehydrogenase (SDHB), leading to a reduction in OCR in prostate and glioblastoma cells (235). Another approach would be to use VLX600, which is undergoing Phase I clinical trial (NCT02222363) and causes mitochondrial dysfunction causing partial inhibition of respiratory complexes I, II and IV. VLX600 also attenuates spare respiratory capacity in similar way as observed here with BAY 87-2243 (53). The finding that VLX600 also triggered a shift towards a glycolytic phenotypic with increased production of lactate may be particularly pertinent for any attempts to combine with AZD3965.

There are similarities with our $MCT1_i$ resistance model, CA46-R, and that generated by Doherty *et al.* and referred to as $Raji^R$. Both exhibit reduced sensitivity to AZD3965 and AR-C122982 respectively although it is difficult to compare the relative shifts in sensitivity as data is only reported at a single dose of AR-C122982 (100 nM). Neither were associated with an increased expression of MCT4. Increased OCR and decreased ECAR were observed in both cases indicating increased oxidative metabolism reduces sensitivity to MCT1 inhibition. In support of this, both models showed increased sensitivity to inhibition of Complex I alone, although the magnitude of sensitisation in $Raji^R$ was far greater than observed in CA46-R cells with $Raji^R$ cell number being reduced by around 95% after just 24 hours of metformin

alone. This may be a reflection of the less specific nature of metformin particularly when used at millimolar concentrations.

The CA46-R resistance phenotype was associated with similar basal levels of intracellular lactate compared to parental cells, but lower AZD3965-induced lactate accumulation and decreased expression of MCT1 and CD147. This is distinct from the Raji^{R} model which exhibited increased basal levels of intracellular lactate and did not report alterations in MCT1 or CD147. No reported changes were described in Raji^{R} with respect to MCT1 inhibitor induced lactate accumulation. Collectively these studies suggest OXPHOS a likely adaptive change but that this may have different consequences depending on the tumour examined. However, the dual targeting of OXPHOS with AZD3965 could have broad potential in BL, even in the presence of a partial acquired resistance.

Chapter 7. General Discussion

This thesis examines the novel, potent and selective monocarboxylate transporter 1 (MCT1) inhibitor AZD3965 and its potential use as a treatment for BL and DLBCL tumours reliant upon MCT1 function. The experimental work reinforced MCT4 expression as a major intrinsic resistance factor to the effects of AZD3965 treatment and consequently this should be used as the basis for patient selection. The IHC methods established can be applied to tumour biopsies prospectively, to determine whether patients should be enrolled on AZD3965 treatment or offered an alternative therapy. The studies suggest DLBCL and BL are priority tumour types for clinical investigation, given the frequently low or negligible expression of MCT4, combined with a comparatively high glycolytic and proliferative rate.

7.1. Establishing a disease setting for AZD3965

The sensitivity of BL to AZD3965 and other MCT1 inhibitors has been previously demonstrated *in vitro* and *in vivo* in the BL cell line, Raji (84, 138). We have expanded this to a wider panel of BL cell lines and importantly made the first identification of DLBCL as a target disease for AZD3965 using preclinical data showing a substantial cytostatic effect (Chapter 4). Encouragingly, using IHC, we were also able to show that low MCT4 expression is a common feature in both BL and DLBCL patient samples independent of COO (GCB/ABC-DLBCL) classification (Figure 3-5, page 77). DLBCL as the most common form of B-NHL (8 cases per 100,000) represents a more prevalent disease population than BL (0.3 cases per 100,000) and is therefore more likely to be investigated clinically (236). Previous studies have shown cell lines from the OXPHOS subtype to be less glycolytic, which we postulated may produce a disparity in the sensitivity to AZD3965 between OXPHOS and BCR subtypes (167). However, CCC classification did not influence sensitivity to AZD3965 *in vitro*. Whether this is also true across a larger panel of ABC-DLBCL cell lines or within *in vivo* models where the tumour microenvironment can influence cellular metabolism is not clear and may warrant further investigation.

Both BL and DLBCL predominantly respond well to aggressive multi-agent chemotherapy However, around a third of DLBCL patients become refractory to treatment where prognosis with salvage therapies is poor (237). A small proportion (~10%) of BL cases also become refractory to treatment. Therefore, the lack of cytotoxicity of AZD3965 does not exclude the potential for clinical utility as a palliative care option in those patients who are refractory to standard treatment. A number of cell lines used here were originally established from

patients following treatment which might suggest that AZD3965 refractory patients will be sensitive to AZD3965. The median age of DLBCL patients is approximately 70 years of age and as the most common form of lymphoma in the elderly, a proportion cannot tolerate standard of care treatment R-CHOP treatment (236, 238). In such patients a well-tolerated agent may also be an important palliative treatment option

Although we have focussed on BL and DLBCL here, a number of other tumour types may warrant further investigation as they exhibit low *MCT4* gene expression including B and T-cell acute lymphoblastic leukaemia and mantle cell lymphoma (Figure 3-1, page 71). However, this is not a common feature of all hematological cancer types as acute myeloid leukaemia and Hodgkin lymphoma cell lines show a more varied expression of *MCT4*. There are also examples of solid tumours which exhibit low *MCT4* expression but the distribution of expression makes potential patient selection for early development more challenging than in BL/DLBCL. Although our data show MCT1+/MCT4- expression is a requirement for sensitivity to MCT1 inhibition in BL and DLBCL, MCT1+/MCT4- does not uniformly denote intrinsic sensitivity to AZD3965. In previous work we have demonstrated relative resistance in neuroblastoma cell lines despite low MCT4 expression and significant intracellular lactate accumulation (119). In addition, the SCLC cell line NCI-H1048 only exhibited a partial response under normoxic conditions despite significant AZD3965-induced lactate accumulation (134).

7.2. Metabolic consequences of AZD3965 treatment

The degree of lactate accumulation observed in BL and DLBCL compares favourably with previous findings under comparable experimental conditions in different cell types. *In vivo* lactate accumulation in Raji and CA46 subcutaneous xenografts was also comparable with fold increases reported in SCLC xenografts (~2-fold) (133, 134). A greater number of studies have measured extracellular lactate some of which show reduced extracellular lactate following MCT1 inhibition consistent with the inhibition of lactate efflux (Table 2-Table 3). The accumulation of early glycolytic intermediates such as G6P is consistent with the accumulation of lactate having a feedback inhibitory effect on glycolysis (Figure 5-15, page 127) (84). However our studies also reveal a concurrent increase in multiple TCA cycle metabolites not previously reported, as most studies have focussed on glycolytic metabolites. This may be reflective of increased oxidative metabolism.

The *in vitro* and *in vivo* metabolic response to AZD3965 revealed some dissimilarities. This may be due to the different methodologies used to interrogate *in vivo* (LC-MS) and *in vitro* (GC-MS) samples. Despite a large number of metabolites detectable by both methods, certain metabolites detected by GC-MS could not be detected by LC-MS and vice versa. Differences between the *in vitro* and *in vivo* response may also be attributed to the environmental factors (Chapter 5). *In vivo* there are also additional considerations around the interaction between tumour cells and the surrounding microenvironment and stroma, the availability of nutrients and varying oxygenation states each of which may influence the metabolic response to AZD3965. This is rather different from the *in vitro* environment where cells are constantly exposed to optimal levels oxygen and nutrients such as glucose and glutamine. This offers several avenues for further investigation. For example, it would be of interest to examine the effect of media composition on sensitivity to AZD3965 through reduced concentrations of glucose and glutamine in order to more accurately reflect physiological concentrations. The importance of MCT1 function under glucose deprivation has been investigated in oxidative tumour cell lines, where lactate uptake through MCT1 and subsequent oxidation is able to compensates for the loss of glucose (108, 239). Increased glutamine oxidation has also been reported in MYC expressing B-cells under glucose deprivation (18). Sensitivity to non-specific MCT1 inhibitor 3-bromopyruvate, sensitises cells to glutamine deprivation however whether this also applies to a truly specific MCT1 inhibitor is unclear (96).

Under hypoxic conditions cells become obligatory glycolytic which might suggest increased sensitivity to MCT1 inhibition although there is also the potential for HIF-1α to up-regulate MCT4 under such conditions and counteract this sensitivity. However, even in SCLC where hypoxia is common, a proportion of low MCT4 tumours exist. In SCLC the metabolic changes observed under hypoxia are somewhat similar to those associated with AZD3965 treatment albeit to a lower magnitude, supporting the model proposed by Sonveaux *et al.* where MCT1 inhibition prevents lactate uptake rather than efflux in oxygenated areas of the tumour limiting glucose availability to the hypoxic regions (108, 133). There is little known about the role of hypoxia in BL/DLBCL, however, recently HIF-1α expression has been demonstrated to be a positive prognostic factor for DLBCL patients receiving R-CHOP (240, 241). This in contrast to solid organ tumours where hypoxia and HIF-1α are usually negative prognostic factors. As MCT4 expression via HIF-1α activation is a potential resistance mechanism the

response of BL/DLBCL cell lines to hypoxia and MCT transporter expression would be of further interest.

7.3. Combination approaches to enhance the efficacy of AZD3965

In DLBCL and BL, AZD3965 treatment has a profound cytostatic effect over 5 days *in vitro* and 24 days *in vivo.* In order to enhance efficacy and induce cell death we examined a number of novel therapies against targets implicated in B-NHL pathophysiology to combine with MCT1 inhibition. We had initially investigated changes in gene expression following treatment with AZD3965 using the Fluidigm® platform with an aim to proposing and testing rational combinations but this was unsuccessful (AstraZeneca placement - *data not shown*). Subsequently the majority of work investigating small molecule inhibitors was concentrated in BL cell lines where the rationale may not be as strong as for DLBCL as they lack the relevant pathway activation to denote sensitivity to a given agent (e.g. *BCL2* overexpression, *PTEN* deletion) which may explain the limited sensitivity as monotherapy and as combination treatments.

Postulating that the increase in TCA cycle metabolites we had observed may suggest increased sensitivity to inhibition of oxidative metabolism we had begun to explore Complex I inhibition using rotenone or metformin prior to the publication of studies combining metformin with inhibition of MCT1 with pharmacological or siRNA approaches (84, 132). Our data show a combination of AZD3965 and BAY 87-2243 causes significant cell death *in vitro* and the first reported evidence of decreased tumour burden with an MCT1 inhibitor and Complex I inhibitor *in vivo.* However, on cessation of treatment we observed growth rates comparable to tumours which had not received AZD3965 and BAY 87-2243 which indicated the need for longer dosing or multiple cycles of treatment to achieve curative activity (Figure 6-15, page 150). Whilst this represents a promising strategy, the clinical development of BAY 87-2243 has been terminated and therefore alternate combinations must be sought if they are to be utilised clinically.

Combination treatment of the low specificity MCT1 inhibitor CHC and doxorubicin have been shown to produce additive effects *in vivo* (123). Cytotoxic chemotherapeutics such as doxorubicin are most efficacious against highly proliferative cells and therefore, as our and

published data show selective MCT1 inhibitors to be cytostatic, combination with these agents might not be optimal. Subsequently, it would be of interest to examine the combination of AZD3965 and an anti-CD20 antibody, rituximab, *in vivo* to trigger antibody dependent cellular toxicity and reduce tumour burden. Also in the clinic, replacement of conventional cytotoxic chemotherapy for more targeted agents such as AZD3965 in combination with rituximab may avoid some of the general cytotoxicity which limit the tolerability of standard therapy particularly in elderly patients which may have other comorbidities as well as reduced liver and kidney function associated with age (242).

7.4. Resistance

Chronic exposure to AZD3965 *in vitro* led to a partial acquired resistance phenotype through the adoption of a more oxidative metabolic phenotype (Figure 5-6, page 117). This is somewhat distinct from a previously reported BL model of acquired resistance to MCT1 inhibition, termed Raji^{R} (84). In both CA46-R and Raji^{R} increased MCT4 expression did not underlie resistance to the compound. This is in contrast to the intrinsic resistance phenotype exhibited by BJAB, and other studies showing the induced expression or artificial overexpression of MCT4 confers resistance to MCT1 inhibitors (84, 134). Both acquired resistance models exhibited increased oxygen consumption. However, uniquely, we observed reductions in CD147 and MCT1 (Figure 5-11, page 122). This could result in reduced plasma membrane expression of MCT1 in CA46-R cells which could be studied by immunofluorescence microscopy. It would be of interest to explore the resistance phenotype in CA46-R in more detail, for example, to investigate whether the resistance phenotype is stable or a more glycolytic and sensitive phenotype remerges following incubation in drug-free culture for extended periods.

In relation to the induction of resistance the pharmacokinetic profile of AZD3965 requires twice-daily dosing *in vivo* in order to maintain drug free plasma concentrations consistent with *in vitro* lactate accumulation. *In vivo,* plasma drug concentrations will obviously fluctuate in contrast to consistent levels achieved *in vitro* which may extend the time required for acquired resistance to occur as the selection pressure exerted *in vivo* may not be as great as with a constant incubation *in vitro* (134). However, since such a significant cytostatic effect was achieved in vivo over a three week period, it would be interesting to extend the dosing in such an experiment, to at least the six week period of treatment

required to elicit resistance *in vitro*. If any tumour growth were evident upon extended treatment *in vivo*, it would be possible to derive a cell line from this and subsequently characterise the resistance mechanism to compare this with CA46-R *in vitro*.

The development of acquired resistance could be investigated through a more chronic dosing schedule, examining any significant outgrowth by isolating tumour cells and culturing *in vitro*.

7.5. Potential biomarkers

As discussed, MCT4 expression represents a predictive biomarker, for resistance to AZD3965. In terms of a relevant pharmacodynamic biomarker *in vitro* and *in vivo* data suggest that intracellular lactate may be a good biomarker to demonstrate target engagement and a consequent change consistent with the mechanism of action. Whether the magnitude of change observed *in vivo* is sufficient to detect in a non-invasive fashion is less clear. However, we did not observe an alteration in AZD3965-induced lactate accumulation between parental and less sensitive CA46-R cells, suggesting that lactate accumulation whilst this reflects target engagement, it may not denote sensitivity or the development of resistance.

Changes in tumour pH have also been investigated which may potentially reflect lactate accumulation, which would be anticipated to be associated with intracellular acidification. MCT1 inhibitor induced reductions in intracellular pH (0.1-0.4 pH units) have been reported in MCT4 expressing multiple myeloma cell lines and greater effects observed in colorectal cancer cells when combined with ablation of MCT4 (125, 132). However, in previous work, we were unable to detect alterations in intracellular pH *in vitro* following treatment with AZD3965 (119). Also, pilot magnetic resonance spectroscopy (MRS) imaging data did not reveal an alteration in pH as a result of AZD3965 treatment *in vivo* (unpublished data) where biochemical lactate changes were measured *ex vivo;* measurements taken from mice with Raji xenografts who had received AZD3965 2 hours earlier were not significantly different from pre-treatment values (pre-treatment: 6.98 ± 0.14, post-treatment 6.99 ± 0.08). Such an endpoint may be confounded as the maintenance of pH homeostasis is not reliant upon monocarboxylate transporters alone. A number of other transporters are involved in proton-coupled transport of substrates and therefore targeting of one transporter can be compensated for.

Investigating potential changes in glucose uptake following AZD3965 treatment with FDG-PET in BL/DLBCL would also be of interest. Both BL and DLBCL exhibit avidity for FDG and FDG-PET-CT is used clinically for disease staging (243, 244). Doherty *et al.* show MCT1 inhibition reduces glucose uptake in Raji cells (78). However, Sonveaux *et al.* show an increase in glucose uptake from oxidative tumours following MCT1 inhibition (84, 108). Importantly, both authors draw conclusions on glucose consumption based on *in vitro* studies. So how AZD3965 influences FDG uptake in a DLBCL mouse model would be of interest before looking toward clinical utility to monitor treatment response.

7.6. Summary

In conclusion, our data support the clinical evaluation of AZD3965 in DLBCL and BL including the clinical selection of patients with low MCT4 expression based on the profound growth inhibitory effects achieved using *in vitro* and *in vivo* models. AZD3965 may have therapeutic utility in patients refractory to current therapy or in the palliative management of poor performance status patients with these diseases. However, approaches to target the glycolytic phenotype are likely to require combination therapies in order to deliver maximal patient benefit. We verify here that potent cell death and tumour regression dual can be achieved through inhibition simultaneous of MCT1 and Complex I.

Chapter 8. References

1. Warburg O, Posener K, Negelein E. Über den Stoffweschsel der Carcinomzelle. Biochem Zeitschr. 1924;152:309-44.
2. Warburg O. On respiratory impairment in cancer cells. Science. 1956;124(3215):269-70.
3. Racker E. Bioenergetics and the problem of tumor growth. Am Sci. 1972;60(1):56-63.
4. Hanahan D, Weinberg RA. Hallmarks of cancer: the next generation. Cell. 2011;144(5):646-74.
5. Berg JM, Tymoczko JL, Stryer L, Stryer LB. Biochemistry. 6th ed. ed. New York: W. H. Freeman ; Basingstoke : Palgrave [distributor]; 2007.
6. Pelicano H, Martin DS, Xu RH, Huang P. Glycolysis inhibition for anticancer treatment. Oncogene. 2006;25(34):4633-46.
7. Webb BA, Forouhar F, Szu F-E, Seetharaman J, Tong L, Barber DL. Structures of human phosphofructokinase-1 and atomic basis of cancer-associated mutations. Nature. 2015;523(7558):111-4.
8. Panieri E, Santoro MM. ROS homeostasis and metabolism: a dangerous liason in cancer cells. Cell Death Dis. 2016;7:e2253.
9. Parsons DW, Jones S, Zhang X, Lin JC-H, Leary RJ, Angenendt P, Mankoo P, Carter H, Siu IM, Gallia GL, Olivi A, McLendon R, Rasheed BA, Keir S, Nikolskaya T, Nikolsky Y, Busam DA, Tekleab H, Diaz LA, Hartigan J, Smith DR, Strausberg RL, Marie SKN, Shinjo SMO, Yan H, Riggins GJ, Bigner DD, Karchin R, Papadopoulos N, Parmigiani G, Vogelstein B, Velculescu VE, Kinzler KW. An Integrated Genomic Analysis of Human Glioblastoma Multiforme. Science. 2008;321(5897):1807.
10. Kanehisa Laboratories, and the KEGG project. Oxidative Phosphorylation [updated 16/6/15; cited 2016]. Available from: http://www.genome.jp/kegg/pathway/map/map00190.html.
11. Langer J. Whole-body PET scan using 18F-FDG. https://en.wikipedia.org/wiki/Positron_emission_tomography2006.
12. Pfeiffer T, Schuster S, Bonhoeffer S. Cooperation and competition in the evolution of ATP-producing pathways. Science. 2001;292(5516):504-7.
13. Miller DM, Thomas SD, Islam A, Muench D, Sedoris K. c-Myc and cancer metabolism. Clin Cancer Res. 2012;18(20):5546-53.

14. Shim H, Dolde C, Lewis BC, Wu CS, Dang G, Jungmann RA, Dalla-Favera R, Dang CV. c-Myc transactivation of LDH-A: implications for tumor metabolism and growth. Proc Natl Acad Sci USA. 1997;94(13):6658-63.
15. Osthus RC, Shim H, Kim S, Li Q, Reddy R, Mukherjee M, Xu Y, Wonsey D, Lee LA, Dang CV. Deregulation of glucose transporter 1 and glycolytic gene expression by c-Myc. J Biol Chem. 2000;275(29):21797-800.
16. Fan Y, Dickman KG, Zong WX. Akt and c-Myc differentially activate cellular metabolic programs and prime cells to bioenergetic inhibition. J Biol Chem. 2010;285(10):7324-33.
17. Wise DR, DeBerardinis RJ, Mancuso A, Sayed N, Zhang XY, Pfeiffer HK, Nissim I, Daikhin E, Yudkoff M, McMahon SB, Thompson CB. Myc regulates a transcriptional program that stimulates mitochondrial glutaminolysis and leads to glutamine addiction. Proc Natl Acad Sci USA. 2008;105(48):18782-7.
18. Le A, Lane AN, Hamaker M, Bose S, Gouw A, Barbi J, Tsukamoto T, Rojas CJ, Slusher BS, Zhang H, Zimmerman LJ, Liebler DC, Slebos RJ, Lorkiewicz PK, Higashi RM, Fan TW, Dang CV. Glucose-independent glutamine metabolism via TCA cycling for proliferation and survival in B cells. Cell Metab. 2012;15(1):110-21.
19. Sun L, Song L, Wan Q, Wu G, Li X, Wang Y, Wang J, Liu Z, Zhong X, He X, Shen S, Pan X, Li A, Wang Y, Gao P, Tang H, Zhang H. cMyc-mediated activation of serine biosynthesis pathway is critical for cancer progression under nutrient deprivation conditions. Cell Res. 2015;25(4):429-44.
20. Gao P, Tchernyshyov I, Chang TC, Lee YS, Kita K, Ochi T, Zeller KI, De Marzo AM, Van Eyk JE, Mendell JT, Dang CV. c-Myc suppression of miR-23a/b enhances mitochondrial glutaminase expression and glutamine metabolism. Nature. 2009;458(7239):762-5.
21. David CJ, Chen M, Assanah M, Canoll P, Manley JL. HnRNP proteins controlled by c-Myc deregulate pyruvate kinase mRNA splicing in cancer. Nature. 2010;463(7279):364-8.
22. Israelsen William J, Dayton Talya L, Davidson Shawn M, Fiske Brian P, Hosios Aaron M, Bellinger G, Li J, Yu Y, Sasaki M, Horner James W, Burga Laura N, Xie J, Jurczak Michael J, DePinho Ronald A, Clish Clary B, Jacks T, Kibbey Richard G, Wulf Gerburg M, Di Vizio D, Mills Gordon B, Cantley Lewis C, Vander Heiden Matthew G. PKM2 Isoform-Specific Deletion Reveals a Differential Requirement for Pyruvate Kinase in Tumor Cells. Cell. 2013;155(2):397-409.

23. Selak MA, Armour SM, MacKenzie ED, Boulahbel H, Watson DG, Mansfield KD, Pan Y, Simon MC, Thompson CB, Gottlieb E. Succinate links TCA cycle dysfunction to oncogenesis by inhibiting HIF-alpha prolyl hydroxylase. Cancer Cell. 2005;7(1):77-85.
24. Jiang BH, Jiang G, Zheng JZ, Lu Z, Hunter T, Vogt PK. Phosphatidylinositol 3-kinase signaling controls levels of hypoxia-inducible factor 1. Cell Growth Differ. 2001;12(7):363-9.
25. Amelio I, Melino G. The p53 family and the hypoxia-inducible factors (HIFs): determinants of cancer progression. Trends Biochem Sci. 2015;40(8):425-34.
26. Zhang H, Gao P, Fukuda R, Kumar G, Krishnamachary B, Zeller KI, Dang CV, Semenza GL. HIF-1 inhibits mitochondrial biogenesis and cellular respiration in VHL-deficient renal cell carcinoma by repression of C-MYC activity. Cancer Cell. 2007;11(5):407-20.
27. Maddocks OD, Vousden KH. Metabolic regulation by p53. J Mol Med. 2011;89(3):237-45.
28. Bensaad K, Tsuruta A, Selak MA, Vidal MN, Nakano K, Bartrons R, Gottlieb E, Vousden KH. TIGAR, a p53-inducible regulator of glycolysis and apoptosis. Cell. 2006;126(1):107-20.
29. Gerin I, Noel G, Bolsee J, Haumont O, Van Schaftingen E, Bommer GT. Identification of TP53-induced glycolysis and apoptosis regulator (TIGAR) as the phosphoglycolate-independent 2,3-bisphosphoglycerate phosphatase. Biochem J. 2014;458(3):439-48.
30. Riscal R, Schrepfer E, Arena G, Cissé Madi Y, Bellvert F, Heuillet M, Rambow F, Bonneil E, Sabourdy F, Vincent C, Ait-Arsa I, Levade T, Thibaut P, Marine J-C, Portais J-C, Sarry J-E, Le Cam L, Linares Laetitia K. Chromatin-Bound MDM2 Regulates Serine Metabolism and Redox Homeostasis Independently of p53. Mol Cell.
31. DeBerardinis RJ, Chandel NS. Fundamentals of cancer metabolism. Sci Adv. 2016;2(5):e1600200.
32. Martinez-Outschoorn UE, Peiris-Pages M, Pestell RG, Sotgia F, Lisanti MP. Cancer metabolism: a therapeutic perspective. Nat Rev Clin Oncol. 2016.
33. Wilson PM, Danenberg PV, Johnston PG, Lenz H-J, Ladner RD. Standing the test of time: targeting thymidylate biosynthesis in cancer therapy. Nat Rev Clin Oncol. 2014;11(5):282-98.
34. Xiang Y, Stine ZE, Xia J, Lu Y, O'Connor RS, Altman BJ, Hsieh AL, Gouw AM, Thomas AG, Gao P, Sun L, Song L, Yan B, Slusher BS, Zhuo J, Ooi LL, Lee CG, Mancuso A, McCallion AS, Le A, Milone MC, Rayport S, Felsher DW, Dang CV. Targeted inhibition of tumor-

specific glutaminase diminishes cell-autonomous tumorigenesis. J Clin Invest. 2015;125(6):2293-306.

35. Shukla K, Ferraris DV, Thomas AG, Stathis M, Duvall B, Delahanty G, Alt J, Rais R, Rojas C, Gao P, Xiang Y, Dang CV, Slusher BS, Tsukamoto T. Design, synthesis, and pharmacological evaluation of bis-2-(5-phenylacetamido-1,2,4-thiadiazol-2-yl)ethyl sulfide 3 (BPTES) analogs as glutaminase inhibitors. J Med Chem. 2012;55(23):10551-63.
36. Stalnecker CA, Ulrich SM, Li Y, Ramachandran S, McBrayer MK, DeBerardinis RJ, Cerione RA, Erickson JW. Mechanism by which a recently discovered allosteric inhibitor blocks glutamine metabolism in transformed cells. Proc Natl Acad Sci USA. 2015;112(2):394-9.
37. Gross MI, Demo SD, Dennison JB, Chen L, Chernov-Rogan T, Goyal B, Janes JR, Laidig GJ, Lewis ER, Li J, Mackinnon AL, Parlati F, Rodriguez ML, Shwonek PJ, Sjogren EB, Stanton TF, Wang T, Yang J, Zhao F, Bennett MK. Antitumor activity of the glutaminase inhibitor CB-839 in triple-negative breast cancer. Mol Cancer Ther. 2014;13(4):890-901.
38. Maddocks Oliver DK, Labuschagne Christiaan F, Adams Peter D, Vousden Karen H. Serine Metabolism Supports the Methionine Cycle and DNA/RNA Methylation through De Novo ATP Synthesis in Cancer Cells. Mol Cell. 2016;61(2):210-21.
39. Sullivan LB, Gui DY, Hosios AM, Bush LN, Freinkman E, Vander Heiden MG. Supporting Aspartate Biosynthesis Is an Essential Function of Respiration in Proliferating Cells. Cell. 2015;162(3):552-63.
40. Mullarky E, Lucki NC, Beheshti Zavareh R, Anglin JL, Gomes AP, Nicolay BN, Wong JC, Christen S, Takahashi H, Singh PK, Blenis J, Warren JD, Fendt SM, Asara JM, DeNicola GM, Lyssiotis CA, Lairson LL, Cantley LC. Identification of a small molecule inhibitor of 3-phosphoglycerate dehydrogenase to target serine biosynthesis in cancers. Proc Natl Acad Sci USA. 2016;113(7):1778-83.
41. Evans JM, Donnelly LA, Emslie-Smith AM, Alessi DR, Morris AD. Metformin and reduced risk of cancer in diabetic patients. BMJ. 2005;330(7503):1304-5.
42. Ben Sahra I, Laurent K, Giuliano S, Larbret F, Ponzio G, Gounon P, Le Marchand-Brustel Y, Giorgetti-Peraldi S, Cormont M, Bertolotto C, Deckert M, Auberger P, Tanti JF, Bost F. Targeting cancer cell metabolism: the combination of metformin and 2-deoxyglucose induces p53-dependent apoptosis in prostate cancer cells. Cancer Res. 2010;70(6):2465-75.

43. Cheong JH, Park ES, Liang J, Dennison JB, Tsavachidou D, Nguyen-Charles C, Wa Cheng K, Hall H, Zhang D, Lu Y, Ravoori M, Kundra V, Ajani J, Lee JS, Ki Hong W, Mills GB. Dual inhibition of tumor energy pathway by 2-deoxyglucose and metformin is effective against a broad spectrum of preclinical cancer models. Mol Cancer Ther. 2011;10(12):2350-62.
44. Shi WY, Xiao D, Wang L, Dong LH, Yan ZX, Shen ZX, Chen SJ, Chen Y, Zhao WL. Therapeutic metformin/AMPK activation blocked lymphoma cell growth via inhibition of mTOR pathway and induction of autophagy. Cell Death Dis. 2012;3:e275.
45. Fendt SM, Bell EL, Keibler MA, Davidson SM, Wirth GJ, Fiske B, Mayers JR, Schwab M, Bellinger G, Csibi A, Patnaik A, Blouin MJ, Cantley LC, Guarente L, Blenis J, Pollak MN, Olumi AF, Vander Heiden MG, Stephanopoulos G. Metformin decreases glucose oxidation and increases the dependency of prostate cancer cells on reductive glutamine metabolism. Cancer Res. 2013;73(14):4429-38.
46. Owen MR, Doran E, Halestrap AP. Evidence that metformin exerts its anti-diabetic effects through inhibition of complex 1 of the mitochondrial respiratory chain. Biochem J. 2000;348 Pt 3:607-14.
47. Bridges HR, Jones AJ, Pollak MN, Hirst J. Effects of metformin and other biguanides on oxidative phosphorylation in mitochondria. Biochem J. 2014;462(3):475-87.
48. Ellinghaus P, Heisler I, Unterschemmann K, Haerter M, Beck H, Greschat S, Ehrmann A, Summer H, Flamme I, Oehme F, Thierauch K, Michels M, Hess-Stumpp H, Ziegelbauer K. BAY 87-2243, a highly potent and selective inhibitor of hypoxia-induced gene activation has antitumor activities by inhibition of mitochondrial complex I. Cancer Med. 2013;2(5):611-24.
49. Schockel L, Glasauer A, Basit F, Bitschar K, Truong H, Erdmann G, Algire C, Hagebarth A, Willems PH, Kopitz C, Koopman WJ, Heroult M. Targeting mitochondrial complex I using BAY 87-2243 reduces melanoma tumor growth. Cancer Metab. 2015;3:11.
50. Bendell JC, Patel MR, Infante JR, Kurkjian CD, Jones SF, Pant S, Burris HA, 3rd, Moreno O, Esquibel V, Levin W, Moore KN. Phase 1, open-label, dose escalation, safety, and pharmacokinetics study of ME-344 as a single agent in patients with refractory solid tumors. Cancer. 2015;121(7):1056-63.
51. Jeyaraju DV, Hurren R, Wang X, MacLean N, Gronda M, Shamas-Din A, Minden MD, Giaever G, Schimmer AD. A novel isoflavone, ME-344, targets the cytoskeleton in acute myeloid leukemia. Oncotarget. 2016.

52. Lim SC, Carey KT, McKenzie M. Anti-cancer analogues ME-143 and ME-344 exert toxicity by directly inhibiting mitochondrial NADH: ubiquinone oxidoreductase (Complex I). Am J Cancer Res. 2015;5(2):689-701.
53. Zhang X, Fryknäs M, Hernlund E, Fayad W, De Milito A, Olofsson MH, Gogvadze V, Dang L, Påhlman S, Schughart LAK, Rickardson L, D'Arcy P, Gullbo J, Nygren P, Larsson R, Linder S. Induction of mitochondrial dysfunction as a strategy for targeting tumour cells in metabolically compromised microenvironments. Nature Communications. 2014;5:3295.
54. Stein M, Lin H, Jeyamohan C, Dvorzhinski D, Gounder M, Bray K, Eddy S, Goodin S, White E, Dipaola RS. Targeting tumor metabolism with 2-deoxyglucose in patients with castrate-resistant prostate cancer and advanced malignancies. Prostate. 2010;70(13):1388-94.
55. Chaneton B, Gottlieb E. Rocking cell metabolism: revised functions of the key glycolytic regulator PKM2 in cancer. Trends Biochem Sci. 2012;37(8):309-16.
56. Parnell KM, Foulks JM, Nix RN, Clifford A, Bullough J, Luo B, Senina A, Vollmer D, Liu J, McCarthy V, Xu Y, Saunders M, Liu XH, Pearce S, Wright K, O'Reilly M, McCullar MV, Ho KK, Kanner SB. Pharmacologic activation of PKM2 slows lung tumor xenograft growth. Mol Cancer Ther. 2013;12(8):1453-60.
57. Vander Heiden MG, Christofk HR, Schuman E, Subtelny AO, Sharfi H, Harlow EE, Xian J, Cantley LC. Identification of small molecule inhibitors of pyruvate kinase M2. Biochem Pharmacol. 2010;79(8):1118-24.
58. Tejeda M, Gaal D, Hullan L, Hegymegi-Barakonyi B, Keri G. Evaluation of the antitumor efficacy of the somatostatin structural derivative TT-232 on different tumor models. Anticancer Res. 2006;26(5A):3477-83.
59. Atsumi T, Chesney J, Metz C, Leng L, Donnelly S, Makita Z, Mitchell R, Bucala R. High expression of inducible 6-phosphofructo-2-kinase/fructose-2,6-bisphosphatase (iPFK-2; PFKFB3) in human cancers. Cancer Res. 2002;62(20):5881-7.
60. Redman R, Pohlmann P, Kurman M, Tapolsky GH, Chesney J. Abstract CT206: PFK-158, first-in-man and first-in-class inhibitor of PFKFB3/ glycolysis: A phase I, dose escalation, multi-center study in patients with advanced solid malignancies. Cancer Res. 2015;75(15 Supplement):CT206.

61. Sheng SL, Liu JJ, Dai YH, Sun XG, Xiong XP, Huang G. Knockdown of lactate dehydrogenase A suppresses tumor growth and metastasis of human hepatocellular carcinoma. FEBS J. 2012;279(20):3898-910.
62. Rajeshkumar NV, Dutta P, Yabuuchi S, de Wilde RF, Martinez GV, Le A, Kamphorst JJ, Rabinowitz JD, Jain SK, Hidalgo M, Dang CV, Gillies RJ, Maitra A. Therapeutic Targeting of the Warburg Effect in Pancreatic Cancer Relies on an Absence of p53 Function. Cancer Res. 2015;75(16):3355-64.
63. Boudreau A, Purkey HE, Hitz A, Robarge K, Peterson D, Labadie S, Kwong M, Hong R, Gao M, Del Nagro C, Pusapati R, Ma S, Salphati L, Pang J, Zhou A, Lai T, Li Y, Chen Z, Wei B, Yen I, Sideris S, McCleland M, Firestein R, Corson L, Vanderbilt A, Williams S, Daemen A, Belvin M, Eigenbrot C, Jackson PK, Malek S, Hatzivassiliou G, Sampath D, Evangelista M, O'Brien T. Metabolic plasticity underpins innate and acquired resistance to LDHA inhibition. Nat Chem Biol. 2016;advance online publication.
64. Poole RC, Sansom CE, Halestrap AP. Studies of the membrane topology of the rat erythrocyte H+/lactate cotransporter (MCT1). Biochemical Journal. 1996;320(Pt 3):817-24.
65. Halestrap AP, Price NT. The proton-linked monocarboxylate transporter (MCT) family: structure, function and regulation. Biochem J. 1999;343 Pt 2:281-99.
66. Wilson MC, Meredith D, Bunnun C, Sessions RB, Halestrap AP. Studies on the DIDS-binding site of monocarboxylate transporter 1 suggest a homology model of the open conformation and a plausible translocation cycle. J Biol Chem. 2009;284(30):20011-21.
67. Manoharan C, Wilson MC, Sessions RB, Halestrap AP. The role of charged residues in the transmembrane helices of monocarboxylate transporter 1 and its ancillary protein basigin in determining plasma membrane expression and catalytic activity. Mol Membr Biol. 2006;23(6):486-98.
68. Yang J, Yan R, Roy A, Xu D, Poisson J, Zhang Y. The I-TASSER Suite: protein structure and function prediction. Nat Methods. 2015;12(1):7-8.
69. Yang J, Zhang Y. I-TASSER server: new development for protein structure and function predictions. Nucleic Acids Res. 2015;43(W1):W174-81.
70. Roy A, Kucukural A, Zhang Y. I-TASSER: a unified platform for automated protein structure and function prediction. Nat Protoc. 2010;5(4):725-38.
71. Zhang Y. I-TASSER server for protein 3D structure prediction. BMC Bioinformatics. 2008;9:40.

72. Broer S, Schneider HP, Broer A, Rahman B, Hamprecht B, Deitmer JW. Characterization of the monocarboxylate transporter 1 expressed in Xenopus laevis oocytes by changes in cytosolic pH. Biochem J. 1998;333 (Pt 1):167-74.
73. Halestrap AP. The monocarboxylate transporter family--Structure and functional characterization. IUBMB Life. 2012;64(1):1-9.
74. Halestrap AP, Wilson MC. The monocarboxylate transporter family--role and regulation. IUBMB Life. 2012;64(2):109-19.
75. Murray CM, Hutchinson R, Bantick JR, Belfield GP, Benjamin AD, Brazma D, Bundick RV, Cook ID, Craggs RI, Edwards S, Evans LR, Harrison R, Holness E, Jackson AP, Jackson CG, Kingston LP, Perry MW, Ross AR, Rugman PA, Sidhu SS, Sullivan M, Taylor-Fishwick DA, Walker PC, Whitehead YM, Wilkinson DJ, Wright A, Donald DK. Monocarboxylate transporter MCT1 is a target for immunosuppression. Nat Chem Biol. 2005;1(7):371-6.
76. MacIver NJ, Michalek RD, Rathmell JC. Metabolic regulation of T lymphocytes. Annu Rev Immunol. 2013;31:259-83.
77. Pierre K, Pellerin L. Monocarboxylate transporters in the central nervous system: distribution, regulation and function. J Neurochem. 2005;94(1):1-14.
78. Manning Fox JE, Meredith D, Halestrap AP. Characterisation of human monocarboxylate transporter 4 substantiates its role in lactic acid efflux from skeletal muscle. J Physiol. 2000;529 Pt 2:285-93.
79. Dimmer KS, Friedrich B, Lang F, Deitmer JW, Broer S. The low-affinity monocarboxylate transporter MCT4 is adapted to the export of lactate in highly glycolytic cells. Biochem J. 2000;350 Pt 1:219-27.
80. Suzuki A, Stern SA, Bozdagi O, Huntley GW, Walker RH, Magistretti PJ, Alberini CM. Astrocyte-neuron lactate transport is required for long-term memory formation. Cell. 2011;144(5):810-23.
81. Broer S, Broer A, Schneider HP, Stegen C, Halestrap AP, Deitmer JW. Characterization of the high-affinity monocarboxylate transporter MCT2 in Xenopus laevis oocytes. Biochem J. 1999;341 (Pt 3):529-35.
82. Philp NJ, Ochrietor JD, Rudoy C, Muramatsu T, Linser PJ. Loss of MCT1, MCT3, and MCT4 Expression in the Retinal Pigment Epithelium and Neural Retina of the 5A11/Basigin-Null Mouse. Investigative Ophthalmology & Visual Science. 2003;44(3):1305-11.

83. Nancolas B, Sessions RB, Halestrap AP. Identification of key binding site residues of MCT1 for AR-C155858 reveals the molecular basis of its isoform selectivity. Biochem J. 2015;466(1):177-88.
84. Doherty JR, Yang C, Scott KE, Cameron MD, Fallahi M, Li W, Hall MA, Amelio AL, Mishra JK, Li F, Tortosa M, Genau HM, Rounbehler RJ, Lu Y, Dang CV, Kumar KG, Butler AA, Bannister TD, Hooper AT, Unsal-Kacmaz K, Roush WR, Cleveland JL. Blocking lactate export by inhibiting the Myc target MCT1 Disables glycolysis and glutathione synthesis. Cancer Res. 2014;74(3):908-20.
85. Gan L, Xiu R, Ren P, Yue M, Su H, Guo G, Xiao D, Yu J, Jiang H, Liu H, Hu G, Qing G. Metabolic targeting of oncogene MYC by selective activation of the proton-coupled monocarboxylate family of transporters. Oncogene. 2016;35(23):3037-48.
86. Kitaoka Y, Takahashi Y, Machida M, Takeda K, Takemasa T, Hatta H. Effect of AMPK activation on monocarboxylate transporter (MCT)1 and MCT4 in denervated muscle. J Physiol Sci. 2014;64(1):59-64.
87. Boidot R, Vegran F, Meulle A, Le Breton A, Dessy C, Sonveaux P, Lizard-Nacol S, Feron O. Regulation of monocarboxylate transporter MCT1 expression by p53 mediates inward and outward lactate fluxes in tumors. Cancer Res. 2012;72(4):939-48.
88. Ullah MS, Davies AJ, Halestrap AP. The plasma membrane lactate transporter MCT4, but not MCT1, is up-regulated by hypoxia through a HIF-1alpha-dependent mechanism. J Biol Chem. 2006;281(14):9030-7.
89. Thomas C, Bishop DJ, Lambert K, Mercier J, Brooks GA. Effects of acute and chronic exercise on sarcolemmal MCT1 and MCT4 contents in human skeletal muscles: current status. American Journal of Physiology - Regulatory, Integrative and Comparative Physiology. 2012;302(1):R1-R14.
90. Kirk P, Wilson MC, Heddle C, Brown MH, Barclay AN, Halestrap AP. CD147 is tightly associated with lactate transporters MCT1 and MCT4 and facilitates their cell surface expression. EMBO J. 2000;19(15):3896-904.
91. Schneiderhan W, Scheler M, Holzmann KH, Marx M, Gschwend JE, Bucholz M, Gress TM, Seufferlein T, Adler G, Oswald F. CD147 silencing inhibits lactate transport and reduces malignant potential of pancreatic cancer cells in in vivo and in vitro models. Gut. 2009;58(10):1391-8.
92. Le Floch R, Chiche J, Marchiq I, Naiken T, Ilc K, Murray CM, Critchlow SE, Roux D, Simon MP, Pouyssegur J. CD147 subunit of lactate/H+ symporters MCT1 and hypoxia-inducible

MCT4 is critical for energetics and growth of glycolytic tumors. Proc Natl Acad Sci USA. 2011;108(40):16663-8.

93. Ibne Noor S, Dietz S, Heidtmann H, Boone CD, McKenna R, Deitmer JW, Becker HM. Analysis of the Binding Moiety mediating the Interaction between Monocarboxylate Transporters and Carbonic Anhydrase II. J Biol Chem. 2015.
94. Becker HM, Hirnet D, Fecher-Trost C, Sultemeyer D, Deitmer JW. Transport activity of MCT1 expressed in Xenopus oocytes is increased by interaction with carbonic anhydrase. J Biol Chem. 2005;280(48):39882-9.
95. Becker HM, Klier M, Schüler C, McKenna R, Deitmer JW. Intramolecular proton shuttle supports not only catalytic but also noncatalytic function of carbonic anhydrase II. Proc Natl Acad Sci USA. 2011;108(7):3071-6.
96. Cardaci S, Rizza S, Filomeni G, Bernardini R, Bertocchi F, Mattei M, Paci M, Rotilio G, Ciriolo MR. Glutamine Deprivation Enhances Antitumor Activity of 3-Bromopyruvate through the Stabilization of Monocarboxylate Transporter-1. Cancer Res. 2012;72(17):4526-36.
97. Pinheiro C, Albergaria A, Paredes J, Sousa B, Dufloth R, Vieira D, Schmitt F, Baltazar F. Monocarboxylate transporter 1 is up-regulated in basal-like breast carcinoma. Histopathology. 2010;56(7):860-7.
98. Hong CS, Graham NA, Gu W, Espindola Camacho C, Mah V, Maresh EL, Alavi M, Bagryanova L, Krotee PA, Gardner BK, Behbahan IS, Horvath S, Chia D, Mellinghoff IK, Hurvitz SA, Dubinett SM, Critchlow SE, Kurdistani SK, Goodglick L, Braas D, Graeber TG, Christofk HR. MCT1 Modulates Cancer Cell Pyruvate Export and Growth of Tumors that Co-express MCT1 and MCT4. Cell Rep. 2016.
99. Polanski R, Hodgkinson C, Fusi A, Nonaka D, Priest L, Kelly P, Trapani F, Bishop P, White A, Critchlow SE, Smith PD, Blackhall FH, Dive C, Morrow CJ. Activity of the Monocarboxylate Transporter 1 inhibitor AZD3965 in Small Cell Lung Cancer. Clinical Cancer Research. 2013.
100. Kim Y, Choi J-W, Lee J-H, Kim Y-S. Expression of lactate/H+ symporters MCT1 and MCT4 and their chaperone CD147 predicts tumor progression in clear cell renal cell carcinoma: immunohistochemical and The Cancer Genome Atlas data analyses. Hum Pathol. 2015;46(1):104-12.

101. Choi JW, Kim Y, Lee JH, Kim YS. Prognostic significance of lactate/proton symporters MCT1, MCT4, and their chaperone CD147 expressions in urothelial carcinoma of the bladder. Urology. 2014;84(1):245 e9-15.
102. de Oliveira AT, Pinheiro C, Longatto-Filho A, Brito MJ, Martinho O, Matos D, Carvalho AL, Vazquez VL, Silva TB, Scapulatempo C, Saad SS, Reis RM, Baltazar F. Co-expression of monocarboxylate transporter 1 (MCT1) and its chaperone (CD147) is associated with low survival in patients with gastrointestinal stromal tumors (GISTs). J Bioenerg Biomembr. 2012;44(1):171-8.
103. Martins SF, Amorim R, Viana-Pereira M, Pinheiro C, Costa RF, Silva P, Couto C, Alves S, Fernandes S, Vilaca S, Falcao J, Marques H, Pardal F, Rodrigues M, Preto A, Reis RM, Longatto-Filho A, Baltazar F. Significance of glycolytic metabolism-related protein expression in colorectal cancer, lymph node and hepatic metastasis. BMC Cancer. 2016;16(1):535.
104. Baek G, Tse YF, Hu Z, Cox D, Buboltz N, McCue P, Yeo CJ, White MA, DeBerardinis RJ, Knudsen ES, Witkiewicz AK. MCT4 Defines a Glycolytic Subtype of Pancreatic Cancer with Poor Prognosis and Unique Metabolic Dependencies. Cell Rep. 2014;9(6):2233-49.
105. Gerlinger M, Santos CR, Spencer-Dene B, Martinez P, Endesfelder D, Burrell RA, Vetter M, Jiang M, Saunders RE, Kelly G, Dykema K, Rioux-Leclercq N, Stamp G, Patard JJ, Larkin J, Howell M, Swanton C. Genome-wide RNA interference analysis of renal carcinoma survival regulators identifies MCT4 as a Warburg effect metabolic target. The Journal of Pathology. 2012;227(2):146-56.
106. Curry JM, Tuluc M, Whitaker-Menezes D, Ames JA, Anantharaman A, Butera A, Leiby B, Cognetti DM, Sotgia F, Lisanti MP, Martinez-Outschoorn UE. Cancer metabolism, stemness and tumor recurrence: MCT1 and MCT4 are functional biomarkers of metabolic symbiosis in head and neck cancer. Cell Cycle. 2013;12(9):1371-84.
107. Pertega-Gomes N, Vizcaino JR, Miranda-Goncalves V, Pinheiro C, Silva J, Pereira H, Monteiro P, Henrique RM, Reis RM, Lopes C, Baltazar F. Monocarboxylate transporter 4 (MCT4) and CD147 overexpression is associated with poor prognosis in prostate cancer. BMC Cancer. 2011;11:312.
108. Sonveaux P, Vegran F, Schroeder T, Wergin MC, Verrax J, Rabbani ZN, De Saedeleer CJ, Kennedy KM, Diepart C, Jordan BF, Kelley MJ, Gallez B, Wahl ML, Feron O, Dewhirst MW. Targeting lactate-fueled respiration selectively kills hypoxic tumor cells in mice. J Clin Invest. 2008;118(12):3930-42.

109. Pavlides S, Whitaker-Menezes D, Castello-Cros R, Flomenberg N, Witkiewicz AK, Frank PG, Casimiro MC, Wang C, Fortina P, Addya S, Pestell RG, Martinez-Outschoorn UE, Sotgia F, Lisanti MP. The reverse Warburg effect: aerobic glycolysis in cancer associated fibroblasts and the tumor stroma. Cell Cycle. 2009;8(23):3984-4001.
110. Colen CB, Shen Y, Ghoddoussi F, Yu P, Francis TB, Koch BJ, Monterey MD, Galloway MP, Sloan AE, Mathupala SP. Metabolic targeting of lactate efflux by malignant glioma inhibits invasiveness and induces necrosis: an in vivo study. Neoplasia. 2011;13(7):620-32.
111. Poole RC, Halestrap AP. Reversible and irreversible inhibition, by stilbenedisulphonates, of lactate transport into rat erythrocytes. Identification of some new high-affinity inhibitors. Biochemical Journal. 1991;275(2):307-12.
112. Halestrap AP, Meredith D. The SLC16 gene family-from monocarboxylate transporters (MCTs) to aromatic amino acid transporters and beyond. Pflugers Arch. 2004;447(5):619-28.
113. Nath K, Guo L, Nancolas B, Nelson DS, Shestov AA, Lee SC, Roman J, Zhou R, Leeper DB, Halestrap AP, Blair IA, Glickson JD. Mechanism of antineoplastic activity of lonidamine. Biochim Biophys Acta. 2016;1866(2):151-62.
114. Davies SP, Reddy H, Caivano M, Cohen P. Specificity and mechanism of action of some commonly used protein kinase inhibitors. Biochemical Journal. 2000;351(1):95-105.
115. Birsoy K, Wang T, Possemato R, Yilmaz OH, Koch CE, Chen WW, Hutchins AW, Gultekin Y, Peterson TR, Carette JE, Brummelkamp TR, Clish CB, Sabatini DM. MCT1-mediated transport of a toxic molecule is an effective strategy for targeting glycolytic tumors. Nat Genet. 2013;45(1):104-8.
116. Draoui N, Schicke O, Seront E, Bouzin C, Sonveaux P, Riant O, Feron O. Antitumor activity of 7-aminocarboxycoumarin derivatives, a new class of potent inhibitors of lactate influx but not efflux. Mol Cancer Ther. 2014.
117. Gurrapu S, Jonnalagadda SK, Alam MA, Ronayne CT, Nelson GL, Solano LN, Lueth EA, Drewes LR, Mereddy VR. Coumarin carboxylic acids as monocarboxylate transporter 1 inhibitors: In vitro and in vivo studies as potential anticancer agents. Bioorg Med Chem Lett. 2016;26(14):3282-6.
118. Critchlow SE, Tate L, inventorsUse of a MCT1 inhibitor in the treatment of cancers expressing MCT1 over MCT4 patent WO 2010089580 A1. 2010.

119. Noble R. Inhibition of Monocarboxylate Transporter-1 (MCT1) as a potential therapeutic approach in oncology [MRes]: Newcastle University; 2013.
120. Busk M, Walenta S, Mueller-Klieser W, Steiniche T, Jakobsen S, Horsman MR, Overgaard J. Inhibition of tumor lactate oxidation: Consequences for the tumor microenvironment. Radiotherapy and Oncology. 2011;99(3):404-11.
121. Amorim R, Pinheiro C, Miranda-Goncalves V, Pereira H, Moyer MP, Preto A, Baltazar F. Monocarboxylate transport inhibition potentiates the cytotoxic effect of 5-fluorouracil in colorectal cancer cells. Cancer Lett. 2015;365(1):68-78.
122. Morais-Santos F, Miranda-Goncalves V, Pinheiro S, Vieira AF, Paredes J, Schmitt FC, Baltazar F, Pinheiro C. Differential sensitivities to lactate transport inhibitors of breast cancer cell lines. Endocrine-Related Cancer. 2014;21(1):27-38.
123. Zhao Z, Wu MS, Zou C, Tang Q, Lu J, Liu D, Wu Y, Yin J, Xie X, Shen J, Kang T, Wang J. Downregulation of MCT1 inhibits tumor growth, metastasis and enhances chemotherapeutic efficacy in osteosarcoma through regulation of the NF-kappaB pathway. Cancer Lett. 2014;342(1):150-8.
124. Miranda-Goncalves V, Honavar M, Pinheiro C, Martinho O, Pires MM, Cordeiro M, Bebiano G, Costa P, Palmeirim I, Reis RM, Baltazar F. Monocarboxylate transporters (MCTs) in gliomas: expression and exploitation as therapeutic targets. Neuro Oncol. 2013;15(2):172-88.
125. Hanson DJ, Nakamura S, Amachi R, Hiasa M, Oda A, Tsuji D, Itoh K, Harada T, Horikawa K, Teramachi J, Miki H, Matsumoto T, Abe M. Effective impairment of myeloma cells and their progenitors by blockade of monocarboxylate transportation. Oncotarget. 2015;6(32):33568-86.
126. Izumi H, Takahashi M, Uramoto H, Nakayama Y, Oyama T, Wang KY, Sasaguri Y, Nishizawa S, Kohno K. Monocarboxylate transporters 1 and 4 are involved in the invasion activity of human lung cancer cells. Cancer Science. 2011;102(5):1007-13.
127. Fang J, Quinones QJ, Holman TL, Morowitz MJ, Wang Q, Zhao H, Sivo F, Maris JM, Wahl ML. The H+-linked monocarboxylate transporter (MCT1/SLC16A1): a potential therapeutic target for high-risk neuroblastoma. Mol Pharmacol. 2006;70(6):2108-15.
128. De Saedeleer CJ, Copetti T, Porporato PE, Verrax J, Feron O, Sonveaux P. Lactate activates HIF-1 in oxidative but not in Warburg-phenotype human tumor cells. PLoS One. 2012;7(10):e46571.

129. Vegran F, Boidot R, Michiels C, Sonveaux P, Feron O. Lactate influx through the endothelial cell monocarboxylate transporter MCT1 supports an NF-kappaB/IL-8 pathway that drives tumor angiogenesis. Cancer Res. 2011;71(7):2550-60.
130. Lamb R, Harrison H, Hulit J, Smith DL, Lisanti MP, Sotgia F. Mitochondria as new therapeutic targets for eradicating cancer stem cells: Quantitative proteomics and functional validation via MCT1/2 inhibition. Oncotarget. 2014;5(22):11029-37.
131. Ovens MJ, Davies AJ, Wilson MC, Murray CM, Halestrap AP. AR-C155858 is a potent inhibitor of monocarboxylate transporters MCT1 and MCT2 that binds to an intracellular site involving transmembrane helices 7-10. Biochem J. 2010;425(3):523-30.
132. Marchiq I, Le Floch R, Roux D, Simon M, Pouyssegur J. Genetic Disruption of Lactate/H+ Symporters (MCTs) and Their Subunit CD147/BASIGIN Sensitizes Glycolytic Tumor Cells to Phenformin. Cancer Res. 2014.
133. Bola BM, Chadwick AL, Michopoulos F, Blount KG, Telfer BA, Williams KJ, Smith PD, Critchlow SE, Stratford IJ. Inhibition of monocarboxylate transporter-1 (MCT1) by AZD3965 enhances radiosensitivity by reducing lactate transport. Mol Cancer Ther. 2014;13(12):2805-16.
134. Polanski R, Hodgkinson CL, Fusi A, Nonaka D, Priest L, Kelly P, Trapani F, Bishop PW, White A, Critchlow SE, Smith PD, Blackhall F, Dive C, Morrow CJ. Activity of the Monocarboxylate Transporter 1 Inhibitor AZD3965 in Small Cell Lung Cancer. Clin Cancer Res. 2014;20(4):926-37.
135. Gray AL, Coleman DT, Shi R, Cardelli JA. Monocarboxylate transporter 1 contributes to growth factor-induced tumor cell migration independent of transporter activity. Oncotarget. 2016.
136. Slack M, Wang T, Wang R. T cell metabolic reprogramming and plasticity. Molecular Immunology. 2015;68(2, Part C):507-12.
137. Bueno V, Binet I, Steger U, Bundick R, Ferguson D, Murray C, Donald D, Wood K. The specific monocarboxylate transporter (MCT1) inhibitor, AR-C117977, a novel immunosuppressant, prolongs allograft survival in the mouse. Transplantation. 2007;84(9):1204-7.
138. AACR 103rd Annual Meeting 2012. Chicago, IL, U.S.A2012. Abstract 3224: Pre-clinical targeting of the metabolic phenotype of lymphoma by AZD3965, a selective inhibitor of monocarboxylate transporter 1 (MCT1).

139. van Hasselt PM, Ferdinandusse S, Monroe GR, Ruiter JP, Turkenburg M, Geerlings MJ, Duran K, Harakalova M, van der Zwaag B, Monavari AA, Okur I, Sharrard MJ, Cleary M, O'Connell N, Walker V, Rubio-Gozalbo ME, de Vries MC, Visser G, Houwen RH, van der Smagt JJ, Verhoeven-Duif NM, Wanders RJ, van Haaften G. Monocarboxylate transporter 1 deficiency and ketone utilization. N Engl J Med. 2014;371(20):1900-7.
140. Merezhinskaya N, Fishbein WN, Davis JI, Foellmer JW. Mutations in MCT1 cDNA in patients with symptomatic deficiency in lactate transport. Muscle & Nerve. 2000;23(1):90-7.
141. Maria Murga Penas E, Schilling G, Behrmann P, Klokow M, Vettorazzi E, Bokemeyer C, Dierlamm J. Comprehensive cytogenetic and molecular cytogenetic analysis of 44 Burkitt lymphoma cell lines: secondary chromosomal changes characterization, karyotypic evolution, and comparison with primary samples. Genes Chromosomes Cancer. 2014;53(6):497-515.
142. Menezes J, Leibold W, Klein G, Clements G. Establishment and characterization of an Epstein-Barr virus (EBC)-negative lymphoblastoid B cell line (BJA-B) from an exceptional, EBV-genome-negative African Burkitt's lymphoma. Biomedicine. 1975;22(4):276-84.
143. Ben-Bassat H, Polliack A, Shlomai Z, Kohn G, Hadar R, Rabinowitz R, Leizerowitz R, Matutes E, Buchier V, Brok-Simoni F, Okon E, Livini N, Schlesinger M. Farage, a Novel Early B Cell Lymphoma Cell Line with Trisomy 11. Leukemia and Lymphoma. 1992;6(6):513-21.
144. Baruch M, Hochberg M, Gabay C, Ben-Bassat H, Shlomai Z, Laskov R. Molecular characterization of an unusual non-Hodgkin's B-lymphoma cell line ("Farage") lacking the ability to produce immunoglobulin polypeptide chains. Leuk Lymphoma. 1996;21(5-6):485-95.
145. Chang H, Blondal JA, Benchimol S, Minden MD, Messner HA. p53 Mutations, c-myc and bcl-2 Rearrangements in Human Non-Hodgkin's Lymphoma Cell Lines. Leuk Lymphoma. 1995;19(1-2):165-71.
146. Gabay C, Ben-Bassat H, Schlesinger M, Laskov R. Somatic mutations and intraclonal variations in the rearranged Vkappa genes of B-non-Hodgkin's lymphoma cell lines. Eur J Haematol. 1999;63(3):180-91.

147. Th'ng KH, Garewal G, Kearney L, Rassool F, Melo JV, White H, Catovsky D, Foroni L, Luzzatto L, Goldman JM. Establishment and characterization of three new malignant lymphoid cell lines. Int J Cancer. 1987;39(1):89-93.
148. Scudiero DA, Shoemaker RH, Paull KD, Monks A, Tierney S, Nofziger TH, Currens MJ, Seniff D, Boyd MR. Evaluation of a soluble tetrazolium/formazan assay for cell growth and drug sensitivity in culture using human and other tumor cell lines. Cancer Res. 1988;48(17):4827-33.
149. Veselkov KA, Vingara LK, Masson P, Robinette SL, Want E, Li JV, Barton RH, Boursier-Neyret C, Walther B, Ebbels TM, Pelczer I, Holmes E, Lindon JC, Nicholson JK. Optimized preprocessing of ultra-performance liquid chromatography/mass spectrometry urinary metabolic profiles for improved information recovery. Anal Chem. 2011;83(15):5864-72.
150. Behrends V, Tredwell GD, Bundy JG. A software complement to AMDIS for processing GC-MS metabolomic data. Anal Biochem. 2011;415(2):206-8.
151. Kind T, Wohlgemuth G, Lee DY, Lu Y, Palazoglu M, Shahbaz S, Fiehn O. FiehnLib: mass spectral and retention index libraries for metabolomics based on quadrupole and time-of-flight gas chromatography/mass spectrometry. Anal Chem. 2009;81(24):10038-48.
152. Stein SE. An integrated method for spectrum extraction and compound identification from gas chromatography/mass spectrometry data. Journal of the American Society for Mass Spectrometry. 1999;10(8):770-81.
153. Jain M, Nilsson R, Sharma S, Madhusudhan N, Kitami T, Souza AL, Kafri R, Kirschner MW, Clish CB, Mootha VK. Metabolite profiling identifies a key role for glycine in rapid cancer cell proliferation. Science. 2012;336(6084):1040-4.
154. Klaassen CD, Casarett LJ, Doull J. Casarett and Doull's toxicology : the basic science of poisons. 8th ed. New York: McGraw-Hill; 2013. xiii, 1454 p. p.
155. Wu M, Neilson A, Swift AL, Moran R, Tamagnine J, Parslow D, Armistead S, Lemire K, Orrell J, Teich J, Chomicz S, Ferrick DA. Multiparameter metabolic analysis reveals a close link between attenuated mitochondrial bioenergetic function and enhanced glycolysis dependency in human tumor cells. Am J Physiol Cell Physiol. 2007;292(1):C125-36.
156. Hirsch FR, Varella-Garcia M, Bunn PA, Di Maria MV, Veve R, Bremnes RM, Barón AE, Zeng C, Franklin WA. Epidermal Growth Factor Receptor in Non–Small-Cell Lung

Carcinomas: Correlation Between Gene Copy Number and Protein Expression and Impact on Prognosis. J Clin Oncol. 2003;21(20):3798-807.

157. Culpin RE, Sieniawski M, Angus B, Menon GK, Proctor SJ, Milne P, McCabe K, Mainou-Fowler T. Prognostic significance of immunohistochemistry-based markers and algorithms in immunochemotherapy-treated diffuse large B cell lymphoma patients. Histopathology. 2013;63(6):788-801.
158. Hans CP, Weisenburger DD, Greiner TC, Gascoyne RD, Delabie J, Ott G, Muller-Hermelink HK, Campo E, Braziel RM, Jaffe ES, Pan Z, Farinha P, Smith LM, Falini B, Banham AH, Rosenwald A, Staudt LM, Connors JM, Armitage JO, Chan WC. Confirmation of the molecular classification of diffuse large B-cell lymphoma by immunohistochemistry using a tissue microarray. Blood. 2004;103(1):275-82.
159. Bomken S, Buechler L, Rehe K, Ponthan F, Elder A, Blair H, Bacon CM, Vormoor J, Heidenreich O. Lentiviral marking of patient-derived acute lymphoblastic leukaemic cells allows in vivo tracking of disease progression. Leukemia. 2013;27(3):718-21.
160. Barretina J, Caponigro G, Stransky N, Venkatesan K, Margolin AA, Kim S, Wilson CJ, Lehar J, Kryukov GV, Sonkin D, Reddy A, Liu M, Murray L, Berger MF, Monahan JE, Morais P, Meltzer J, Korejwa A, Jane-Valbuena J, Mapa FA, Thibault J, Bric-Furlong E, Raman P, Shipway A, Engels IH, Cheng J, Yu GK, Yu J, Aspesi P, Jr., de Silva M, Jagtap K, Jones MD, Wang L, Hatton C, Palescandolo E, Gupta S, Mahan S, Sougnez C, Onofrio RC, Liefeld T, MacConaill L, Winckler W, Reich M, Li N, Mesirov JP, Gabriel SB, Getz G, Ardlie K, Chan V, Myer VE, Weber BL, Porter J, Warmuth M, Finan P, Harris JL, Meyerson M, Golub TR, Morrissey MP, Sellers WR, Schlegel R, Garraway LA. The Cancer Cell Line Encyclopedia enables predictive modelling of anticancer drug sensitivity. Nature. 2012;483(7391):603-7.
161. Lymphoma Association. Diffuse large B-cell lymphoma 2013 [updated 08/13; cited 2014 30/04/14]. Available from: http://www.lymphomas.org.uk/sites/default/files/pdfs/Burkitt-lymphoma.pdf.
162. Shaffer AL, 3rd, Young RM, Staudt LM. Pathogenesis of human B cell lymphomas. Annu Rev Immunol. 2012;30:565-610.
163. Alizadeh AA, Eisen MB, Davis RE, Ma C, Lossos IS, Rosenwald A, Boldrick JC, Sabet H, Tran T, Yu X, Powell JI, Yang L, Marti GE, Moore T, Hudson J, Jr., Lu L, Lewis DB, Tibshirani R, Sherlock G, Chan WC, Greiner TC, Weisenburger DD, Armitage JO, Warnke R, Levy R, Wilson W, Grever MR, Byrd JC, Botstein D, Brown PO, Staudt LM. Distinct types of

diffuse large B-cell lymphoma identified by gene expression profiling. Nature. 2000;403(6769):503-11.

164. Rosenwald A, Wright G, Chan WC, Connors JM, Campo E, Fisher RI, Gascoyne RD, Muller-Hermelink HK, Smeland EB, Giltnane JM, Hurt EM, Zhao H, Averett L, Yang L, Wilson WH, Jaffe ES, Simon R, Klausner RD, Powell J, Duffey PL, Longo DL, Greiner TC, Weisenburger DD, Sanger WG, Dave BJ, Lynch JC, Vose J, Armitage JO, Montserrat E, Lopez-Guillermo A, Grogan TM, Miller TP, LeBlanc M, Ott G, Kvaloy S, Delabie J, Holte H, Krajci P, Stokke T, Staudt LM, Lymphoma/Leukemia Molecular Profiling P. The use of molecular profiling to predict survival after chemotherapy for diffuse large-B-cell lymphoma. N Engl J Med. 2002;346(25):1937-47.
165. Scott DW. Cell-of-Origin in Diffuse Large B-Cell Lymphoma: Are the Assays Ready for the Clinic? Am Soc Clin Oncol Educ Book. 2015:e458-66.
166. Monti S, Savage KJ, Kutok JL, Feuerhake F, Kurtin P, Mihm M, Wu B, Pasqualucci L, Neuberg D, Aguiar RC, Dal Cin P, Ladd C, Pinkus GS, Salles G, Harris NL, Dalla-Favera R, Habermann TM, Aster JC, Golub TR, Shipp MA. Molecular profiling of diffuse large B-cell lymphoma identifies robust subtypes including one characterized by host inflammatory response. Blood. 2005;105(5):1851-61.
167. Caro P, Kishan AU, Norberg E, Stanley IA, Chapuy B, Ficarro SB, Polak K, Tondera D, Gounarides J, Yin H, Zhou F, Green MR, Chen L, Monti S, Marto JA, Shipp MA, Danial NN. Metabolic signatures uncover distinct targets in molecular subsets of diffuse large B cell lymphoma. Cancer Cell. 2012;22(4):547-60.
168. Coiffier B, Thieblemont C, Van Den Neste E, Lepeu G, Plantier I, Castaigne S, Lefort S, Marit G, Macro M, Sebban C, Belhadj K, Bordessoule D, Ferme C, Tilly H. Long-term outcome of patients in the LNH-98.5 trial, the first randomized study comparing rituximab-CHOP to standard CHOP chemotherapy in DLBCL patients: a study by the Groupe d'Etudes des Lymphomes de l'Adulte. Blood. 2010;116(12):2040-5.
169. Pfreundschuh M, Kuhnt E, Trumper L, Osterborg A, Trneny M, Shepherd L, Gill DS, Walewski J, Pettengell R, Jaeger U, Zinzani PL, Shpilberg O, Kvaloy S, de Nully Brown P, Stahel R, Milpied N, Lopez-Guillermo A, Poeschel V, Grass S, Loeffler M, Murawski N, MabThera International Trial G. CHOP-like chemotherapy with or without rituximab in young patients with good-prognosis diffuse large-B-cell lymphoma: 6-year results of an open-label randomised study of the MabThera International Trial (MInT) Group. Lancet Oncol. 2011;12(11):1013-22.

170. Camicia R, Winkler HC, Hassa PO. Novel drug targets for personalized precision medicine in relapsed/refractory diffuse large B-cell lymphoma: a comprehensive review. Mol Cancer. 2015;14:207.
171. Lenz G, Staudt LM. Aggressive lymphomas. N Engl J Med. 2010;362(15):1417-29.
172. Hummel M, Bentink S, Berger H, Klapper W, Wessendorf S, Barth TF, Bernd HW, Cogliatti SB, Dierlamm J, Feller AC, Hansmann ML, Haralambieva E, Harder L, Hasenclever D, Kuhn M, Lenze D, Lichter P, Martin-Subero JI, Moller P, Muller-Hermelink HK, Ott G, Parwaresch RM, Pott C, Rosenwald A, Rosolowski M, Schwaenen C, Sturzenhofecker B, Szczepanowski M, Trautmann H, Wacker HH, Spang R, Loeffler M, Trumper L, Stein H, Siebert R, Molecular Mechanisms in Malignant Lymphomas Network Project of the Deutsche K. A biologic definition of Burkitt's lymphoma from transcriptional and genomic profiling. N Engl J Med. 2006;354(23):2419-30.
173. Schmitz R, Ceribelli M, Pittaluga S, Wright G, Staudt LM. Oncogenic mechanisms in Burkitt lymphoma. Cold Spring Harb Perspect Med. 2014;4(2).
174. Ribrag V, Koscielny S, Bosq J, Leguay T, Casasnovas O, Fornecker LM, Recher C, Ghesquieres H, Morschhauser F, Girault S, Gouill SL, Ojeda-Uribe M, Mariette C, Cornillon J, Cartron G, Verge V, Chassagne-Clement C, Dombret H, Coiffier B, Lamy T, Tilly H, Salles G. Rituximab and dose-dense chemotherapy for adults with Burkitt's lymphoma: a randomised, controlled, open-label, phase 3 trial. Lancet. 2016.
175. Cairo MS, Sposto R, Perkins SL, Meadows AT, Hoover-Regan ML, Anderson JR, Siegel SE, Lones MA, Tedeschi-Blok N, Kadin ME, Kjeldsberg CR, Wilson JF, Sanger W, Morris E, Krailo MD, Finlay JL. Burkitt's and Burkitt-like lymphoma in children and adolescents: a review of the Children's Cancer Group experience. Br J Haematol. 2003;120(4):660-70.
176. Sweetenham JW, Pearce R, Taghipour G, Blaise D, Gisselbrecht C, Goldstone AH. Adult Burkitt's and Burkitt-like non-Hodgkin's lymphoma--outcome for patients treated with high-dose therapy and autologous stem-cell transplantation in first remission or at relapse: results from the European Group for Blood and Marrow Transplantation. J Clin Oncol. 1996;14(9):2465-72.
177. Tan Z, Xie N, Banerjee S, Cui H, Fu M, Thannickal VJ, Liu G. The monocarboxylate transporter 4 is required for glycolytic reprogramming and inflammatory response in macrophages. J Biol Chem. 2015;290(1):46-55.
178. Calvo-Vidal MN, Cerchietti L. The metabolism of lymphomas. Curr Opin Hematol. 2013;20(4):345-54.

179. Plummer R, Veal G, Maxwell R, Payne G, Griffin M, O'Carrigan B, D'Arcangelo D, Halford S, Jones P, Hirschberg S, Banerji U. A first-in-human first-in-class trial of the monocarboxylate transporter 1 (MCT1) inhibitor AZD3965 in patients with advanced solid tumours. 14th International Congress on Targeted Anticancer Therapies; Washington, DC, USA.2016.
180. Chen L, Monti S, Juszczynski P, Daley J, Chen W, Witzig TE, Habermann TM, Kutok JL, Shipp MA. SYK-dependent tonic B-cell receptor signaling is a rational treatment target in diffuse large B-cell lymphoma. Blood. 2008;111(4):2230-7.
181. Polo JM, Juszczynski P, Monti S, Cerchietti L, Ye K, Greally JM, Shipp M, Melnick A. Transcriptional signature with differential expression of BCL6 target genes accurately identifies BCL6-dependent diffuse large B cell lymphomas. Proc Natl Acad Sci USA. 2007;104(9):3207-12.
182. Bradley WD, Arora S, Busby J, Balasubramanian S, Gehling VS, Nasveschuk CG, Vaswani RG, Yuan CC, Hatton C, Zhao F, Williamson KE, Iyer P, Mendez J, Campbell R, Cantone N, Garapaty-Rao S, Audia JE, Cook AS, Dakin LA, Albrecht BK, Harmange JC, Daniels DL, Cummings RT, Bryant BM, Normant E, Trojer P. EZH2 inhibitor efficacy in non-Hodgkin's lymphoma does not require suppression of H3K27 monomethylation. Chem Biol. 2014;21(11):1463-75.
183. Cheng S, Coffey G, Zhang XH, Shaknovich R, Song Z, Lu P, Pandey A, Melnick AM, Sinha U, Wang YL. SYK inhibition and response prediction in diffuse large B-cell lymphoma. Blood. 2011;118(24):6342-52.
184. Lunt SY, Vander Heiden MG. Aerobic glycolysis: meeting the metabolic requirements of cell proliferation. Annu Rev Cell Dev Biol. 2011;27:441-64.
185. Jurica MS, Mesecar A, Heath PJ, Shi W, Nowak T, Stoddard BL. The allosteric regulation of pyruvate kinase by fructose-1,6-bisphosphate. Structure. 1998;6(2):195-210.
186. Chandel NS. Navigating metabolism. xv, 248 pages p.
187. Birsoy K, Wang T, Chen WW, Freinkman E, Abu-Remaileh M, Sabatini DM. An Essential Role of the Mitochondrial Electron Transport Chain in Cell Proliferation Is to Enable Aspartate Synthesis. Cell. 2015;162(3):540-51.
188. Luo W, Brouwer C. Pathview: an R/Bioconductor package for pathway-based data integration and visualization. Bioinformatics. 2013;29(14):1830-1.
189. DeBerardinis RJ, Mancuso A, Daikhin E, Nissim I, Yudkoff M, Wehrli S, Thompson CB. Beyond aerobic glycolysis: Transformed cells can engage in glutamine metabolism that

exceeds the requirement for protein and nucleotide synthesis. Proc Natl Acad Sci USA. 2007;104(49):19345-50.

190. Amelio I, Cutruzzola F, Antonov A, Agostini M, Melino G. Serine and glycine metabolism in cancer. Trends Biochem Sci. 2014;39(4):191-8.
191. Chaneton B, Hillmann P, Zheng L, Martin AC, Maddocks OD, Chokkathukalam A, Coyle JE, Jankevics A, Holding FP, Vousden KH, Frezza C, O'Reilly M, Gottlieb E. Serine is a natural ligand and allosteric activator of pyruvate kinase M2. Nature. 2012;491(7424):458-62.
192. Cerchietti LC, Polo JM, Da Silva GF, Farinha P, Shaknovich R, Gascoyne RD, Dowdy SF, Melnick A. Sequential transcription factor targeting for diffuse large B-cell lymphomas. Cancer Res. 2008;68(9):3361-9.
193. Petitjean A, Mathe E, Kato S, Ishioka C, Tavtigian SV, Hainaut P, Olivier M. Impact of mutant p53 functional properties on TP53 mutation patterns and tumor phenotype: lessons from recent developments in the IARC TP53 database. Hum Mutat. 2007;28(6):622-9.
194. Roschewski M, Staudt LM, Wilson WH. Diffuse large B-cell lymphoma-treatment approaches in the molecular era. Nat Rev Clin Oncol. 2014;11(1):12-23.
195. Jokinen E, Koivunen JP. MEK and PI3K inhibition in solid tumors: rationale and evidence to date. Therapeutic Advances in Medical Oncology. 2015;7(3):170-80.
196. Pfeifer M, Grau M, Lenze D, Wenzel SS, Wolf A, Wollert-Wulf B, Dietze K, Nogai H, Storek B, Madle H, Dorken B, Janz M, Dirnhofer S, Lenz P, Hummel M, Tzankov A, Lenz G. PTEN loss defines a PI3K/AKT pathway-dependent germinal center subtype of diffuse large B-cell lymphoma. Proc Natl Acad Sci USA. 2013;110(30):12420-5.
197. Ezell SA, Wang S, Bihani T, Lai Z, Grosskurth SE, Tepsuporn S, Davies BR, Huszar D, Byth KF. Differential regulation of mTOR signaling determines sensitivity to AKT inhibition in diffuse large B cell lymphoma. Oncotarget. 2016;7(8):9163-74.
198. Schmitz R, Young RM, Ceribelli M, Jhavar S, Xiao W, Zhang M, Wright G, Shaffer AL, Hodson DJ, Buras E, Liu X, Powell J, Yang Y, Xu W, Zhao H, Kohlhammer H, Rosenwald A, Kluin P, Muller-Hermelink HK, Ott G, Gascoyne RD, Connors JM, Rimsza LM, Campo E, Jaffe ES, Delabie J, Smeland EB, Ogwang MD, Reynolds SJ, Fisher RI, Braziel RM, Tubbs RR, Cook JR, Weisenburger DD, Chan WC, Pittaluga S, Wilson W, Waldmann TA, Rowe M, Mbulaiteye SM, Rickinson AB, Staudt LM. Burkitt lymphoma pathogenesis and

therapeutic targets from structural and functional genomics. Nature. 2012;490(7418):116-20.

199. Sander S, Calado DP, Srinivasan L, Köchert K, Zhang B, Rosolowski M, Rodig SJ, Holzmann K, Stilgenbauer S, Siebert R, Bullinger L, Rajewsky K. Synergy between PI3K Signaling and MYC in Burkitt Lymphomagenesis. Cancer Cell. 2012;22(2):167-79.
200. Schuetz JM, Johnson NA, Morin RD, Scott DW, Tan K, Ben-Nierah S, Boyle M, Slack GW, Marra MA, Connors JM, Brooks-Wilson AR, Gascoyne RD. BCL2 mutations in diffuse large B-cell lymphoma. Leukemia. 2012;26(6):1383-90.
201. Iqbal J, Sanger WG, Horsman DE, Rosenwald A, Pickering DL, Dave B, Dave S, Xiao L, Cao K, Zhu Q, Sherman S, Hans CP, Weisenburger DD, Greiner TC, Gascoyne RD, Ott G, Müller-Hermelink HK, Delabie J, Braziel RM, Jaffe ES, Campo E, Lynch JC, Connors JM, Vose JM, Armitage JO, Grogan TM, Staudt LM, Chan WC. BCL2 Translocation Defines a Unique Tumor Subset within the Germinal Center B-Cell-Like Diffuse Large B-Cell Lymphoma. The American Journal of Pathology. 2004;165(1):159-66.
202. Souers AJ, Leverson JD, Boghaert ER, Ackler SL, Catron ND, Chen J, Dayton BD, Ding H, Enschede SH, Fairbrother WJ, Huang DC, Hymowitz SG, Jin S, Khaw SL, Kovar PJ, Lam LT, Lee J, Maecker HL, Marsh KC, Mason KD, Mitten MJ, Nimmer PM, Oleksijew A, Park CH, Park CM, Phillips DC, Roberts AW, Sampath D, Seymour JF, Smith ML, Sullivan GM, Tahir SK, Tse C, Wendt MD, Xiao Y, Xue JC, Zhang H, Humerickhouse RA, Rosenberg SH, Elmore SW. ABT-199, a potent and selective BCL-2 inhibitor, achieves antitumor activity while sparing platelets. Nat Med. 2013;19(2):202-8.
203. Johnson-Farley N, Veliz J, Bhagavathi S, Bertino JR. ABT-199, a BH3 mimetic that specifically targets Bcl-2, enhances the antitumor activity of chemotherapy, bortezomib and JQ1 in “double hit” lymphoma cells. Leuk Lymphoma. 2015;56(7):2146-52.
204. Young RM, Shaffer AL, 3rd, Phelan JD, Staudt LM. B-cell receptor signaling in diffuse large B-cell lymphoma. Semin Hematol. 2015;52(2):77-85.
205. Wilson WH, Young RM, Schmitz R, Yang Y, Pittaluga S, Wright G, Lih CJ, Williams PM, Shaffer AL, Gerecitano J, de Vos S, Goy A, Kenkre VP, Barr PM, Blum KA, Shustov A, Advani R, Fowler NH, Vose JM, Elstrom RL, Habermann TM, Barrientos JC, McGreivy J, Fardis M, Chang BY, Clow F, Munneke B, Moussa D, Beaupre DM, Staudt LM. Targeting B cell receptor signaling with ibrutinib in diffuse large B cell lymphoma. Nat Med. 2015;21(8):922-6.

206. Wang Y, Zhang LL, Champlin RE, Wang ML. Targeting Bruton's tyrosine kinase with ibrutinib in B-cell malignancies. Clin Pharmacol Ther. 2015;97(5):455-68.
207. Ott G, Rosenwald A, Campo E. Understanding MYC-driven aggressive B-cell lymphomas: pathogenesis and classification. Blood. 2013;122(24):3884-91.
208. Delmore JE, Issa GC, Lemieux ME, Rahl PB, Shi J, Jacobs HM, Kastritis E, Gilpatrick T, Paranal RM, Qi J, Chesi M, Schinzel AC, McKeown MR, Heffernan TP, Vakoc CR, Bergsagel PL, Ghobrial IM, Richardson PG, Young RA, Hahn WC, Anderson KC, Kung AL, Bradner JE, Mitsiades CS. BET bromodomain inhibition as a therapeutic strategy to target c-Myc. Cell. 2011;146(6):904-17.
209. Trabucco SE, Gerstein RM, Evens AM, Bradner JE, Shultz LD, Greiner DL, Zhang H. Inhibition of Bromodomain Proteins for the Treatment of Human Diffuse Large B-cell Lymphoma. Clin Cancer Res. 2015;21(1):113-22.
210. Mertz JA, Conery AR, Bryant BM, Sandy P, Balasubramanian S, Mele DA, Bergeron L, Sims RJ, 3rd. Targeting MYC dependence in cancer by inhibiting BET bromodomains. Proc Natl Acad Sci USA. 2011;108(40):16669-74.
211. Martínez-Reyes I, Diebold Lauren P, Kong H, Schieber M, Huang H, Hensley Christopher T, Mehta Manan M, Wang T, Santos Janine H, Woychik R, Dufour E, Spelbrink Johannes N, Weinberg Samuel E, Zhao Y, DeBerardinis Ralph J, Chandel Navdeep S. TCA Cycle and Mitochondrial Membrane Potential Are Necessary for Diverse Biological Functions. Mol Cell.61(2):199-209.
212. Li N, Ragheb K, Lawler G, Sturgis J, Rajwa B, Melendez JA, Robinson JP. Mitochondrial Complex I Inhibitor Rotenone Induces Apoptosis through Enhancing Mitochondrial Reactive Oxygen Species Production. Journal of Biological Chemistry. 2003;278(10):8516-25.
213. Lewis KA, Tzilivakis J, Warner DJ, Green A. An international database for pesticide risk assessments and management. Human and Ecological Risk Assessment: An International Journal. 2016;22(4):1050-64.
214. Morales DR, Morris AD. Metformin in Cancer Treatment and Prevention. Annu Rev Med. 2014.
215. Janzer A, German NJ, Gonzalez-Herrera KN, Asara JM, Haigis MC, Struhl K. Metformin and phenformin deplete tricarboxylic acid cycle and glycolytic intermediates during cell transformation and NTPs in cancer stem cells. Proc Natl Acad Sci USA. 2014;111(29):10574-9.

216. Chandel Navdeep S, Avizonis D, Reczek Colleen R, Weinberg Samuel E, Menz S, Neuhaus R, Christian S, Haegebarth A, Algire C, Pollak M. Are Metformin Doses Used in Murine Cancer Models Clinically Relevant? Cell Metab.23(4):569-70.
217. Dowling RJ, Lam S, Bassi C, Mouaaz S, Aman A, Kiyota T, Al-Awar R, Goodwin PJ, Stambolic V. Metformin Pharmacokinetics in Mouse Tumors: Implications for Human Therapy. Cell Metab. 2016;23(4):567-8.
218. He L, Wondisford FE. Metformin action: concentrations matter. Cell Metab. 2015;21(2):159-62.
219. Honigberg LA, Smith AM, Sirisawad M, Verner E, Loury D, Chang B, Li S, Pan Z, Thamm DH, Miller RA, Buggy JJ. The Bruton tyrosine kinase inhibitor PCI-32765 blocks B-cell activation and is efficacious in models of autoimmune disease and B-cell malignancy. Proc Natl Acad Sci USA. 2010;107(29):13075-80.
220. Lannutti BJ, Meadows SA, Herman SEM, Kashishian A, Steiner B, Johnson AJ, Byrd JC, Tyner JW, Loriaux MM, Deininger M, Druker BJ, Puri KD, Ulrich RG, Giese NA. CAL-101, a p110δ selective phosphatidylinositol-3-kinase inhibitor for the treatment of B-cell malignancies, inhibits PI3K signaling and cellular viability. Blood. 2011;117(2):591-4.
221. Chou T, Martin N. CompuSyn for Drug Combinations: PC Software and User's Guide: A Computer Program for Quantitation of Synergism and Antagonism in Drug Combinations, and the Determination of IC50 and ED50 and LD50 Values: Paramus; 2005.
222. Chou T-C. Drug Combination Studies and Their Synergy Quantification Using the Chou-Talalay Method. Cancer Res. 2010;70(2):440-6.
223. Greco WR, Bravo G, Parsons JC. The search for synergy: a critical review from a response surface perspective. Pharmacol Rev. 1995;47(2):331-85.
224. Chou TC. Theoretical basis, experimental design, and computerized simulation of synergism and antagonism in drug combination studies. Pharmacol Rev. 2006;58(3):621-81.
225. Sabharwal SS, Schumacker PT. Mitochondrial ROS in cancer: initiators, amplifiers or an Achilles' heel? Nat Rev Cancer. 2014;14(11):709-21.
226. Chang E, Liu H, Unterschemmann K, Ellinghaus P, Liu S, Gekeler V, Cheng Z, Berndorff D, Gambhir SS. 18F-FAZA PET imaging response tracks the reoxygenation of tumors in mice upon treatment with the mitochondrial complex I inhibitor BAY 87-2243. Clin Cancer Res. 2015;21(2):335-46.

227. Shortt J, Martin BP, Newbold A, Hannan KM, Devlin JR, Baker AJ, Ralli R, Cullinane C, Schmitt CA, Reimann M, Hall MN, Wall M, Hannan RD, Pearson RB, McArthur GA, Johnstone RW. Combined inhibition of PI3K-related DNA damage response kinases and mTORC1 induces apoptosis in MYC-driven B-cell lymphomas. Blood. 2013;121(15):2964-74.
228. Graham GG, Punt J, Arora M, Day RO, Doogue MP, Duong JK, Furlong TJ, Greenfield JR, Greenup LC, Kirkpatrick CM, Ray JE, Timmins P, Williams KM. Clinical pharmacokinetics of metformin. Clin Pharmacokinet. 2011;50(2):81-98.
229. Wheaton WW, Weinberg SE, Hamanaka RB, Soberanes S, Sullivan LB, Anso E, Glasauer A, Dufour E, Mutlu GM, Budigner GS, Chandel NS. Metformin inhibits mitochondrial complex I of cancer cells to reduce tumorigenesis. Elife. 2014;3:e02242.
230. Kordes S, Pollak MN, Zwinderman AH, Mathôt RA, Weterman MJ, Beeker A, Punt CJ, Richel DJ, Wilmink JW. Metformin in patients with advanced pancreatic cancer: a double-blind, randomised, placebo-controlled phase 2 trial. Lancet Oncol. 2015;16(7):839-47.
231. Bayer Healthcare AG. An open-label, Phase I, dose-escalation study to characterize the safety, tolerability, pharmacokinetics, and maximum tolerated dose of BAY 87-2243 given once daily in subjects with advanced malignancies 2013 [cited 2016 20/07/16]. Available from: http://trialfinder.bayerscheringpharma.de/html/pdf/15044_Study_Synopsis_CTP.pdf.
232. Salpeter SR, Greyber E, Pasternak GA, Salpeter EE. Risk of fatal and nonfatal lactic acidosis with metformin use in type 2 diabetes mellitus. Cochrane Database Syst Rev. 2010(4):CD002967.
233. Zhang G, Frederick DT, Wu L, Wei Z, Krepler C, Srinivasan S, Chae YC, Xu X, Choi H, Dimwamwa E, Ope O, Shannan B, Basu D, Zhang D, Guha M, Xiao M, Randell S, Sproesser K, Xu W, Liu J, Karakousis GC, Schuchter LM, Gangadhar TC, Amaravadi RK, Gu M, Xu C, Ghosh A, Xu W, Tian T, Zhang J, Zha S, Liu Q, Brafford P, Weeraratna A, Davies MA, Wargo JA, Avadhani NG, Lu Y, Mills GB, Altieri DC, Flaherty KT, Herlyn M. Targeting mitochondrial biogenesis to overcome drug resistance to MAPK inhibitors. J Clin Invest. 2016;126(5):1834-56.
234. Caino MC, Altieri DC. Molecular Pathways: Mitochondrial Reprogramming in Tumor Progression and Therapy. Clin Cancer Res. 2016;22(3):540-5.

235. Chae YC, Angelin A, Lisanti S, Kossenkov AV, Speicher KD, Wang H, Powers JF, Tischler AS, Pacak K, Fliedner S, Michalek RD, Karoly ED, Wallace DC, Languino LR, Speicher DW, Altieri DC. Landscape of the mitochondrial Hsp90 metabolome in tumours. Nat Commun. 2013;4.
236. Smith A, Crouch S, Lax S, Li J, Painter D, Howell D, Patmore R, Jack A, Roman E. Lymphoma incidence, survival and prevalence 2004-2014: sub-type analyses from the UK's Haematological Malignancy Research Network. Br J Cancer. 2015;112(9):1575-84.
237. Friedberg JW. Relapsed/Refractory Diffuse Large B-Cell Lymphoma. ASH Education Program Book. 2011;2011(1):498-505.
238. Sarkozy C, Coiffier B. Diffuse Large B-cell Lymphoma in the Elderly: A Review of Potential Difficulties. Clin Cancer Res. 2013;19(7):1660-9.
239. De Saedeleer CJ, Porporato PE, Copetti T, Perez-Escuredo J, Payen VL, Brisson L, Feron O, Sonveaux P. Glucose deprivation increases monocarboxylate transporter 1 (MCT1) expression and MCT1-dependent tumor cell migration. Oncogene. 2013.
240. Evens AM, Sehn LH, Farinha P, Nelson BP, Raji A, Lu Y, Brakman A, Parimi V, Winter JN, Schumacker PT, Gascoyne RD, Gordon LI. Hypoxia-inducible factor-1 {alpha} expression predicts superior survival in patients with diffuse large B-cell lymphoma treated with R-CHOP. J Clin Oncol. 2010;28(6):1017-24.
241. Powell JR, Dojcinov S, King L, Wosniak S, Gerry S, Casbard A, Bailey H, Gallop-Evans E, Maughan T. Prognostic significance of hypoxia inducible factor-1α and vascular endothelial growth factor expression in patients with diffuse large B-cell lymphoma treated with rituximab. Leuk Lymphoma. 2013;54(5):959-66.
242. Pfreundschuh M. How I treat elderly patients with diffuse large B-cell lymphoma. Blood. 2010;116(24):5103-10.
243. Weiler-Sagie M, Bushelev O, Epelbaum R, Dann EJ, Haim N, Avivi I, Ben-Barak A, Ben-Arie Y, Bar-Shalom R, Israel O. (18)F-FDG avidity in lymphoma readdressed: a study of 766 patients. J Nucl Med. 2010;51(1):25-30.
244. Valls L, Badve C, Avril S, Herrmann K, Faulhaber P, O'Donnell J, Avril N. FDG-PET imaging in hematological malignancies. Blood Rev. 2016;30(4):317-31.

Chapter 9. Appendices

Appendix A: Metabolic pathway analysis with Pathview

```
#Download and load necessary packages
#source("http://bioconductor.org/biocLite.R")
#biocLite()
#biocLite("pathview")
#install.packages("ggplot2")
#biocLite("GOstats")
#biocLite("gplots")
library(pathview)
library(ggplot2)
library(GOstats)
library(gplots)

#2h data only all events
#ANALYSIS REQUIRES COMPOUND NAMES AS KEGG_IDs
my_data = read.csv("~/KEGG_IDs.csv") #Read in CSV

View(my_data)
my_data = my_data[complete.cases(my_data),]

#Remove unicode characters from excel sheet (spaces)
my_data$KEGG.id = gsub("\xa0", "", my_data$KEGG.id)

#Filter on P-value
my_data = my_data[my_data$T.Test < 0.05,]

#Filter on 2h data
cpd_fc = my_data[my_data$Time..h.==2,]$Log2.Fold.Change

#Convert to character vector
cpd_id = as.character(my_data[my_data$Time..h.==2,]$KEGG.id)
names(cpd_fc) = cpd_id

#Use KEGG pathway IDs to map changes onto given pathways

#TCA CYCLE
pathview(cpd.data=cpd_fc, pathway.id="00020", species="hsa",
    limit=list(gene=1, cpd=c(round(min(cpd_fc)), round(max(cpd_fc)))),
    low=list(gene="red", cpd="blue"),
    mid=list(gene="light grey", cpd="light grey"),
    high=list(gene="blue", cpd="red")

#GLYCOLYSIS
pathview(cpd.data=cpd_fc_24, pathway.id="00010", species="hsa",
    limit=list(gene=1, cpd=c(round(min(cpd_fc)), round(max(cpd_fc))),
    low=list(gene="red", cpd="blue"),
    mid=list(gene="light grey", cpd="light grey"),
    high=list(gene="blue", cpd="red")
```

Appendix B: Patient samples used for MCT1 and MCT4 scoring by IHC

ID	Disease type	COO subtype	MYC FISH status	MCT1	MCT4
16/611	BL	n/a	Y	300	0
16/768	BL	n/a	Y	300	0
16/817	BL	n/a	N	300	0
16/391	BL	n/a	Y	300	0
16/818	BL	n/a	Y	300	0
16/827	BL	n/a	Y	300	0
16/558	BL	n/a	N	300	0
16/841	BL	n/a	Y	300	0
16/511	BL	n/a	Y	300	2
16/321	BL	n/a	n.d	300	10
PR29428/07	DLBCL	ABC	N	170	0
PR32298/07	DLBCL	GCB	N	240	0
PR42830/07	DLBCL	ABC	N	300	0
PR3089/08	DLBCL	ABC	N	220	0
PR9008/08	DLBCL	ABC	N	290	0
PR13580/08	DLBCL	ABC	Y	100	0
PR23480/08	DLBCL	GCB	n.d	300	0
PR29746/08	DLBCL	GCB	N	20	0
PR43029/09	DLBCL	GCB	n.d	70	0
PR32817/11	DLBCL	GCB	n.d	200	0
PR29109/11	DLBCL	GCB	n.d	20	0
PR23302/11	DLBCL	GCB	n.d	20	0
PR20297/04	DLBCL	GCB	Y	240	0
PR28506/05	DLBCL	GCB	N	130	0
PR40579/05	DLBCL	ABC	N	110	0
PR14004/04	DLBCL	GCB	N	100	0
PR25724/06	DLBCL	ABC	N	170	0
PR28320/06	DLBCL	ABC	N	170	0
PR40465/06	DLBCL	ABC	N	100	0
PR16937/07	DLBCL	GCB	N	140	0
PR19169/07	DLBCL	GCB	N	280	0
PR21027/07	DLBCL	n.d	n.d	290	0

ID	Disease type	COO subtype	MYC FISH status	MCT1	MCT4
PR29951/07	DLBCL	GCB	Y	300	0
PR5697/08	DLBCL	ABC	N	50	0
PR15963/08	DLBCL	ABC	N	150	0
PR25086/08	DLBCL	GCB	Y	300	0
PR24199/08	DLBCL	GCB	N	270	0
PR40812/08	DLBCL	GCB	Y	290	0
PR43968/08	DLBCL	GCB	N	280	0
PR2676/09	DLBCL	ABC	Y	120	0
PR19148/09	DLBCL	ABC	n.d	290	0
PR29270/09	DLBCL	GCB	Y	300	0
PR29864/09	DLBCL	GCB	n.d	200	0
PR25618/07	DLBCL	GCB	N	150	0
PR6621/07	DLBCL	ABC	N	260	0
PR2486/07	DLBCL	GCB	N	240	0
PR36972/06	DLBCL	GCB	n.d	120	0
PR32034/06	DLBCL	GCB	N	260	0
PR23084/06	DLBCL	GCB	Y	280	0
PR36304/03	DLBCL	GCB	N	30	0
PR3902/04	DLBCL	ABC	N	170	0
PR20367/08	DLBCL	GCB	n.d	300	0
PR40146/03	DLBCL	GCB	n.d	280	0
05/13561	DLBCL	ABC	Y	200	0
1210827	DLBCL	ABC	N	280	0
PR20761/05	DLBCL	GCB	N	290	0
PR9693/07	DLBCL	GCB	N	180	0
07H12708	DLBCL	GCB	Y	20	0
P06/8605	DLBCL	ABC	N	300	0
P07/14124	DLBCL	GCB	N	90	0
P05/7489	DLBCL	GCB	N	210	0
PR3219/06	DLBCL	GCB	N	300	0
07H13399	DLBCL	GCB	n.d	70	0
PR34622/09	DLBCL	ABC	N	90	0
PR28424/07	DLBCL	ABC	N	20	0
PR13924/07	DLBCL	GCB	Y	290	0
PR37065/04	DLBCL	GCB	n.d	300	0
PR3035/09	DLBCL	ABC	N	170	0

ID	Disease type	COO subtype	MYC FISH status	MCT1	MCT4
PR26840/05	DLBCL	GCB	N	260	0
PR23944/07	DLBCL	ABC	n.d	200	0
PR1825/05	DLBCL	GCB	N	300	0
PR41673/08	DLBCL	GCB	n.d	50	0
08/02315	DLBCL	GCB	n.d	250	0
04/4472 A5	DLBCL	GCB	N	280	0
PR22517/06	DLBCL	GCB	n.d	40	0
07H8249	DLBCL	ABC	N	80	0
PR21189/06	DLBCL	GCB	n.d	50	0
PR21012/07	DLBCL	ABC	n.d	280	0
PR16109/04	DLBCL	GCB	n.d	230	0
PR15362/08	DLBCL	GCB	n.d	250	0
PR40855/06	DLBCL	GCB	N	300	0
08/10760	DLBCL	ABC	N	10	0
PR35436/05	DLBCL	GCB	n.d	260	0
04/12376	DLBCL	GCB	N	300	0
PR11576/15	DLBCL	ABC	N	300	0
PR30622/14	DLBCL	ABC	n.d	250	0
PR41399/13	DLBCL	ABC	n.d	130	0
PR31383/13	DLBCL	GCB	N	300	0
PR48484/15	DLBCL	GCB	N	240	0
PR53103/13	DLBCL	GCB	n.d	160	0
PR31909/14	DLBCL	GCB	Y	300	0
PR4823/15	DLBCL	GCB	n.d	110	0
PR41003/14	DLBCL	GCB	N	260	0
PR09549/16	DLBCL	GCB	N	300	0
PR18025/15	DLBCL	GCB	n.d	300	0
PR47674/14	DLBCL	GCB	N	300	0
PR47462/14	DLBCL	GCB	N	300	0
PR33799/13	DLBCL	GCB	Y	130	0
PR23721/14	DLBCL	GCB	Y	250	0
PR16506/06	DLBCL	GCB	N	110	2
PR14330/08	DLBCL	GCB	N	300	2
713474	DLBCL	ABC	N	230	2
PR4666/05	DLBCL	ABC	N	50	2
PR12775/14	DLBCL	ABC	n.d	90	2

ID	Disease type	COO subtype	MYC FISH status	MCT1	MCT4
PR06607/15	DLBCL	GCB	N	30	2
PR15175/11	DLBCL	ABC	n.d	280	4
PR10234/08	DLBCL	ABC	N	270	5
PR1592/06	DLBCL	GCB	N	100	5
PR36943/09	DLBCL	GCB	N	200	10
PR43202/11	DLBCL	GCB	n.d	300	10
PR17512/07	DLBCL	GCB	N	250	10
PR23739/14	DLBCL	ABC	n.d	220	15
PR14786/11	DLBCL	GCB	n.d	100	20
PR24260/05	DLBCL	GCB	N	180	20
PR33076/04	DLBCL	ABC	n.d	270	20
PR14748/14	DLBCL	ABC	n.d	300	20
PR32466/08	DLBCL	GCB	N	220	30
PR20422/06	DLBCL	GCB	N	170	40
PR21162/08	DLBCL	GCB	n.d	120	40
PR3257/06	DLBCL	GCB	N	90	60
PR35058/15	DLBCL	ABC	N	60	80
PR06734/15	DLBCL	GCB	N	200	90
08H06103	DLBCL	GCB	N	270	100
PR4068/06	DLBCL	GCB	N	220	110
PR26201/05	DLBCL	GCB	N	230	120
P06/16727-4	DLBCL	GCB	n.d	280	150
PR10496/05	DLBCL	GCB	N	140	160
PR32255/11	DLBCL	ABC	n.d	240	170
PR1266/08	DLBCL	ABC	n.d	300	190
PR15144/06	DLBCL	GCB	N	260	200
PR41023/06	DLBCL	GCB	n.d	300	250

Table 10: BL/DLBCL samples stained for MCT1 and MCT4 expression by IHC
Individual cases were sorted by disease type (BL or DLBCL) and then by MCT4 expression. Cell of Origin status is indicated where defined (ABC/GCB), not determined (n.d) or not applicable (n/a). Presence of MYC translocation as identified by FISH is indicated as confirmed (Y), no evidence (N) or not defined (?). BL and DLBCL patient samples were scored for intensity and extent of staining to produce a single expression score (H-score).

Appendix C: *TP53* mutational status in B-NHL

Sample Name	Morphology	*TP53* status	Structure-Function Class	*MCT1*	*MCT4*	PubMed
Akata	BL	MUT	n/a			1915267
AKUA	BL	MUT	non-functional			8402660
AS283A	BL	MUT	n/a			2052620
BL113	BL	MUT	non-functional			2052620
BL-37	BL	MUT	non-functional			2052620
BL-41	BL	MUT	non-functional	9.84	4.47	15188009
BL-49	BL	MUT	non-functional			2052620
BL-60	BL	MUT	non-functional			2052620
BL-70	BL	MUT	non-functional	8.76	4.51	15188009
BL-99	BL	MUT	n/a			2052620
BRG-A	BL	MUT	n/a			9399658
BRG-M	BL	MUT	non-functional			9399658
CA46	BL	MUT	non-functional	9.19	4.87	8402660
CW678	BL	MUT	non-functional	8.63	4.89	2052620
Daudi	BL	MUT	non-functional	8.63	4.89	15188009
DG-75	BL	MUT	functional			9525742
EB-1	BL	MUT	non-functional	9.17	4.68	15188009
EB2	BL	MUT	non-functional	8.93	4.85	15188009
EB3	BL	MUT	n/a			2052620
GA-10	BL	MUT	non-functional	9.30	4.85	11482875
JD 38	BL	MUT	non-functional			2052620
Jijoye	BL	MUT	non-functional			1915267
KK125	BL	MUT	non-functional			2052620
Louckes	BL	MUT	non-functional			1915267
MC116	BL	MUT	non-functional	9.19	5.32	2052620
Namalwa	BL	MUT	non-functional	9.54	5.56	2052620
P3HR-1	BL	MUT	non-functional			2052620
PP984	BL	MUT	non-functional			2052620
Raji	BL	MUT	non-functional	9.52	5.03	1915267
Ramos	BL	MUT	non-functional			2052620
SG568	BL	MUT	n.d			8402660
ST486	BL	MUT	non-functional	8.71	4.72	15188009

TE-161-T	BL	WT	n/a			15188009
BJAB	DLBCL	MUT	non-functional			1915267
CTB-1	DLBCL	WT	n/a			15188009
DB	DLBCL	MUT	non-functional	8.99	4.79	15188009
DOHH-2	DLBCL	WT	n/a	8.41	4.71	15188009
Farage	DLBCL	MUT	n.d			2748725
HBL-1	DLBCL	MUT	non-functional			8412324
HT	DLBCL	MUT	non-functional	9.50	6.28	15188009
KARPAS-422	DLBCL	MUT	n/a	9.23	4.61	15188009
OCILY1	DLBCL	MUT	non-functional			8274734
OCILY17	DLBCL	MUT	non-functional			8274734
OCILY2	DLBCL	MUT	non-functional			8274734
OCILY7	DLBCL	MUT	non-functional			8274734
Ly-8C3	DLBCL	MUT	non-functional			8274734
NU-DHL-1	DLBCL	MUT	non-functional	10.11	5.07	22460905
OCILY10	DLBCL	WT	n/a	9.21	5.12	19021061
OCILY18	DLBCL	MUT	n.d			8574164
OCILY3	DLBCL	WT	n/a	8.80	4.66	19021061
OCILY4	DLBCL	MUT	non-functional			8574164
Pfeiffer	DLBCL	MUT	n.d			21394100
RIVA	DLBCL	MUT	non-functional	10.01	6.49	22460905
SU-DHL-1	DLBCL	MUT	non-functional	10.20	4.98	15188009
SU-DHL-10	DLBCL	MUT	n/a	9.61	5.39	22460905
SU-DHL-4	DLBCL	MUT	non-functional	9.34	5.03	22460905
SU-DHL-6	DLBCL	MUT	n/a	9.46	4.73	22460905
SU-DHL-8	DLBCL	MUT	non-functional	9.16	5.18	22460905
Toledo	DLBCL	MUT	n/a	8.63	4.95	22460905
TUR	DLBCL	MUT	n/a			15188009
WSU-DLCL2	DLBCL	MUT	non-functional	9.60	4.90	22460905

Table 11: Summary of *TP53* status and *MCT1/MCT4* gene expression in BL and DLBCL
Relative expression of *MCT1* and *MCT4* mRNA (RMA-normalised) from CCLE for BL and DLBCL cell lines listed within the IARC *TP53* mutation database (160, 193).

Appendix D: LC-MS Metabolites

Analyte short name	Name
_Acetoacetyl_CoA	Acetoacetyl coenzyme A
_acetylCoA	Acetyl coenzyme A
_adenine	Adenine
_adipic_acid	Adipic acid
_ADP	Adenosine diphosphate
_ADP_ribose	Adenosine diphosphoribose
_aKET_B	Alpha ketoglutarate
_AMP	Adenosine monophosphate
_Arginine	Arginine
_Asparagine	Asparagine
_Aspartic_acid	Aspartic acid
_ATP	Adenosine triphosphate
_benzoic_acid	Benzoic acid
_cAMP	Cyclic adenosine monophosphate
_cGMP	Cyclic guanosine monophosphate
_cis_aconitic_acid	Cis aconitic acid
_citrate	Citrate
_citrulline	Citrulline
_CMP	Cytidine monophosphate
_CoA	Coenzyme A
_coumaric_acid	Coumaric acid
_Creatine	Creatine
_Creatinine	Creatinine
_Cystine	Cystine
_cytosine	Cytosine
_dADP	2'deoxyadenosine monophosphate
_dAMP	2'deoxyadenosine diphosphate
_dATP	2'deoxyadenosine triphosphate
_dCDP	2'deoxycytidine diphosphate
_dCMP	2'deoxycytidine monophosphate
_dCTP	2'deoxycytidine triphosphate
_dGMP	2' deoxyguanosine 5-monophosphate
_Dihydroxy_Acetone_Phosphate	Dihydroxyacetone phosphate

_dinitrosalicylic_acid	Dinitrosalicylic acid
_dUMP	2'deoxyuridine monophosphate
_dUTP	2'deoxyuridine triphosphate
_FAD	Flavin adenine dinucleotide
_FBP	Fructose bisphosphate
_ferrulic_acid	Ferrulic acid
_folate	Folate
_Fructose__1_P	Fructose-1-phosphate
_Fructose_6_P	Fructose-6-phosphate
_fumarate	Fumarate
_G3P	Glycerate-3-phosphate
_Galactose_1	Galactose-1-phosphate
_GAP	Glyceraldehyde-3-phosphate
_GBP	Glycerate bisphosphate
_GDP	Guanosine diphosphate
_glucosamine6P	Glucosamine-6-phosphate
_Glucose_1_P	Glucose-1-phosphate
_Glucose_6_P	Glucose-6-phosphate
_glucuronic_acid	Glucuronic acid
_glutamate	Glutamate
_glutamine	Glutamine
_glutaric_acid	Glutaric acid
_glutathione_ox	Glutathione (Oxidised)
_glutathione_red	Glutathione (Reduced)
_glyoxyllic_acid	Glyoxyllic acid
_GMP	Guanosine monophosphate
_GTP	Guanosine triphosphate
_guanine	Guanine
_guanosine	Guanosine
_Histidine	Histidine
_HPPA	Hydroxyphenyl propionic acid
_Hydroxy_glutaric_Acid	Hydroxymethyl glutaric acid
_Hydroxymethyl_Glutaryl_CoA	Hydroxymethyl glutaryl coenzyme A
_ICA	Indoleacrylic acid
_IMP	Inosine monophosphate
_inosine	Inosine

_Isobutyryl_CoA	Isobutyryl coenzyme A
_isocitrate_sp	Isoctirate
_Isoleucine	Isoleucine
_Isovaleryl_CoA	Isovaleryl coenzyme A
_itaconic_acid	Itaconic acid
_lactate	Lactate
_Leucine	Leucine
_malate	Malate
_maleic_acid	Maleic acid
_malonic_acid	Malonic acid
_Malonyl_CoA	Malonyl coenzyme A
_Mannose_6_P	Mannose 6 phosphate
_Mesaconic_Acid	Mesaconic acid
_Methionine	Methionine
_Methyl_Malonyl_CoA	Methylmalonyl coenzyme A
_methylxanthine	Methylxanthine
_NAD	Nicotinamide adenine dinucleotide
_NADH	Reduced NAD
_NADP	Nicotinamide adenine dinucleotide phosphate
_NADPH	Reduced NADP
_NAG	N-acetyl glucosamine
_nicotinic_acid	Nicotinic acid
_nitrophenol	Nitrophenol
_orotic_acid	Orotic acid
_palmitic_acid	Palmitic acid
_pantothenic_acid	Pantothenic acid
_Pcreatine	Phosphocreatine
_PEP	Phosphophenolpyruvate
_PG	6-phosphogluconate
_phenylalanine	Phenylalanine
_phthalic_acid	Phthalic acid
_Proline	Proline
_Proprionyl_CoA	Proprionyl coenzyme A
_Pserine	Phosphoserine
_pyruvate	Pyruvate
_riboflavin	Riblofalvin

_Ribose_5_P	Ribose 5 phosphate
_ribulose_5_P	Ribulose-5-phosphate
_S_5_Adenosyl_L_Cysteine	S-5-Adenosyl-L-Cysteine
_S_5_Adenosyl_L_Cysteine_1	S-5-Adenosyl-L-Cysteine-1
_S_5Adenosyl_L_Homocysteine	S-5-Adenosyl-L-Homocysteine
_salicylic_acid	Salicylic acid
_serine	Serine
_shikimic_acid	Shikimic acid
_sorbitol_mannitol	Sorbitol or mannitol
_succinate	Succinate
_Succinyl_CoA	Succinyl coenzyme A
_Threonine	Threonine
_thymine	Thymine
_TIA	2, trans-3-enol pyruvic acid
_tryptophan	Tryptophan
_tyrosine	Tyrosine
_UDP	Uridine diphosphate
_UDP_glucA	Uridine diphosphate glucuronic acid
_UDP_glucose	Uridine diphosphate glucose
_UMP	Uridine monophosphate
_uracil	Uracil
_uridine	Uridine
_Valine	Valine
_xylulose_5_P	Xyulose 5 phosphate

Table 12: Array of metabolites detectable by LC-MS

Appendix E: AZD3965 induced metabolic changes *in vitro*

Cell line	Metabolites	Log_2 FC	P-value
CA46	α-ketoglutarate	0.72	0.02364856
CA46	Aspartic acid	-0.55	0.01123613
CA46	Benzoic acid	0.76	0.03698818
CA46	Cis-aconitic acid	1.92	0.00186559
CA46	Citrate	2.50	0.03527132
CA46	Fructose bisphosphate	-3.16	0.03645213
CA46	Fructose-1-phosphate	-1.46	0.01015639
CA46	Fructose-6-phosphate	1.38	0.03452481
CA46	Fumarate	1.17	0.00030609
CA46	Glucose-6-phosphate	1.37	0.02149326
CA46	Hydroxy-glutaric acid	0.61	0.00423076
CA46	Inosine monophosphate	0.88	0.01666035
CA46	Isocitrate	2.21	0.0233072
CA46	Lactate	0.95	8.63E-05
CA46	Malate	0.66	0.0005867
CA46	Mannose-6-phosphate	1.39	0.0147361
CA46	Phosphocreatine	-0.82	0.00559057
CA46	Phosphoserine	-4.27	0.00011756
CA46	Succinate	0.62	0.0009613
CA46	Xyulose-5-phosphate	-0.84	0.00307755
Daudi	α-ketoglutarate	0.95	0.00130228
Daudi	Adenosine monophosphate	-0.54	0.00417053
Daudi	Aspartic acid	-0.54	0.02443934
Daudi	Cyclic adenosine monophosphate	1.36	0.03651374
Daudi	Cis-aconitic acid	2.29	0.00180616
Daudi	Citrate	1.86	0.03120898
Daudi	Creatine	-0.77	0.01865185
Daudi	2' deoxyuridine-monophosphate	-0.63	0.03069022
Daudi	Fructose bisphosphate	-3.20	0.01142309
Daudi	Fructose-1-phosphate	-1.13	0.00400372
Daudi	Fumarate	0.81	0.02688549
Daudi	Glucose-6-phosphate	0.59	0.00398842
Daudi	Glutamate	-0.52	0.00580551

Cell line	Metabolites	Log_2 FC	P-value
Daudi	Glyoxyllic acid	0.66	0.0327116
Daudi	Guanosine	-2.08	0.01324557
Daudi	Lactate	0.97	0.00066579
Daudi	Malate	0.90	0.00330235
Daudi	Mannose-6-phosphate	0.59	0.02457415
Daudi	Orotic acid	-1.22	9.34E-05
Daudi	Phosphocreatine	-2.15	0.0001488
Daudi	6-phosphogluconate	0.93	0.04639125
Daudi	Proline	-0.86	0.01248772
Daudi	S-5-adenosyl-L-cysteine	-1.38	0.00186336
Daudi	Thymidine monophosphate	-0.66	0.00078543
Raji	α-ketoglutarate	0.55	0.00422628
Raji	Aspartic acid	-1.02	0.00748999
Raji	cis Aconitic acid	2.19	1.95E-05
Raji	Citrate	4.21	0.00637086
Raji	Creatine	-0.70	0.0101281
Raji	2'deoxyuridine triphosphate	0.62	0.03859534
Raji	Fructose-6-phosphate	1.41	0.03921023
Raji	Glyceraldehyde-3-phosphate	2.00	0.00063439
Raji	Glucose-1-phosphate	0.74	0.013916
Raji	Glucose-6-phosphate	0.95	0.03814738
Raji	Glutamate	-0.59	0.01808727
Raji	Hydroxy-glutaric acid	0.87	0.00015756
Raji	Inosine monophosphate	1.75	0.00027764
Raji	Isocitrate	2.62	0.00238449
Raji	Lactate	0.59	0.04441402
Raji	Malate	0.50	0.0064463
Raji	Phosphoserine	-4.75	0.00588106
Farage	α-ketoglutarate	1.01	0.00039321
Farage	Aspartic acid	-0.86	0.01500082
Farage	Benzoic acid	-0.54	0.03676635
Farage	cis-Aconitic acid	1.43	0.00187777
Farage	Fumarate	1.24	0.04946194
Farage	Galactose-1-phosphate	0.57	0.04257316
Farage	Glyceraldehyde-3-phosphate	1.96	0.02487211

Cell line	Metabolites	Log_2 FC	P-value
Farage	Glucose-6-phosphate	1.88	0.01368217
Farage	Glyoxyllic acid	1.63	0.03285017
Farage	Isocitrate	2.06	0.03556178
Farage	Malate	1.00	0.04061783
Farage	Orotic acid	0.93	0.03812001
OCILY18	α-ketoglutarate	1.52	0.00075014
OCILY18	Aspartic acid	-0.94	0.00100529
OCILY18	cis-Aconitic acid	2.38	2.59E-06
OCILY18	Citrate	2.76	0.00065383
OCILY18	Cytidine-monophosphate	-0.70	0.03042743
OCILY18	2'deoxycytidine monophosphate	-0.92	0.01832797
OCILY18	Fructose-1-phosphate	-1.34	0.00195119
OCILY18	Fructose-6-phosphate	1.66	0.0049803
OCILY18	Fumarate	0.60	0.0269773
OCILY18	Glyceraldehyde-3-phosphate	1.43	0.00252289
OCILY18	Glucose-6-phosphate	1.87	1.07E-05
OCILY18	Glutamate	-0.59	0.01381352
OCILY18	Glyoxyllic acid	1.52	5.60E-05
OCILY18	Hydroxy glutaric acid	1.38	0.00202169
OCILY18	Inosine monophosphate	1.50	7.89E-05
OCILY18	Isocitrate	3.40	0.00017889
OCILY18	Lactate	0.62	0.0065629
OCILY18	Malate	0.56	0.00150088
OCILY18	Mannose-6-phosphate	1.88	0.00027798
OCILY18	Nicotinamide adenine dinucleotide	-0.51	0.00945742
OCILY18	Phosphocreatine	-0.91	0.00340449
OCILY18	Phosphoserine	-4.61	0.00041349
OCILY18	Pyruvate	-1.00	0.00038491
OCILY18	Ribose-5-phosphate	-0.61	0.0085644
OCILY18	Tyrosine	-0.65	0.00239074
OCILY18	Uridine-diphosphate-glucose	-1.05	0.00015616
OCILY18	Uridine monophosphate	-0.80	4.92E-05
OCILY18	Uridine	-1.14	0.0133522
IMR-32	α-ketoglutarate	1.40	0.00020957
IMR-32	cis Aconitic acid	2.05	0.00029976

Cell line	Metabolites	Log_2 FC	P-value
IMR-32	Citrate	3.40	1.73E-05
IMR-32	2'deoxyuridine monophosphate	-0.58	0.0205305
IMR-32	Fructose-1-phosphate	-0.85	0.00038287
IMR-32	Fructose-6-phosphate	1.32	0.00041635
IMR-32	Fumarate	1.85	0.00024637
IMR-32	Glycerate-3-phosphate	1.22	3.46E-05
IMR-32	Glucose-6-phosphate	2.00	4.15E-05
IMR-32	Reduced glutathione	1.43	0.04179682
IMR-32	Hydroxy-glutaric acid	0.59	0.00538379
IMR-32	Isocitrate	2.23	0.00058534
IMR-32	Lactate	0.72	0.00024147
IMR-32	Malate	1.50	9.05E-06
IMR-32	Mannose-6-phosphate	1.87	3.71E-05
IMR-32	Phosphophenolpyruvate	1.74	0.00343812
IMR-32	Phosphoserine	-2.74	0.00018128
IMR-32	Pyruvate	0.94	0.00021128
IMR-32	Ribulose-5-phosphate	0.71	0.04060115
IMR-32	Succinate	1.02	9.15E-05
IMR-32	Tryptophan	-0.58	0.01842709
SH-SY5Y	α-ketoglutarate	1.77	6.81E-06
SH-SY5Y	Adenosine monophosphate	0.55	0.02528411
SH-SY5Y	Aspartic acid	-0.97	8.03E-05
SH-SY5Y	cis-Aconitic acid	1.69	0.00024036
SH-SY5Y	Citrate	2.45	5.21E-07
SH-SY5Y	Creatine	0.72	0.00325851
SH-SY5Y	Fructose-6-phosphate	1.25	3.48E-05
SH-SY5Y	Fumarate	0.83	0.00234584
SH-SY5Y	Glycerate-3-phosphate	0.78	9.17E-05
SH-SY5Y	Glyceraldehyde-3-phosphate	1.20	0.00074528
SH-SY5Y	Glycerate bisphosphate	-1.60	0.00264423
SH-SY5Y	Glucose-6-phosphate	1.21	0.00016866
SH-SY5Y	Glutamate	-0.56	5.79E-05
SH-SY5Y	Glyoxyllic acid	1.60	0.00055379
SH-SY5Y	Guanosine monophosphate	1.47	0.00870991
SH-SY5Y	Hydroxy-glutaric acid	1.04	0.00011156

Cell line	Metabolites	Log_2 FC	P-value
SH-SY5Y	Isocitrate	1.93	4.42E-05
SH-SY5Y	Lactate	0.74	0.0001002
SH-SY5Y	Malate	0.62	8.75E-05
SH-SY5Y	Mannose-6-phosphate	1.21	0.00173694
SH-SY5Y	Orotic acid	1.09	0.00288852
SH-SY5Y	Phosphocreatine	-0.71	0.00017369
SH-SY5Y	Phosphophenolpyruvate	0.55	0.00020893
SH-SY5Y	Phosphoserine	-4.14	8.81E-05
SH-SY5Y	Pyruvate	0.51	0.00285791
SH-SY5Y	Ribulose-5-phosphate	0.83	0.00031764
SH-SY5Y	Succinate	0.51	0.01035155
SH-SY5Y	Uridine-diphosphate-glucose	-0.58	0.02061405
SH-SY5Y	Xyulose-5-phosphate	0.90	0.00028449

Table 13: Full list of significantly altered metabolites following treatment with AZD3965 *in vitro.*
Metabolic changes following 2 hour treatment with AZD3965 in BL (CA46, Daudi, Raji), DLBCL (Farage and OCILY18) and neuroblastoma (IMR-32, SH-SY5Y) cells. Substantial alterations in intracellular metabolite concentrations relative to time-matched DMSO controls (+/- 0.5 Log_2 fold change), with associated P-values below 0.05 (two-tailed *t*-test) are indicated.